Modelling Simulation and Optimization of Innovative Hybrid Separation Processes for Energy Savings

by

Dragan Nikolić

6 July 2010

A thesis submitted for the degree of Doctor of Philosophy
of the University of Western Macedonia, Kozani, Greece

University of Western Macedonia, Department of Mechanical Engineering,
Sialvera & Bakola Str., 50100 Kozani, Greece

ABSTRACT

Adsorption and membrane systems have become highly important gas separation technologies in chemical manufacturing, petroleum and natural gas refining and new clean energy concepts. The global market for the industrial gas business was worth 63 billion dollars in 2008. For instance, over 41 million tons/year of hydrogen and 100 million tons/year of oxygen is produced worldwide. Pressure swing adsorption (PSA) has attracted increasing interest because of its low energy requirements as well as low capital investment costs in comparison to the traditional separation processes. PSA has become state-of-the-art technology for small to intermediate scale oxygen and nitrogen production from air, small to large-scale gas drying, hydrogen recovery from different petrochemical processes (steam-methane reforming off gas or coke oven gas), and trace impurity removal from contaminated gases. Membranes found applications in similar areas: processing of natural gas, hydrogen recovery from various chemical and petrochemical sources, oxygen and nitrogen production from air, and carbon dioxide removal.

PSA is able to produce high purity gases at very high recovery. However, the capital costs and energy requirements are still considerably high since modern industrial PSA units typically utilize layered beds containing up to four adsorbents and, depending on the production volume, anywhere between four and sixteen columns. On the other hand, current membranes systems offer low energy consumption, dramatically lower investment costs, continuous production and ease of operation. However, membranes are not able to produce high purity gases yet (due to a limited selectivity). Therefore, why not combine these two worlds: reliable PSA technology able to produce high purity gases with the low cost membrane systems to try to increase the performance (in terms of energy requirements and overall product recovery), decrease the overall capital investment costs and reduce negative impact on the environment (for instance, by removing the most common pollutants, carbon monoxide and carbon dioxide)?

To do so, first it is necessary to develop an integrated modelling, simulation and optimization framework for complex gas separation processes including: 1) Pressure Swing Adsorption processes (PSA); 2) Membrane processes for gas separations; 3) Hybrid PSA/Membrane processes, and apply these technologies in processes of industrial interest.

A detailed modelling of typical modern multi-bed industrial PSA units comprising several multi-layered adsorption beds operating in tandem has been presented. The modelling framework is sufficiently general to support arbitrary number of beds, all feasible bed configurations, all operating steps and all feasible inter-bed connectivities. Four different mass transfer mechanisms (local equilibrium, linear driving force, surface diffusion and particle diffusion), three thermal operating modes (isothermal, adiabatic and non-isothermal) and several approaches to model gas-solid phase equilibria (Henry's law or extended Langmuir adsorption isotherms and ideal/real adsorbed solution theory) have been implemented. Two approaches to modelling of bed interactions in a multi-bed PSA process have been developed: a) bed network super-structure approach; b) *VirtualBeds* approach. Two approaches to control the execution of a PSA process have been proposed: a) by using a set of operating procedures to govern the bed network super-structure; b) a novel, more robust approach by using a state transition network (STN) to govern the state of adsorbent columns and gas valves.

Developed modelling and optimization framework has been applied on three most common industrial separation processes and results compared to the results available in the literature. Two large-scale multi-component separation processes (oxygen production from air and hydrogen recovery from steam methane reforming off gas) have been used to illustrate the applicability and potential of the proposed approach in terms of power consumption minimization and improvement of product purity and recovery. The number of beds, PSA cycle configuration and various operating and design parameters have been systematically optimized using recent advances on process optimization. It has been shown that by employing multi-bed configurations and multi-layered adsorption columns it is possible to achieve much higher recovery for the same purity (compared to a one-bed single-layer PSA).

The state-of-the-art general Stefan-Maxwell equations coupled with Ideal/Real Adsorbed Solution Theory to predict gas-solid phase equilibrium have been employed to model mass transfer phenomena in a porous solid and porous support within a membrane. The modelling framework has been applied on several hydrocarbons separation processes and results compared to the results available in the literature, obtained from experiments or molecular dynamics simulations.

Hybrid PSA/membrane concept has been applied on the process of hydrogen production from steam methane reformer off gas, three distinct hybrid schemes have been analyzed and possibilities for process improvement discussed. The overall hydrogen recovery for given minimum requirements in product purity has been systematically maximized using the recent advances on process optimization while optimizing the number of beds, PSA cycle configuration and various PSA and membrane operating and design parameters. The optimization results have been compared to the optimization results of the PSA only case. The benefits of hybrid systems have been assessed in terms of reduction of adsorption columns size, improvements in the overall hydrogen recovery, reduction of the carbon dioxide content in the feed and waste gas streams and improvements in a calorific value of the waste gas streams (used as a fuel in the steam methane reforming process).

ACKNOWLEDGMENTS

It is often said that writing a PhD is a work of many. This is also the case with this PhD. First and foremost, I am indebted to my family and friends who always unselfishly committed themselves to my well being. Their help can never be physically repaid and without their support this thesis would never been done.

I gratefully acknowledge the supervision of Professor Eustathios Kikkinides and Professor Michalis Georgiadis who offered sound guidance, coordination of the project and countless practical advices.

The realization of this study was only possible through the cooperation with members of other teams participating in this Marie Curie Research Training Network. I thank all of them for their effort, involvement and support.

I also want to thank Dr. Apostolos Giovanoglou for our numerous brainstorming sessions and help in adapting to a new living environment.

Financial support from PRISM EC-funded RTN (Contract number MRTN-CT-2004-512233) is gratefully acknowledged.

Finally, without the music of The Skatalites, Toots & the Maytals, The Melodians, Desmond Dekker, Derrick Morgan, New York Ska-Jazz Ensemble, Flogging Molly, Locomondo, Azra, Ekaterina Velika and many other who provided moments of calm this thesis would never come to an end.

LIST OF FIGURES

Figure 2.1	Principle of PSA operation	23
Figure 2.2	Pressure changes during a single PSA cycle (two-beds, one pressure equalization)	24
Figure 2.3	Adsorbent layer	31
Figure 2.4	Adsorbent particle	35
Figure 2.5	Adsorbent column with multiple adsorbent layers	44
Figure 2.6	Multi-bed PSA flow-sheet	46
Figure 2.7	A main building block of the multi-bed PSA flowsheet	46
Figure 2.8	Sample four-bed PSA flow-sheet (generated in gPROMS)	47
Figure 2.9	Algorithm of the operating procedure generator	48
Figure 2.10	*VirtualBeds* PSA approach	49
Figure 2.11	Pressure history in a real column and *VirtualBed*	52
Figure 2.12	State transition network with all possible state transitions	53
Figure 2.13	Effects of adsorption step duration for fixed feed velocity on N_2 purity	63
Figure 2.14	Effects of adsorption step duration for fixed feed velocity on N_2 recovery	63
Figure 2.15	Effects of adsorption step duration for fixed feed velocity on power requirements per cycle	64
Figure 2.16	Effects of feed velocity for a fixed duration of adsorption step on N_2 purity	65
Figure 2.17	Effects of feed velocity for a fixed duration of adsorption step on N_2 recovery	65
Figure 2.18	Effects of adsorption step duration for a fixed amount of feed on N_2 purity	66
Figure 2.19	Effects of adsorption step duration for a fixed amount of feed on N_2 recovery	67
Figure 2.20	Effects of adsorption step duration for a fixed amount of feed on power requirements per cycle	67
Figure 2.21	Effects of blowdown step duration on N_2 purity	68
Figure 2.22	Effects of blowdown step duration on N_2 recovery	69
Figure 2.23	Effects of velocity of purge gas for fixed purge step duration on N_2 purity	70
Figure 2.24	Effects of velocity of purge gas for fixed purge step duration on N_2 recovery	70
Figure 2.25	Effects of velocity of purge gas for fixed purge step duration on power requirements per cycle	71
Figure 2.26	Effects of purge step duration for fixed purge gas velocity on N_2 purity	72
Figure 2.27	Effects of purge step duration for fixed purge gas velocity on N_2 recovery	72
Figure 2.28	Effects of purge step duration for a fixed amount of purge gas on N_2 purity	73
Figure 2.29	Effects of purge step duration for a fixed amount of purge gas on N_2 recovery	74
Figure 2.30	Effects of pressurization step duration on N_2 purity	75
Figure 2.31	Effects of pressurization step duration on N_2 recovery	75
Figure 2.32	Effects of pressurization step duration on power requirements per cycle	76
Figure 2.33	Effects of the feed to the purge gas pressure ratio on N_2 purity	77
Figure 2.34	Effects of the feed to the purge gas pressure ratio on N_2 recovery	77
Figure 2.35	Effects of the feed to the purge gas pressure ratio on power requirements per cycle	78
Figure 2.36	Effects of column geometry on N_2 purity	79
Figure 2.37	Effects of column geometry on N_2 recovery	79
Figure 2.38	Effects of feed pressure on product purity	82
Figure 2.39	Effects of feed pressure on O_2 purity/recovery	83
Figure 2.40	Effects of particle radius on O_2 purity	84
Figure 2.41	Effects of particle radius on O_2 purity/recovery	84

Figure 2.42 Effects of bed length on O_2 purity 85
Figure 2.43 Effects of bed length on O_2 purity/recovery 85
Figure 2.44 Effects of cycle time on O_2 purity 86
Figure 2.45 Effects of cycle time on O_2 purity/recovery 86
Figure 2.46 Steam-methane reformer system 87
Figure 2.47. Sequence of steps for configuration A 89
Figure 2.48 Sequence of steps for configuration B 89
Figure 2.49. Simulation results of Run I 92
Figure 2.50. Simulation results of Run II 94
Figure 2.51. Simulation results of the Set III 96
Figure 2.52. Simulation and optimization results (II layers) 103
Figure 2.53. Case study I, II: optimal recovery (purity 99.9^+ %) 111
Figure 2.54. Case study I, II: optimal feed pressure (purity 99.9^+ %) 112
Figure 2.55. Case study I, II: optimal purge/feed ratio (purity 99.9^+ %) 112
Figure 2.56. Case study I, II: optimal recovery (purity 99.99^+ %) 113
Figure 2.57. Case study I, II: optimal feed pressure (purity 99.99^+ %) 113
Figure 2.58. Case study I, II: optimal purge/feed ratio (purity 99.99^+ %) 114
Figure 2.59. Case study II: optimal carbon/zeolite ratio (purity 99.9^+ %) 115
Figure 2.60. Case study II: optimal carbon/zeolite ratio (purity 99.99^+%) 115
Figure 2.61. Case study III: optimal power and specific power (purity 99.5^+ %) 116
Figure 2.62. Case study III: optimal productivity and recovery (purity 99.5^+ %) 117
Figure 2.63. Case study III: optimal feed flowrate and purge/feed ratio (purity 99.5^+ %) 117
Figure 2.64. Case study III: optimal particle radius and L/D ratio (purity 99.5^+ %) 118
Figure 2.65. Case study III: optimal step times (purity 99.5^+ %) 118
Figure 2.66. Case study III: optimal feed pressure (purity 99.5^+ %) 119
Figure 2.67. Concentration profiles (configuration C8, two layers): a) after adsorption step, b) after 1st pressure equalization, c) after 2^{nd} pressure equalization, d) after 3^{rd} pressure equalization 122
Figure 3.1 Principle of a membrane operation 128
Figure 3.2 Ranges of membrane based separations 128
Figure 3.3 The topology of the membrane unit 130
Figure 3.4 Topology of the Permeate/Retentate compartment model 131
Figure 3.5 Topology of the membrane model 133
Figure 3.6 Topology of the support layer 138
Figure 3.7 Methane/Ethane permeation fluxes as a function of ethane composition at 303K; (above: this thesis; below: van der Graaf et al, 1999) 142
Figure 3.8 Selectivity toward ethane as a function of ethane composition at 303K; (above: this thesis; below: van der Graaf et al, 1999) 143
Figure 3.9 Methane/Ethane permeation fluxes as a function of total pressure at 303K (1:1 mixture); (above: this thesis; below: van der Graaf et al, 1999) 144
Figure 3.10 Selectivity toward ethane as a function of total pressure at 303K (1:1 mixture); (above: this thesis; below: van der Graaf et al, 1999) 145
Figure 3.11 Methane/Ethane permeation fluxes as a function of temperature (1:1 mixture, P_{tot}=1bar); (above: this thesis; below: van der Graaf et al, 1999) 146
Figure 3.12 Selectivity toward ethane as a function of temperature (1:1 mixture, P_{tot}=1bar); (above: this thesis; below: van der Graaf et al, 1999) 147
Figure 3.13 Comparison of selectivities for binary mixture permeation through a silicalite-1 membrane for ethane/methane equimolar feed mixture at 303 K as a function of the total feed pressure, permeate pressure 20 kPa; (above: this thesis; below: Kapteijn et al, 2000) 149
Figure 3.14 Comparison of selectivities for binary mixture permeation through a silicalite-1 membrane for propane/methane mixture at 303 K and 100 kPa

	total feed pressure as a function of the propane pressure, permeate pressure 10 kPa; (above: this thesis; below: Kapteijn et al, 2000)	150
Figure 3.15	Comparison of IAS and CBMC mixture loadings for Methane-Ethane mixture at T=303K in silicalite and P_{total}=100kPa; (above: this thesis; below: Krishna and Paschek, 2000)	153
Figure 3.16	Comparison of IAS and CBMC mixture loadings for Methane-Propane mixture at T=303K in silicalite and P_{total}=100kPa; (above: this thesis; below: Krishna and Paschek, 2000)	154
Figure 3.17	Comparison of IAS and CBMC mixture loadings for Ethane-Propane mixture at T=303K in silicalite and P_{total}=100kPa; (above: this thesis; below: Krishna and Paschek, 2000)	155
Figure 3.18	Comparison of IAS, RAS and CBMC mixture loadings for n-Butane/iso-Butane at 303K in silicalite; (above: this thesis; below: Krishna and Paschek, 2000)	156
Figure 4.1	Sample hybrid PSA-Membrane configuration	159
Figure 4.2	PSA inlet /outlet streams	163
Figure 4.3	Hybrid Case 1: Mem-PSA	164
Figure 4.4	Hybrid Case 2: PSA-Mem	165
Figure 4.5	Hybrid Case 3: Mem-PSA-Mem	166
Figure 4.6	Comparison of the recovery: PSA-Only vs. Mem-PSA (X_{CO2}=3%)	175
Figure 4.7	Comparison of the recovery: PSA-Only vs. Mem-PSA (X_{CO2}=4%)	176
Figure 4.8	Comparison of the recovery: PSA-Only vs. Mem-PSA (X_{CO2}=5%)	176
Figure 4.9	Comparison of the recovery: PSA-Only vs. Mem-PSA (X_{CO2}=6%)	177
Figure 4.10	Comparison of the overall recovery (Mem-PSA case)	177
Figure 4.11	Comparison of the recovery: Membrane vs. PSA vs. Overall (Mem-PSA case, X_{CO2}=3%)	178
Figure 4.12	Comparison of the recovery: Membrane vs. PSA vs. Overall (Mem-PSA case, X_{CO2}=4%)	178
Figure 4.13	Comparison of the recovery: Membrane vs. PSA vs. Overall (Mem-PSA case, X_{CO2}=5%)	179
Figure 4.14	Comparison of the recovery: Membrane vs. PSA vs. Overall (Mem-PSA case, X_{CO2}=6%)	179
Figure 4.15	Comparison of the recovery: Membrane vs. PSA vs. Overall (Mem-PSA case, configuration C4)	180
Figure 4.16	Comparison of the recovery: Membrane vs. PSA vs. Overall (Mem-PSA case, configuration C5b)	180
Figure 4.17	Comparison of the recovery: Membrane vs. PSA vs. Overall (Mem-PSA case, configuration C8)	181
Figure 4.18	Comparison of L/D ratio: Mem-PSA vs. PSA-Only (X_{CO2}=3%)	181
Figure 4.19	Comparison of L/D ratio: Mem-PSA vs. PSA-Only (X_{CO2}=4%)	182
Figure 4.20	Comparison of L/D ratio: Mem-PSA vs. PSA-Only (X_{CO2}=5%)	182
Figure 4.21	Comparison of L/D ratio: Mem-PSA vs. PSA-Only (X_{CO2}=6%)	183
Figure 4.22	Comparison of L/D ratio (Mem-PSA case)	183
Figure 4.23	Difference between L/D of PSA-Only and Mem-PSA case (given in %)	184
Figure 4.24	Comparison of AC/Z ratio: Mem-PSA vs. PSA-Only (X_{CO2}=3%)	184
Figure 4.25	Comparison of AC/Z ratio: Mem-PSA vs. PSA-Only (X_{CO2}=4%)	185
Figure 4.26	Comparison of AC/Z ratio: Mem-PSA vs. PSA-Only (X_{CO2}=5%)	185
Figure 4.27	Comparison of AC/Z ratio: Mem-PSA vs. PSA-Only (X_{CO2}=6%)	186
Figure 4.28	Comparison of AC/Z ratio (Mem-PSA case)	186
Figure 4.29	Comparison of P_{feed}: Mem-PSA vs. PSA-Only (X_{CO2}=3%)	187
Figure 4.30	Comparison of P_{feed}: Mem-PSA vs. PSA-Only (X_{CO2}=4%)	187
Figure 4.31	Comparison of P_{feed}: Mem-PSA vs. PSA-Only (X_{CO2}=5%)	188
Figure 4.32	Comparison of P_{feed}: Mem-PSA vs. PSA-Only (X_{CO2}=6%)	188

Figure 4.33 Comparison of P_{feed} (Mem-PSA case) 189
Figure 4.34 Comparison of Purge/feed ratio: Mem-PSA vs. PSA-Only (X_{CO2}=3%) 189
Figure 4.35 Comparison of Purge/feed ratio: Mem-PSA vs. PSA-Only (X_{CO2}=4%) 190
Figure 4.36 Comparison of Purge/feed ratio: Mem-PSA vs. PSA-Only (X_{CO2}=5%) 190
Figure 4.37 Comparison of Purge/feed ratio: Mem-PSA vs. PSA-Only (X_{CO2}=6%) 191
Figure 4.38 Comparison of Purge/feed ratio (Mem-PSA case) 191
Figure 4.39 Comparison of the membrane recovery (Mem-PSA case) 192
Figure 4.40 Comparison of the membrane area (Mem-PSA case) 192
Figure 4.41 Comparison of the membrane thickness (Mem-PSA case) 193
Figure 4.42 Comparison of the membrane support thickness (Mem-PSA case) 193
Figure 4.43 Comparison of the membrane retentate flowrates (Mem-PSA case) 194
Figure 4.44 Comparison of the membrane permeate flowrates (Mem-PSA case) 194
Figure 4.45 Comparison of the membrane H_2 and CH_4 purity (Mem-PSA-Mem case) 198
Figure 4.46 Comparison of the membrane area (Mem-PSA-Mem case) 199
Figure 4.47 Comparison of the membrane thickness (Mem-PSA-Mem case) 199
Figure 4.48 Support thickness (Mem-PSA-Mem case) 200

LIST OF TABLES

Table 2.1	Overview of typical PSA industrial processes	22
Table 2.2.	Overview of single-bed PSA studies	26
Table 2.3.	Overview of two-bed PSA studies	27
Table 2.4.	Overview of multi-bed PSA studies	28
Table 2.5	*VirtualBed* lookup table	50
Table 2.6	Geometrical and transport characteristics	57
Table 2.7	Base case parameters	57
Table 2.8	Input parameters for the simulation [(a)]	58
Table 2.9	Input parameters for the simulation [(b)]	59
Table 2.10	Comparison of the experimental and simulation results	60
Table 2.11	Absolute deviations from the experimental data	61
Table 2.12	Overall average absolute deviations from the experimental data	62
Table 2.13	Absolute deviations from the experimental data	62
Table 2.14	Absolute deviations from the experimental data	64
Table 2.15	Absolute deviations from the experimental data	66
Table 2.16	Absolute deviations from the experimental data	68
Table 2.17	Absolute deviations from the experimental data	69
Table 2.18	Absolute deviations from the experimental data	71
Table 2.19	Absolute deviations from the experimental data	73
Table 2.20	Absolute deviations from the experimental data	74
Table 2.21	Absolute deviations from the experimental data	76
Table 2.22	Absolute deviations from the experimental data	78
Table 2.23	Parameters for rPSA simulation	80
Table 2.24	Comparison of simulation results	81
Table 2.25	Phase equilibrium data for activated carbon	87
Table 2.26	Geometrical and transport characteristics of PSA process	88
Table 2.27	One-bed four-step PSA configuration	90
Table 2.28	Four-bed six-step PSA configuration	90
Table 2.29	Eight-bed eight-step PSA configuration	90
Table 2.30	Twelve-bed ten-step PSA configuration	90
Table 2.31.	Input parameters for Run I	92
Table 2.32.	Simulation results of Run I	92
Table 2.33.	Runtime parameters for Run II	93
Table 2.34.	Simulation results of Run II	94
Table 2.35.	Runtime parameters for Set III	95
Table 2.36.	Simulation results for Set III	95
Table 2.37.	PSA configuration C1	98
Table 2.38.	PSA configuration C2	98
Table 2.39.	PSA configuration C4	99
Table 2.40.	PSA configuration C5a	99
Table 2.41.	PSA configuration C5b	99
Table 2.42.	PSA configuration C8	99
Table 2.43.	Typical sensitivity ratios (Case studies I and II)	104
Table 2.44.	Typical sensitivity ratios (Case study III)	107
Table 2.45.	Various design, operating and transport characteristics (Case studies I and II)	108
Table 2.46.	Various design, operating and transport characteristics (Case study III)	109
Table 2.47.	Langmuir parameters and heat of adsorption for activated carbon	109
Table 2.48.	Langmuir parameters and heat of adsorption for zeolite 5A	109
Table 2.49.	LRC parameters and heat of adsorption for zeolite 5A	110

Table 2.50.	Runtime parameters (Case studies I and II)	110
Table 2.51.	Runtime parameters (Case study III)	110
Table 2.52.	Optimization durations	110
Table 2.53.	The feed and the final pressure after the last pressure equalization (Case studies I and II)	120
Table 2.54.	Average waste gas composition after blowdown step (Case studies I and II)	120
Table 2.55.	Average waste gas composition after purge step (Case studies I and II)	120
Table 2.56.	Comparison of the results	123
Table 3.1	Membrane parameters	140
Table 3.2	Diffusion parameters	140
Table 3.3	Adsorption parameters	141
Table 3.4	Pure component parameters for dual-site Langmuir model	152
Table 3.5	Wilson non-ideality parameters for mixture isotherms	152
Table 4.1	Feed characteristics	167
Table 4.2	Diffusion coefficients and activation energies for diffusion	167
Table 4.3	Langmuir parameters for Silicalite-1	167
Table 4.4	Base case parameters (membrane)	168
Table 4.5	PSA runtime parameters (all case studies)	168
Table 4.6.	Computational statistics	172
Table 4.7	PSA averaged waste gas compositions (PSA-Only case)	195
Table 4.8	Membrane retentate/permeate compositions (Mem-PSA case, 3%)	195
Table 4.9	PSA averaged waste gas compositions (Mem-PSA case, 3%)	195
Table 4.10	Difference in waste gas H_2 and CO_2 compositions: PSA-Only vs Mem-PSA (3%)	196
Table 4.11	Waste gas flowrates: PSA-Only vs Mem-PSA (3%)	196
Table 4.12	Membrane cut (Mem-PSA case)	196
Table 4.13	Membrane optimization results (PSA-Mem case)	197
Table 4.14	Membrane retentate/permeate compositions (PSA-Mem case)	197
Table 4.15	Optimization results (Mem-PSA-Mem case, 3%)	200
Table 4.16	Membrane compositions (Mem-PSA-Mem case, 3%)	201

TABLE OF CONTENTS

Abstract 1

Acknowledgments 4

List of figures 6

List of tables 10

1. INTRODUCTION 17

1.1. Problem definition 17

1.2. Challenges 18

1.3. Thesis structure 18

2. PRESSURE SWING ADSORPTION 21

2.1. Introduction 21

2.2. Principles of operation 23

2.3. Literature review 25

2.3.1. Overview of multi-bed PSA studies 25

2.3.2. Overview of optimization PSA studies 29

2.4. Mathematical modelling 31

2.4.1. Adsorption layer model 31

2.4.1.1. General balance equations 31

2.4.1.2. Mass balance 32

2.4.1.3. Heat balance 32

2.4.1.4. Momentum balance 33

2.4.1.5. Equation of state 34

2.4.1.6. Thermo-physical properties 34

2.4.1.7. Axial dispersion 34

2.4.1.8. Transport properties 35

2.4.2. Adsorbent particle model 35

2.4.2.1. General equations for mass and heat balance 35

2.4.2.2. Local equilibrium (LEQ) 37

2.4.2.3. Linear driving force (LDF) 37

2.4.2.4. Surface diffusion (SD) 38

2.4.2.5. Pore diffusion (PD) 39

2.4.2.6. Gas-solid phase equilibria 41

2.4.3. Adsorption column model 43

2.4.4. Multi-bed PSA model 45

2.4.4.1. Bed network super-structure approach 45

2.4.4.2. VirtualBeds approach 48

2.4.5. Gas valve model 54

2.5. Single-bed PSA simulation case studies 55

2.5.1. Diffusion controlled separation 55
2.5.1.1. Effects of adsorption step duration for fixed feed velocity 62
2.5.1.2. Effects of feed velocity for a fixed duration of adsorption step 64
2.5.1.3. Effects of adsorption step duration for a fixed amount of feed 66
2.5.1.4. Effects of blowdown step duration 68
2.5.1.5. Effects of velocity of purge gas for fixed purge step duration 69
2.5.1.6. Effects of purge step duration for fixed purge gas velocity 71
2.5.1.7. Effects of purge step duration for a fixed amount of purge gas 73
2.5.1.8. Effects of pressurization step duration 74
2.5.1.9. Effects of the feed to the purge gas pressure ratio 76
2.5.1.10. Effects of column geometry 78
2.5.2. Equilibrium controlled separation 80
2.5.2.1. Effects of feed pressure 82
2.5.2.2. Effects of particle radius 83
2.5.2.3. Effects of bed length 84
2.5.2.4. Effects of cycle time 86
2.6. Multi-bed PSA case studies 87
2.6.1. Simulation Run I 91
2.6.2. Simulation Run II 93
2.6.3. Simulation Run III 94
2.7. Multi-bed PSA optimization case studies 97
2.7.1. Optimization problems 97
2.7.2. Parametric analysis 100
2.7.2.1. Effect of particle size 100
2.7.2.2. Effect of column length/diameter ratio 100
2.7.2.3. Effect of feed and purge gas pressures 101
2.7.2.4. Effect of feed flowrate 101
2.7.2.5. Effect of purge flowrate (purge/feed ratio) 101
2.7.2.6. Effect of cycle/step times 101
2.7.2.7. Effect of carbon/zeolite ratio (AC/Z ratio) 102
2.7.2.8. Effect of number of beds and cycle design 103
2.7.3. Formulation of the optimization problem 103
2.7.3.1. Case study I: Hydrogen recovery from SMROG (single layer) 104
2.7.3.2. Case study II: Hydrogen recovery from SMROG (double layer) 105
2.7.3.3. Case study III: Oxygen production from air 106
2.7.4. Optimization results 107
2.7.4.1. Case study I: Hydrogen recovery from SMROG (single layer) 111
2.7.4.2. Case study II: Hydrogen recovery from SMROG (double layer) 114
2.7.4.3. Case study III: Oxygen production from air 116

2.7.5. Discussion 119
2.7.5.1. Case studies I and II 119
2.7.5.2. Case study III 123
3. MEMBRANES 125
3.1. Introduction 125
3.2. Principles of operation 127
3.3. Literature review 129
3.4. Mathematical modelling 130
3.4.1. Permeate/Retentate compartments 131
3.4.2. Porous membrane 133
3.4.3. Support layer 138
3.5. Simulation case studies 140
3.5.1. Separation of hydrocarbons: GMS – EL 140
3.5.2. Separation of hydrocarbons: GMS – IAS vs. GMS – EL 148
3.5.3. Separation of hydrocarbons: GMS – IAS vs. GMS – RAS vs. GMS – CBMC 151
4. HYBRID PSA/MEMBRANE 157
4.1. Introduction 157
4.2. Principles of operation 158
4.3. Literature review 158
4.4. Mathematical modelling 161
4.5. Analysis 161
4.5.1. Membrane attached to feed stream (Mem-PSA) 164
4.5.2. Membrane attached to waste gases stream (PSA-Mem) 165
4.5.3. Membranes attached to both feed and waste gases streams (Mem-PSA-Mem) 166
4.6. Optimization case studies 167
4.6.1. Formulation of the optimization problem 168
4.6.1.1. Case 1: PSA-Only 169
4.6.1.2. Case 2: Mem-PSA 169
4.6.1.3. Case 3: PSA-Mem 171
4.6.1.4. Case 4: Mem-PSA-Mem 171
4.6.2. Optimization results and discussion 172
4.6.2.1. Case 1 and 2: PSA-Only and Mem-PSA 172
4.6.2.2. Case 3: PSA-Mem 197
4.6.2.3. Case 4: Mem-PSA-Mem 198
5. CONCLUSIONS AND FUTURE WORK 203
5.1. Recommendations for Future Directions 205
6. NOMENCLATURE 209
7. LIST OF REFERENCES 213

Chapter 1

Introduction

1.1. Problem definition

Adsorption and membrane systems have become highly important gas separation technologies in chemical manufacturing, petroleum and natural gas refining and new clean energy concepts. Importance of these technologies can be depicted from the fact that over 41 million tons/year of hydrogen and 100 million tons/year of oxygen is produced worldwide (Ritter and Ebner, 2007).

Pressure swing adsorption (PSA) has attracted increasing interest because of its low energy requirements as well as low capital investment costs in comparison to the traditional separation processes (such as cryogenic processes). PSA is able to produce high purity gases at high recovery; however, capital costs and energy requirements of PSA systems are still considerably high because modern industrial PSA units typically utilize layered beds containing up to four adsorbents and, depending on the production volume, anywhere between four and sixteen columns.

At the current level, membrane systems offer low energy consumption, dramatically lower investment costs, and ease of operation. However, they are not able to produce high purity gases yet (due to a limited selectivity). Therefore, why not combine these two worlds: reliable PSA technology able to produce high purity gases with the low cost membrane systems to bust the performance (in terms of energy requirements and overall product recovery), decrease the overall capital costs and reduce negative impact on the environment (for instance, by removing the most common pollutants, carbon monoxide and carbon dioxide)?

To do so it was necessary to develop an integrated modelling, simulation and optimization framework for complex gas separation processes including: pressure wing

adsorption processes, membrane processes for gas separations, and hybrid PSA/Membrane processes, apply these technologies in processes of industrial interest, and qualitatively and quantitatively describe their performance, detect problems/bottlenecks and prescribe a solution (or a set of solutions) to them.

1.2. Challenges

Exploring the capabilities of the hybrid technology is not an easy task. Both processes are quite complex and involve mathematical modelling at different scales. For instance, the mathematical model of an adsorption column should include equations for mass, heat and momentum transfer and gas/solid phase equilibrium at bulk flow level and particle level (coupled at the particle surface). Moreover, several adsorption columns typically operate in tandems with very complex, time-dependant column inter-connections making the problem more difficult. Thus, even a simple mathematical model of the adsorption column requires a huge number of partial differential and algebraic equations to be solved simultaneously. In addition, dynamic nature of PSA processes operating in a cyclic steady state (CSS) and complex columns' interconnections make the system highly difficult for a man to control it. Finally, the computational requirements and amount of memory needed for the problem solution are so high that the problem could not have been solved until the recent advances in the computer science field. To the authors best knowledge the computer program that, based on a rigorous multi-bed multi-layer PSA model, is capable of calculating the optimal PSA step sequence and optimal values of all design and operating parameters at the same time does not exist. Membrane separation processes are somewhat simpler due to a steady-state nature. However, similar problems arise regarding the model complexity. In this thesis, the abovementioned problems have been analyzed and the solutions proposed.

1.3. Thesis structure

The abovementioned challenges have been addressed in the following four chapters:

Chapter 2

In this chapter, the detailed models of typical modern multi-bed industrial PSA units consisting of several multi-layered adsorption columns operating in tandem have been presented. The coupled set of mixed algebraic and partial differential equations for mass, heat and momentum balance at bulk gas and particle level, gas-solid phase equilibrium equations and complex boundary conditions represent the core of the modelling framework. The modelling framework is sufficiently general to support arbitrary number of beds, all feasible bed configurations, all operating steps and all feasible inter-bed connectivities. Four different mass transfer mechanisms (local equilibrium, linear driving force, surface diffusion and particle diffusion), three thermal operating modes (isothermal, adiabatic and non-isothermal) and several approaches to model gas-solid phase equilibrium (Henry's law or extended Langmuir adsorption isotherms and ideal/real adsorbed solution theory) have been implemented. Two different approaches to modelling of multi-bed PSA have been proposed: a) bed network super-structure approach (the most complete one, where all columns are simulated), suitable for a rigorous study of bed interactions during a

cycle, and b) *VirtualBeds approach* (a modified *Unibed* approach employed to reduce the size of the DAE system and speed up process simulation), suitable for process optimization. Two approaches to control the execution of a PSA process have been proposed: a) by using a set of operating procedures to govern the bed network super-structure; b) a novel, more robust approach by using a state transition network (STN) to govern the state of adsorbent columns and gas valves. The first approach employs the auxiliary program for automatic generation of operating procedures, which generates operating procedures for the whole network of beds according to the given number of beds and sequence of operating steps in one bed. The second relies on a state transition network representation, implemented as a deterministic Finite State Machine (FSM) where the next possible state is uniquely determined for a given state and input values.

The developed modelling framework has been applied on two typical industrial gas separation processes (oxygen and nitrogen production from air) and results compared to the experimental and simulation results available in the literature. A medium scale hydrogen recovery from steam methane reforming off gas (SMROG) process has been used to investigate the effects of number of beds on the separation quality and to analyse trade-offs between capital and operating costs and separation quality.

Finally, an optimization framework has been built on top of the STN approach and the case dependant optimization strategies have been proposed. Two large-scale multicomponent separation processes (oxygen production from air and hydrogen recovery from steam methane reforming off gas) have been used to illustrate the applicability and potential of the proposed approach in terms of power consumption minimization and improvement of product purity and recovery. The number of beds, PSA cycle configuration and various operating and design parameters have been systematically optimized using recent advances in process optimization.

Chapter 3

In this chapter, the detailed modelling of porous membranes for gas separations has been presented. The state-of-the-art general Stefan-Maxwell equations coupled with Ideal or Real gas Adsorbed Solution Theory to predict gas-solid phase equilibrium have been implemented to model mass transfer phenomena in porous solid and porous support. The modelling framework has been applied on several hydrocarbons separation processes and results compared to the results available in the literature, obtained from experiments or molecular dynamics simulations.

Chapter 4

In the last part, hybrid PSA/membrane concept has been applied on the process of hydrogen production from steam methane reforming off gas mixture, various hybrid schemes have been analyzed and possibilities for process improvement discussed. Three distinct hybrid schemes have been selected and optimized: membrane attached to feed stream (Mem-PSA), membrane attached to waste gas streams (PSA-Mem), and membranes attached to both feed and waste gases streams (Mem-PSA-Mem). The overall hydrogen recovery for given minimum requirements in product purity has been systematically maximized using the recent advances on process optimization while optimizing the number of beds, PSA cycle configuration and various PSA and membrane operating and design

parameters. The optimization results have been compared to the optimization results of the PSA only case. The benefits of hybrid systems have been assessed in terms of reduction of adsorption columns size, improvements in the overall hydrogen recovery, reduction of the carbon dioxide content in the feed and waste gas streams and improvements in a calorific value of the waste gas streams (used as a fuel in the steam methane reforming process).

Chapter 5

This chapter summarizes the research and explores future directions for development of hybrid gas separation processes.

Chapter 2

Pressure Swing Adsorption

2.1. Introduction

Pressure swing adsorption (PSA) is a gas separation process, which has attracted increasing interest because of its low energy requirements as well as low capital investment costs in comparison to the traditional separation processes (Ruthven, 1984, Yang, 1987). The major industrial applications of PSA include small to intermediate scale oxygen and nitrogen production from air, small to large-scale gas drying, hydrogen recovery from different petrochemical processes (steam-methane reforming off gas or coke oven gas), and trace impurity removal from contaminated gases.

Adsorption has become the state of the art technology for the following applications (Sircar, 2006):

- Small to very large scale production of H_2 from various source gases
- Small to intermediate scale production of O_2 and N_2 enriched air from ambient air
- Small to large scale gas drying
- Trace impurity removal from contaminated gases

Other typical industrial processes are summarized in Table 2.1.

Table 2.1 Overview of typical PSA industrial processes

Process	Components
Air fractionation (production of O_2 and N_2 enriched air)	H_2O, CO_2, N_2, O_2, Ar
Production of 90-93% O_2 from air for home medical use	H_2O, CO_2, N_2, O_2, Ar
Production of H_2 and CO_2 from steam-methane reformer (SMR) off-gas	H_2O, CO_2, CO, CH_4, H_2, N_2
Production of CO from SMR off-gas	H_2O, H_2, C_1-C_5 alkanes and alkenes
Production of H_2 from refinery off-gas (ROG)	H_2O, chlorofluorohydrocarbons, alcohols, ketones, BTX, N_2 (air)
Production of CH_4 and CO_2 from landfill gas	CO_2, CH_4, trace chlorofluorohydrocarbons, H_2O
Gas drying	H_2O, N_2, CH_4, CO_2, alcohols
Air brake drying	H_2O, CO_2, N_2, O_2, Ar
Separation of normal paraffins from isoparaffins and cyclic hydrocarbons	*n*-C_8H_{18}, *i*-C_8H_{18}, cyclohexane

Hydrogen production

The growing requirements for hydrogen in chemical manufacturing, petroleum refining, and the newly emerging clean energy concepts will place greater demands on sourcing, production capacity and supplies of hydrogen. Currently, about 41 million tons/year of hydrogen is produced worldwide (Ritter and Ebner, 2007), with 80% of it being produced from natural gas by steam reforming, partial oxidation and autothermal reforming. Hydrogen is used commercially to produce CO, syngas, ammonia, methanol, and higher alcohols, urea and hydrochloric acid (Ritter and Ebner, 2007). It is also used in Fischer Tropsch reactions, as a reducing agent (metallurgy), and to upgrade petroleum products and oils (hydrogenation).

Oxygen/nitrogen production from air

Over 100 million tons/year of oxygen is produced worldwide (Ritter and Ebner, 2007). The largest amount produced by non-cryogenic technology is the production of medium purity nitrogen (95 to 99.5%) and oxygen (up to 95%). Typically, various types of zeolites (molecular sieves) are employed. Sometime, a desorption step is performed at pressures below the atmospheric pressures and this process is referred to as Vacum Swing Adsorption (VSA).

2.2. Principles of operation

In PSA processes, the less strongly (or less rapidly) adsorbed species passes throughout the adsorbent bed and are recovered as the raffinate product. The extracted product consists of adsorbed species removed during a desorption step. The selectivity in a PSA process comes from differences in either adsorption equilibrium (equilibrium-controlled) or adsorption rate (kinetic-controlled) between the components to be separated. Although the overall performance of PSA depends on both equilibrium and kinetics, the relative importance varies for different applications. A vast majority of industrial PSA systems are equilibrium-based separations.

All adsorption separation processes must involve two basic steps: *adsorption* during which the more adsorbable components adsorb and *regeneration* during which these components are removed from the adsorbent. The essential feature of PSA process is that regeneration is achieved by reducing the total pressure, rather than increasing temperature or purging with displacing agent. The process operates under (near) isothermal conditions. Therefore, a useful capacity is given by the difference in loadings between two points (1 and 2) on the *same isotherm* as given in Figure 2.1.

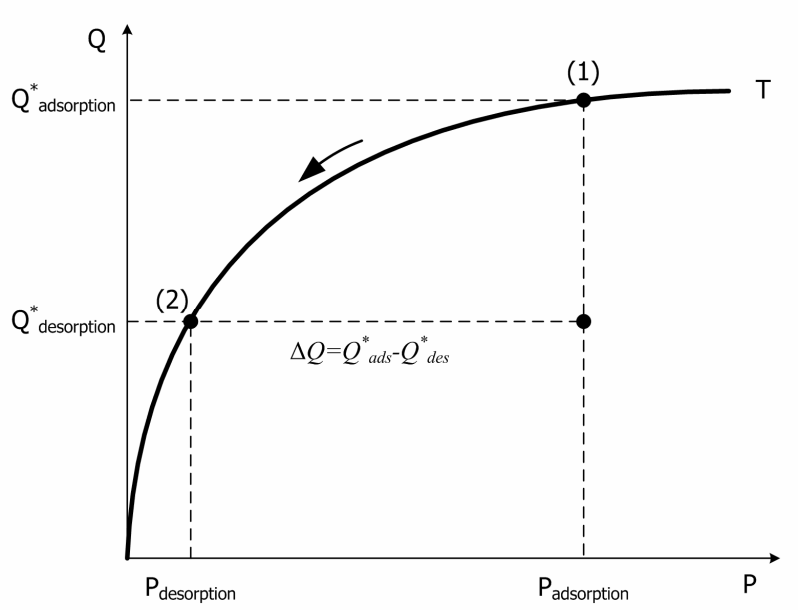

Figure 2.1 Principle of PSA operation

A major advantage of PSA is that the pressure can be changed more rapidly than temperature, making possible to operate PSA process on a much faster cycle, thereby increasing the throughout per unit of adsorbent per unit of time. However if the more adsorbable component is too strongly adsorbed a very high vacuum is required for regeneration and PSA process becomes uneconomical. In that case, thermal swing adsorption (TSA) is preferred option.

The essential feature of PSA process is that it operates under transient conditions, whereas most other separation process such as absorption, extraction or distillation operate

under steady-state conditions. As a consequence, PSA process has to be described by a coupled set of partial differential equations, usually solved numerically.

From an operational point of view PSA is an intrinsic dynamic process operating in a cyclic manner with each bed undergoing the same sequence of steps. The typical operating steps include pressurization with feed or pure product, high-pressure adsorption, pressure equalization(s), blowdown, and purge. An introduction of pressure equalization steps led to significant improvements in the PSA efficiency. Pressure equalization steps allow large savings in mechanical energy necessary to pressurize beds making the PSA process economically feasible. A typical pressure change during a single PSA cycle is illustrated in Figure 2.2. The PSA cycle sequence includes the following operating steps: pressure equalization (repressurization from the other columns), counter-current pressurization, adsorption, pressure equalization (depressurization to the other columns), counter-current blowdown and counter-current purge.

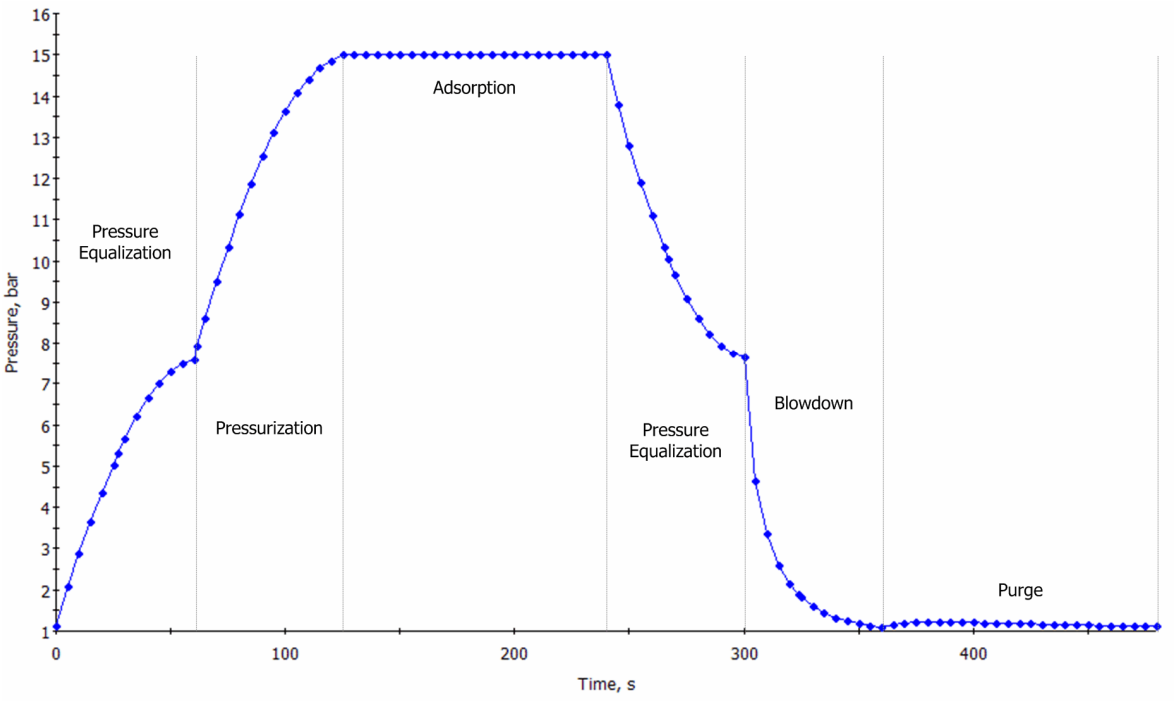

Figure 2.2 Pressure changes during a single PSA cycle (two-beds, one pressure equalization)

The major breakthrough in PSA technology came in the early 1970's with the development of a 4-bed, multi-layer PSA process. Since that time modifications have added additional beds, typically 7 to 10 beds (up to 16), and sometimes tanks for storing intermediate process streams between cycle stages. Along with more beds and tanks came more complex cycle sequencing to achieve higher throughputs with the same or even less volume of adsorbent distributed in the additional beds.

2.3. Literature review

Over the last three decades, numerous PSA studies have appeared in the literature. In this thesis an overview of PSA studies is split into four groups: single-bed PSA, two-beds PSA, multi-bed PSA and optimization PSA studies, covering all areas of interest: modelling of a single adsorption column as a building block of the multi-bed PSA, modelling of adsorbent bed interactions in multi-bed PSA configurations and finally optimization studies. Special focus is put on a critical review of multi-bed and PSA optimization studies.

The summary of single-bed PSA studies is given in Table 2.2. The key literature contributions involving two- and multi-bed configurations under certain assumptions are summarized in Table 2.3 and Table 2.4. Good overviews can be also found in Ruthven (1984) and Yang (1987).

2.3.1. Overview of multi-bed PSA studies

One of the earliest attempts to realistically describe bed interactions is presented by Chou and Huang (1994a) and is based on incorporating a gas valve equation into a PSA model to control a flowrate. The authors gave comparison between three available approaches: frozen solid (pressure changes instantly so there is no change in solid phase), linear pressure change and gas valve equation (pressures and flowrates change according to the gas valve equation). This approach gave much better prediction of pressure history and phenomena occurring during pressure changing steps compared to use of the linear pressure change. The results obtained are in good agreement with experimental data. The proposed approach was followed to study the dynamic behaviour of two and four bed PSA processes in a subsequent work (1994b).

Warmuzinski and Tanczyk (1997) developed a generic multi-bed PSA model. The main features of their approach include support for multicomponent mixtures, LDF approximation, one or two adsorbent layers and linear pressure changes. The model was used to study the separation of coke oven gas in a five-bed eight-step PSA process. In a subsequent publication in 1998, the same authors presented an experimental verification of the model using a case study concerning hydrogen recovery from a $H_2/N_2/CH_4/CO$ mixture. Two different configurations have been used: four-bed seven-step and two-bed five-step PSA configuration. In both cases, the satisfactory agreement between theoretical predictions and experimental data was achieved.

Lee and co-workers (1998) developed a mathematical model for the separation of hydrogen from coke oven gas ($H_2/CH_4/N_2/CO/CO_2$) using two adsorbent layers (activated carbon and zeolite 5A). The model employs Linear Driving Force theory, heat balance for both bulk gas and solid phase, Ergun equation for pressure drop and Langmuir/Freundlich isotherm. They carried out breakthrough experiments in the layered bed and investigated adsorption dynamics. In 1999, they used the same model to analyze effects of carbon-to-zeolite ratio on separation quality. System considered was separation of hydrogen from coke oven gas in a two-bed seven-step PSA configuration. Simulation results agreed well with the experimental ones.

Table 2.2. Overview of single-bed PSA studies

Ref	Mass balance	Heat balance	Moment. balance	Isotherm, adsorbent	No. beds	No. steps	Bed interactions	No. layers	Application
Warmuzinski and Tanczyk, 1997	LDF	-	-	Linear, CMS	1	4	-	1	Air separation
Park et al, 1998	PD	-	-	Langmuir, alumina	1	4	-	1	Air separation
Park et al, 2000	LEQ, SD, PD	Bulk gas	-	IAS/LRC, AC	1	5	-	1	H_2, CO_2, CH_4
Sircar and Golden, 2000	BDPD	Bulk gas	-	Langmuire, 5A	1	5	-	1	H_2, CH_4
Jiang et al, 2003	PD	-	-	Linear, MS RS-10	1	4	-	1	Air separation, theoretical study
Jiang et al, 2005	PD	-	-	Linear, MS RS-10	1	4	-	1	Air separation, experimental study
Cruz et al, 2003	4 different LDF	Bulk gas	Ergun	Linear, 13X	1	-	-	1	Air separation
Raghavan et al, 1986	LDF	Bulk gas, solids	-	Langmuir/Freundlich, 5A	1	5	-	1	H_2, CO H_2, CO_2
Doong and Yang, 1987	DGM	Bulk gas	-	Langmuir, 5A	1	-	Linear	1	Air separation
Raghavan et al, 1987	LDF	Bulk gas	Ergun	Langmuir, AC+5A	1	-	-	2	H_2, CO_2, CH_4, CO
Farooq and Ruthven, 1989	LDF	Bulk gas	Ergun	Langmuir, AC+5A	1	-	-	2	H_2, CO_2, CH_4, CO
Lu and Rodrigues, 1994	DG, LDF - DG, LDF-DGSD, LDF-DGSD	-	-	Langmuir, 4A, 5A, CMS	1	4	-	1	Air separation
Le Van, 1995	LDF	Bulk gas	Darcy	Langmuir, 13X	1	4	-	1	CO_2 sequestr.
Chabani and Tondeur, 2000	LDF	Bulk gas	-	Langmuir, AC	1	4	-	1	H_2, CH_4
Mendes and Costa, 2001	LDF	Bulk gas	Ergun	Dual-site Langmuir, 13X	1	4	Valve eq.	1	CO_2 capture
Ko et al, 2003	Bi-LDF	Bulk gas, solid	Ergun	Langmuir, 4A	1	5	-	1	Propane, propylene

Table 2.3. Overview of two-bed PSA studies

Ref	Mass balance	Heat balance	Moment. balance	Isotherm, adsorbent	No. beds	No. steps	Bed interactions	No. layers	Application
Barg et al, 2000	LDF, PD	Bulk gas	-	LRC, AC	2	4	Only one bed is simulated	1	H_2, CH_4
Jiang et al, 2003	LDF	-	-	Linear, CMS	2	6	Frozen ads.	1	Air separation
Wakao et al, 1979	LDF	-	-	Langmuir, CMS/5A	2	4	Valve eq.	1	Air separation
Hassan et al, 1987	LDF, PD	-	Darcy	Linear-Langmuir, 5A	1, 2	2, 6	Valve eq.	1	Air separation
Kapoor and Yang, 1989	LDF	Bulk gas	Ergun	Langmuir/Freundlich, AC+5A	2	7	-	2	H_2, CH_4, CO, N_2, CO_2
Hartzog and Sircar, 1994	LDF	Bulk gas	Ergun	Dual-site Langmuir, 13X	1, 2	3, 6	Valve eq.	Inert + ads.	Air separation
Yang et al, 1995	LDF, DG	Bulk gas	Darcy	Langmuir	2	4	-	1	Air separation
Botte et al, 1998	LDF	Bulk gas	Ergun	LRC, AC+5A	2	6	-	1	Air separation

Cho and co-workers (1998) developed a mathematical model for the separation of hydrogen from steam methane reformer off gas. They investigated the effects of carbon-to-zeolite ratio on adsorber dynamics. In a subsequent study (2000) they investigated the purification of hydrogen from cracked gas mixture (H_2/CH_4/CO/CO_2) using a double-layer four-bed eight-step PSA configuration. Operation of only one bed has been simulated and pressure during pressure equalization steps has been estimated using simple equations. Influences of feed flowrate, duration of adsorption step and carbon-to-zeolite ratio on process performance have been investigated.

Secchi and co-workers (2000) studied the modelling and optimization of an industrial six-beds twelve-steps PSA unit for hydrogen purification. The model employed LDF approximation, nonisothermal operating, neglected pressure drop, Langmuir isotherm, three adsorbent layers and linear pressure change during pressure changing steps. The effects of step durations on process performance were systematically analyzed.

Sircar and Golden (2000) presented an overview of industrial PSA processes for hydrogen production, simultaneous production of hydrogen and carbon dioxide, and for production of ammonia synthesis gas. The selection of adsorbents for hydrogen purification was also investigated. Configurations of four, nine (two series of adsorbents: six + three) and ten beds have been analyzed in detail. The same authors (2000) carried out a parametric study of multi-bed PSA systems for the separation of hydrogen from a H_2/CH_4 mixture. Three different PSA configurations were analyzed: four-bed seven-step

(one pressure equalization), four bed nine-step (two pressure equalizations), and five-bed twelve-step. Effects of various process variables on the separation quality were evaluated.

Table 2.4. Overview of multi-bed PSA studies

Ref	Mass balance	Heat balance	Moment. balance	Isotherm, adsorbent	No. beds	No. steps	Bed interactions	No. layers	Application
Raghavan and Ruthven, 1985	LEQ	-	-	Langmuir, 5A	4	6	Valve eq.	1	Air separation
Doong and Yang, 1986	LDF	Bulk gas	-	LRC, AC+5A	5	8	Linear	1 or 2	H_2, CH_4, CO, N_2
Yang and Doong, 1986	LDF	Bulk gas	-	LRC, AC/5A	2, 4	5, 7	-	1	H_2, CH_4, N_2
Alpay and Scot, 1992	LEQ	Bulk gas	-	Ext. Langmuir, 13X	2, 3	4, 6	-	1	CO_2 from flue gases
Kikkinides and Yang, 1993a	-	-	-	AC, zeolite, silica gel	9, 10	9, 11, 6+7	-	-	Overview of commercial PSA processes
Ruthven, 1992	LDF	Bulk gas	Darcy	Langmuir, AC	4, 5	7, 9, 12	-	1	H_2, CH_4
Kikkinides and Yang, 1993b	LDF	Bulk gas	Darcy	Langmuir, Alumina+AC+zeolite	6	12	Stored in buffer	inert + 2 ads.	H_2, CH_4, CO
Lu et al, 1993	LDF	Bulk gas	Ergun	Langmuir, AC+5A	4	8	Only one bed is simulated; data stored in the buffer	2	H_2, CO_2, CH_4, CO
Yang and Lee, 1998	LDF	Bulk gas	Ergun	Dual-site Langmuir, APHP+5A	5	11	Valve eq.	2	N_2, CH_4, CO_2, CO, H_2,
Cruz et al, 2003	LDF	Bulk gas	-	Langmuir, 13X	4, 5	4, 5, 5	Linear	1	CO_2, N_2, H_2O

A general conclusion from the previous contributions is that in most of the previous studies either complex mathematical models and simple bed arrangements, or simple mathematical models and complex bed arrangements have been presented. Mass balance is usually represented by the LDF approximation and heat balance by the typical bulk gas equation. Detailed mass and heat transfer mechanisms at the particle level are often neglected. Transport properties such as mass and heat transfer coefficients, gas diffusivities (molecular, Knudsen, surface), and mass and heat axial dispersion coefficients are often assigned to constant values. Furthermore, most of the previous contributions focus on a relatively small number of units with simple bed interactions (frozen solid model, the

linear pressure change or the information about streams are stored in data buffers for later use). Moreover, simulations of multi-bed PSA processes are usually carried out by simulating only one bed with the exception of the works of Sircar and Golden (2000) and Jiang et al (2003).

2.3.2. Overview of optimization PSA studies

Smith and Westerberg (1990) developed a program to determine the optimal schedule of a PSA process. The optimization problem was formulated as a mixed-integer nonlinear optimization problem. They showed that, in most cases, nonlinear constraints can be linearized by using proper variable transformations and the whole problem can be transformed into the mixed-integer linear optimization. The program calculates the optimal schedule based on the given set of operating steps and constraints (such as steps that require bed inter-connections, continuous operating of the compressor or continuous production). The basic model has been extended to support more flexible schedules, that is to determine the best subset and sequence of steps based on a given set of operating steps. The extended program has been applied on the industrial process for hydrogen purification (*Polybed*). However, the features introduced in the modified model were not fully employed. The sequence of steps was predetermined and only the optimal schedule has been determined. In the subsequent publication in 1991, the same authors employed the optimization model on the simple integral model of a PSA process and applied it on the process of hydrogen purification from a hydrogen/methane waste stream. The objective was to maximize total annual profit while optimizing the structure, schedule and operating of the process. The optimal schedules for four different number of pressure equalizations (zero to three) have been presented as well as the effect of various variables on total annual profit, annual capital and annual operating costs of the process.

The work of Nilchan and Pantelides (1998) is the first key contribution towards a formal PSA optimization framework. They introduced a novel mathematical programming approach to the optimization of general periodic adsorption process, which comprises the rigorous mathematical model of an adsorption bed, periodic boundary conditions, cycle timing constraints and bed interaction constraints. Two different techniques for determining the cyclic steady state (CSS) have been applied: dynamic simulation (DS) and complete (both in space and time) discretization (CD). Bed interactions have been described by gas valve equations. The developed model has been applied in modelling and optimization of nitrogen production from air where two-bed four-step PSA configuration has been used.

Biegler and co-workers (2003) proposed an algorithm to accelerate the CSS convergence by using a Newtonian-based method with accurate sensitivity calculation to achieve fast and robust convergence. They applied the method on two different single-bed oxygen VSA cycles, and chose to maximize oxygen recovery using the tank pressure, gas valve constant (from the bed to the tank), adsorption and desorption times as optimization decision variables. The same authors in 2004 developed a robust simulation and optimization framework for multi-bed PSA processes and investigated the effect of different operating parameters on process performance using a five-bed eleven-step PSA configuration for the separation of hydrogen from $H_2/CH_4/N_2/CO/CO_2$ mixture. To simulate the behavior of a five-bed PSA configuration two different approaches were employed: *Unibed* and *Multibed*. The *Unibed* approach assumes that all beds undergo

identical steps so only one bed is needed to simulate the multi-bed cycle. Information about the effluent streams are stored in data buffers and linear interpolation is used to obtain information between two time points. The *Multibed* approach considers a multi-bed process as a sequence of repetitive stages within the cycle. A black box and a simultaneous tailored framework to solve the optimization problem were presented. In the black box approach, sensitivities are calculated at CSS by using the perturbation method, while in the simultaneous framework either by perturbation or direct sensitivity approach by the DASPK package.

Mendes and co-workers (2003) developed an efficient and robust cyclic adsorption processes simulator, and proposed a systematic theoretical optimization method to design and optimize small- and large-scale PSA units. The system of partial differential equations was solved by an adaptive multiresolution approach, ensuring great stability and accuracy of the simulated solution. The proposed optimization procedure was applied in a case study involving oxygen production from air. This work was then extended in 2006 by the same authors to optimize cycles that are more complex, to analyze different types of adsorbents and different operating conditions. A performance analysis is presented for two different types of adsorbents using the Skarstrom cycle with one equalization step (PSA and VSA).

Sankararao and Gupta (2007) developed a general procedure for the optimization of PSA processes by using multi-objective optimization techniques. An adaptation of a multi-objective simulated annealing (MOSA-aJG) has been developed and employed in a PSA process for oxygen production from air. The rigorous single adsorption bed model previously developed by the same authors was applied on the basic two-bed four-step Scarstrom cycle.

As it has been clearly illustrated in previous works, the selection of optimal design and operating parameters is a difficult task due to several reasons: highly complex mathematical models (large number of partial differential and algebraic equations necessary to describe the multi-scale transport phenomena in adsorbent column and adsorbent particles), a large number of trade-offs between the key variables, and excessive computational requirements to reach the cyclic steady state. In addition, calculation of the optimal number of beds and optimal schedule coupled with the optimization of design and operating variables makes the system of intractable size. In the previous contributions typical objective functions have been employed (e.g. product purity and recovery, power requirements or profit) and different scenarios used to reduce the computational requirements for the solution of the problem: a) fixed number of beds, fixed schedule and complex PSA model employed, and subset of operating and design parameters optimized (Nilchan and Pantelides, 1998; Biegler et al, 2003, 2004; Mendes et al, 2003, 2006; Sankarao and Gupta, 2007); b) very simple PSA model employed, and number of beds, schedule and subset of operating and design parameters optimized (Smith and Westerberg, 1991). The effect of number of beds and different cycle configurations (sequence and duration of steps) has been systematically analyzed by Smith and Westerberg only. However, very simple PSA model has been used (with a priori given important parameters, such as efficiency and bed utilization) which rather roughly predicts PSA process performance (purity and recovery) therefore making it practically insensitive on many design and operating variables. In addition, very few contributions consider optimization studies of PSA processes with multilayered adsorbents.

2.4. Mathematical modelling

PSA is a typical multi-scale process: all industrial scale PSA processes consist of several adsorbent columns inter-connected by gas valves; each column comprises one or more adsorbent layers; adsorbent layers are made of adsorbent particles packed into beds; adsorbent particles may consist of several micro-pellets forming the macro-pellet (as in the case of zeolite adsorbents). Thus, the mathematical modelling of a PSA process has to take into account the simultaneous mass, heat and momentum balances at adsorbent column and adsorbent particle level, gas-solid phase equilibrium, transport and thermo-physical properties of the fluids and a complicated set of boundary conditions for each operating step (due to a knotty nature of adsorbent column connections). As the result, the mathematical model of a PSA process is a complex system of coupled partial differential and algebraic equations at different scales: PSA flowsheet, adsorbent column, adsorbent particle and in certain situations even at the molecular level. In order to deal with such a complex system it is necessary to build–up a hierarchical system of mathematical models each describing particular scale in a PSA process. Therefore, as far as this work is concerned the following scales exist:

- Multi-bed PSA flow-sheet
- Adsorption column
- Adsorbent layer
- Adsorbent particle

Lower-level models, which represent building blocks for the more complex ones, will be presented first.

2.4.1. Adsorption layer model

2.4.1.1. General balance equations

An adsorption layer model should take into the account the simultaneous mass, heat and momentum balances in the bulk flow, equations for transport and thermo-physical properties of the gas mixture and a set of boundary conditions for inlet and outlet from the layer and for the interface between the bulk gas and particle surface. The result of the model is a set of functions of time, axial position and number of components in the layer for the composition/concentration, temperature, velocity and pressure.

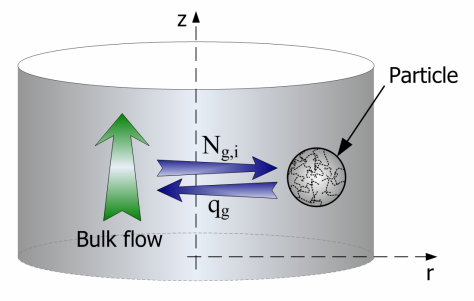

Figure 2.3 Adsorbent layer

The following general assumptions have been adopted:

- The flow pattern in the layer is described by axially dispersed plug flow (no variations in radial direction across the adsorber)
- The adsorbent is represented by uniform micro-porous spheres

The general balance equation is given in the following form:

$$\frac{D\psi}{Dt} = \psi_g + \nabla D \nabla \psi \tag{2.1}$$

where ψ is concentration of mass, heat or momentum, D is diffusivity, $\frac{D\psi}{Dt}$ is substantial derivative, ψ_g is generation term and $\nabla D \nabla \psi$ is diffusion term.

For the *bulk gas flow*, convection and diffusion in x and y directions can be neglected leading to the following general transport equation:

$$\underset{(1)}{\frac{\partial(u\psi)}{\partial z}} + \underset{(2)}{\frac{\partial \psi}{\partial t}} = \underset{(3)}{\psi_g} + \underset{(4)}{\frac{\partial}{\partial z}\left(D\frac{\partial \psi}{\partial z}\right)} \tag{2.2}$$

where the terms (1) to (4) are: (1) convection term, (2) accumulation term, (3) generation term, (4) diffusion term.

2.4.1.2. Mass balance

Applying general equation 2.2 on the mass transfer in the bulk gas flow ($\psi = C_i$, $D = D_{z,i}$), after few simple mathematical operations, we get:

$$\varepsilon_{bed}\frac{\partial(uC_i)}{\partial z} + \varepsilon_{bed}\frac{\partial C_i}{\partial t} + (1-\varepsilon_{bed})N_{g,i} = \varepsilon_{bed}\frac{\partial}{\partial z}\left(D_{z,i}\frac{\partial C_i}{\partial z}\right),\ \forall z \in (0,\ L),\ i = 1,\ N_{comp} \tag{2.3}$$

where the term $N_{g,i}$ is a generation term given per unit volume of adsorbent which quantifies the mass transfer occurring between bulk flow and particles. The actual expression for the generation term depends on the nature of the resistances to the mass transfer (gas film around particles, macro or micro pores etc). This analysis will be given in the next section.

2.4.1.3. Heat balance

Applying general equation 2.2 on the heat transfer in the bulk gas flow ($\psi = \rho c_p T$, $D = a = \frac{\lambda}{\rho c_p}$), after few simple mathematical operations we get:

$$\varepsilon_{bed}\frac{\partial(\rho c_p T u)}{\partial z} + \varepsilon_{bed}\frac{\partial(\rho c_p T)}{\partial t} = (1-\varepsilon_{bed})q_g + q_{wall} + \varepsilon_{bed}\frac{\partial}{\partial z}\left(\lambda\frac{\partial T}{\partial z}\right),\ \forall z \in (0,\ L) \tag{2.4}$$

where q_g and q_{wall} are generation terms, again given per unit volume of adsorbent. q_g quantifies the heat transfer between bulk flow and particles, while q_{wall} takes into account heat losses through the column walls. Again, the actual expression for q_g depends on the nature of the resistances to the heat transfer and will be given in the next section.

In general, three thermal operating modes exist in PSA: *isothermal*, *non-isothermal* and *adiabatic*. In the case of gas purification, system can be assumed approximately isothermal. Therefore, the heat balance becomes:

$$\frac{\partial T}{\partial z} = 0, \ \forall z \in (0, \ L) \tag{2.5}$$

In the case of adiabatic column, the term q_{wall} in equation 2.4 is equal to zero and the equations becomes:

$$\frac{\partial \left(\rho c_p T u\right)}{\partial z} + \frac{\partial \left(\rho c_p T\right)}{\partial t} = \frac{1-\varepsilon_{bed}}{\varepsilon_{bed}} q_g + \frac{\partial}{\partial z}\left(\lambda \frac{\partial T}{\partial z}\right), \ \forall z \in (0, \ L) \tag{2.6}$$

If the heat transfer through the column wall cannot be neglected (*non-isothermal* mode), the following equation can be used:

$$q_{wall} = \frac{2k_{h,wall}}{R_{bed}}\left(T - T_{wall}\right), \ \forall z \in (0, \ L) \tag{2.7}$$

where $k_{h,wall}$ is a heat transfer coefficient between the bulk flow and the wall and T_{wall} is the temperature of the wall.

2.4.1.4. Momentum balance

The pressure drop is an important variable in modelling of fixed beds having a high impact on the separation quality and operating costs. The hydrodynamics of flow through porous media is the most commonly described by using one of the following correlations for pressure drop:

- Blake-Kozeny

$$-\frac{\partial P}{\partial z} = 180\frac{\left(1-\varepsilon_{bed}\right)^2}{\varepsilon_{bed}^3}\frac{\mu u}{\left(2R_p\right)^2}, \ \forall z \in (0, \ L) \tag{2.8}$$

- Ergun

$$-\frac{\partial P}{\partial z} = 150\frac{\left(1-\varepsilon_{bed}\right)^2}{\varepsilon_{bed}^3}\frac{^2\mu u|u|}{\left(2R_p\right)^2} + 1.75\frac{1-\varepsilon_{bed}}{\varepsilon_{bed}^3}\frac{\rho u}{2R_p}, \ \forall z \in (0, \ L) \tag{2.9}$$

2.4.1.5. Equation of state

The mass and heat balances are coupled through the concentration dependence on temperature and pressure. In many cases, an ideal gas equation satisfactorily predicts that dependency:

$$P = \sum_{i=1}^{N_{comp}} C_i RT, \ \forall z \in [0, \ L] \tag{2.10}$$

However, in mixtures that are more complex it may be necessary to employ one of numerous gas equations of state, given in general form:

$$P = f\left(C_1,...,C_{N_{comp}},T\right), \ \forall z \in [0, \ L] \tag{2.11}$$

2.4.1.6. Thermo-physical properties

Physical properties of the gas mixture can be assumed constant or calculated by using some of the available correlations or thermo-physical packages. In either case, physical properties are functions of temperature, pressure and composition, given in general form:

$$\rho, \lambda, c_p, \mu = f\left(T, P, C_1,...,C_{N_{comp}}\right), \ \forall z \in [0, \ L] \tag{2.12}$$

2.4.1.7. Axial dispersion

Axial concentration and temperature gradients always exist in packed beds. Hence, a diffusive mass and heat transfer will always occur and tend to degrade the performance of the process. An accurate prediction of mass and heat axial dispersion coefficients is therefore very important for detailed modelling of the flow through the packed bed. Several correlations for prediction of mass and heat axial dispersion coefficients exist in the literature. Wakao (1978, 1979) developed one of the most widely used:

$$D_{z,i} = \frac{D_{m,i}}{\varepsilon_{bed}}\left(20 + 0.5ScRe\right), \ \forall z \in [0, \ L], \ i = 1,\ldots, N_{comp} \tag{2.13}$$

$$\lambda_z = \lambda_{bg}\left(7 + 0.5PrRe\right), \ \forall z \in [0, \ L] \tag{2.14}$$

The molecular diffusivity for a binary mixture can be calculated by using Chapman-Enskog equation (Yang, 1987):

$$D_{m,i} = 1.8583 \times 10^{-3} \sqrt{\frac{T^3 \dfrac{1}{MW_i}}{P\sigma_{12}^2 \Omega_{12}}}, \ \forall r \in \left[0, \ R_p\right], \ i = 1, \ 2 \tag{2.15}$$

where σ_{12}, ε_{12} are constants in Lennard-Jones potential-energy function given by:

$$\sigma_{12} = \frac{\sigma_1 + \sigma_2}{2}, \ \varepsilon_{12} = \sqrt{\varepsilon_1 \varepsilon_2} \tag{2.16}$$

and Ω_{12} is a collision integral which is a function of $\frac{k_B T}{\varepsilon_{12}}$.

2.4.1.8. Transport properties

Transport properties are assigned constant values or predicted using appropriate correlations. In general any appropriate correlation can be used. Some of the most commonly used were developed by Wakao (1978, 1979):

$$Sh = \frac{k_{f,i} R_p}{D_{m,i}} = \left(2.0 + 1.1 Sc^{0.33} Re^{0.6}\right), \ \forall z \in [0, \ L], \ i = 1, \ldots, N_{comp} \tag{2.17}$$

$$Nu = \frac{k_h R_p}{\lambda} = \left(2.0 + 1.1 Pr^{0.33} \, \mathrm{Re}^{0.6}\right), \ \forall z \in [0, \ L] \tag{2.18}$$

2.4.2. Adsorbent particle model

Similar to the bulk gas flow, the adsorption particle model should take into account the simultaneous mass and heat balance, equations for transport and thermo-physical properties of the gas mixture and a set of boundary conditions at the particle surface and particle centre. The result of the model is a set of functions of time, radial position and number of components for composition/concentration of the gas within pores, composition/concentration of the gas adsorbed in the particle and temperature.

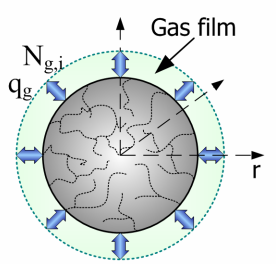

Figure 2.4 Adsorbent particle

The main assumptions made in deriving the equations for the mass and heat balance are:

- all particles are represented by uniform spheres
- only changes in the radial direction occur - transport in θ and φ directions can be neglected

2.4.2.1. General equations for mass and heat balance

Starting from the general balance equation 2.2 after few simple mathematical operations, we get the general expression for the mass transfer in spherical particles:

$$\varepsilon_p \frac{\partial C_i^p}{\partial t} + \left(1-\varepsilon_p\right) N_{gi}^p = \varepsilon_p N_i^p, \ \forall r \in \left(0, \ R_p\right), \ i = 1, \ldots, N_{comp} \tag{2.19}$$

where C_i^p is concentration of component *i* in the gas phase, N_{gi}^p is the generation term of the component *i* and N_i^p is molar flux of component *i*. In general, the molar flux is given as the sum of gaseous diffusion, convective flux due to diffusion, surface flux and viscous flow. Gaseous and surface fluxes follow Fick's first law of diffusion while the other terms can usually be neglected. The equations for the gaseous and surface molar fluxes within the particle are given by (assuming the constant diffusivities):

$$\begin{aligned} \left(N_i^p\right)_{gaseous} &= D_{e,i}\left(\frac{\partial^2 C_i^p}{\partial r^2} + \frac{2}{r}\frac{\partial C_i^p}{\partial r}\right) \\ \left(N_i^p\right)_{surface} &= D_{s,i}\left(\frac{\partial^2 Q_i^p}{\partial r^2} + \frac{2}{r}\frac{\partial Q_i^p}{\partial r}\right) \end{aligned} \tag{2.20}$$

where $D_{e,i}$ is the effective diffusivity (usually a combined effect of Knudsen and molecular diffusion), $D_{s,i}$ is surface diffusivity and Q_i^p is the concentration of the gas adsorbed in the particle. Which expression is used depends on the type of the adsorbent as well as the pore size. In large pores (where the pore diameter is ten times greater than mean free path) the molecular diffusion will be dominant. In smaller pores, the Knudsen diffusion may prevail. The mean free path is given by the following equation:

$$Mean\ free\ path = \frac{1}{\sqrt{2} n \pi \sigma^2} \tag{2.21}$$

where *n* is gas number density in molecules/volume and σ is a collision parameter (Yang, 1987). On the other hand, in zeolites the gas is transported within the particle primarily by surface diffusion.

Starting from the general balance equation 2.2, after few simple mathematical operations we get the general expression for the heat transfer in spherical particles:

$$\frac{\partial\left(\rho^p c_p^p T^p + \varepsilon_p \rho_{pg} c_{pg} T^p\right)}{\partial t} + q_g^p = \lambda^p \left(\frac{\partial^2 T^p}{\partial r^2} + \frac{2}{r}\frac{\partial T^p}{\partial r}\right), \ \forall r \in \left(0, \ R_p\right) \tag{2.22}$$

where T^p is temperature within the particle (temperature of the gas and solid phase are assumed equal) and q_g^p is the generation term.

The mass transfer within particles can be described by several diffusion mechanisms. The most common found in the literature are: (i) local equilibrium (LEQ), (ii) linear driving force (LDF), (iii) surface diffusion (SD), (iv) pore diffusion (PD). First two mechanisms (LEQ and LDF) try to significantly simplify the solution. This can be done by introducing certain assumptions which will result in the expressions for generation terms in equations 2.3 and 2.4 as functions of bulk flow concentrations and temperature. The last two mechanisms (SD and PD) are more rigorous approaches, which take into account mass and heat balances at both levels (bulk gas flow and particle level). In the next sections, a derivation for mass and heat balances will be given for all four mechanisms.

2.4.2.2. Local equilibrium (LEQ)

Local equilibrium is the simplest approach to modelling of the inter-particle mass transfer. The main assumption is that there is no mass or heat transfer resistance, that is the mass transfer through the particles is instantaneous and the gas phase is in equilibrium with the solid phase at any radial position. Thus, the gas concentration within the particles is equal to the concentration in the bulk flow:

$$C_i^p = C_i,\ \forall r \in \left[0,\ R_p\right], \forall z \in \left[0,\ L\right],\ i = 1,\ldots, N_{comp} \tag{2.23}$$

and the gas phase is in equilibrium with the solid phase:

$$Q_i\ = Q_i^*,\ \forall r \in \left[0,\ R_p\right], \forall z \in \left[0,\ L\right], i = 1,\ldots, N_{comp} \tag{2.24}$$

The generation term in the equation 2.3 is given by a sum of adsorbed amounts of components in the gas mixture and accumulation in the gas phase within particles:

$$N_{g,i} = \rho^p \frac{\partial Q_i^*}{\partial t} + \varepsilon_p \frac{\partial C_i}{\partial t}, \forall z \in \left(0, L\right),\ i = 1,\ldots, N_{comp} \tag{2.25}$$

Similar to the mass transfer, the heat transfer is also assumed instantaneous. Therefore, the temperature of particles is assumed the same as the temperature of the bulk flow.

$$T^p = T,\ \forall r \in \left[0,\ R_p\right], \forall z \in \left[0,\ L\right] \tag{2.26}$$

Thus, the generation term in the equation 2.4 is given by the following equation:

$$q_g = \frac{\partial\left(\rho^p c_p^p T + \varepsilon_p \rho_{pg} c_{p,pg} T\right)}{\partial t} + \rho^p \sum_{i=1}^{N_{comp}} \Delta H_{ads,i} \frac{\partial Q_i^*}{\partial t}, \forall z \in \left(0, L\right) \tag{2.27}$$

2.4.2.3. Linear driving force (LDF)

LDF approximation is one of the most widely used in adsorber models. However, one should keep in mind the conditions needed to derive the equation. Detailed derivation is given in Glueckauf (1947, 1955) and Yang (1997) and the applicability of this approximation to cyclic processes has been discussed by Nakao and Suzuki (1983) and by Raghavan and Ruthven (1986).

According to the LDF approach, the gas film resistance is neglected and the overall uptake rate in a particle is expressed as a function of the bulk gas flow concentration:

$$\frac{\partial \bar{Q}_i}{\partial t} = \frac{15 D_{e,i}}{R_p^2}\left(Q_i^* - \bar{Q}_i\right),\ \forall z \in \left[0,\ L\right], i = 1,\ldots, N_{comp} \tag{2.28}$$

where $\bar{Q}_i$ is the volume-averaged adsorbed amount per unit volume of sorbent, Q_i^* is adsorbed amount in equilibrium with the gas phase, and $D_{e,i}$ is the effective diffusivity usually measured experimentally. The same equation can be obtained by assuming a parabolic concentration profile within the particle and finding its analytical solution (Yang, 1987). The generation term in the equation 2.3 is given as a sum of adsorbed amounts of components in the gas mixture and accumulation in the gas phase within particles:

$$N_{g,i} = \rho^p \frac{\partial \overline{Q}_i}{\partial t} + \varepsilon_p \frac{\partial C_i}{\partial t}, \forall z \in (0, L),\ i = 1, \ldots, N_{comp} \tag{2.29}$$

The temperature of particles is assumed equal to the temperature of the bulk flow:

$$T^p = T,\ \forall r \in \left[0,\ R_p\right], \forall z \in [0,\ L] \tag{2.30}$$

and the generation term in equation 2.4 is given by the following equation:

$$q_g = \frac{\partial \left(\rho^p c_p^p T + \varepsilon_p \rho_{pg} c_{p,pg} T\right)}{\partial t} + \rho^p \sum_{i=1}^{N_{comp}} \Delta H_{ads,i} \frac{\partial \overline{Q}_i}{\partial t}, \forall z \in (0, L) \tag{2.31}$$

2.4.2.4. Surface diffusion (SD)

The surface diffusion is a dominant mass transfer mechanism in many adsorptive gas separation processes (as it is a case with diffusion within zeolite micro-crystals). It is assumed that all adsorption happens at the particle surface where the gas phase is in equilibrium with the solid phase, and that the gas phase does not exist within the particles:

$$C_i^p = 0,\ \forall r \in \left[0,\ R_p\right), \forall z \in [0,\ L],\ i = 1, \ldots, N_{comp} \tag{2.32}$$

$$Q_i = Q_i^*,\ r = R_p,\ \forall z \in [0,\ L],\ i = 1, \ldots, N_{comp} \tag{2.33}$$

Adsorbed phase is then transported towards particle centre by surface diffusion (Fick's first law of diffusion):

$$\frac{\partial Q_i}{\partial t} = \frac{\partial}{\partial r}\left(D_{s,i} \frac{\partial Q_i}{\partial r}\right),\ \forall r \in \left(0,\ R_p\right),\ \forall z \in [0,\ L],\ i = 1, \ldots, N_{comp} \tag{2.34}$$

Mass transfer between the bulk flow and particles is carried out through the gas film around particles. In that case, the generation term in equation 2.3 is given by:

$$N_{g,i} = \frac{3k_f}{R_p}\left(C_i - C_i^p\Big|_{r=R_p}\right),\ \forall z \in [0,\ L],\ i = 1, \ldots, N_{comp} \tag{2.35}$$

At the particle surface we have a continuity equation:

$$k_{f,i}\left(C_i - C_i^p\Big|_{r=R_p}\right) = D_{s,i} \frac{\partial Q_i}{\partial r}\Big|_{r=R_p},\ \ r = R_p,\ \forall z \in [0,\ L],\ i = 1,\ N_{comp} \tag{2.36}$$

At the particle centre it is assumed there is no mass transfer:

$$\left.\frac{\partial Q_i}{\partial r}\right|_{r=0} = 0,\ r = 0,\ \forall z \in [0,\ L],\ i = 1, \ldots, N_{comp} \tag{2.37}$$

Since all adsorption happens at the particle surface and there is no gas phase within the particles, the temperature is given by the following equation:

$$\frac{\partial T^p}{\partial t} = \frac{\partial}{\partial r}\left(\lambda^p \frac{\partial T^p}{\partial r}\right),\ \forall r \in \left(0,\ R_p\right),\ \forall z \in [0,\ L] \tag{2.38}$$

Similar to the mass transfer, the heat transfer between the bulk flow and particles is carried out through the gas film around them. Therefore, the equation for the generation term is given by:

$$q_g = \frac{3k_h}{R_p}\left(T - T^p\big|_{r=R_p}\right), \forall z \in [0,\ L] \tag{2.39}$$

In that case, the temperature at $r = R_p$ should be calculated from the following continuity equation:

$$k_h\left(T - T^p\big|_{r=R_p}\right) = \lambda^p\left(\frac{\partial T^p}{\partial r}\right)\Bigg|_{r=R_p}, \quad r = R_p, \forall z \in [0,\ L] \tag{2.40}$$

At the particle centre it is assumed there is no heat transfer:

$$\left(\frac{\partial T^p}{\partial r}\right)\Bigg|_{r=0} = 0,\ r = 0, \forall z \in [0,\ L] \tag{2.41}$$

2.4.2.5. Pore diffusion (PD)

This model is applicable to the adsorbents with a monodisperse pore structure: activated carbon, alumina, silica gel. It is assumed that within the pores, gas is transported by combined molecular and Knudsen diffusion. Thus, the mass balance can be given by the following equation:

$$\varepsilon_p \frac{\partial C_i^p}{\partial t} + \left(1-\varepsilon_p\right)\rho^p \frac{\partial Q_i}{\partial t} = \varepsilon_p \frac{\partial}{\partial r}\left(D_{e,i}\frac{\partial C_i^p}{\partial r}\right), \forall r \in \left(0,\ R_p\right),\ \forall z \in [0,\ L],\ i = 1,\ldots,N_{comp} \tag{2.42}$$

The gas phase within pores is assumed in equilibrium with the adsorbed phase:

$$Q_i = Q_i^*,\ \forall r \in \left[0,\ R_p\right],\ \forall z \in [0,\ L],\ i = 1,\ldots,N_{comp} \tag{2.43}$$

The effective diffusivity in equation 2.42 can be calculated from the following equation:

$$D_{e,i} = \frac{\varepsilon_p}{\tau_p}\frac{D_{m,i}D_{k,i}}{D_{m,i}+D_{k,i}},\ \forall r \in \left[0,\ R_p\right],\ i = 1,\ldots,N_{comp} \tag{2.44}$$

The free molecular diffusivity ($D_{m,i}$) and the Knudsen diffusivity ($D_{k,i}$) can be calculated from the kinetic gas theory. For instance, the Kauzmann correlation (Yang, 1987) can be used to calculate the Knudsen diffusivity:

$$D_{k,i} = 9.7\times10^3 R_{pore}\sqrt{\frac{T^p}{MW_i}},\ \forall r \in \left[0,\ R_p\right],\ i = 1,\ldots,N_{comp} \tag{2.45}$$

while the molecular diffusivity for binary systems can be calculated from Chapman-Enskog equation, and it is independent of the composition. However, in multicomponent gas mixtures the diffusivity is concentration dependant, which has to be taken into account. In that case, General Stefan-Maxwell equations can be used to describe multicomponent diffusion (Krishna, 1993), given in a general form:

$$-\frac{\partial C_i^p}{\partial r}=\sum_{j=1}^{N_{comp}}\frac{x_j N_i^p - x_i N_j^p}{\varepsilon_p Đ_{ij}}+\frac{N_i^p}{Đ_{i,Kn}},\ z\in[0,L],\ r\in(0,R_p),i,j=1,...,N_{comp} \tag{2.46}$$

where $Đ_{ij}$ is Stefan Maxwell diffusivity, $Đ_{i,Kn}$ is Knudsen diffusivity, x_i and x_j are molar fractions, and N_i^p and N_j^p are molar fluxes of components *i* and *j*. Detailed discussion and applications of Stefan-Maxwell equations can be found in Chapter 3 and Krishna (1993).

Particle heat balance is given by the following equation:

$$\frac{\partial\left(\rho^p c_p^p T^p+\varepsilon_p\rho_{pg}c_{pg}T^p\right)}{\partial t}+\rho^p\sum_{i=1}^{N_{comp}}\Delta H_{ads,i}\frac{\partial Q_i^p}{\partial t}=\lambda^p\left(\frac{\partial^2 T^p}{\partial r^2}+\frac{2}{R_p}\frac{\partial T^p}{\partial r}\right),\ z\in[0,L],\ r\in(0,R_p) \tag{2.47}$$

Mass transfer between the bulk flow and particles is carried out through the gas film around particles. In that case, the generation term in equation 2.3 is given by:

$$N_{g,i}=\frac{3k_f}{R_p}\left(C_i-C_i^p\big|_{r=R_p}\right),\forall z\in[0,\ L],\ i=1,\ldots,N_{comp} \tag{2.48}$$

At the particle surface, we have a continuity equation:

$$k_{f,i}\left(C_i-C_i^p\big|_{r=R_p}\right)=D_{e,i}\frac{\partial C_i^p}{\partial r}\Big|_{r=R_p},\ \ r=R_p,\ \forall z\in[0,\ L],\ i=1,\ N_{comp} \tag{2.49}$$

while at the centre of the particle it is assumed that there is no mass transfer:

$$\left.\frac{\partial Q_i}{\partial r}\right|_{r=0}=0,\ r=0,\ \forall z\in[0,\ L],i=1,\ldots,N_{comp} \tag{2.50}$$

Similarly to the mass transfer, the heat transfer between the bulk flow and particles is carried out through the gas film around the particles. Therefore, the equation for the generation term in equation 2.4 is given by:

$$q_g=\frac{3k_h}{R_p}\left(T-T^p\big|_{r=R_p}\right),\forall z\in[0,\ L] \tag{2.51}$$

In that case, the temperature at the particle surface can be calculated from the following continuity equation:

$$k_h\left(T-T^p\big|_{r=R_p}\right)=\lambda^p\left(\frac{\partial T^p}{\partial r}\right)\Bigg|_{r=R_p},\ \ r=R_p,\forall z\in[0,\ L] \tag{2.52}$$

At the particle centre, it is assumed there is no heat transfer:

$$\left.\frac{\partial T^p}{\partial r}\right|_{r=0}=0,\ r=0,\forall z\in[0,\ L] \tag{2.53}$$

2.4.2.6. Gas-solid phase equilibria

Accurate models for prediction of gas-solid equilibrium are extremely important for a rigorous modelling of pressure swing adsorption. They should accurately calculate the amount of gas adsorbed within the adsorbent particles as a function of pressure, temperature and composition of the gas. Such equations are commonly given as the amount adsorbed as a function of the composition/partial pressure at the given temperature (adsorption isotherms). In general, there are three different categories of single gas and gas mixtures isotherms: Langmuir-type correlations, the Gibbs approach and the Potential-theory approach. More details are given in Ruthven (1984) and Yang (1987). From the modelling point of view, the most widely used multi-component adsorption isotherms are: Henry's law, Extended Langmuir equation, Loading Ratio Correlation (LRC), and Ideal Adsorbed Solution Theory (IAST). Each of them will be briefly described here.

Henry's Law

At sufficiently low concentrations, the amount of adsorbed gas is a linear function of the concentration. This linear relationship is commonly referred to as Henry's law and given by the following equation:

$$Q_i^* = H_i C_i^p,\ \forall r \in \left[0,\ R_p\right], \forall z \in \left[0,\ L\right], i = 1, \ldots, N_{comp} \tag{2.54}$$

where H_i is a function of pressure and temperature:

$$H_i = f\left(T^p, P\right) \tag{2.55}$$

An important term in both mass and heat balance equations that has to be calculated is a total derivative per time $\frac{\partial Q_i^*}{\partial t}$. Q_i^* is in general case a function of pressure, temperature and component concentrations:

$$Q_i^* = f\left(T, P, C_i^p\right),\ i = 1, ..., N_{comp} \tag{2.56}$$

Thus, the total derivative per time is given by:

$$\frac{\partial Q_i^*}{\partial t} = \frac{\partial Q_i^*}{\partial T}\frac{\partial T}{\partial t} + \frac{\partial Q_i^*}{\partial P}\frac{\partial P}{\partial t} + \sum_k \frac{\partial Q_i^*}{\partial C_k}\frac{\partial C_k}{\partial t},\ i, k = 1, \ldots, N_{comp} \tag{2.57}$$

For constant pressure and temperature, the total derivative simplifies to:

$$\frac{\partial Q_i^*}{\partial t} = \sum_k \frac{\partial Q_i^*}{\partial C_k^p}\frac{\partial C_k^p}{\partial t},\ i, k = 1, \ldots, N_{comp} \tag{2.58}$$

In case of linear adsorption isotherm, the time derivative is simple and given by the following equation:

$$\frac{\partial Q_i^*}{\partial t} = H_i \frac{\partial C_i^p}{\partial t},\ \forall r \in \left[0,\ R_p\right],\ \forall z \in \left[0,\ L\right],\ i = 1,\ N_{comp} \tag{2.59}$$

Extended Langmuir isotherm

The single component Langmuir isotherm can easily be extended for a multi-component mixture:

$$Q_i^* = Q_{m,i} \frac{b_i P_i}{1 + \sum_j b_j P_j},\ i, j = 1, \ldots, N_{comp} \tag{2.60}$$

$$Q_{m,i} = a_{i,1} + \frac{a_{i,2}}{T^p},\ i = 1, \ldots, N_{comp} \tag{2.61}$$

$$b_i = b_{i,1} \exp\left(\frac{b_{i,2}}{T^p}\right) \tag{2.62}$$

In this case, calculation of the total derivative $\frac{\partial Q_i^*}{\partial t}$ is somewhat more complex. Starting from the same equation 2.58 after several mathematical operations, we get the following equation:

$$\frac{\partial Q_i^*}{\partial t} = \frac{Q_{m,i} b_i}{\left(1 + \sum_j b_j C_j^p\right)^2} \sum_k Der_k \frac{\partial C_k^p}{\partial t},\ \forall r \in \left[0,\ R_p\right],\ \forall z \in \left[0,\ L\right],\ i, j, k = 1, ..., N_{comp} \tag{2.63}$$

where the term Der_k is given by:

$$Der_k = \begin{cases} 1 + \sum_j b_j C_j^p - b_i C_i^p, & if\ \ k = i \\ -b_k C_i^p, & if\ \ k \neq i \end{cases} \tag{2.64}$$

Adsorbed Solution Theory

Adsorbed Solution Theory is a special case in treatment of the mixed adsorbate as a solution in equilibrium with the gas phase. The fundamental equations for liquids are applied to the adsorbed phase. A detailed derivation can be found in Myers and Prausnitz (1965) and practical considerations in O'Brien and Myers (1988) and Yang (1997).

In general, any suitable single component adsorption isotherm can be used together with the adsorbed solution theory. However, the Langmuir isotherm is the most commonly used one since it can accurately predict the experimental data. Thus, the following set of equations (2.65 to 2.73) needed to be solved simultaneously is given here for the Langmuir isotherm:

$$\pi_i^* = \int_0^{P_i^0} \frac{Q_{pure,i}^*}{P} dP \xrightarrow[isotherm]{Langmuir} \pi_i^* = Q_{m,i}\left(1 + b_i P_i^0\right), \forall z \in \left[0,\ L\right],\ i = 1, \ldots, N_{comp} \tag{2.65}$$

$$\pi_i^* = \pi_{i+1}^*, \forall r \in \left[0,\ R_p\right], \forall z \in \left[0,\ L\right],\ i = 1, \ldots, N_{comp} - 1 \tag{2.66}$$

$$Q_{pure,i}^* = Q_{m,i} \frac{b_i P_i}{1 + b_i P_i}, \forall r \in \left[0,\ R_p\right], \forall z \in \left[0,\ L\right],\ i = 1, \ldots, N_{comp} \tag{2.67}$$

$$Q_{m,i} = a_{i,1} + \frac{a_{i,2}}{T}, \quad \forall r \in \left[0,\ R_p\right], \forall z \in \left[0,\ L\right],\ i = 1,\ldots,N_{comp} \tag{2.68}$$

$$b_i = b_{i,1} \exp\left(\frac{b_{i,2}}{T^p}\right), \forall r \in \left[0,\ R_p\right], \forall z \in \left[0,\ L\right],\ i = 1,\ldots,N_{comp} \tag{2.69}$$

$$X_i^* P_i^0 \gamma_i = X_i P, \forall r \in \left[0,\ R_p\right], \forall z \in \left[0,\ L\right],\ i = 1,\ldots,N_{comp} \tag{2.70}$$

$$\sum X_i^* = 1, \forall r \in \left[0,\ R_p\right], \forall z \in \left[0,\ L\right],\ i = 1,\ldots,N_{comp} \tag{2.71}$$

$$\frac{1}{Q_{total}} = \sum_i \frac{X_i^*}{Q_{pure,i}^*} + \frac{RT^p}{A} \sum_i X_i^* \left(\frac{\partial \ln \gamma_i}{\partial \pi_i^*}\right)_{X_i^*}, \forall r \in \left[0,\ R_p\right], \forall z \in \left[0,\ L\right],\ i = 1,\ldots,N_{comp} \tag{2.72}$$

$$Q_i^* = X_i^* Q_{total}, \forall r \in \left[0,\ R_p\right], \forall z \in \left[0,\ L\right],\ i = 1,\ldots,N_{comp} \tag{2.73}$$

In above equations, π_i^* is spreading pressure, P_i^0 is the equilibrium "vapour pressure" for pure component *i* at the same spreading pressure and the same temperature as the adsorbed mixture, γ_i is the activity coefficient of component *i*, X_i^* is the mole fraction in adsorbed phase and X_i is the mole fraction in gas phase. Many different equations are available for calculating the activity coefficients in equation 2.70. For instance, the Wilson equation coupled with the appropriate equation of state (UNIQUAC, for instance) have been successfully employed (Yang, 1987).

For the special case of ideal solution where γ_i is unity, we get the Ideal Adsorbed Solution Theory (IAST), and equation 2.70 reduces to Raoult's law:

$$X_i^* P_i^0 = X_i P, \forall r \in \left[0,\ R_p\right], \forall z \in \left[0,\ L\right],\ i = 1,\ldots,N_{comp} \tag{2.74}$$

and equation 2.72 now becomes:

$$\frac{1}{Q_{total}} = \sum_i \frac{X_i^*}{Q_{pure,i}^*}, \forall r \in \left[0,\ R_p\right], \forall z \in \left[0,\ L\right],\ i = 1,\ldots,N_{comp} \tag{2.75}$$

2.4.3. Adsorption column model

The functionality of the adsorption model is simple. It hosts one or multiple adsorption layers and define boundary condition equations for three points:

- Boundary conditions at the column inlet (z=0 position)
- Boundary conditions at the column inlet (z=L position)
- Bondary conditions (that is continuity equations) for layer interconnections

Boundary conditions depend on the operating step that is currently performed, and the boundary condition equations for twelve different operating steps have been developed:

- Closed system
- Co-current pressurization
- Adsorption

- Pressure equalization (depressurization to the other bed)
- Pressure equalization (repressurization from the other bed)
- Pressure equalization at both bed ends (depressurization to the other bed)
- Pressure equalization at both bed ends (repressurization from the other bed)
- Co-current depressurization
- Counter-current blowdown
- Counter-current purge
- Counter-current pressurization
- Co-current purge with strong adsorbate

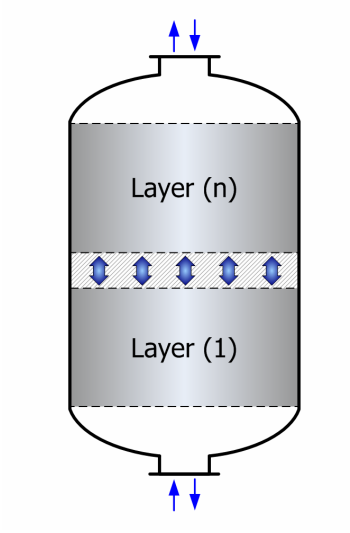

Figure 2.5 Adsorbent column with multiple adsorbent layers

For the **first** and the **last** adsorption layer, Danckwert's boundary conditions have been applied:

- For stream inlet into the layer:

$$u\left(C_i - C_i^{in}\right) = D_{z,i}\frac{\partial C_i}{\partial z},\ z = 0 \text{ or } z = L,\ i = 1,\ N_{comp} \tag{2.76}$$

$$\rho c_p u\left(T - T^{in}\right) = \lambda_z \frac{\partial T}{\partial z},\ z = 0 \text{ or } z = L \tag{2.77}$$

$$u = u^{in},\ z = 0 \text{ or } z = L \tag{2.78}$$

- For stream outlet from the layer or closed bed end:

$$\frac{\partial C_i}{\partial z} = 0,\ z = 0 \text{ or } z = L,\ i = 1,\ N_{comp} \tag{2.79}$$

$$\frac{\partial T}{\partial z} = 0,\ z = 0 \text{ or } z = L \tag{2.80}$$

$$\frac{\partial u}{\partial z} = 0,\ z = 0 \text{ or } z = L \tag{2.81}$$

where u^{in}, C_i^{in} and T^{in} are interstitial velocity, concentration and temperature of the inlet stream into the layer.

Bondary conditions for layer interconnections are given by the following equations:

$$C_i(L)\big|_{k-1} = C_i(0)\big|_k,\ k = 2, N_{layers}; i = 1, N_{comp} \tag{2.82}$$

$$T(L)\big|_{k-1} = T(0)\big|_k,\ k = 2, N_{layers} \tag{2.83}$$

$$P(L)\big|_{k-1} = P(0)\big|_k,\ k = 2, N_{layers} \tag{2.84}$$

$$U(L)\big|_{k-1} = U(0)\big|_k,\ k = 2, N_{layers} \tag{2.85}$$

$$\left.\frac{\partial P(L)}{\partial z}\right|_{k-1} = \left.\frac{\partial P(0)}{\partial z}\right|_k,\ k = 2, N_{layers} \tag{2.86}$$

$$D_{z,i}(L)\left.\frac{\partial C_i(L)}{\partial z}\right|_{k-1} = D_{z,i}(0)\left.\frac{\partial C_i(0)}{\partial z}\right|_k,\ k = 2, N_{layers}; i = 1, N_{comp} \tag{2.87}$$

$$\lambda_z(L)\left.\frac{\partial T(L)}{\partial z}\right|_{k-1} = \lambda_z(L)\left.\frac{\partial T(0)}{\partial z}\right|_k,\ k = 2, N_{layers} \tag{2.88}$$

$$\left.\frac{\partial U(L)}{\partial z}\right|_{k-1} = \left.\frac{\partial U(0)}{\partial z}\right|_k,\ k = 2, N_{layers} \tag{2.89}$$

2.4.4. Multi-bed PSA model

Multi-bed PSA model is the main model of a PSA plant and its major role is a mathematical description of complex bed inter-connections. Two distinct approaches to modelling of bed interactions have been developed:

- Bed network superstructure approach
- *VirtualBeds* approach (modified *Unibed* approach)

2.4.4.1. Bed network super-structure approach

The single bed PSA model provides the basis for the automatic generation of a flowsheet via a network-superstructure of single adsorbent beds. The main building block of the multi-bed PSA model is illustrated in Figure 2.7. The central part of the building block is the adsorption column model. Feed, purge gas, and strong adsorptive component streams are connected to the corresponding column's ends via gas valves. This is also the case for light and waste product streams. The bed is properly connected to all other beds in the system at both ends via gas valves. Such a configuration makes the flowsheet sufficiently general to support all feasible bed interconnections. This way all possible

operating steps in a PSA process can be supported. The main building block can be replicated accordingly through an input parameter representing the number of beds in the flowsheet. Multi-bed PSA flowsheet is given in Figure 2.6 while a typical four-bed PSA flowsheet (as generated in gPROMS) is shown in Figure 2.8.

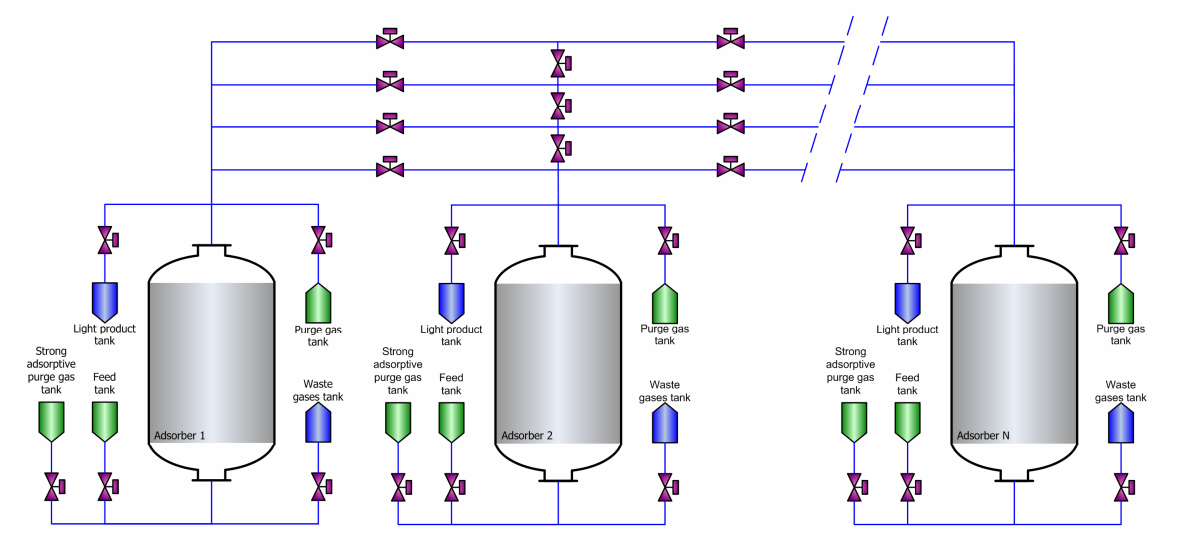

Figure 2.6 Multi-bed PSA flow-sheet

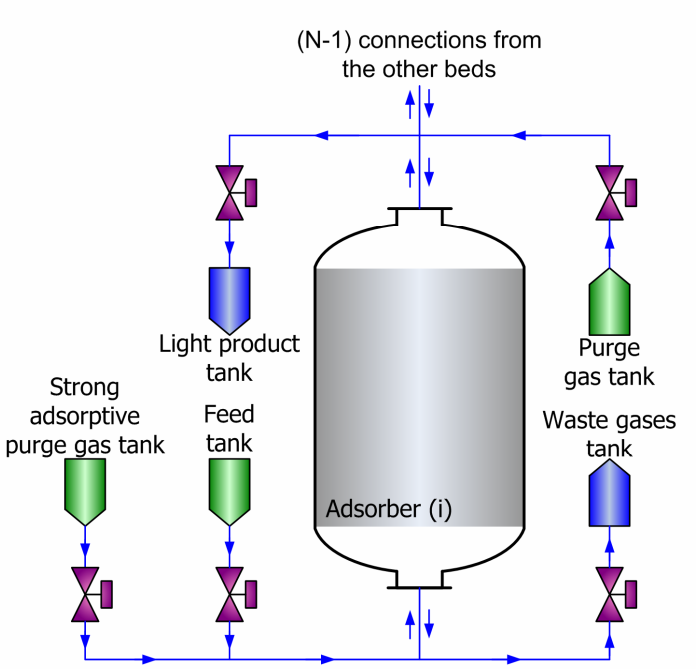

Figure 2.7 A main building block of the multi-bed PSA flowsheet

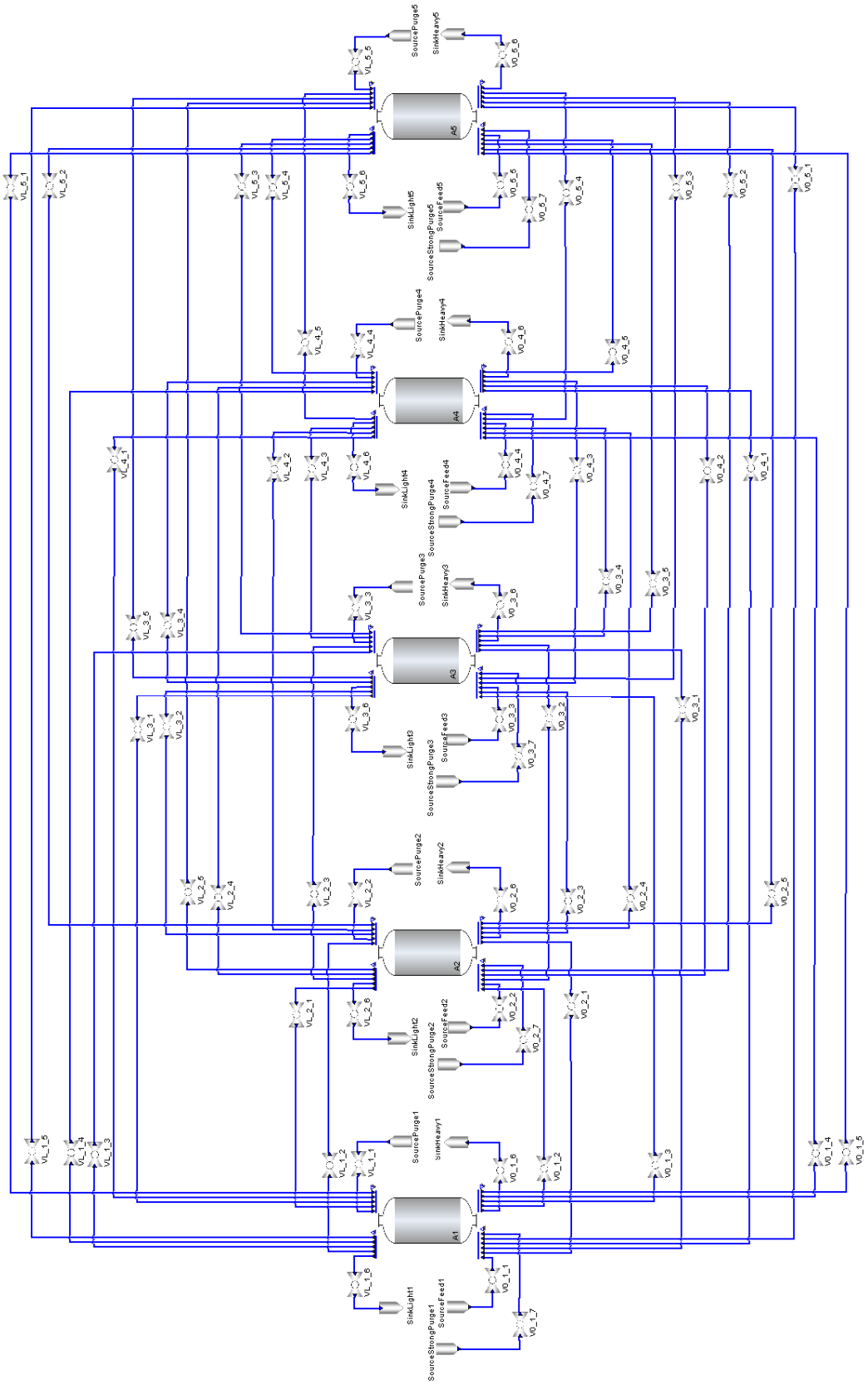

Figure 2.8 Sample four-bed PSA flow-sheet (generated in gPROMS)

Operating procedures

The execution of a PSA process in the gPROMS environment is controlled by using a set of operating procedures. Procedures for controlling the operation of multi-bed PSA processes are highly complex due to a large number of interactions. Hence, an auxiliary program for automatic generation of operating procedures has been developed. This program generates operating procedures for the whole network of beds according to the given number of beds and sequence of operating steps in one bed. Operating procedures govern the network by opening or closing the appropriate valves at the desired level and changing the state of each bed. This auxiliary program allows the automatic generation of a gPROMS source code for a given number of beds and sequence of operating steps in one bed. It also generates gPROMS tasks ensuring feasible connectivities between the units according to the given sequence. A simplified algorithm illustrating the generation of operating procedures is presented in Figure 2.9. The program is not limited only to PSA configurations where beds undergo the same sequence of steps, but it can also handle more complex configurations such as those concerning the production of two valuable components.

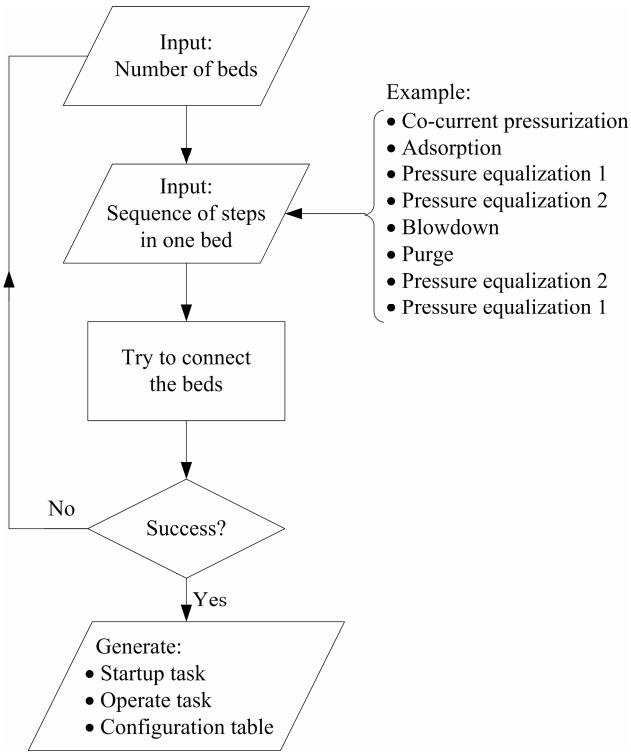

Figure 2.9 Algorithm of the operating procedure generator

2.4.4.2. VirtualBeds approach

A systematic optimization procedure, to determine the optimal design and operating conditions in a PSA system demands significant computational requirements. It is therefore necessary to reduce the size of the underlying model being optimized. In this thesis, we use a modification of the *Unibed* approach suggested by Biegler and co-workers (2003). The *Unibed* approach assumes that all beds undergo identical steps so that only one bed is

needed to simulate the multi-bed cycle. Information about the effluent streams is stored in data buffers and linear interpolation is used to obtain information between two points in time. To this end, external software (gPROMS foreign object named *VirtualBed*) has been developed in gPROMS. The modified *VirtualBeds* approach is presented in Figure 2.10. The maximum number of pressure equalization steps supported is fixed to four, thus, four *VirtualBed* models are employed. Each *VirtualBed* is connected to a real adsorption column by gas valves. According to this approach, whenever the real column undergoes a pressure equalization step it interacts with one of the *VirtualBeds* (not with the real adsorption column). Therefore, the number of variables/equations is significantly reduced (up to one order of magnitude), compared to the full bed-network superstructure approach. The *VirtualBed* and *Unibed* approaches differ in few implementation details only. More specifically, the *VirtualBed* represents an independent model (not only a data buffer), and it is connected to a real bed model via gas valves thus behaving as the adsorption column. It should be noted that the final cyclic steady state (CSS) reached is the same as in the case when the full PSA network is used.

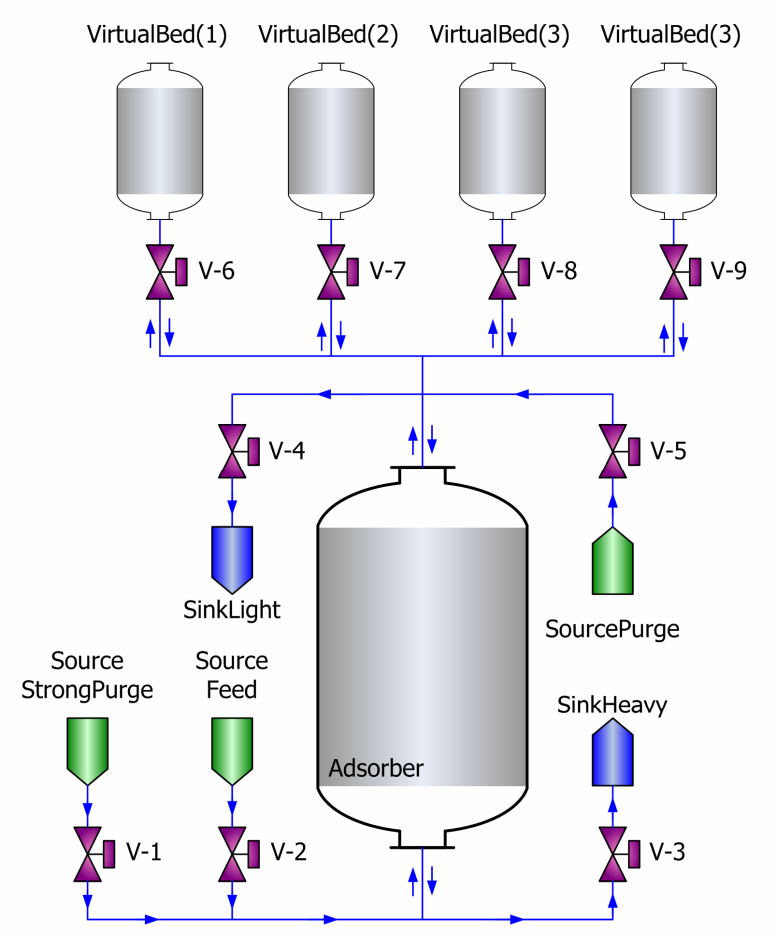

Figure 2.10 ***VirtualBeds*** **PSA approach**

The *VirtualBed* foreign object contains four callable functions:

- *SaveHistory* (saves the pressure, enthalpy and composition history)
- *GetPressure* (restores the pressure history)
- *GetEnthalpy* (restores the enthalpy history)
- *GetFraction* (restores the composition history)

SaveHistory function

This function is used by real adsorption column model to save the pressure, enthalpy and composition of the stream entering or exiting the column during the pressure equalization steps (repressurization and depressurization respectively). It takes five arguments:

- Operating step
- Number of moles transferred
- Pressure
- Mass specific enthalpy
- Mass fraction for each component

One VirtualBed holds two histories: during repressurization and during depressurization which is controlled by the *Operating step* flag. The process of the history recording is based on the relation between the number of moles exchanged between two beds and corresponding pressure (and enthalpy and composition) in the column, that is the pressure in the bed is proportional to the number of moles flowed in or out of the bed. More precisely, at the beginning of pressure equalization step (for instance depressurization to the other bed), we have certain pressure in the column and the flowrate is controlled by the gas valve equation. For example, after certain time N(1) moles of gas leave the bed and the pressure decreases to P(1). When N(2) moles leave the bed the pressure will further decrease to P(2), and so on. Obviously, at each point we have complete information about the gas stream (pressure, enthalpy and composition). This way we can build the lookup table (that is a history) given in Table 2.5.

Table 2.5 *VirtualBed* lookup table

Time [s]	Total number of moles exchanged [mol]	Pressure [Pa]	Enthalpy [J/kg]	Fraction, [-]			
				1	2	…	n
t(1)	N(1)	P(1)	h(1)	X1(1)	X2(1)	…	Xn(1)
t(2)	N(2)	P(2)	h(2)	X1(2)	X2(2)	…	Xn(2)
...	…	…	…	…	…	…	…
t(n)	N(n)	P(n)	h(n)	X1(n)	X2(n)	…	Xn(n)

When the same bed is now being repressurized from the virtual bed (by using previously recorded P, h and x history) the reverse process is taking place. The starting pressure in the *VirtualBed* is the first value from the previously recorded history (that is the

highest pressure). When certain amount of gas (let us say N moles) enters the real column the pressure in it will increase. The pressure in the *VirtualBed* will decrease and it will be pressure for the number of moles N that entered the column (taken from the history). Let us say it is somewhere between zero and N(1). The values for the P, h and x for the values of number of moles laying between two points in the history will be calculated by using linear interpolation (which is a good approximation since pressure linearly depends on number of moles). The same stands for enthalpy and composition. When the new depressurization step is about to start, the previous history is deleted and new values are stored. The same procedure stands for both depressurization and repressurization steps, and the *VirtualBed* records both histories.

It should be noticed that the history is empty at the beginning of the simulation. This issue has been solved by using default pressure, enthalpy and mass fraction in the first cycle which is presented in Figure 2.11 (Region I at the beginning of the 1st cycle; the default pressure is used). For all following cycles, the history is available.

The next issue is that the pressure (and the other variables) in the *VirtualBed* **during** the simulation does not exactly match the pressure history in the real column compared to the case when the full multi-bed configuration is used (that is when virtual beds are not used). However, at the cyclic steady state that difference disappears.

GetPressure function

Function returns pressure from the corresponding pressure history and it takes three arguments:

- Operating step
- Number of moles
- Default pressure

The parameter Operating step is used to obtain the current step (de- or re-pressurization history). If the history is currently empty, it returns *Default pressure*. If *Number of moles* is greater than the last value in the history, the last (the highest) value is always returned (Region II in Figure 2.11, the 1st cycle).

GetEnthalpy function

Function returns mass specific enthalpy from the corresponding history and it takes three arguments:

- Operating step
- Number of moles
- Default mass specific enthalpy

If the history is currently empty, it returns *Default mass specific enthalpy*. If *Number of moles* is greater than the last value in the history, the last (the highest) value is returned.

GetFraction function

Function returns mass fraction for each component from the corresponding history and it takes three arguments:

- Operating step
- Number of moles
- Default mass fraction

If the history is currently empty, it returns *Default mass fraction*. If *Number of moles* is greater than the last value in the history, the last (the highest) value is returned.

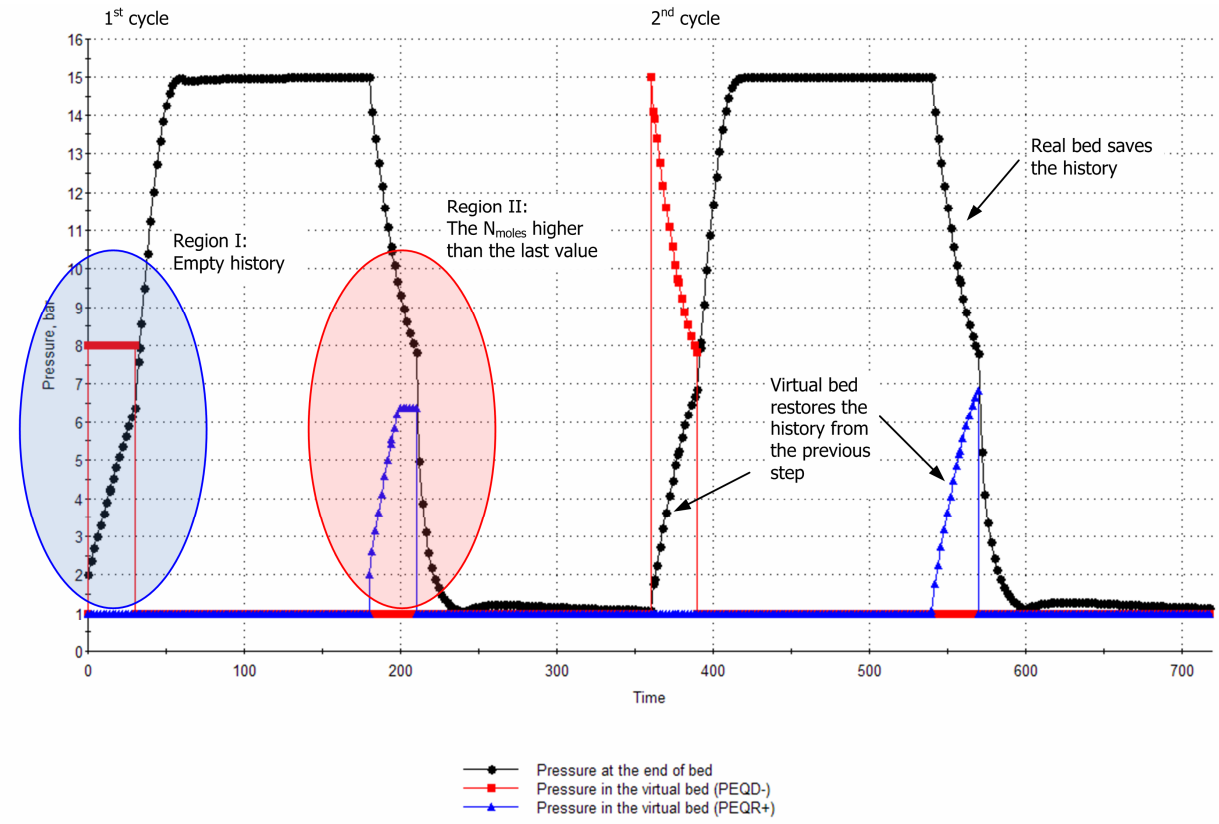

Figure 2.11 Pressure history in a real column and *VirtualBed*

State Transition Network approach

Controlling the execution of a PSA process by using a set of operating procedures has got some drawbacks: the development of operating procedures for multi-bed PSA flowsheets is a time consuming task and special software developments need to be done; it cannot be directly used in optimization studies. Thus, a new, more robust method is needed which relies on a state transition network (STN) representation of the process. States are represented by operating steps (that is an adsorbent column can be in one of the operating states such as pressurization, adsorption, purge etc); inputs are the time elapsed in the process, the time within the current cycle and several input parameters known a priory at the time of execution. Each state (the operating step) includes a set of boundary conditions and gas valves states (open/closed). A deterministic Finite State Machine (FSM) is implemented where the next possible state is uniquely determined for a given (current) state and input values. State transitions are decisions when the state change should occur (based on the input values). This way, it is possible to control the execution of the process

by specifying few parameters such as the number of beds, the sequence of steps in one bed, the number of pressure equalization steps, and the start time and duration of each step. An STN graph with all possible state transitions is presented in Figure 2.12. The overall idea is to identify which state transitions are feasible and conditions under which a particular state change occurs for a given current state. For instance, from the Pressurization step (either by feed or by light product) it is possible to switch to Adsorption step only. On the other hand, from Adsorption step it is possible to go to many other states such as CoCurrent depressurization, Blowdown, Pressure equalization or Purge by strong adsorptive, depending on a PSA sequence that we want to simulate. In general, the cycle time and the time elapsed in the process are used to identify the position within the cycle. More specifically, by defining certain process parameters (such as the number of pressure equalization steps, NoPEQ), and for a given sequence of steps in one bed and duration of certain steps in the cycle it is possible to distinguish between allowed and forbidden steps and make the decision about the transition.

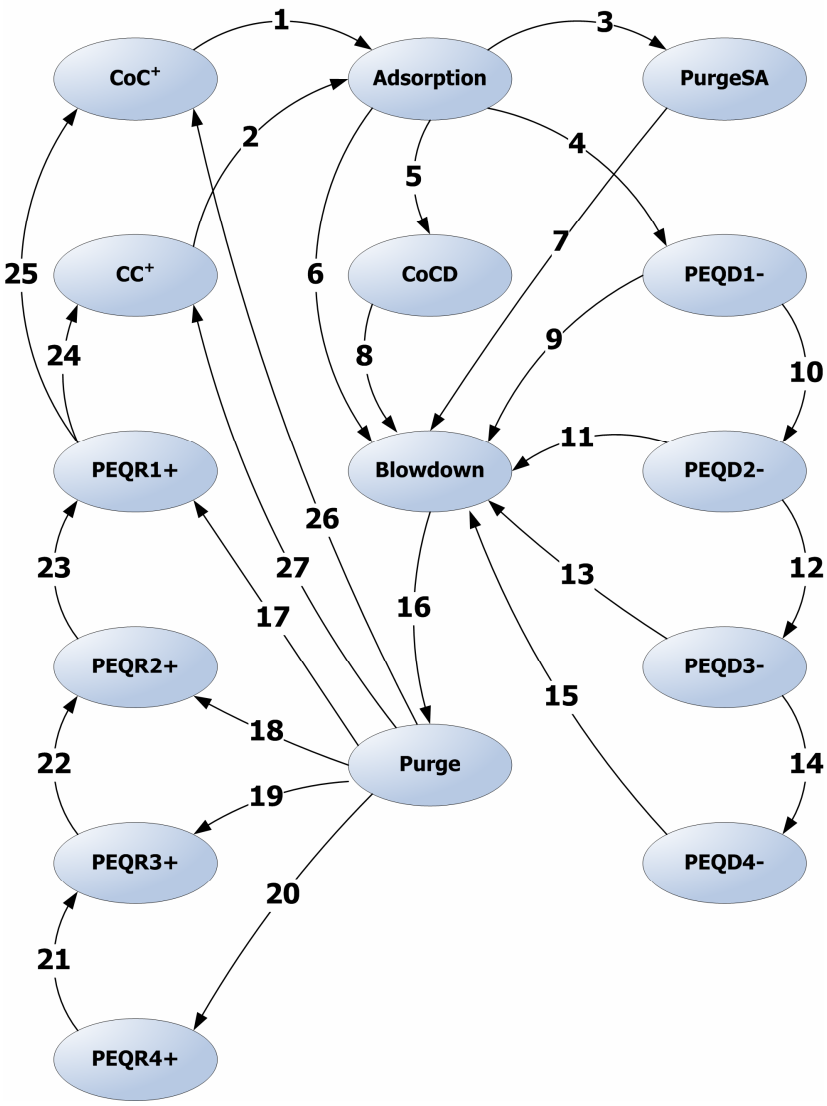

Figure 2.12 State transition network with all possible state transitions

2.4.5. Gas valve model

The velocity of the gas stream entering or leaving the adsorption bed is calculated by a valve equation recommended by the Fluids Control Institute Inc (Chou and Huang, 1994a and 1994b) given by:

$$F = \begin{cases} C_v\, SP\, P_{in} \sqrt{\left| \dfrac{1-\left(\dfrac{P_{out}}{P_{in}}\right)^2}{\sum x_i MW_i\; T} \right|}, & if\;\; P_{out} > P_{crit} \cdot P_{in} \\ C_v\, SP\, P_{in} \sqrt{\left| \dfrac{1-\left(P_{crit}\right)^2}{\sum x_i MW_i\; T} \right|}, & if\;\; P_{out} \le P_{crit} \cdot P_{in} \end{cases} \tag{2.90}$$

Critical pressure in equation 2.90 is given by the following equation:

$$P_{crit} = \left(\frac{2}{1+\kappa}\right)^{\frac{\kappa}{1-\kappa}} \tag{2.91}$$

The theoretical power needed for compression of ideal gas is given by:

$$Power = \left(\frac{\kappa}{\kappa-1}\right) RT_{feed} \left(\left(\frac{P_{feed}}{P_{low}}\right)^{\frac{\kappa-1}{\kappa}} - 1 \right) \frac{N_{feed}}{\tau_{cycle}} \tag{2.92}$$

2.5. Single-bed PSA simulation case studies

In the previous section, a generic modelling framework has been presented. In this section, the modelling framework has been applied on two most common gas separation processes (oxygen and nitrogen production from air) to check its predictive power. Equilibrium- and diffusion-controlled separations, as well as two mass transfer mechanisms of different complexity (Linear Driving Force and Pore diffusion) have been considered and simulation results compared to the results available in the literature.

2.5.1. Diffusion controlled separation

The developed modelling framework first has been applied on the process of nitrogen production from air, investigated in the work of Shin and Knaebel (1987, 1988). This gas separation is based on differences in intra-particle diffusion rates through molecular sieve type RS-10. Systematic experiments were conducted in a pilot plant to study the following variables:

- The duration of adsorbent step for a constant feed velocity
- Feed velocity (for a fixed duration of adsorption step)
- The duration of adsorbent step for a fixed amount of feed
- The duration of blowdown step
- Purge gas velocity for a fixed duration of purge step
- The duration of purge step for a constant purge gas velocity
- The duration of purge step for a fixed amount of purge gas
- The duration of pressurization step
- Feed/purge step pressure ratio
- Column geometry (length/diameter ratio)

The test results were compared to predictions of a mathematical model (Shin and Knaebel, 1987). In all cases, the trends of product purity and net recovery of both theory and experiment were in a close agreement. Since the theory accurately portrays the overall behaviour of the process, the transport mechanisms embodied in the theory may provide insight into diffusion-induced separation by PSA. In addition, by reviewing the results of the parametric studies of the variables, it has been possible to gain an intuitive understanding of the relations between factors that affect process performance.

In this work the effective diffusivity, axial dispersion coefficient, and mass transfer coefficient are taken by Shin and Knaebel. Phase equilibrium is given as a linear function of gas phase concentration (Henry's law). The design characteristics of the adsorbent and packed bed are also adopted from the work of Shin and Knaebel (1987, 1988). The axial domain is discretized using orthogonal collocation on finite elements of third order with 20 elements. The radial domain within the particles is discretized using the same method of third order with five elements. Shin and Knaebel used six collocation points for discretization of the axial domain and eight collocation points for the radial domain. The bed is considered clean initially. The target is to separate nitrogen from an air stream using molecular sieve RS-10. Here oxygen is the preferably adsorbed component due to higher

diffusivity. The PSA configuration consists of one bed and four operating steps (pressurization with feed, high-pressure adsorption, counter-current blowdown, and counter-current purge).

The pore diffusion model presented in the Chapter 2.4.2.5 has been applied on the described problem. Gas valve constants and corresponding stem positions have been properly selected to produce the same flow rates as in the work of Shin and Knaebel (1988). Since several parameters have been changed during the simulations, corresponding modifications in stem positions of the gas valves have been made. The stem positions of the gas valves for the base case are 0.15 for feed inlet, 0.002 for feed outlet, 0.7 for blowdown, and 0.3 for purge. All the other cases have been modified according to the base case. This was necessary because the flow rate through the gas valve linearly depends on the valve pressure difference for a given stem position (e.g. in order to increase the flowrate through the gas valve the stem position should be linearly increased). For example, for the experimental set 5-8, since the feed velocity was increased, the stem position for the product outlet also increased (in the same proportion).

The design characteristics of the adsorbent and packed bed used in experimental work and simulations are given in Table 2.6 and the base experimental case is shown in Table 2.7. Input parameters for the simulation are given in Table 2.8 and Table 2.9.

Comparison between experimental and simulation results of this work and the work of Shin and Knaebel (1988) is given in Table 2.10 while the comparison of absolute deviations between experimental and simulation results of this work and the work of Shin and Knaebel (1988) is given in Table 2.11.

The overall conclusion is that the modeling approach presented in this work predicts satisfactorily the behavior of PSA process and the overall average absolute deviation from experimental data is limited to 1.97% in purity and 2.23% in recovery, while the deviations between Shin and Knaebel's (1988) theoretical and experimental results were 1.81% and 2.52% respectively, as shown in the Table 2.12. These small differences can be attributed to the use of a gas valve equation employed to calculate the flowrate and pressure at the end of the column, as opposed to linear pressure histories during pressure changing steps used in the original work of Shin and Knaebel (1988). It should be emphasized that the gas valve equation results in exponential pressure histories during the pressure changing steps. Moreover, different number of discretization points and different package for thermo-physical property calculations have been used compared to the work of Shin and Knaebel (1988).

Table 2.6 Geometrical and transport characteristics

Parameter	Value	Units
Particle density	1790	kg/m^3
Bulk density	724	kg/m^3
Particle radius	8×10^{-4}	m
Bed void fraction	0.6	-
Bed inner diameter	0.0208	m
Bed length	1.016	m
Effective diffusivity of O_2	3×10^{-7}	m^2/s
Effective diffusivity of N_2	6×10^{-9}	m^2/s
Adsorption isotherm O_2	3.822	$(mol/m^3$ solid$)/(mol/m^3$ gas$)$
Adsorption isotherm O_2	8.178	$(mol/m^3$ solid$)/(mol/m^3$ gas$)$
Mass transfer coefficient O_2	10	m/s
Mass transfer coefficient N_2	10	m/s
Mass axial dispersion coefficient	10^{-6}	m^2/s

Table 2.7 Base case parameters

Parameter	Value
Feed volume (on STP)	2.54e-4 m^3
Purge gas volume (on STP)	1.66e-5 m^3
Duration of pressurization step	15 s
Duration of adsorption step	35 s
Duration of blowdown step	2 s
Duration of purge step	3 s
Stem position for pressurization	0.150
Stem position for feed outlet	0.002
Stem position for blowdown	0.700
Stem position for purge outlet	0.300

STP - standard pressure and temperature, T = 273.15^0C, P = 101,325 Pa

Table 2.8 Input parameters for the simulation [(a)]

	Duration [s]							Feed data		
No.	**Press**	**Ads**	**Blow**	**Purge**	**P_{high} [kPa]**	**P_{low} [kPa]**	**T [C]**	**V_{STP} [m^3]**	**F [10^6 m^3/s]**	**U [m/s]**
1	15	25	2	3	3.58	1.17	23.5	1.82E-04	3.7278	1.097E-02
2	15	30	2	3	3.58	1.18	22.0	2.18E-04	3.7022	1.090E-02
3	15	35	2	3	3.58	1.17	23.0	2.54E-04	3.7098	1.092E-02
4	15	40	2	3	3.58	1.16	23.5	2.91E-04	3.7252	1.096E-02
5	15	35	2	3	3.58	1.17	24.5	2.18E-04	3.2002	9.418E-03
6	15	35	2	3	3.58	1.17	24.5	2.54E-04	3.7286	1.097E-02
7	15	35	2	3	3.58	1.16	25.5	2.73E-04	4.0210	1.183E-02
8	15	35	2	3	3.58	1.17	25.0	2.91E-04	4.2790	1.259E-02
9	15	35	2	3	3.58	1.19	23.0	3.93E-04	5.7400	1.689E-02
10	15	50	2	3	3.58	1.19	22.0	3.93E-04	4.0044	1.179E-02
11	15	70	2	3	3.58	1.18	22.0	3.93E-04	2.8603	8.418E-03
12	15	100	2	3	3.58	1.19	21.2	3.93E-04	1.9968	5.877E-03
13	15	35	6	3	3.58	1.10	24.0	2.91E-04	4.2646	1.255E-02
14	15	35	10	3	3.58	1.09	24.0	2.91E-04	4.2646	1.255E-02
15	15	35	15	3	3.58	1.07	25.5	2.91E-04	4.2861	1.261E-02
16	15	35	6	3	3.58	1.09	25.0	2.91E-04	4.2790	1.259E-02
17	15	35	6	3	3.58	1.10	27.0	2.91E-04	4.3077	1.268E-02
18	15	35	6	3	3.58	1.11	26.0	2.91E-04	4.2933	1.264E-02
19	15	35	6	3	3.58	1.11	25.5	2.91E-04	4.2861	1.261E-02
20	15	35	2	3	3.58	1.12	25.5	2.91E-04	4.2861	1.261E-02
21	15	35	2	5	3.58	1.10	25.0	2.91E-04	4.2790	1.259E-02
22	15	35	2	8	3.58	1.08	24.2	2.91E-04	4.2675	1.256E-02
23	15	35	2	11	3.58	1.07	24.0	2.91E-04	4.2646	1.255E-02
24	15	35	2	2	3.58	1.15	24.8	3.49E-04	5.1284	1.509E-02
25	15	35	2	5	3.58	1.09	25.8	3.49E-04	5.1456	1.514E-02
26	15	35	2	9	3.58	1.06	26.3	3.49E-04	5.1542	1.517E-02
27	15	35	2	12	3.58	1.05	24.8	3.49E-04	5.1284	1.509E-02
28	11	35	2	3	3.58	1.12	26.7	2.91E-04	4.3034	1.266E-02
29	20	35	2	3	3.58	1.10	25.2	2.91E-04	4.2818	1.260E-02
30	25	35	2	3	3.58	1.13	23.6	2.91E-04	4.2589	1.253E-02
31	15	35	2	3	2.00	1.13	22.3	3.93E-04	10.250	3.017E-02
32	15	35	2	3	3.58	1.23	23.0	3.93E-04	5.7400	1.689E-02
33	15	35	2	3	6.20	1.54	24.5	3.93E-04	3.3312	9.804E-03
34	15	35	2	3	2.00	1.13	22.3	1.31E-04	3.4168	1.006E-02
35	15	35	2	3	6.20	1.52	25.4	6.63E-04	5.6368	1.659E-02
42	15	35	2	3	3.58	1.20	24.0	3.93E-04	5.7594	1.695E-02
43	15	35	2	3	3.58	1.25	24.5	3.93E-04	5.7691	1.698E-02

Table 2.9 Input parameters for the simulation [(b)]

	Purge gas data			Stem positions (for CV=1e-6)			
No.	**V_{STP} [m^3]**	**F [m^3/s]**	**U [m/s]**	**Press**	**Ads Out**	**Blow**	**Purge Out**
1	1.66E-05	8.6697	2.55E-02	0.150	0.0020	0.700	0.300
2	1.66E-05	8.5528	2.52E-02	0.150	0.0020	0.700	0.300
3	1.66E-05	8.6551	2.55E-02	0.150	0.0020	0.700	0.300
4	1.66E-05	8.7445	2.57E-02	0.150	0.0020	0.700	0.300
5	1.66E-05	8.6990	2.56E-02	0.150	0.00172	0.700	0.300
6	1.66E-05	8.6990	2.56E-02	0.150	0.00200	0.700	0.300
7	1.66E-05	8.8035	2.59E-02	0.150	0.00215	0.700	0.300
8	1.66E-05	8.7136	2.56E-02	0.150	0.00229	0.700	0.300
9	1.66E-05	8.5096	2.50E-02	0.150	0.0045	0.700	0.300
10	1.66E-05	8.4809	2.50E-02	0.150	0.0032	0.700	0.300
11	1.66E-05	8.5528	2.52E-02	0.150	0.0023	0.700	0.300
12	1.66E-05	8.4579	2.49E-02	0.150	0.0016	0.700	0.300
13	1.66E-05	9.2370	2.72E-02	0.150	0.0020	0.700	0.300
14	1.66E-05	9.3217	2.74E-02	0.150	0.0020	0.700	0.300
15	1.66E-05	9.5439	2.81E-02	0.150	0.0020	0.700	0.300
16	1.66E-05	9.3531	2.75E-02	0.150	0.0023	0.700	0.300
17	3.09E-05	17.368	5.11E-02	0.150	0.0023	0.700	0.558
18	4.39E-05	24.371	7.17E-02	0.150	0.0023	0.700	0.793
19	6.02E-05	33.364	9.82E-02	0.150	0.0023	0.700	1.088
20	1.66E-05	9.1179	2.68E-02	0.150	0.0023	0.700	0.300
21	2.76E-05	9.2458	2.72E-02	0.150	0.0023	0.700	0.299
22	4.42E-05	9.4002	2.77E-02	0.150	0.0023	0.700	0.300
23	6.07E-05	9.4700	2.79E-02	0.150	0.0023	0.700	0.299
24	4.39E-05	35.143	1.03E-01	0.150	0.0027	0.700	1.190
25	4.39E-05	14.881	4.38E-02	0.150	0.0027	0.700	0.476
26	4.39E-05	8.5154	2.51E-02	0.150	0.0027	0.700	0.264
27	4.39E-05	6.4150	1.89E-02	0.150	0.0027	0.700	0.198
28	1.66E-05	9.1545	2.69E-02	0.150	0.0023	0.700	0.300
29	1.66E-05	9.2743	2.73E-02	0.150	0.0023	0.700	0.300
30	1.66E-05	8.9797	2.64E-02	0.150	0.0023	0.700	0.300
31	1.66E-05	8.9403	2.63E-02	0.150	0.0055	0.700	0.300
32	1.66E-05	8.2329	2.42E-02	0.150	0.0031	0.700	0.300
33	1.66E-05	6.6090	1.95E-02	0.150	0.0018	0.700	0.300
34	1.66E-05	8.9403	2.63E-02	0.150	0.0018	0.700	0.300
35	1.66E-05	6.7162	1.98E-02	0.150	0.0030	0.700	0.300
42	1.66E-05	8.4672	1.98E-02	0.150	0.0045	0.700	0.300
43	1.66E-05	8.1422	1.98E-02	0.150	0.0045	0.700	0.300

Table 2.10 Comparison of the experimental and simulation results

	Recovery, %			Purity, %			Power, W
No.	**Exp. data**	**Shin & Knaebel**	**This work**	**Exp. data**	**Shin & Knaebel**	**This work**	**This work**
1	6.44	6.38	6.96	99.75	100.00	99.31	6.18
2	8.16	8.64	8.50	99.55	99.89	98.92	5.63
3	10.65	10.92	9.94	99.00	99.09	98.55	5.31
4	12.39	12.15	11.30	98.35	98.59	98.15	5.01
5	7.07	8.25	8.52	99.60	99.88	98.95	5.18
6	9.41	9.85	9.95	98.85	99.41	98.54	5.31
7	11.67	11.72	10.72	98.30	98.77	98.33	5.45
8	12.99	12.13	11.41	97.80	98.49	98.11	5.46
9	25.84	17.02	21.23	90.80	95.39	94.47	5.52
10	21.36	16.09	21.21	90.70	96.23	94.75	4.54
11	22.74	15.50	21.20	91.40	96.18	94.78	3.57
12	22.18	22.74	21.08	91.20	96.02	94.77	2.64
13	9.39	8.35	8.45	98.25	99.70	99.74	6.20
14	7.40	6.32	7.85	98.90	99.82	99.91	6.19
15	5.10	5.00	7.38	99.00	99.88	99.97	6.12
16	9.19	8.59	9.82	98.45	99.63	99.60	6.29
17	7.07	7.62	8.56	98.50	99.76	99.79	6.26
18	6.43	6.99	7.42	98.70	99.83	99.89	6.19
19	5.41	6.13	6.12	98.80	99.93	99.96	6.65
20	11.51	12.44	11.28	97.95	98.71	98.25	5.79
21	9.72	9.67	9.43	98.50	99.42	99.40	6.12
22	6.74	6.59	7.26	98.85	99.79	99.91	6.33
23	3.37	4.08	5.46	99.00	99.96	99.99	6.33
24	16.63	14.33	10.86	95.85	97.47	98.69	5.85
25	10.76	11.55	9.62	96.80	98.72	99.57	6.52
26	8.57	8.47	8.81	97.30	99.15	99.84	6.69
27	8.26	7.21	8.44	97.65	99.10	99.91	6.62
28	7.35	8.56	11.35	98.75	99.87	98.22	6.11
29	11.95	14.27	11.17	97.70	97.92	98.31	5.50
30	13.30	16.07	11.20	97.00	96.57	98.24	4.89
31	41.56	37.64	26.38	82.30	82.27	89.23	1.46
32	22.46	16.07	15.11	93.70	94.97	96.70	5.45
33	12.54	8.00	8.99	98.20	100.00	99.06	12.62
34	13.83	13.09	9.86	93.80	94.45	96.06	0.99
35	23.05	16.73	14.25	93.70	97.58	97.75	14.13
42	22.40	16.46	20.51	89.00	94.40	94.96	5.95
43	22.37	16.15	20.06	82.30	89.72	90.12	5.42

Table 2.11 Absolute deviations from the experimental data

	In recovery, %		In purity, %	
No.	**Shin & Knaebel**	**This work**	**Shin & Knaebel**	**This work**
1	-0.06	0.52	0.25	-0.44
2	0.48	0.34	0.34	-0.63
3	0.27	-0.71	0.09	-0.45
4	-0.24	-1.09	0.24	-0.20
5	1.18	1.45	0.28	-0.65
6	0.44	0.54	0.56	-0.31
7	0.05	-0.95	0.47	0.03
8	-0.86	-1.58	0.69	0.31
9	-8.82	-4.61	4.59	3.67
10	-5.27	-0.15	5.53	4.05
11	-7.24	-1.54	4.78	3.38
12	0.56	-1.10	4.82	3.57
13	-1.04	-0.94	1.45	1.49
14	-1.08	0.45	0.92	1.01
15	-0.10	2.28	0.88	0.97
16	-0.60	0.63	1.18	1.15
17	0.55	1.49	1.26	1.29
18	0.56	0.99	1.13	1.19
19	0.72	0.71	1.13	1.16
20	0.93	-0.23	0.76	0.30
21	-0.05	-0.29	0.92	0.90
22	-0.15	0.52	0.94	1.06
23	0.71	2.09	0.96	0.99
24	-2.30	-5.77	1.62	2.84
25	0.79	-1.14	1.92	2.77
26	-0.10	0.24	1.85	2.54
27	-1.05	0.18	1.45	2.26
28	1.21	4.00	1.12	-0.53
29	2.32	-0.78	0.22	0.61
30	2.77	-2.10	-0.43	1.24
31	-3.92	-15.18	-0.03	6.93
32	-6.39	-7.35	1.27	3.00
33	-4.54	-3.55	1.80	0.86
34	-0.74	-3.97	0.65	2.26
35	-6.32	-8.80	3.88	4.05
42	-5.94	-1.89	5.40	5.96
43	-6.22	-2.31	7.42	7.82
Max negative deviation, %	**-8.82**	**-15.18**	**-0.43**	**-0.65**
Max positive deviation, %	**2.77**	**4.00**	**7.42**	**7.82**
Overall average deviation, %	**2.52**	**2.23**	**1.81**	**1.97**

Table 2.12 Overall average absolute deviations from the experimental data

Overall average absolute deviation	Shin and Knaebel	This work
In purity	1.81%	1.97%
In recovery	2.52%	2.23%

2.5.1.1. Effects of adsorption step duration for fixed feed velocity

The amount of feed is increased proportionally to the duration in order to ensure a constant feed velocity at inlet of the bed. All the other parameters have been kept constant.

Experimental and simulation results are given in Figure 2.13, Figure 2.14 and Figure 2.15. The results indicate that the product purity decreases as the adsorption step duration increases while the opposite trend hold for the product recovery. This verifies the trade-off between purity and recovery in diffusion based separations.

Simulation results of this work and Shin and Knaebel (1988) work are in good agreement with the experimental data. However, purities predicted by both models are slightly higher than experimental. Absolute deviations from the experimental data are summarized in the Table 2.13.

The power requirement per one cycle decreases as the adsorption step duration increases although the amount of feed increases. However, the total energy consumption for one cycle increases as the amount of feed increases.

Table 2.13 Absolute deviations from the experimental data

Average absolute deviation	Shin and Knaebel	This work
In purity	0.23%	0.43%
In recovery	0.26%	0.67%

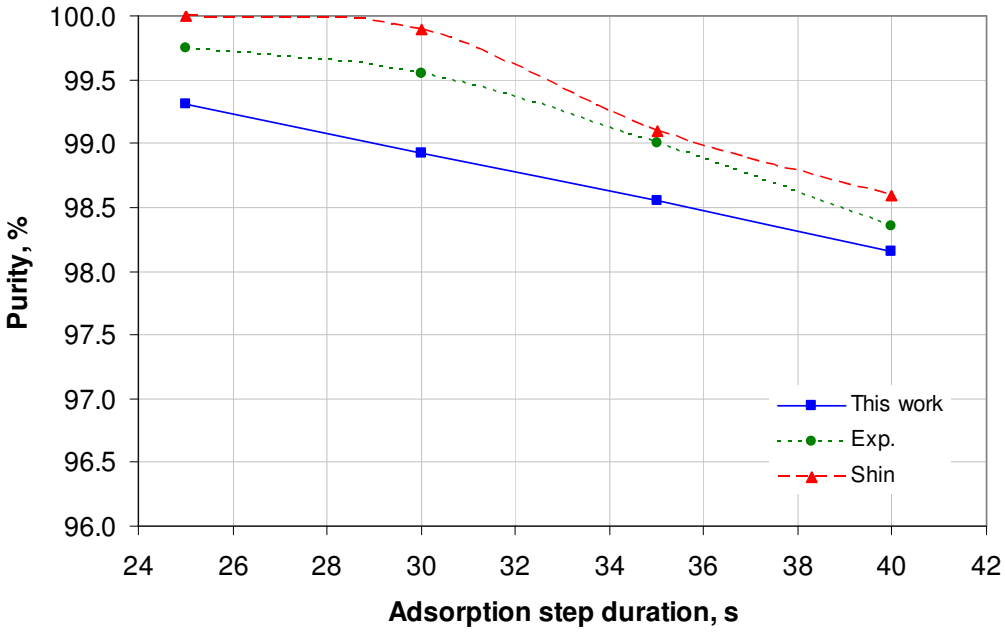

Figure 2.13 Effects of adsorption step duration for fixed feed velocity on N_2 purity

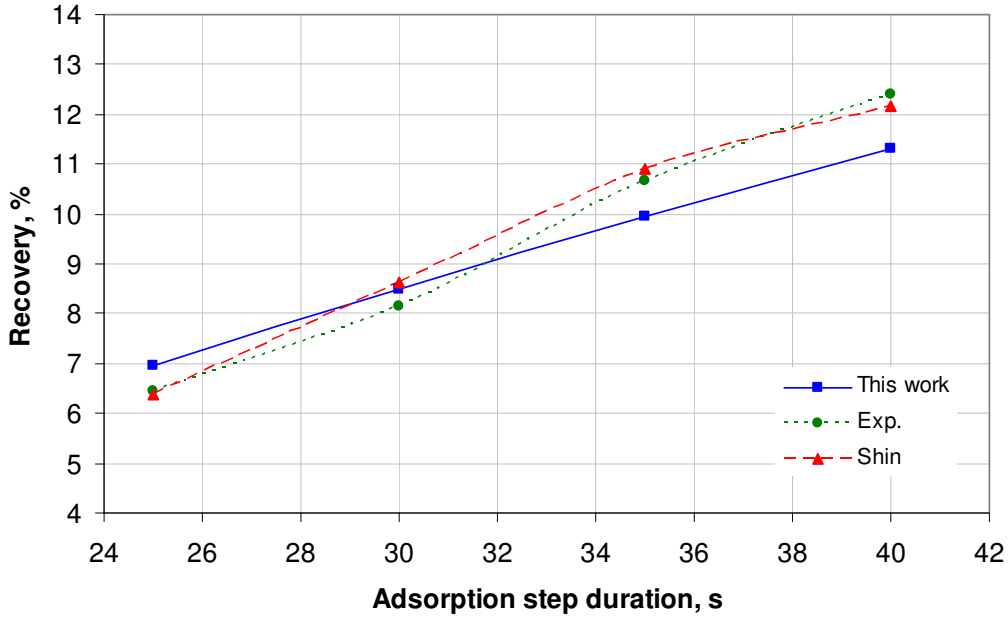

Figure 2.14 Effects of adsorption step duration for fixed feed velocity on N_2 recovery

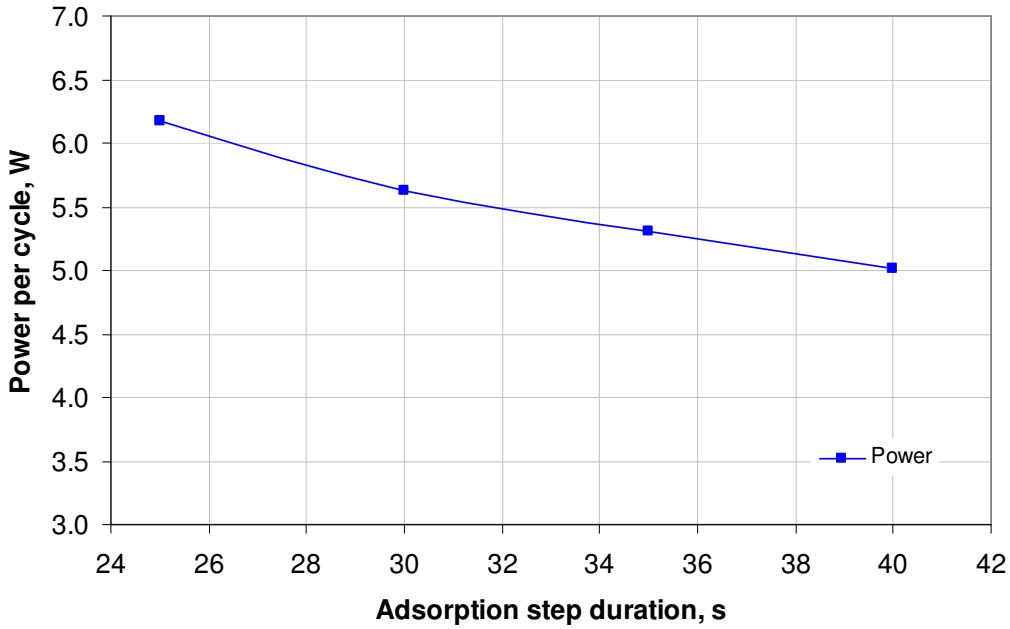

Figure 2.15 Effects of adsorption step duration for fixed feed velocity on power requirements per cycle

2.5.1.2. Effects of feed velocity for a fixed duration of adsorption step

In this section, effects of feed velocity on the separation quality have been investigated. All the other parameters have been kept constant.

Experimental and simulation results are given in Figure 2.16 and Figure 2.17. The results show the same trend as in the previous case.

The simulation results of both Shin and Knaebel and this work in terms of purity and recovery are in good agreement with the experimental data. Absolute deviations from experimental data are summarized in Table 2.14.

Table 2.14 Absolute deviations from the experimental data

Average absolute deviation	Shin and Knaebel	This work
In purity	0.50%	0.32%
In recovery	0.63%	1.13%

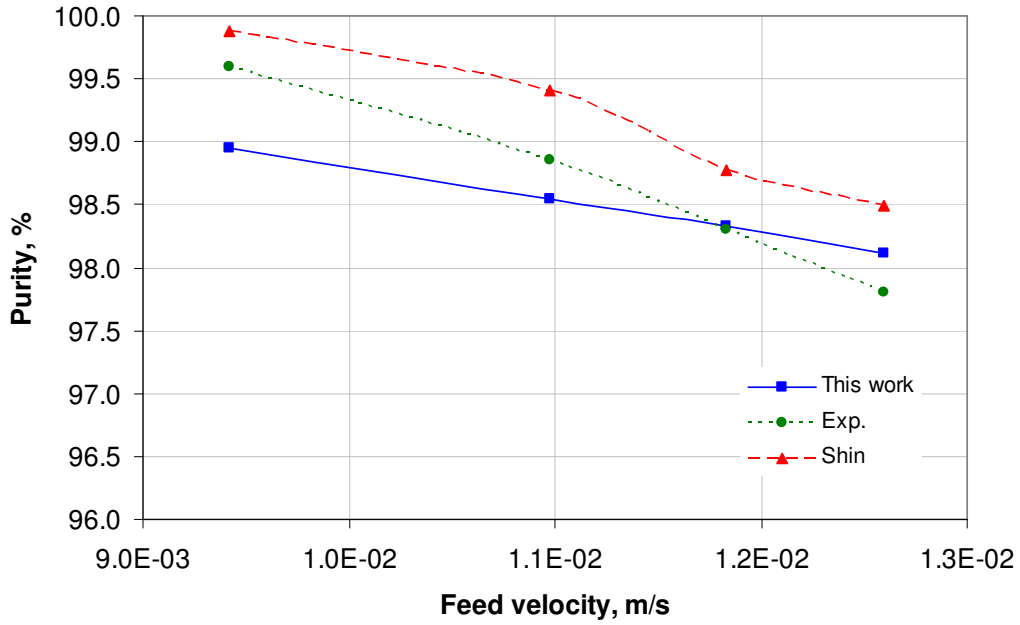

Figure 2.16 Effects of feed velocity for a fixed duration of adsorption step on N_2 purity

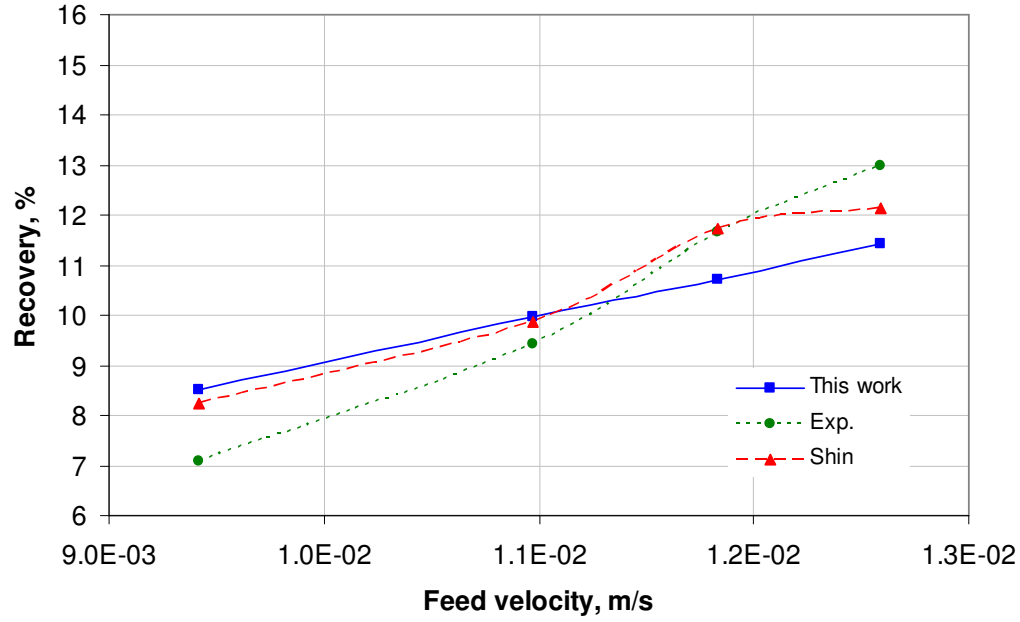

Figure 2.17 Effects of feed velocity for a fixed duration of adsorption step on N_2 recovery

2.5.1.3. Effects of adsorption step duration for a fixed amount of feed

Here the effect of adsorption step duration has been investigated for a fixed amount of feed. All the other parameters have been kept constant.

Experimental and simulation results are shown in Figure 2.18, Figure 2.19 and Figure 2.20. The results indicate that the product purity increased with the adsorption step duration (for longer adsorption steps the components have more available time to diffuse thus resulting in better separation). This is also the case for product recovery.

Shin and this work simulation results, are in acceptable agreement with the experimental data. However, purities predicted by this work are higher and recoveries are lower compared to experimental. Absolute deviations are summarized in Table 2.15.

The power requirement per one cycle is depicted in Figure 2.20. As the feed step duration increases the power consumption over one cycle decreases.

Table 2.15 Absolute deviations from the experimental data

Average absolute deviation	Shin and Knaebel	This work
In purity	4.93%	5.89%
In recovery	5.47%	8.12%

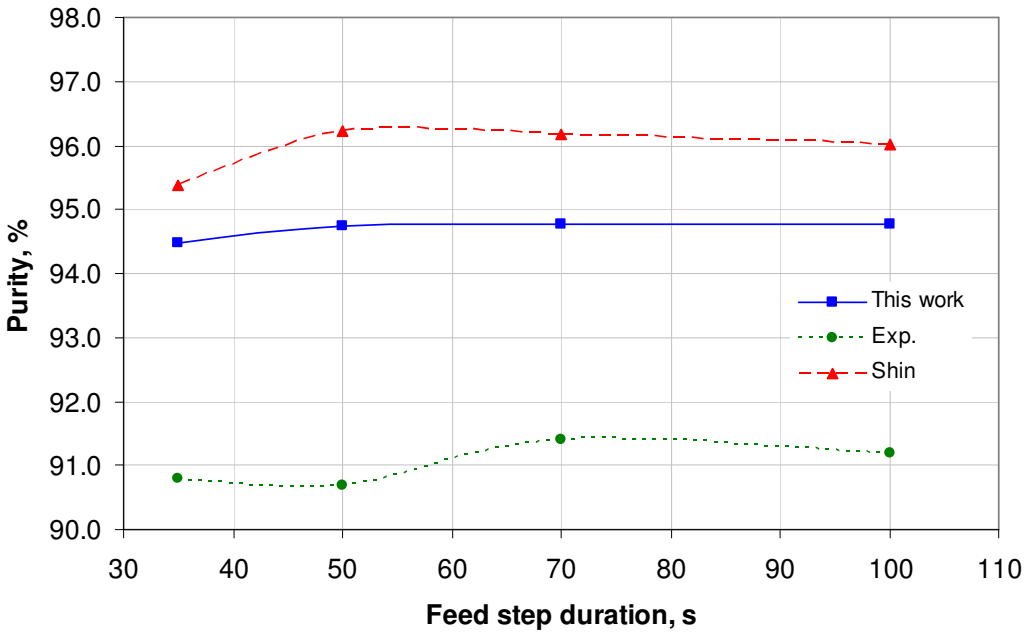

Figure 2.18 Effects of adsorption step duration for a fixed amount of feed on N_2 purity

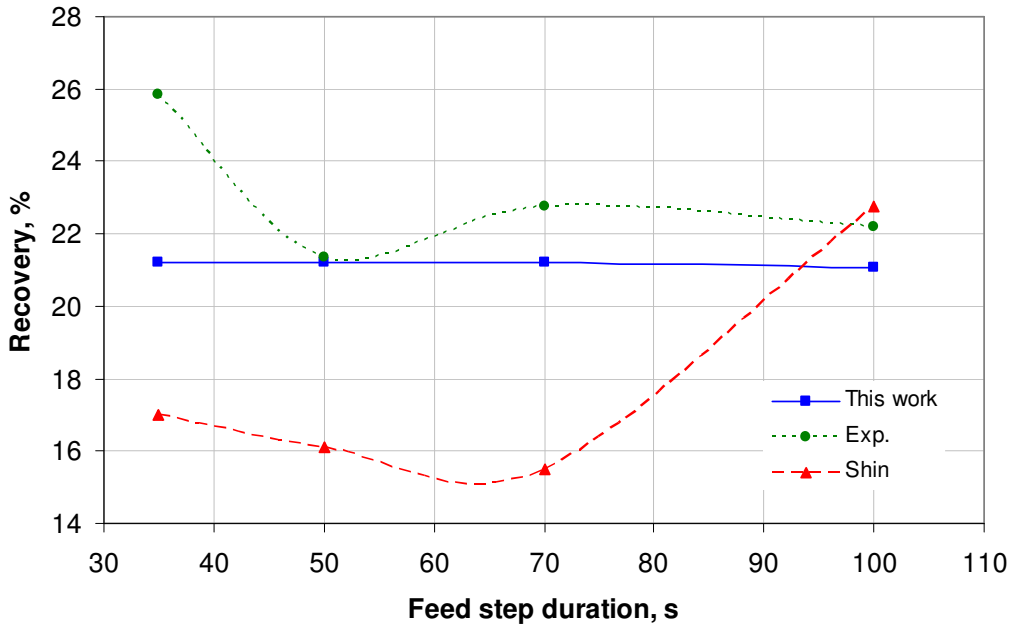

Figure 2.19 Effects of adsorption step duration for a fixed amount of feed on N_2 recovery

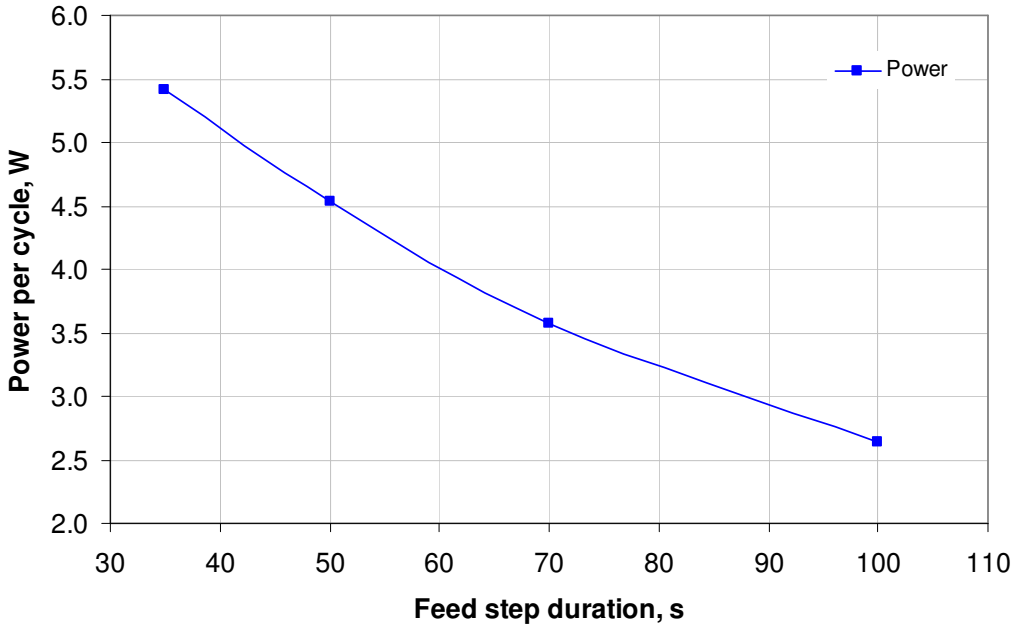

Figure 2.20 Effects of adsorption step duration for a fixed amount of feed on power requirements per cycle

2.5.1.4. Effects of blowdown step duration

In this case the effect of blowdown step duration is investigated for a fixed amount of feed and purge gas. All the other parameters have been kept constant.

Experimental and simulation results are shown in Figure 2.21 and Figure 2.22. The results indicate a small increase in product purity. This can be attributed to the fact that since a higher amount of gas leaves the bed during blowdown a better cleaning of the bed is achieved. On the other hand, product recovery decreases as the blowdown step duration increases. This can be attributed to the longer blowdown time which results in a higher amount of gas to be directed to the waste stream. The model predicts well the overall behaviour of the process when the blowdown time increases. Absolute deviations from experimental data are summarized in Table 2.16.

Table 2.16 Absolute deviations from the experimental data

Average absolute deviation	Shin and Knaebel	This work
In purity	1.08%	1.16%
In recovery	0.74%	1.22%

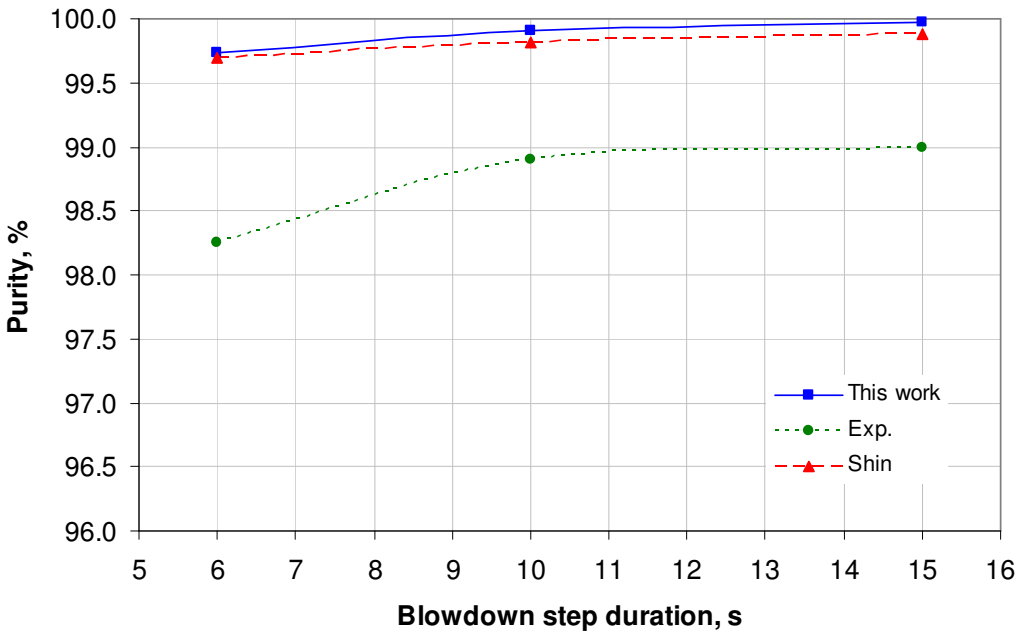

Figure 2.21 Effects of blowdown step duration on N_2 purity

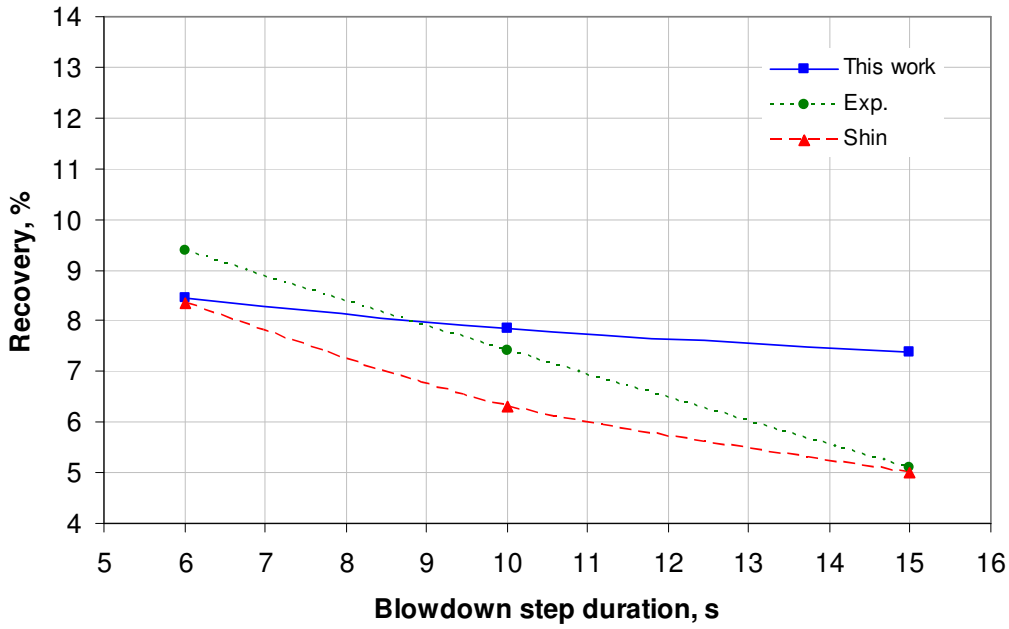

Figure 2.22 Effects of blowdown step duration on N_2 recovery

2.5.1.5. Effects of velocity of purge gas for fixed purge step duration

Here influence of purge gas velocity for fixed purge step duration is investigated. All the other parameters have been kept constant.

Experimental and simulation results are given in Figure 2.23, Figure 2.24 and Figure 2.25. The results show a small increase in product purity (larger amount of the purge gas causes better cleaning of the bed) and decrease in product recovery (higher amount of gas leaves the column with the waste stream). Absolute deviations are summarized in Table 2.17.

Table 2.17 Absolute deviations from the experimental data

Average absolute deviation	Shin and Knaebel	This work
In purity	1.18%	1.20%
In recovery	0.61%	0.96%

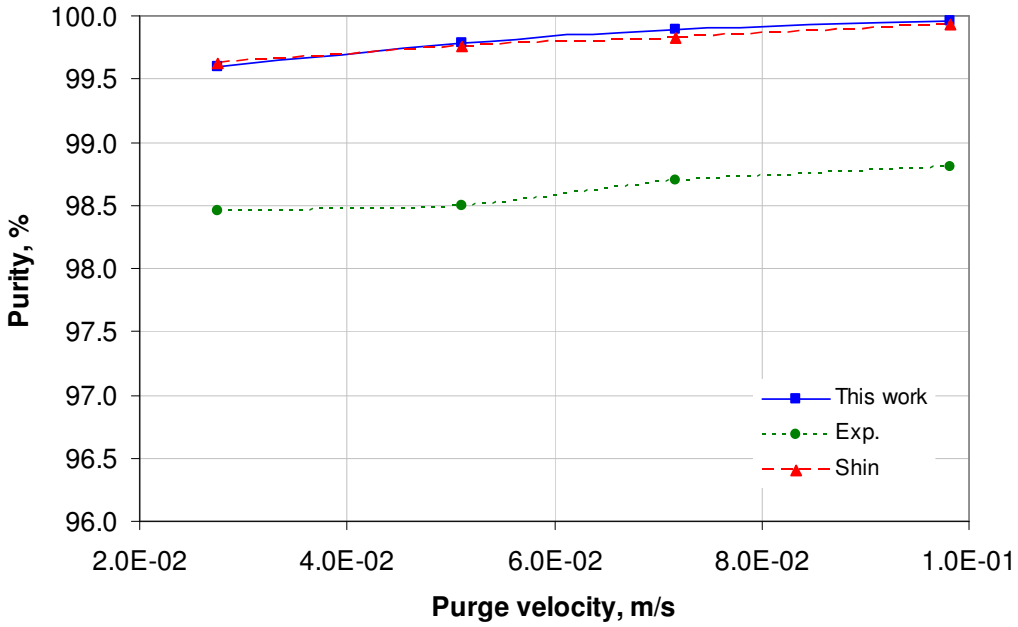

Figure 2.23 Effects of velocity of purge gas for fixed purge step duration on N_2 purity

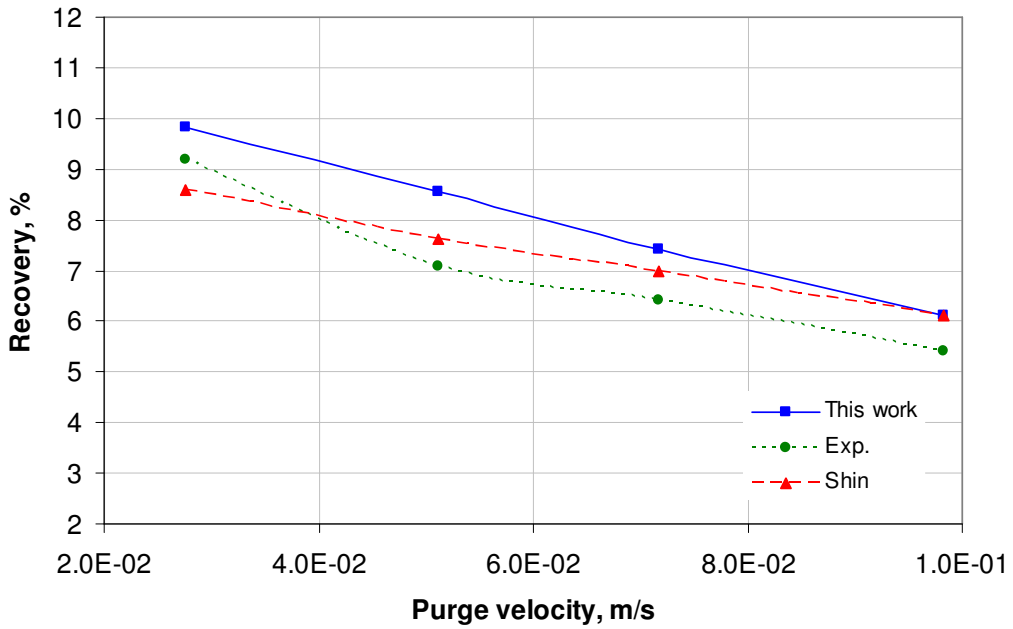

Figure 2.24 Effects of velocity of purge gas for fixed purge step duration on N_2 recovery

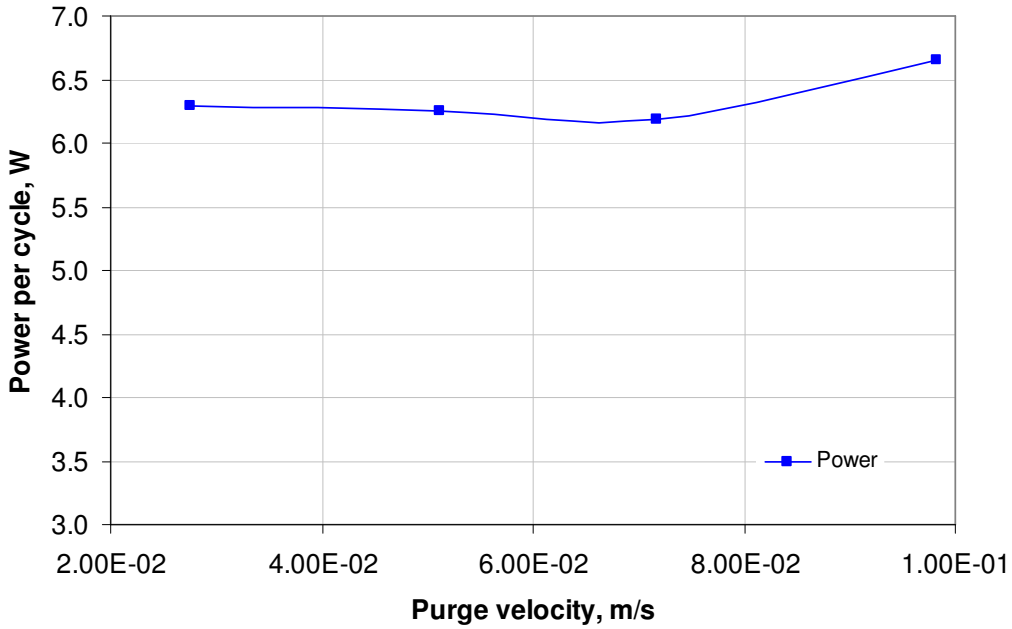

Figure 2.25 Effects of velocity of purge gas for fixed purge step duration on power requirements per cycle

2.5.1.6. Effects of purge step duration for fixed purge gas velocity

Here the influence of purge gas velocity for a fixed purge gas velocity is investigated. All the other parameters were kept constant.

Experimental and simulation results are depicted in Figure 2.26 and Figure 2.27. The results illustrate that the product purity increases as the step duration increases due to the higher amount of purge gas which leads to a cleaned bed. On the other hand, the product recovery decreases with the purge step duration due to the higher amount of gas leaving the column as a waste stream. The model predicts very well the behaviour of the system, and the simulation results are in very good agreement with the experimental. Absolute deviations from experimental data are given in Table 2.18.

Table 2.18 Absolute deviations from the experimental data

Average absolute deviation	Shin and Knaebel	This work
In purity	0.90%	0.81%
In recovery	0.46%	0.78%

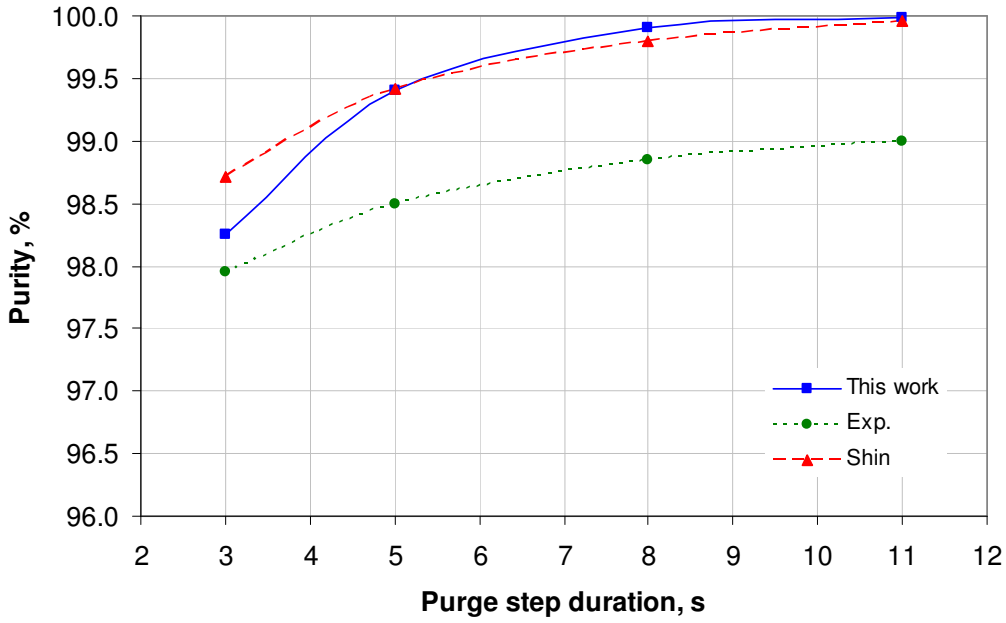

Figure 2.26 Effects of purge step duration for fixed purge gas velocity on N_2 purity

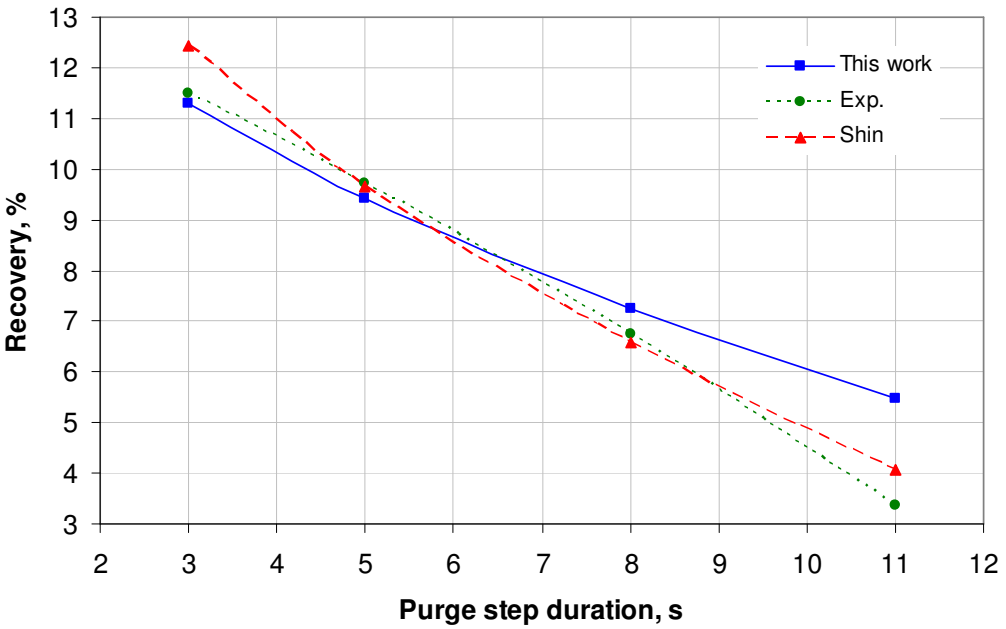

Figure 2.27 Effects of purge step duration for fixed purge gas velocity on N_2 recovery

2.5.1.7. Effects of purge step duration for a fixed amount of purge gas

Experimental and simulation results are shown in Figure 2.28 and Figure 2.29. The results illustrate that product purity increases with the purge step duration since more time is available for the gas to be desorbed and then diffuse out of the particles. Product recovery decreases with the purge step duration since higher amount of gas leaves the column as a waste stream. The simulation results are in very good agreement with the experimental data. Absolute deviations from experimental data are given in Table 2.19.

Table 2.19 Absolute deviations from the experimental data

Average absolute deviation	Shin and Knaebel	This work
In purity	1.71%	2.60%
In recovery	1.06%	1.73%

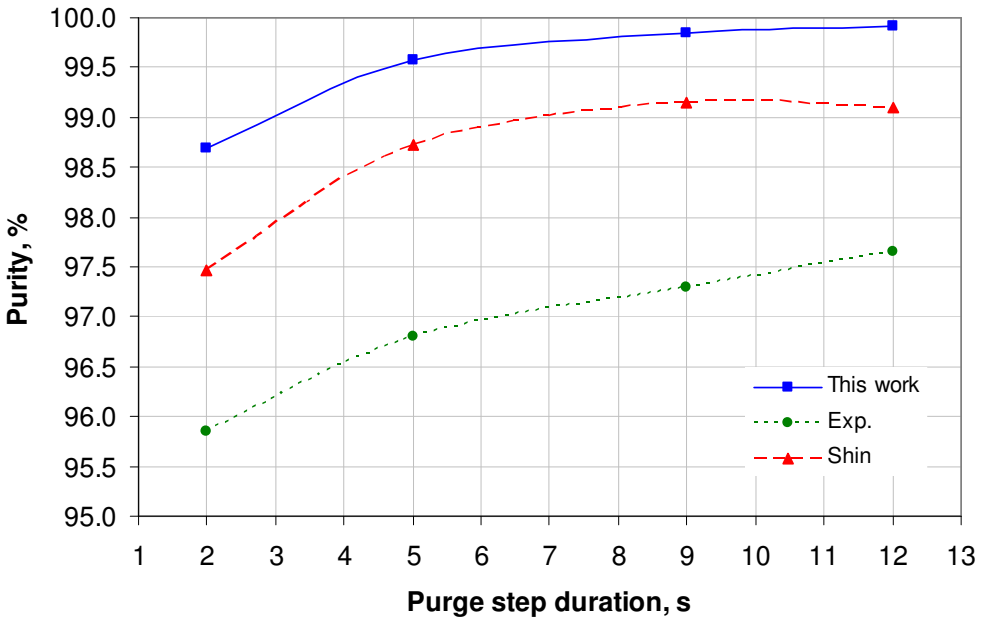

Figure 2.28 Effects of purge step duration for a fixed amount of purge gas on N_2 purity

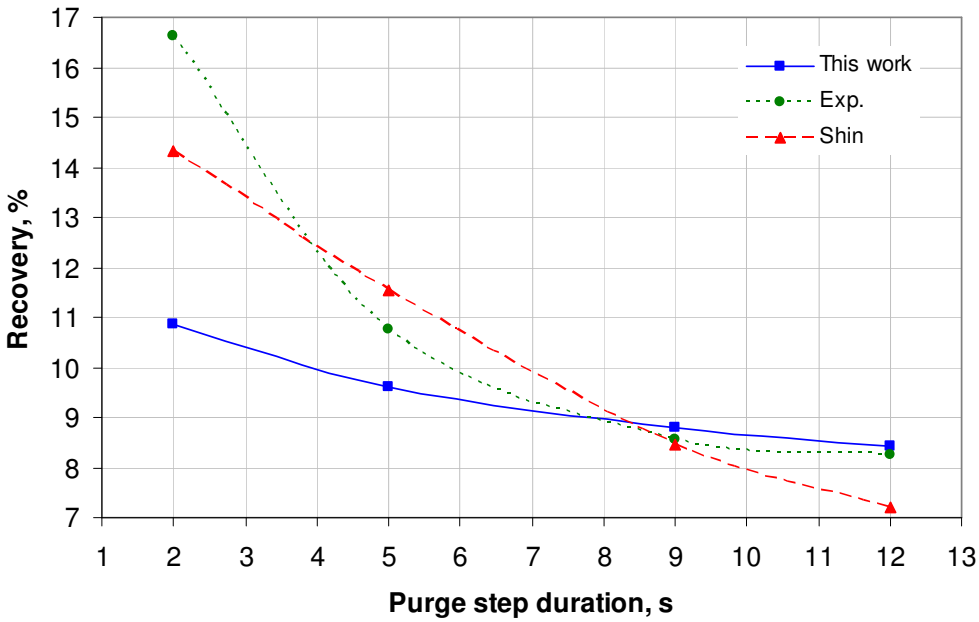

Figure 2.29 Effects of purge step duration for a fixed amount of purge gas on N_2 recovery

2.5.1.8. Effects of pressurization step duration

Experimental and simulation results are given in Figure 2.30, Figure 2.31 and Figure 2.32. It is expected that the product purity decreases as the duration of pressurization step increases since more feed enters the column. On the other hand, the product recovery increases (because more product is produced). However, simulation results show no significant change in both the product purity and recovery. This can be attributed to the response of the gas valve. Flow through the valve is proportional to its pressure drop. When the final pressure is achieved, there is no flow through the valve. Since the feed is continuously consumed by the adsorbent the flow is never zero. However, the system does not illustrate any effect due to the increased pressurization time. Also, the values of the gas valve coefficient / stem position which controls the feed inlet are chosen as quite high and analysis shows that the column reaches 90% of the final pressure in the first few seconds. Hence, the system does not react on the pressurization time changes within an observed time interval. Absolute deviations from experimental data are given in Table 2.20.

Table 2.20 Absolute deviations from the experimental data

Average absolute deviation	Shin and Knaebel	This work
In purity	0.59%	0.79%
In recovery	2.10%	2.29%

The power consumption per one cycle decreases with the pressurization time. The total energy necessary for one cycle remains almost constant.

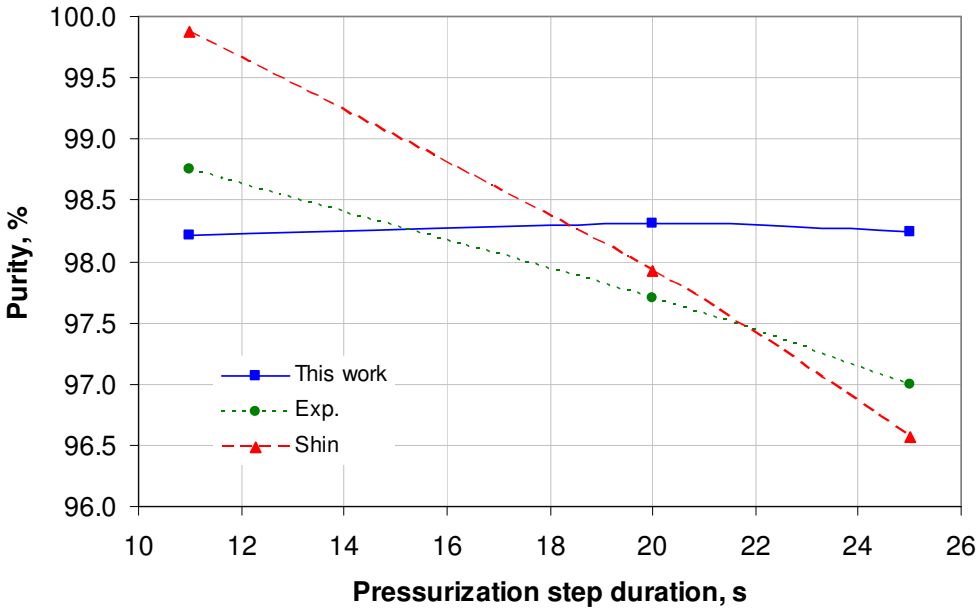

Figure 2.30 Effects of pressurization step duration on N_2 purity

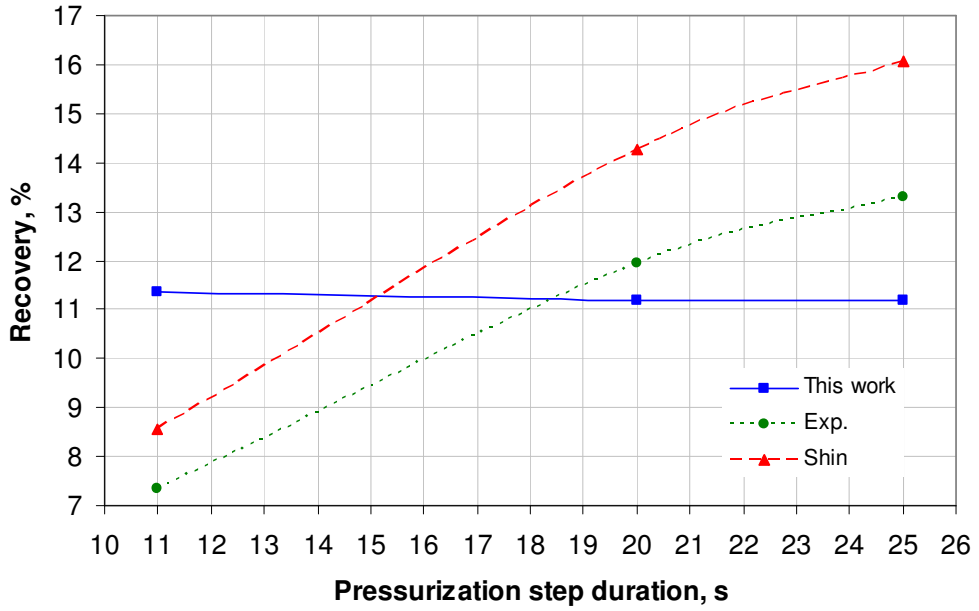

Figure 2.31 Effects of pressurization step duration on N_2 recovery

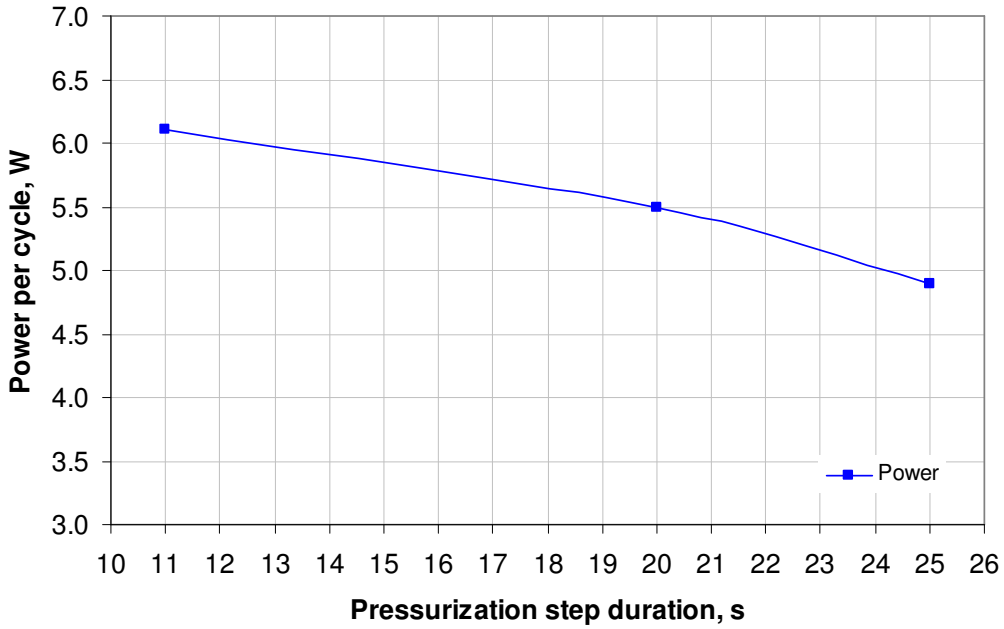

Figure 2.32 Effects of pressurization step duration on power requirements per cycle

2.5.1.9. Effects of the feed to the purge gas pressure ratio

In this set of experiments, the effect of feed to purge gas pressure ratio is investigated assuming the other parameters are kept constant.

Experimental and simulation results are shown in Figure 2.33, Figure 2.34 and Figure 2.35. It is seen that the product purity increases with the feed pressure which is according to the theory for linear adsorption isotherms. Product recovery decreases with the feed pressure since during the blowdown step more gas leaves the bed. Absolute deviations from experimental data are given in Table 2.21.

The power requirements per one cycle increase (for compression of the feed to the higher pressures).

Table 2.21 Absolute deviations from the experimental data

Average absolute deviation	Shin and Knaebel	This work
In purity	1.53%	3.42%
In recovery	4.38%	7.77%

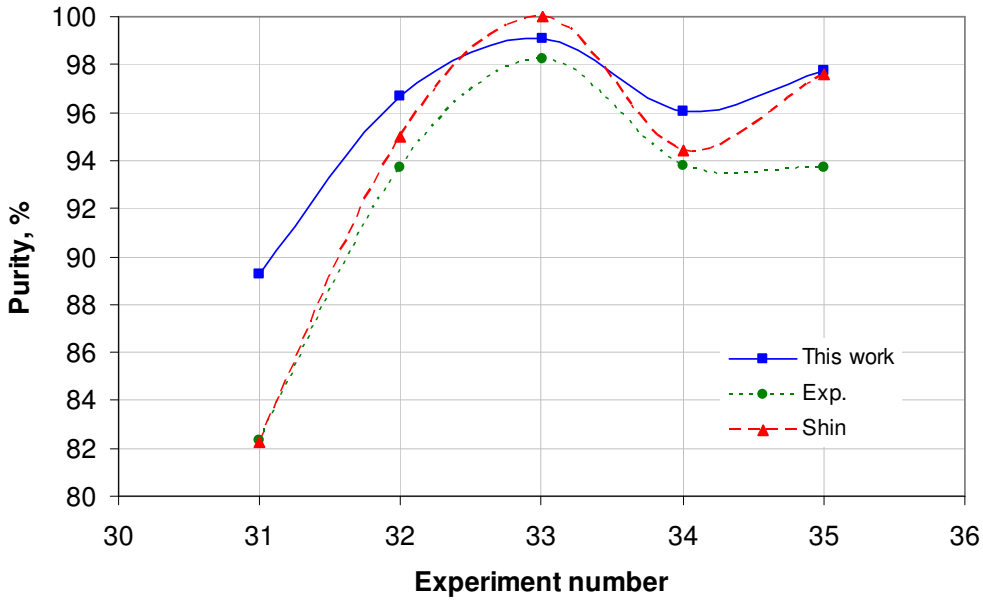

Figure 2.33 Effects of the feed to the purge gas pressure ratio on N_2 purity

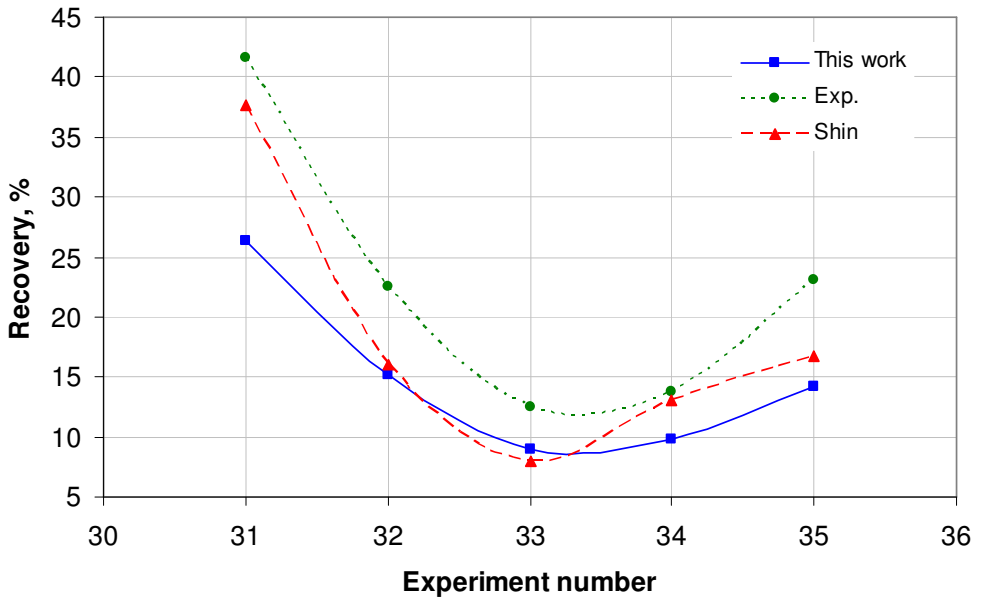

Figure 2.34 Effects of the feed to the purge gas pressure ratio on N_2 recovery

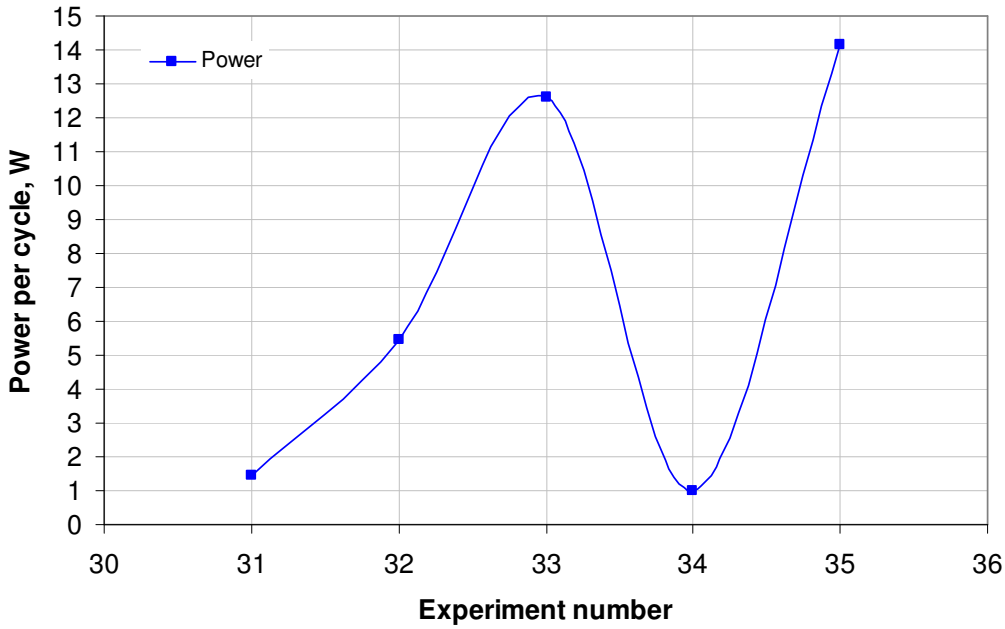

Figure 2.35 Effects of the feed to the purge gas pressure ratio on power requirements per cycle

2.5.1.10. Effects of column geometry

In this case, the effect of length to diameter ratio is investigated. All the other parameters are kept constant.

Experimental and simulation results are given in Figure 2.36 and Figure 2.37. Length/diameter ratios were 48.846, 7.208 and 1.716, respectively. The results indicate that a column with a low L/d ratio gives poorer separation (lower purity and lower recovery). Due to the larger bed diameter, interstitial velocities are lower, thus resulting in lower Pecklet number. As it was illustrated by Shin and Knaebel (1987), there is a slight compensation due to increase in the axial dispersion coefficient, which imposes an increase in the Pecklet number, but this effect is not significant in comparison with the effect of velocity on Pecklet number. On the other hand, shorter bed length results in a sooner of the breakthrough. Absolute deviations from experimental data are given in Table 2.22.

Table 2.22 Absolute deviations from the experimental data

Average absolute deviation	Shin and Knaebel	This work
In purity	6.41%	6.89%
In recovery	6.08%	2.10%

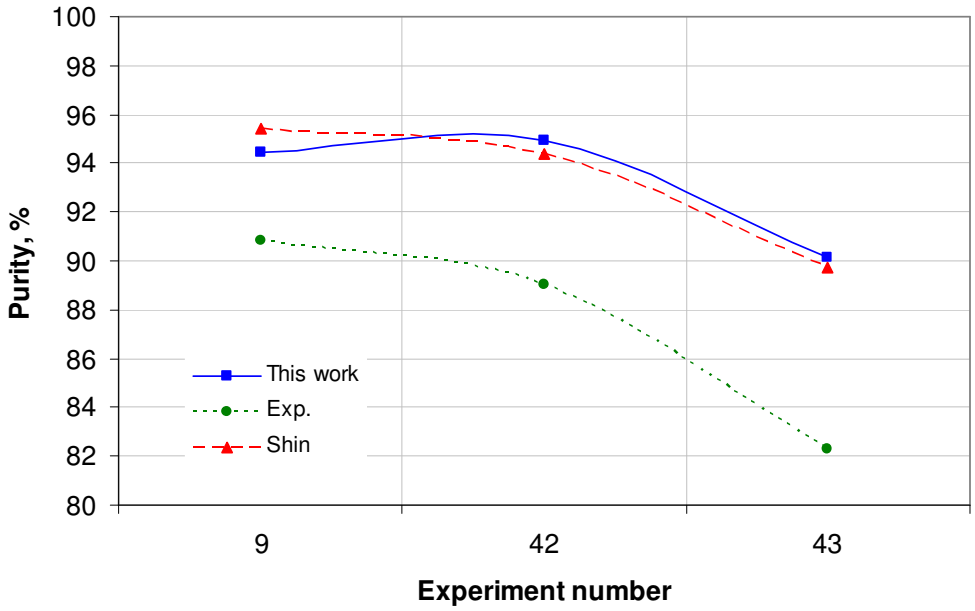

Figure 2.36 Effects of column geometry on N_2 purity

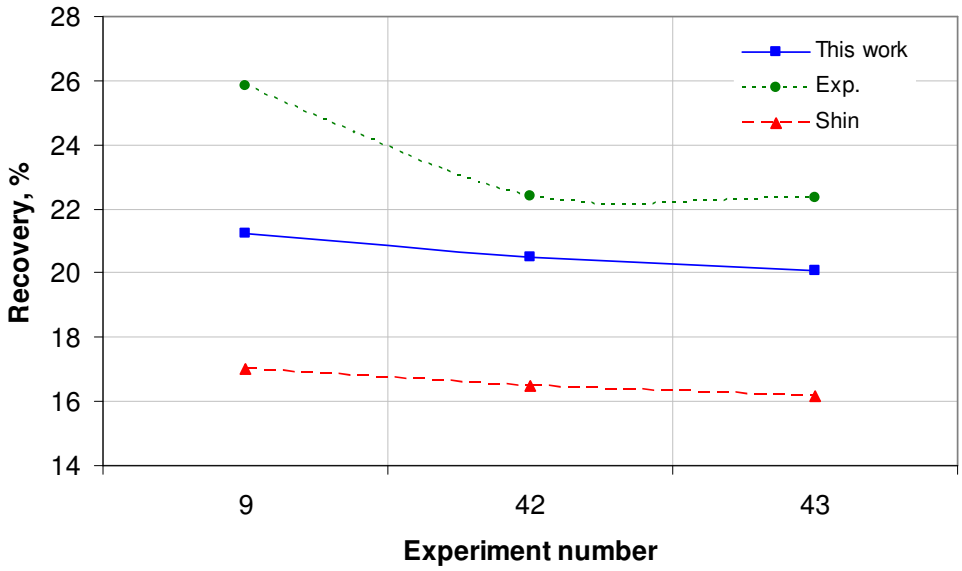

Figure 2.37 Effects of column geometry on N_2 recovery

2.5.2. Equilibrium controlled separation

In this section, the developed modelling framework has been applied on the equilibrium-controlled process of oxygen production from air using zeolite 5A, investigated in the work of Nilchan and Pantelides (1998). The authors used single-bed Rapid Pressure Swing Adsorption (rPSA) process, which offers a very simple configuration and quite high adsorbent productivity (due to very short cycle time). As in the original work, the linear driving force (LDF) approximation has been employed to describe the mass transfer within adsorbent particles.

Nilchan and Pantelides have investigated the effect of four parameters on the purity and recovery of O_2:

- Particle radius
- Feed pressure
- Cycle time
- Column length

The effective diffusivity, axial dispersion coefficient and the design characteristics of the adsorbent and packed bed are adopted from the work of Nilchan and Pantelides (1998) and given in Table 2.23. Phase equilibrium is given as a linear function of gas phase concentration (Henry's law). The axial domain is discretized using orthogonal collocation on finite elements of third order with 50 elements (both in Nilchan and Pantelides and in this work). The column is initially at atmospheric pressure (1 bar) and saturated with air (79% of nitrogen and 21% of oxygen). The target is to separate oxygen from an air stream using zeolite 5A. Here nitrogen is the preferably adsorbed component. The rPSA configuration consists of one bed and two operating steps (pressurization with feed and counter-current depressurization). Since the bed end at z=L is open all time, the rPSA process exhibits self-purging features as explained in Nilchan and Pantelides (1998).

Table 2.23 Parameters for rPSA simulation

Property	Value	Units
Pore diameter	$0.12\ 10^{-6}$	m
Axial dispersion coefficient	10^{-3}	m^2/s
Adsorbent void fraction	0.55	-
Bed void fraction	0.35	-
Bed bulk density	800	kg/m^3
Particle tortuosity factor	3	-
Adsorption isotherm O_2	1.43×10^{-6}	mol/(kg Pa)
Adsorption isotherm N_2	3.08×10^{-6}	mol/(kg Pa)
Atmospheric pressure	1	bar
Exhaust pressure	1	bar
Product delivery rate at P_{atm}	10^{-5}	m^3/s
Gas viscosity	1.8×10^{-5}	Pas

The comparison of simulation results is given in Table 2.24. The overall absolute deviation of the results of Nilchan and Pantelides from the ones obtained in this work is 4.42% in product purity.

Table 2.24 Comparison of simulation results

		This work			Nilchan and Pantelides (1998)*	Absolute deviation
No.	**P_{feed}, Pa**	**Purity, %**	**Recovery, %**	**Power, W**	**Purity, %**	**Purity, %**
1	1.60E+05	66.13	6.23	25.45	62.00	4.13
2	1.80E+05	80.71	5.46	45.09	76.00	4.71
3	2.00E+05	89.19	4.65	70.16	85.00	4.19
4	2.12E+05	92.21	4.20	87.73	89.35	2.86
5	2.20E+05	93.69	3.93	100.48	91.00	2.69
6	2.40E+05	96.09	3.35	135.98	94.00	2.09
No.	**R_p, m**	**Purity, %**	**Recovery, %**	**Power, W**	**Purity, %**	**Purity, %**
7	1.00E-04	71.58	5.04	56.73	67.00	4.58
8	1.50E-04	92.21	4.20	87.73	89.35	2.86
9	2.00E-04	96.85	3.21	120.51	93.00	3.85
10	2.50E-04	97.36	2.54	153.29	87.00	10.36
No.	**Length, m**	**Purity, %**	**Recovery, %**	**Power, W**	**Purity, %**	**Purity, %**
11	0.6	81.20	3.55	91.39	83.00	-1.8
12	0.7	86.32	3.80	90.77	87.00	-0.68
13	0.8	89.44	3.99	89.57	88.80	0.64
14	0.9	91.24	4.12	88.48	89.50	1.74
15	1.0	92.21	4.20	87.73	89.35	2.86
16	1.1	92.72	4.25	87.31	88.30	4.42
17	1.2	92.91	4.26	87.14	87.40	5.51
18	1.3	92.94	4.27	87.11	85.80	7.14
19	1.4	92.89	4.26	87.15	84.00	8.89
20	1.5	92.79	4.25	87.20	82.10	10.69
No.	**τ_{cycle}, s**	**Purity, %**	**Recovery, %**	**Power, W**	**Purity, %**	**Purity, %**
21	2	93.71	3.51	106.68	86.30	7.41
22	3	92.21	4.20	87.73	89.35	2.86
21	4	89.96	4.68	76.91	87.30	2.66
21	5	87.39	5.02	69.58	82.80	4.59

* Values for product purities are taken from diagrams. Therefore, they could slightly differ from the original values

2.5.2.1. Effects of feed pressure

The effect of feed pressure is illustrated in figures Figure 2.38 and Figure 2.39. It is clear that product purity increases with the feed pressure. This is in full agreement with the theory since for linear adsorption isotherms purity always increases for higher feed pressures. Product recovery decreases because during the blowdown step more gas leaves the bed. The absolute deviation of purity from the results of Nilchan and Pantelides (1998) is 3.45%. The power requirement per one cycle also increases with the feed pressure since more energy is needed for compression of the gas.

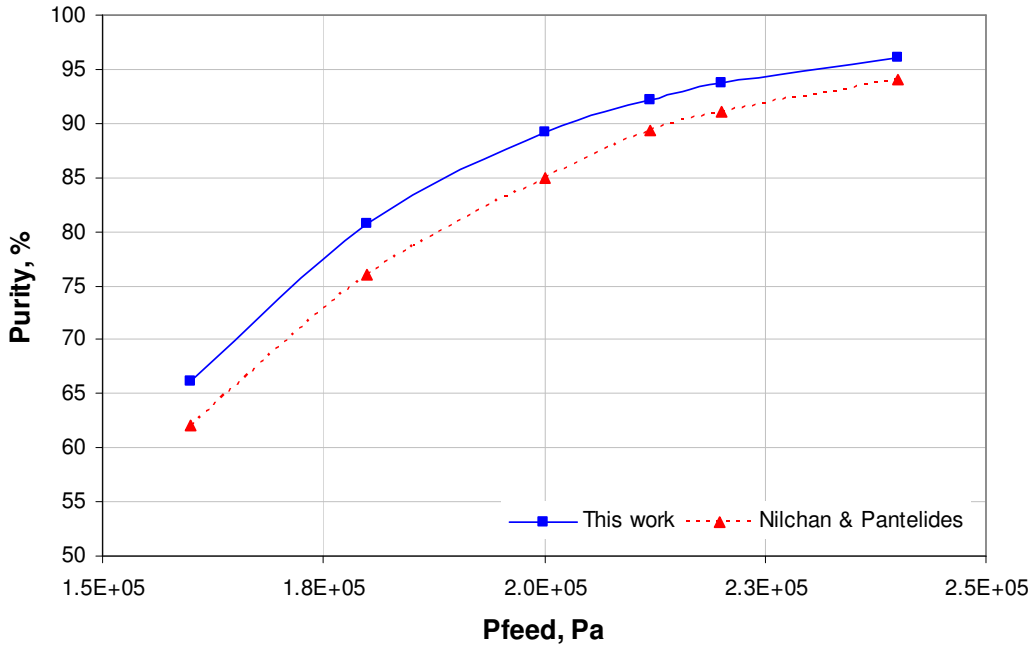

Figure 2.38 Effects of feed pressure on product purity

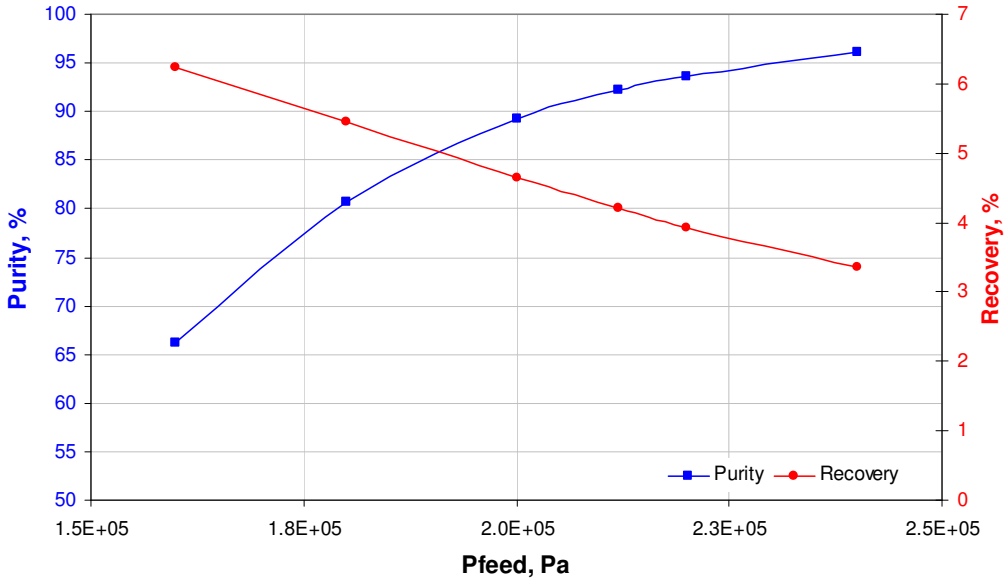

Figure 2.39 Effects of feed pressure on O_2 purity/recovery

2.5.2.2. Effects of particle radius

The effects of particle radius are illustrated in Figure 2.40 and Figure 2.41. It is clear that the product purity reaches the maximum. This can be justified since both adsorbed amount (Q) and pressure drop (ΔP) are affected by the particle radius (both are function of $1/R_{particle}$), an opposite effect is imposed on product purity. As $R_{particle}$ increases the effect on Q becomes more dominant and thus purity decreases. Product recovery decreases because significant amount of product is lost during depressurization. The average absolute deviation in purity from the work of Nilchan and Pantelides is 5.41%. The power requirement per one cycle increases with the particle radius due to a lower pressure drop.

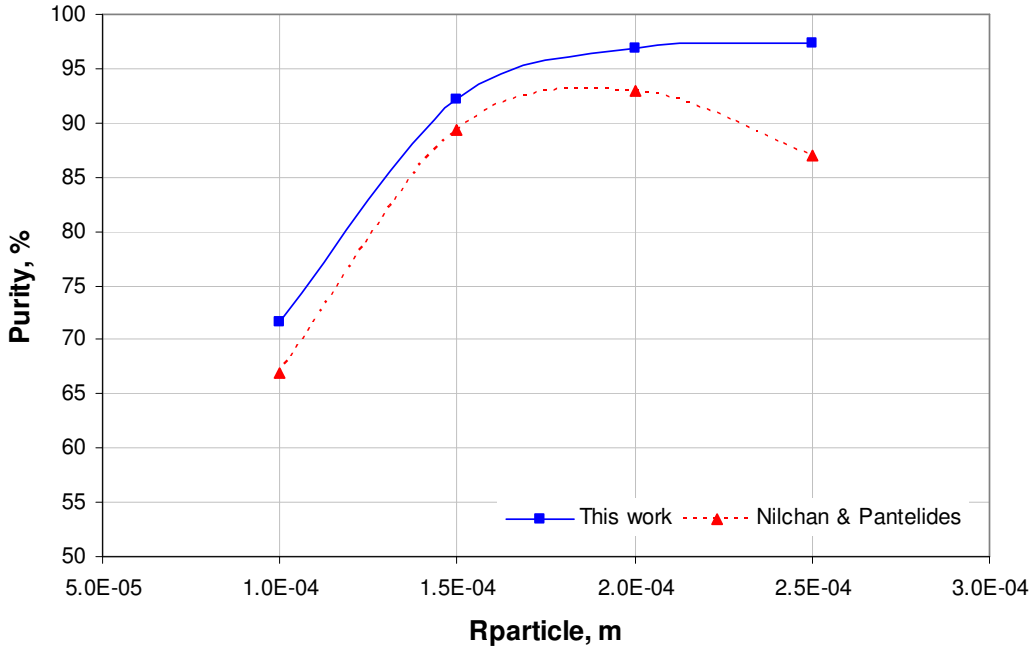

Figure 2.40 Effects of particle radius on O_2 purity

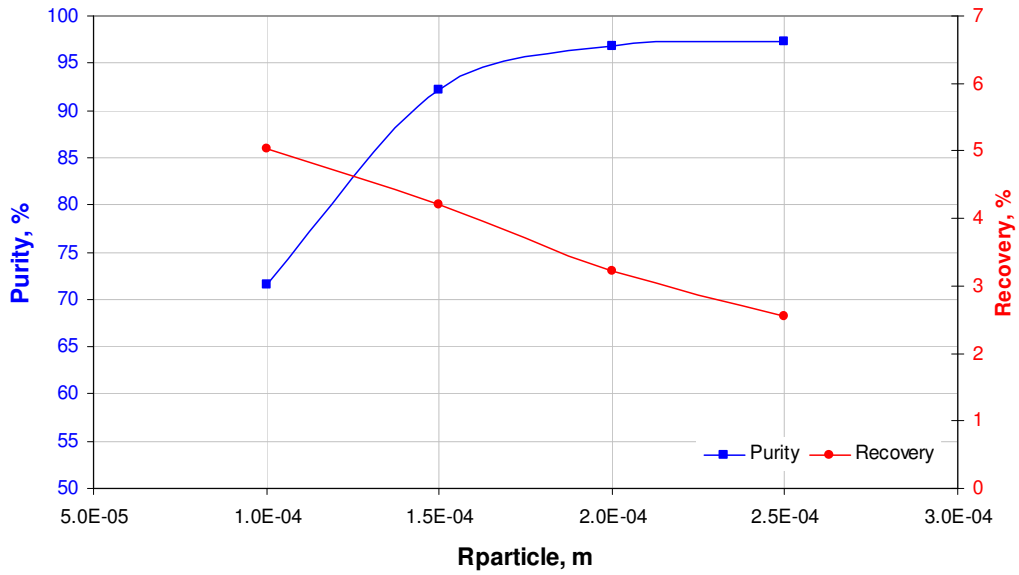

Figure 2.41 Effects of particle radius on O_2 purity/recovery

2.5.2.3. Effects of bed length

The effect of bed length is illustrated in Figure 2.42 and Figure 2.43. It is noticed that the product purity increases with the bed length and so does product recovery. Increase in the bed length (for constant feed amount and pressure) shifts the time point at which

breakthrough takes place. The average absolute deviation in purity from the work of Nilchan and Pantelides is 4.44%.

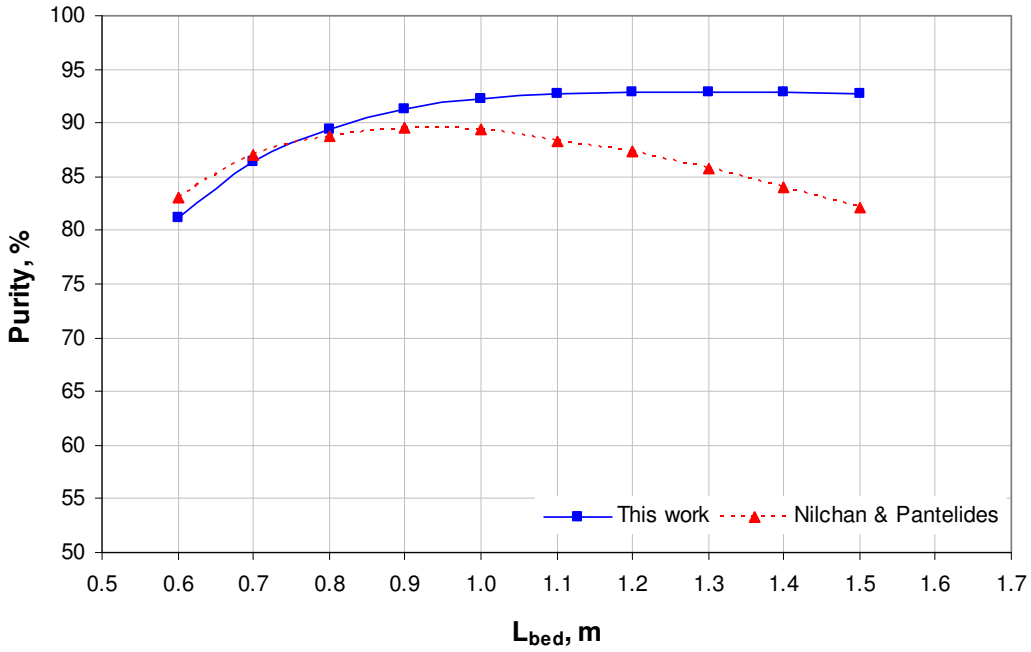

Figure 2.42 Effects of bed length on O_2 purity

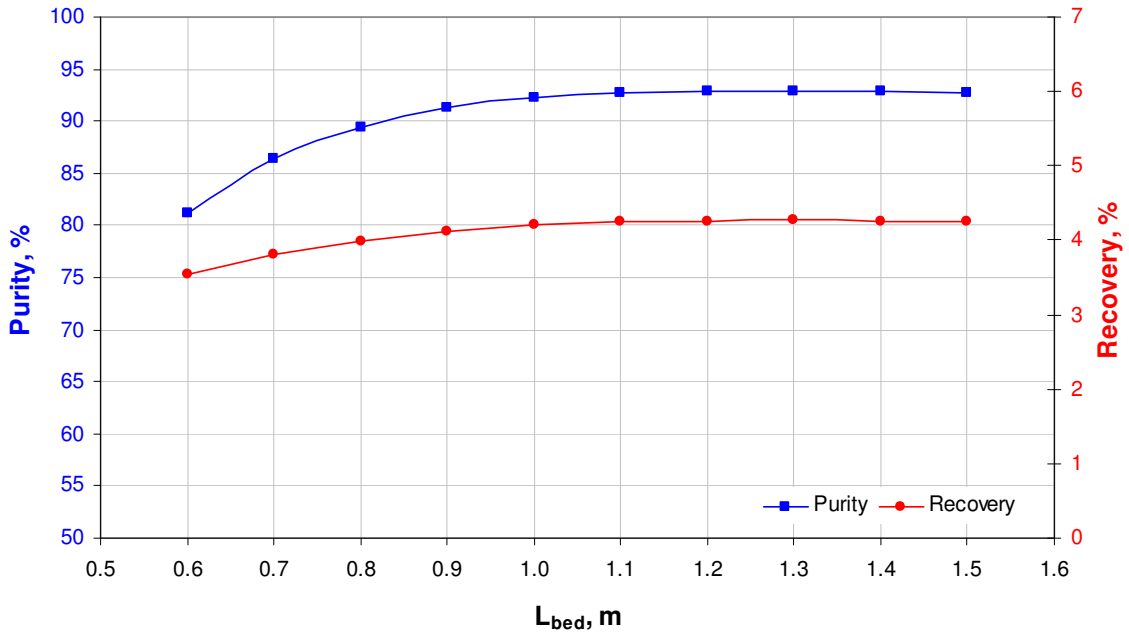

Figure 2.43 Effects of bed length on O_2 purity/recovery

2.5.2.4. Effects of cycle time

The effect of cycle time is illustrated in Figure 2.44 and Figure 2.45. As the cycle time increases the product purity decreases. This could be explained by the fact that the breakthrough curve reaches the end of the bed and therefore lowers purity. From the other side, product recovery increases with the cycle time because during the longer cycle much more product is generated. The average absolute deviation in purity from the work of Nilchan and Pantelides is 4.38%. Finally, the power requirement per one cycle decreases with the cycle time.

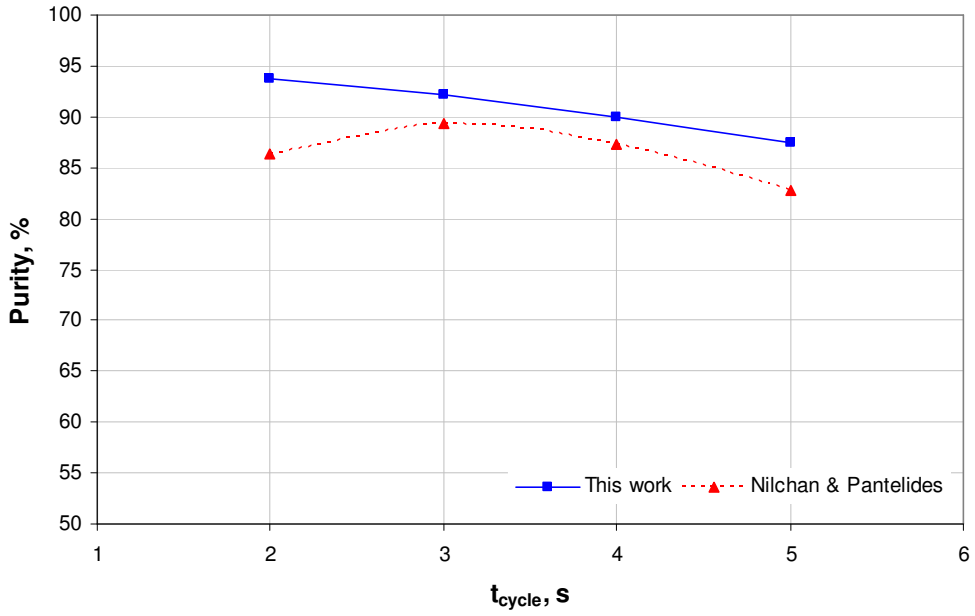

Figure 2.44 Effects of cycle time on O_2 purity

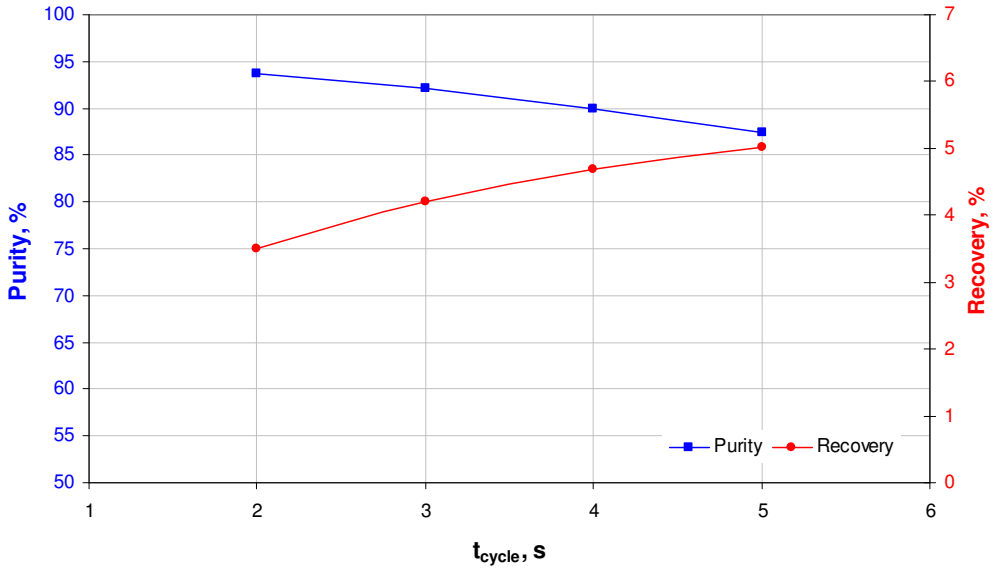

Figure 2.45 Effects of cycle time on O_2 purity/recovery

2.6. Multi-bed PSA case studies

In this section, a medium scale hydrogen recovery from steam methane reforming off gas process using activated carbon as an adsorbent has been used to investigate the effects of number of beds on the separation quality and analyse the trade-offs between capital and operating costs and separation quality. A simplified flowshet of the steam methane reformer is given in Figure 2.46.

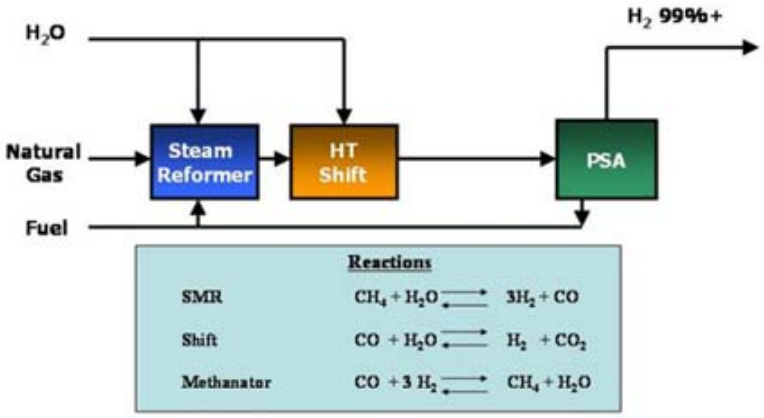

Figure 2.46 Steam-methane reformer system

In this case, the non-isothermal linear driving force model has been used for simulation purposes. The geometrical data of a column, adsorbent and adsorption isotherm parameters for activated carbon have been adopted from the work of Park et al (1998) and given in Table 2.26 and Table 2.25. The effective diffusivity, axial dispersion coefficients, and heat transfer coefficient are assumed constant in accordance with the work of Park et al (1998) as well.

Table 2.25 Phase equilibrium data for activated carbon

Comp.	a_1 (mol/kg)	a_2 (K)	b_1 (Pa^{-1})	b_2 (K)	$-\Delta H_{ads}$ (J/mol)
H_2	4.32E-3	0.00	5.040E-9	850.5	7861.73
CO	0.92E-3	0.52	5.896E-9	1730.9	16677.42
CH_4	-1.70E-3	1.98	19.952E-9	1446.7	18752.69
CO_2	-14.20E-3	6.63	24.775E-9	1496.6	25572.61

Table 2.26 Geometrical and transport characteristics of PSA process

Parameter	Value	Units
Temperature of the feed	297	K
Temperature of the purge gas	297	K
Temperature of the wall	297	K
Feed pressure	26.3E5	Pa
Purge pressure	1E5	Pa
Gas valve constant	1E-5	-
Particle density	850	kg/m^3
Particle radius	3×10^{-3}	m
Bed void fraction	0.36	-
Bed inner diameter	0.1	m
Bed length	1.0	m
Molar fraction of H_2 in feed	0.755	-
Molar fraction of CO in feed	0.040	-
Molar fraction of CH_4 in feed	0.035	-
Molar fraction of CO_2 in feed	0.170	-
Effective diffusivity of H_2	1.0	1/s
Effective diffusivity of CO	0.3	1/s
Effective diffusivity of CH_4	0.4	1/s
Effective diffusivity of CO_2	0.1	1/s
Heat capacity of the particles	878.64	J/(kgK)
Heat transfer coefficient (wall)	138.07	$W/(m^2K)$
Heat axial dispersion coefficient	10^{-3}	m^2/s
Mass axial dispersion coefficient	10^{-3}	m^2/s

Two different PSA cycle configurations have been employed. The following sequence of steps served as a basis for both of them: pressurization, adsorption, pressure equalization (depressurization to other beds), blowdown, purge, and pressure equalization (repressurization from other beds). The cycle configurations differ only in the first step. In the first configuration (configuration A), pressurization has been carried out by using the feed stream whereas in the second (configuration B) by using the light product stream (pure hydrogen). All the other steps are identical (as given in Figure 2.47 and Figure 2.48). All configurations have been generated using the auxiliary program described in section 2.4.4.1. Flowsheets of one, four, eight, and twelve beds have been simulated. These configurations differ only in the number of pressure equalization steps introduced. Thus, one-bed configuration contains no pressure equalization steps, four-bed involves one, eight-bed configuration two, and twelve-bed flowsheet involves three pressure equalization steps. An overview of operating steps employed in these configurations is presented in Table 2.27, Table 2.28, Table 2.29 and Table 2.30, where *CoCP* stands for co-current pressurization, *Ads* for adsorption, *EQD1*, *EQD2* and *EQD3* are the pressure equalization steps (depressurization to the other bed), *Blow* represents counter-current blowdown, *Purge* is the counter-counter purge step, and *EQR3*, *EQR2* and *EQR1* are the pressure equalization steps (repressurization from the other bed).

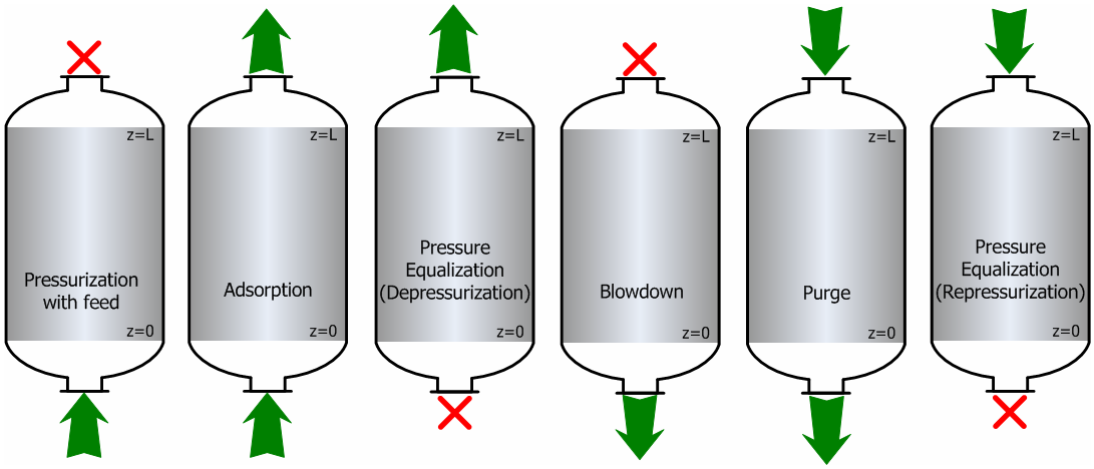

Figure 2.47. Sequence of steps for configuration A

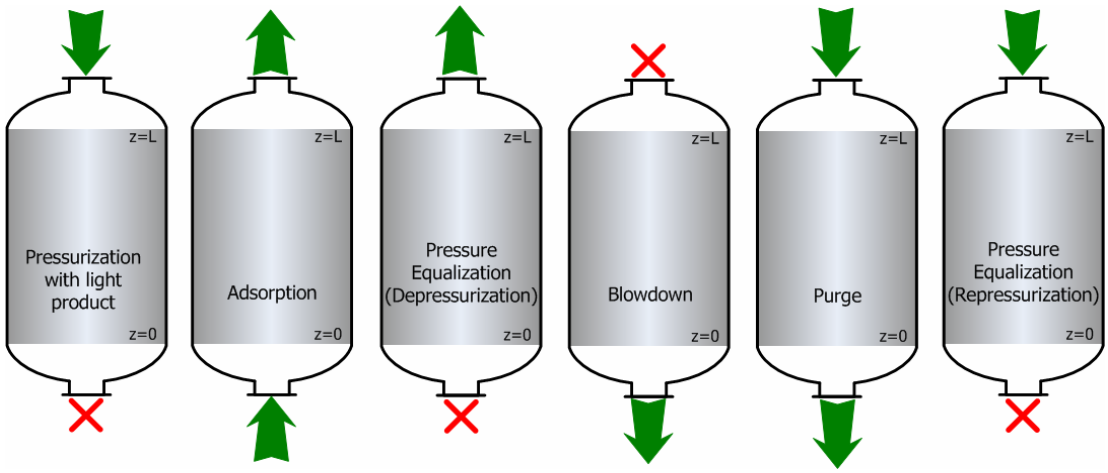

Figure 2.48 Sequence of steps for configuration B

Table 2.27 One-bed four-step PSA configuration

	I	II	III	IV
Bed 1	CoCP	Ads	Blow	Purge

Table 2.28 Four-bed six-step PSA configuration

	I	IIa	IIb	III	IV	Va	Vb	VI
Bed 1	CoCP	Ads	Ads	EQD1	Blow	Purge	Purge	EQR1
Bed 2	Purge	EQR1	CoCP	Ads	Ads	EQD1	Blow	Purge
Bed 3	Blow	Purge	Purge	EQR1	CoCP	Ads	Ads	EQD1
Bed 4	Ads	EQD1	Blow	Purge	Purge	EQR1	CoCP	Ads

Table 2.29 Eight-bed eight-step PSA configuration

	I	II	III	IV	V	VI	VII	VIII
Bed 1	CoCP	Ads	EQD1	EQD2	Blow	Purge	EQR2	EQR1
Bed 2	EQR1	CoCP	Ads	EQD1	EQD2	Blow	Purge	EQR2
Bed 3	EQR2	EQR1	CoCP	Ads	EQD1	EQD2	Blow	Purge
Bed 4	Purge	EQR2	EQR1	CoCP	Ads	EQD1	EQD2	Blow
Bed 5	Blow	Purge	EQR2	EQR1	CoCP	Ads	EQD1	EQD2
Bed 6	EQD2	Blow	Purge	EQR2	EQR1	CoCP	Ads	EQD1
Bed 7	EQD1	EQD2	Blow	Purge	EQR2	EQR1	CoCP	Ads
Bed 8	Ads	EQD1	EQD2	Blow	Purge	EQR2	EQR1	CoCP

Table 2.30 Twelve-bed ten-step PSA configuration

	I	IIa	IIb	III	IV	V	VI	VIIa	VIIb	VIII	IX	X
Bed 1	CoCP	Ads	Ads	EQD1	EQD2	EQD3	Blow	Purge	Purge	EQR3	EQR2	EQR1
Bed 2	EQR1	CoCP	Ads	Ads	EQD1	EQD2	EQD3	Blow	Purge	Purge	EQR3	EQR2
Bed 3	EQR2	EQR1	CoCP	Ads	Ads	EQD1	EQD2	EQD3	Blow	Purge	Purge	EQR3
Bed 4	EQR3	EQR2	EQR1	CoCP	Ads	Ads	EQD1	EQD2	EQD3	Blow	Purge	Purge
Bed 5	Purge	EQR3	EQR2	EQR1	CoCP	Ads	Ads	EQD1	EQD2	EQD3	Blow	Purge
Bed 6	Purge	Purge	EQR3	EQR2	EQR1	CoCP	Ads	Ads	EQD1	EQD2	EQD3	Blow
Bed 7	Blow	Purge	Purge	EQR3	EQR2	EQR1	CoCP	Ads	Ads	EQD1	EQD2	EQD3
Bed 8	EQD3	Blow	Purge	Purge	EQR3	EQR2	EQR1	CoCP	Ads	Ads	EQD1	EQD2
Bed 9	EQD2	EQD3	Blow	Purge	Purge	EQR3	EQR2	EQR1	CoCP	Ads	Ads	EQD1
Bed 10	EQD1	EQD2	EQD3	Blow	Purge	Purge	EQR3	EQR2	EQR1	CoCP	Ads	Ads
Bed 11	Ads	EQD1	EQD2	EQD3	Blow	Purge	Purge	EQR3	EQR2	EQR1	CoCP	Ads
Bed 12	Ads	Ads	EQD1	EQD2	EQD3	Blow	Purge	Purge	EQR3	EQR2	EQR1	CoCP

For simulation purposes, the axial domain is discretized using orthogonal collocation on finite elements of third order with 20 elements. In terms of numerical stability and accuracy, other superior discretization methods exist (e.g. adaptive multiresolution approach by Cruz et al, 2003a) which overcome problems of non-physical oscillations or the divergence of the numerical method in the computed solution in the presence of steep, fast moving fronts. These methods are capable of locally refining the grid in the regions where the solution exhibits sharp features and this way allowing nearly constant discretization error throughout the computational domain. This approach has been successfully applied in the simulation and optimization of cyclic adsorption processes (Cruz et al, 2003b and 2005). However, in all case studies considered in this thesis, the contribution of diffusive/dispersive terms is significant and numerical simulations did not reveal any non-physical oscillations. Thus, the orthogonal collocation on finite elements was considered as an adequate discretization scheme in terms of accuracy and stability. The bed is initially assumed clean (99.999% H_2).

Three different sets of simulations have been carried out: Run I, Run II, and Run III.

2.6.1. Simulation Run I

In simulation Run I the configuration A has been employed (pressurization with feed). The effect of number of beds and cycle time (due to introduction of pressure equalization steps) on the separation quality has been investigated. The following operating conditions have been selected: constant duration of adsorption and purge steps, and constant feed and purge gas flowrates. The input parameters are given in Table 2.31, and the simulation results are summarized in Table 2.32 and Figure 2.49.

The results clearly illustrate that, as the number of beds increases, an improved product purity (~3%) and product recovery (~38%) are achieved. The improved purity can be attributed to the fact that flowsheets with lower number of beds process more feed per cycle (feed flowrate is constant but more feed is needed to repressurize beds from the lower pressure). The noticeable increase in product recovery is a direct result of the pressure equalization steps. On the other hand, power requirements and adsorbent productivity decrease due to the lower amount of feed processed per unit time (the power and productivity of the eight-bed configuration are lower than the power and productivity of the twelve-bed configuration due to higher cycle time). The purity of the twelve-bed configuration is lower than the purity of the four and eight-bed ones. This interesting trend can be attributed to the fact that during the third pressure equalization a small breakthrough takes place thus contaminating the pressurized bed.

Table 2.31. Input parameters for Run I

Parameter	Number of beds			
	1	4	8	12
$sp_{PressCoC}$	0.1000	0.060	0.030	0.0500
sp_{AdsIn}	0.3600	0.3600	0.3600	0.3600
sp_{AdsOut}	0.0035	0.0015	0.0015	0.0015
sp_{Blow}	0.8000	0.5000	0.2500	0.4000
$sp_{PurgeIn}$	0.2250	0.2250	0.2250	0.2250
$sp_{PurgeOut}$	0.0300	0.0300	0.030	0.0300
sp_{PEQ1}	-	0.0040	0.0025	0.0030
sp_{PEQ2}	-	-	0.0050	0.0040
sp_{PEQ3}	-	-	-	0.0080
Feed flowrate, m^3/s	3.60E-6	3.60E-6	3.60E-6	3.60E-6
Purge flowrate, m^3/s	2.25E-6	2.25E-6	2.25E-6	2.25E-6
τ_{cycle}, s	60	80	160	120

Table 2.32. Simulation results of Run I

No. beds	O_2 purity (%)	O_2 recovery (%)	Power (W)	Productivity (mol/kgs)
1	96.87	34.40	5290.2	9.18E-02
4	99.50	58.06	2794.9	4.85E-02
8	99.58	68.87	1198.7	2.08E-02
12	99.36	72.50	1393.6	2.42E-02

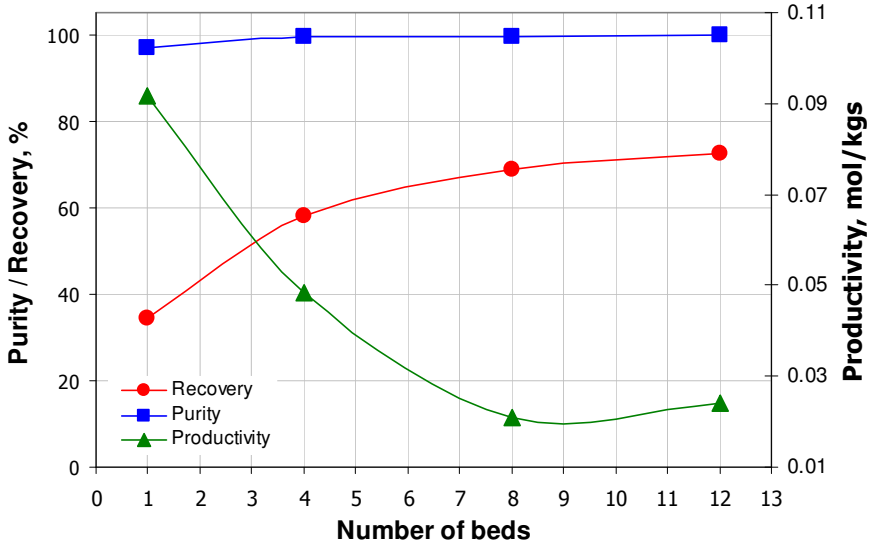

Figure 2.49. Simulation results of Run I

2.6.2. Simulation Run II

In simulation Run II the configuration A has been employed (pressurization with feed). The effect of number of beds for constant power requirements and constant adsorbent productivity on the separation quality has been analyzed. The following operating conditions have been selected: constant adsorbent productivity, constant cycle time, and constant amount of feed processed per cycle. The input parameters are given in Table 2.33 and the simulation results are summarized in Table 2.34 and Figure 2.50.

The results show that, increasing the number of beds, a slight increase in the product purity (~1%) and a significant increase in product recovery (~52%) are achieved. In this run the amount of feed processed per cycle is constant and improve in the purity cannot be attributed to the PSA design characteristics and operating procedure. Due to the same reasons described in Run I, the purity of the twelve-bed configuration is lower than the purity of the eight-bed one. The power requirements and adsorbent productivity remain constant due to the constant amount of feed processed per cycle.

Table 2.33. Runtime parameters for Run II

Parameter	Number of beds			
	1	4	8	12
$sp_{PressCoC}$	0.0300	0.0450	0.0500	0.0500
sp_{AdsIn}	0.1200	0.1300	0.3300	0.3600
sp_{AdsOut}	0.0004	0.00035	0.0014	0.0015
sp_{Blow}	0.2000	0.2200	0.3000	0.4000
$sp_{PurgeIn}$	0.5625	0.1500	0.3000	0.2250
$sp_{PurgeOut}$	0.0075	0.0200	0.0400	0.0300
sp_{PEQ1}	-	0.0025	0.0020	0.0300
sp_{PEQ2}	-	-	0.0040	0.0040
sp_{PEQ3}	-	-	-	0.0080
Feed flowrate, m^3/s	1.20E-6	1.30E-6	3.30E-6	3.60E-6
Purge flowrate, m^3/s	0.75E-6	1.15E-6	3.00E-6	2.25E-6
τ_{cycle}, s	120	120	120	120

Table 2.34. Simulation results of Run II

No. beds	O_2 purity (%)	O_2 recovery (%)	Power (W)	Productivity (mol/kgs)
1	98.11	20.21	1442.0	2.50E-02
4	99.29	38.40	1406.9	2.44E-02
8	99.79	65.25	1409.2	2.45E-02
12	99.36	72.50	1393.6	2.42E-02

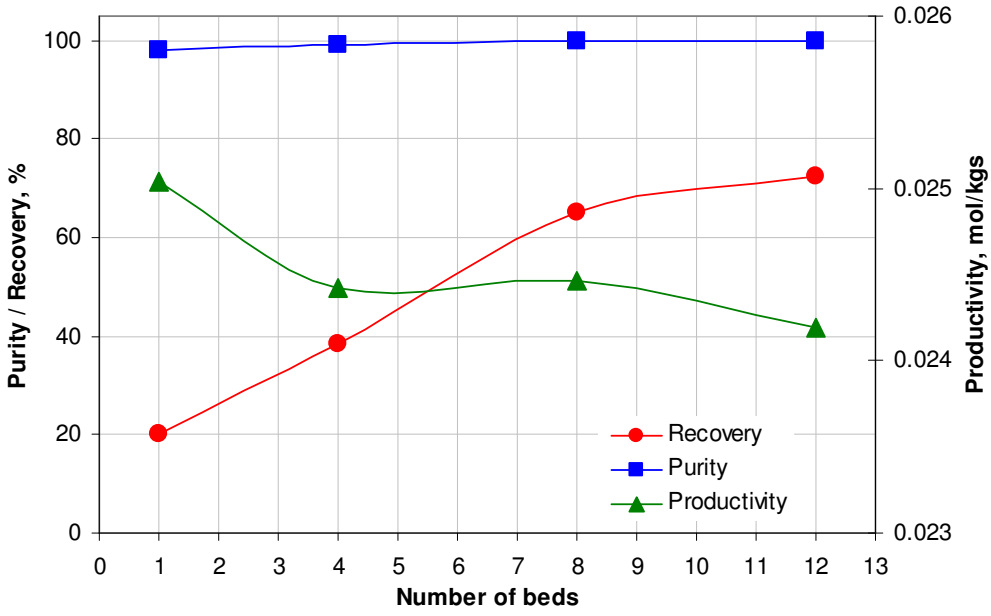

Figure 2.50. Simulation results of Run II

2.6.3. Simulation Run III

In simulation Run III the configuration B (pressurization with light product) is used. The effect of number of beds for constant power requirements and constant adsorbent productivity on separation quality has been investigated. The following operating conditions have been selected: constant adsorbent productivity, constant duration of adsorption and purge steps, constant feed and purge gas flowrates, constant cycle time, and constant amount of feed processed per cycle. The input parameters are given in Table 2.35 and the simulation results are presented in Table 2.36 and Figure 2.51.

The results illustrate that the number of beds does not affect the product purity, productivity and power requirements (since the amount of feed per cycle is constant). However, a huge improvement in the product recovery (~64%) is achieved due to three pressure equalization steps. Similar to the results in Run I and II the purity of the twelve-bed con-figuration is lower than the purity of the eight-bed one.

The above analysis reveals typical trade-offs between capital and operating costs and separation quality. Thus, by increasing the number of beds a higher product

purity/recovery is achieved while higher capital costs are required (due to a larger number of beds). On the other hand, energy demands are lower due to energy conservation imposed by the existence of pressure equalization steps.

Table 2.35. Runtime parameters for Set III

Parameter	Number of beds			
	1	4	8	12
$sp_{PressCoC}$	0.0030	0.0030	0.0500	0.0040
sp_{AdsIn}	0.4000	0.3333	0.3450	0.5000
sp_{AdsOut}	0.00088	0.00085	0.0015	0.0014
sp_{Blow}	0.2500	0.4000	0.3000	0.4000
$sp_{PurgeIn}$	0.0900	0.1333	0.3000	0.2000
$sp_{PurgeOut}$	0.0140	0.0200	0.0400	0.0300
sp_{PEQ1}	-	0.0050	0.0020	0.0030
sp_{PEQ2}	-	-	0.0040	0.0040
sp_{PEQ3}	-	-	-	0.0080
Feed flowrate, m^3/s	4.00E-6	3.33E-6	3.45E-6	5.00E-6
Purge flowrate, m^3/s	0.90E-6	1.33E-6	3.00E-6	2.00E-6
τ_{cycle}, s	120	120	120	120

Table 2.36. Simulation results for Set III

No. beds	O_2 purity (%)	O_2 recovery (%)	Power (W)	Productivity (mol/kgs)
1	99.87	1.41	1887.8	2.03E-02
4	99.97	28.47	1180.8	2.05E-02
8	99.97	50.58	1193.8	2.07E-02
12	99.83	65.16	1190.9	2.07E-02

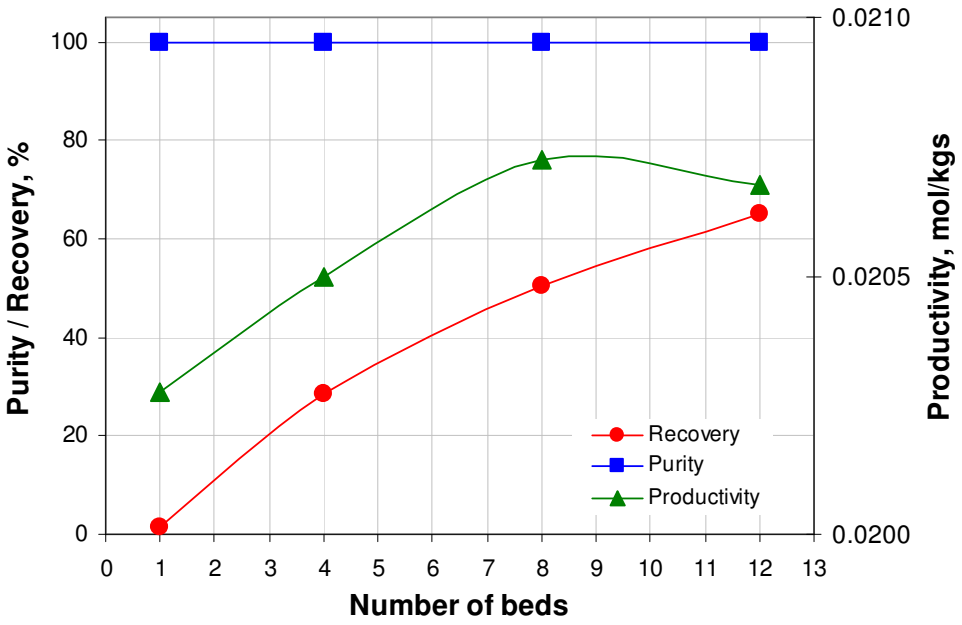

Figure 2.51. Simulation results of the Set III

2.7. Multi-bed PSA optimization case studies

The selection of optimal design and operating parameters is a difficult task due to several reasons: highly complex mathematical models (large number of partial differential and algebraic equations necessary to describe the multi-scale transport phenomena in adsorbent column and adsorbent particles), a large number of trade-offs between the key variables, and excessive computational requirements to reach the cyclic steady state. In addition, calculation of the optimal number of beds and optimal schedule coupled with the optimization of design and operating variables makes the system of intractable size. In the previous contributions typical objective functions have been employed (e.g. product purity and recovery, power requirements or profit) and different scenarios used to reduce the computational requirements for the solution of the problem: a) fixed number of beds, fixed schedule and complex PSA model employed, and subset of operating and design parameters optimized (Nilchan and Pantelides, 1998; Jiang et al, 2003, 2004; Cruz et al, 2003, 2005; Sankarao and Gupta, 2007); b) very simple PSA model employed, and number of beds, schedule and subset of operating and design parameters optimized (Smith and Westerberg, 1991). The effect of number of beds and different cycle configurations (sequence and duration of steps) has been systematically analyzed by Smith and Westerberg only. However, very simple PSA model has been used (with a priori given important parameters, such as efficiency and bed utilization) which rather roughly predicts PSA process performance (purity and recovery) therefore making it practically insensitive on many design and operating variables. In addition, very few contributions consider optimization studies of PSA processes with multilayered adsorbents.

In this thesis, based on the developed modelling framework we try to develop an optimization approach for PSA processes. The existence of multiple objectives in a PSA process requires a systematic optimization procedure. The proposed approach relies on the following steps:

- Analysis of the process and selection of the optimal adsorbent, its adsorbent equilibrium and diffusion data
- Identification of the most important design and operating variables, and dependencies of the key process performance variables (e.g. purity, recovery, productivity, power requirements etc) on the input (design and operating) parameters, as well as their relative importance – sensitivities
- Formulation of case-dependent objective function(s)

2.7.1. Optimization problems

The proposed optimization approach has been applied on three different gas separation problems:

- Case study I: hydrogen recovery from steam methane reformer off-gas by using activated carbon
- Case study II: hydrogen recovery from steam methane reformer off-gas by using two layered adsorbent columns (activated carbon and zeolite 5A)
- Case study III: oxygen production from air by using zeolite 5A

The problem of simultaneously defining the optimal number of beds, operating schedule and process design is computationally expensive and potentially not feasible with current optimization techniques and computational resources; thus, certain simplifications have to be made. More specifically, the process schedule and process design/operation have been optimized independently. Therefore, the first task is to define PSA configurations of interest. We start with a single bed PSA configuration. Next, it is assumed that the maximum number of pressure equalizations is three (which is the usual case in industrial PSA plants), so that we need three more configurations to investigate the effect of the number of pressure equalizations. Next, it is of a great importance to analyze effects of co-current depressurization step (a step commonly performed in large scale industrial PSA plants) on separation quality; thus, two additional configurations have been added to our set of configurations. Hence, one + three + two = six configurations are needed. Clearly, a larger number of beds is necessary to accommodate more pressure equalizations. In addition, an appropriate increase in the number of beds should be done if the same number of beds cannot accommodate a configuration in which one pressure equalization step is replaced by co-current depressurization (as in the case for two-beds). Final, all configurations are so designed that they do not include any idle time. Keeping the abovementioned demands in mind, in case studies I and II, six different PSA cycle configurations with one, two, four, five, and eight beds have been selected and optimized. Configuration C1 includes no pressure equalization steps, C2 and C4 include one pressure equalization step, C5a and C5b include two, and C8 includes three pressure equalization steps. Configurations C4 and C5b contain one additional co-current depressurization step during which the product gas is used to purge another column (the limiting factor is that impurities are not allowed to breakthrough and contaminate purged column). Configurations C4, C5a, C5b, and C8 are carefully designed to continuously produce hydrogen, consume the feed and use part of the pure product from adsorption step to finally counter-currently repressurize other columns. The sequence of steps for all configurations is summarized in Table 2.37 to Table 2.42.

Table 2.37. PSA configuration C1

Bed	**1**	**2**	**3**	**4**
B-1	CC	Ads	Blow	Purge

Table 2.38. PSA configuration C2

Bed	**1**	**2**	**3**	**4**	**5**	**6**	**7**	**8**
B-1	EQR1	CC	Ads	Ads	EQD1	Blow	Purge	Purge
B-2	EQD1	Blow	Purge	Purge	EQR1	CC	Ads	Ads

Table 2.39. PSA configuration C4

Bed	1	2	3	4	5	6	7	8
B-1	EQR1	CC	Ads	Ads^{CC}	EQD1	CoCD	Blow	Purge
B-2	Blow	Purge	EQR1	CC	Ads	Ads^{CC}	EQD1	CoCD
B-3	EQD1	CoCD	Blow	Purge	EQR1	CC	Ads	Ads^{CC}
B-4	Ads	Ads^{CC}	EQD1	CoCD	Blow	Purge	EQR1	CC

Table 2.40. PSA configuration C5a

Bed	1	2	3	4	5	6	7	8	9	10
B-1	EQR2	EQR1	CC	Ads	Ads^{CC}	EQD1	EQD2	Blow	Purge	Purge
B-2	Purge	Purge	EQR2	EQR1	CC	Ads	Ads^{CC}	EQD1	EQD2	Blow
B-3	EQD2	Blow	Purge	Purge	EQR2	EQR1	CC	Ads	Ads^{CC}	EQD1
B-4	Ads^{CC}	EQD1	EQD2	Blow	Purge	Purge	EQR2	EQR1	CC	Ads
B-5	CC	Ads	Ads^{CC}	EQD1	EQD2	Blow	Purge	Purge	EQR2	EQR1

Table 2.41. PSA configuration C5b

Bed	1	2	3	4	5	6	7	8	9	10
B-1	EQR2	EQR1	CC	Ads	Ads^{CC}	EQD1	EQD2	CoCD	Blow	Purge
B-2	Blow	Purge	EQR2	EQR1	CC	Ads	Ads^{CC}	EQD1	EQD2	CoCD
B-3	EQD2	CoCD	Blow	Purge	EQR2	EQR1	CC	Ads	Ads^{CC}	EQD1
B-4	Ads^{CC}	EQD1	EQD2	CoCD	Blow	Purge	EQR2	EQR1	CC	Ads
B-5	CC	Ads	Ads^{CC}	EQD1	EQD2	CoCD	Blow	Purge	EQR2	EQR1

Table 2.42. PSA configuration C8

Bed	1	2	3	4	5	6	7	8	9	10	11	12	13	14	15	16
B-1	EQR3	EQR2	EQR1	CC	CC	Ads^{CC}	Ads^{CC}	Ads	EQD1	EQD2	EQD3	Blow	Blow	Purge	Purge	Purge
B-2	Purge	Purge	EQR3	EQR2	EQR1	CC	CC	Ads^{CC}	Ads^{CC}	Ads	EQD1	EQD2	EQD3	Blow	Blow	Purge
B-3	Blow	Purge	Purge	Purge	EQR3	EQR2	EQR1	CC	CC	Ads^{CC}	Ads^{CC}	Ads	EQD1	EQD2	EQD3	Blow
B-4	EQD3	Blow	Blow	Purge	Purge	Purge	EQR3	EQR2	EQR1	CC	CC	Ads^{CC}	Ads^{CC}	Ads	EQD1	EQD2
B-5	EQD1	EQD2	EQD3	Blow	Blow	Purge	Purge	Purge	EQR3	EQR2	EQR1	CC	CC	Ads^{CC}	Ads^{CC}	Ads
B-6	Ads^{CC}	Ads	EQD1	EQD2	EQD3	Blow	Blow	Purge	Purge	Purge	EQR3	EQR2	EQR1	CC	CC	Ads^{CC}
B-7	CC	Ads^{CC}	Ads^{CC}	Ads	EQD1	EQD2	EQD3	Blow	Blow	Purge	Purge	Purge	EQR3	EQR2	EQR1	CC
B-8	EQR1	CC	CC	Ads^{CC}	Ads^{CC}	Ads	EQD1	EQD2	EQD3	Blow	Blow	Purge	Purge	Purge	EQR3	EQR2

2.7.2. Parametric analysis

A systematic case-dependent parametric analysis provides significant insight into the most critical design and operating parameters, and their effect on the process performance variables such as product purity, recovery, power consumption etc.

Several parametric studies have been reported in the literature for specific PSA systems (Yang and Doong, 1986; Wankat, 1987; Shin and Knaebel, 1988; Farooq et al, 1989; Lu et al, 1993; Kikkinides et al, 1993; Chou and Huang, 1994; Yang and Lee, 1998; Warmuzinsky and Tanczyk, 1998; Nilchan and Pantelides, 1998; Park et al, 1998, 2000; Lee et al, 1999; Sircar and Golden, 2000; Waldron and Sircar, 2000; Mendes et al, 2001; Jee et al, 2002; Jiang et al, 2003, 2004; Cruz et al, 2003, 2005; Kim et al, 2005; Sankararao and Gupta, 2007). The parameters studied in this work include particle size, column length and diameter (length/diameter ratio), feed and purge gas pressures, feed and purge gas flowrates, cycle- and step-times, distribution of adsorbents in multilayered adsorption columns, number of beds and PSA cycle design (sequence of steps). The effect of these parameters is well documented in the literature and the parametric studies performed in this work have been carried out only in cases when it was necessary to clarify the effect of certain parameter on the process performance (such as carbon to zeolite ratio). Thus, once the base case parameters have been selected, only one variable at the time has been varied, and its effect analyzed.

2.7.2.1. Effect of particle size

Particle size is an important design parameter whose influence on the separation quality can be qualitatively assessed according to the well-known linear driving force (LDF) approach. The LDF coefficient is inversely proportional to the square of particle radius and significantly affects the mass transfer within particles. On the other hand, a decrease in particle size leads to an increase in a pressure drop, which results in an earlier breakthrough and degradation of the performance. Several attempts in the literature tried to explicitly exploit this trade-off. For instance, Wankat (1987) used the method of decreasing the adsorbent particle diameter while at the same time keeping the pressure drop constant (that is keeping the ratio L_{bed}/R_p^2 constant). Such technique resulted in fat, "pan-cake" column designs (very short columns with large diameter) which are capable to significantly reduce the dimensions of the column and amount of adsorbent. In this work, for the systems under consideration a detailed analysis has revealed that in the range of particle radius, bed length and diameter and velocities used, a smaller diameter has been always the preferable choice.

2.7.2.2. Effect of column length/diameter ratio

The parametric analyses as well as both case studies have been carried out for the constant amount of adsorbent that is for the constant column volume. Thus, only one degree of freedom exists (column length, diameter or length/diameter ratio). In this work, length/diameter ratio has been utilized. Simulation results indicate that as the length/diameter ratio (L/D) increases, product purity increases while recovery passes through a maximum. Also higher L/D ratios cause higher pressure drops thus leading to an

earlier breakthrough and decrease in purity. Thus, this parameter is employed as an optimization decision variable in all case studies.

2.7.2.3. Effect of feed and purge gas pressures

An increase in the feed pressure (for a constant amount of feed) causes an increase in product purity since the adsorbent capacity increases as the pressure increases (in the range of pressures of interest in this work). On the other hand, as feed pressure increases, power consumption also increases. Therefore, it is necessary to find the optimal feed pressure, which ensures feasible pressure equalization and co-current depressurization steps at minimum costs. In other words, to effectively use void gas in the column, the length of unused bed (LUB) has to be high enough to adsorb strong adsorptive components moving towards the end of column during co-current depressurization steps. This ensures that the product leaving the column is completely pure and can be used to repressurize or purge other columns. High LUB can be achieved by interrupting the adsorption step long before the concentration front reaches the end. This is done in practice by: (i) decreasing the feed flowrate (in the case of constant length), (ii) extending the column length (in the case of constant feed flowrate), (iii) increasing the adsorbent capacity for a constant amount of feed by increasing the feed pressure, (iv) increasing the D_e/R_p^2 ratio either by increasing D_e or decreasing the particle radius. In this work in case studies I and II, the feed pressure is used to control the LUB (since the feed is available at high pressures as the product of steam methane reforming). Also, the feed pressure was employed in case study III as an optimization variable due to its high effect on the power requirements. Purge gas pressure is assumed constant in all case studies and fixed to 1atm.

2.7.2.4. Effect of feed flowrate

A higher feed flowrate leads to a decrease in product purity and increase in product recovery. In addition, the power consumption is directly proportional to the feed flowrate. Thus, the feed flowrate was chosen as an optimization decision variable in all case studies.

2.7.2.5. Effect of purge flowrate (purge/feed ratio)

The purge/feed ratio is one of the most important operating variables in PSA whose increase might lead to an increase in purity and to a significant decrease in recovery. Hence, it was employed as an optimization decision variable in all case studies.

2.7.2.6. Effect of cycle/step times

The effect of cycle and step times on process performance is important. For instance, as the duration of pressurization (by using feed stream) increases, product purity decreases but recovery increases. This can be justified by the increased amount adsorbed during the prolonged step duration, which lowers the purity. According to Shin and Knaebel (1988) the effect on product recovery is rather complicated since decrease in purity also decreases recovery but at the same time the product quantity increases in larger rates and the overall effect is an increase in recovery. In addition, a longer pressurization step increases power

requirements. Regarding the duration of the adsorption step for a constant amount of feed, longer adsorption time leads to an increase in purity and decrease in recovery. Purge and blowdown step times have similar effects: as the duration increases, product purity increases but recovery decreases (longer time allows more impurities to desorb while at the same time more product is loss during the step). The power requirements slightly increase since larger quantities of feed are needed to repressurize the bed. The step times are not independent variables, and in a typical multi-bed PSA process only the duration of one or two steps can be independently varied at the same time.

2.7.2.7. Effect of carbon/zeolite ratio (AC/Z ratio)

In this thesis, the carbon/zeolite ratio is defined as the fraction of activated carbon of the total column length. This way it is more convenient to visualize the simulation and optimization results. As presented in the work of Yang and Lee (1998), Lee et al (1999) and Park et al (1998, 2000), the product recovery increases as the zeolite fraction increase while purity passes through a maximum. In addition, it is noticed that this effect is more important at lower pressures. To prove the abovementioned conclusions a parametric study has been carried out to establish dependencies of product purity and recovery on the carbon/zeolite ratio. In addition, two optimization problems have been solved utilizing only the carbon/zeolite ratio as optimization variable: a) maximization of product recovery for a given minimum purity (e.g. 99.99%) while optimizing carbon/zeolite ratio, and b) maximization of purity for a given minimum recovery (e.g. 55%) while optimizing carbon/zeolite ratio. The following base case properties have been used: configuration C1 (one bed, no pressure equalizations), feed pressure=15bar, L/D=5, and purge/feed ratio=1.5. Simulation results as presented in Figure 2.52 support the conclusions drawn in the literature: the existence of an optimal carbon/zeolite ratio and the qualitative dependence of purity and recovery on the carbon/zeolite ratio. Optimization studies also indicate that it is possible to find: a) maximum recovery for a given minimum requirement in purity, and b) maximum purity for a given recovery. The effect of carbon/zeolite ratio is systematically optimized in Case study II.

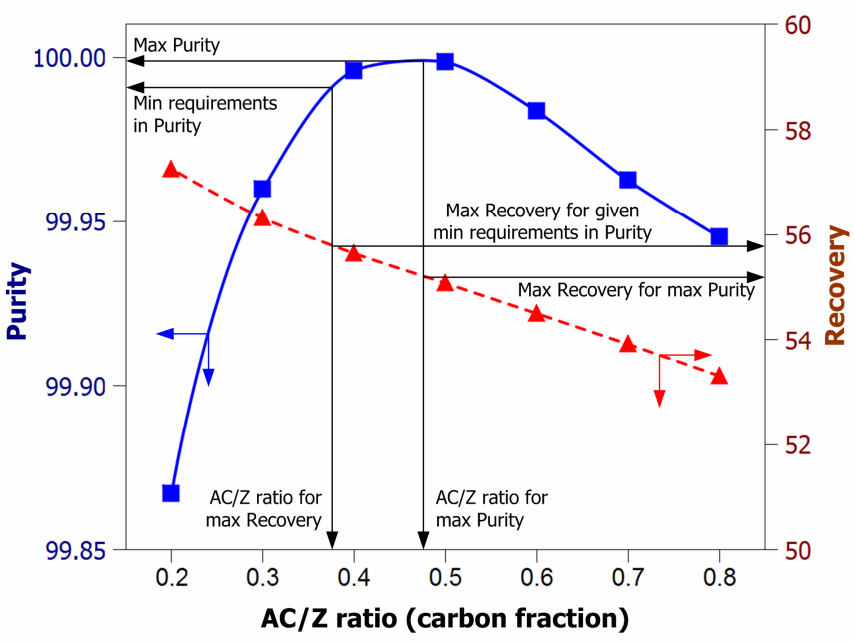

Figure 2.52. Simulation and optimization results (II layers)

2.7.2.8. Effect of number of beds and cycle design

The number of beds and sequence of steps are important decision parameters because well-designed multi-bed PSA processes offer significant advantages such as continuous production and consumption of the feed, increased product recovery and energy savings. This can be achieved by using co-current depressurization steps (to repressurize and purge other columns), while simultaneously carrying out a number of certain operating steps. For instance, it is possible to repressurize the column by using high pressure product from the adsorption step thus reducing investments in additional equipment such as storage tanks or compressors. The effect of step sequence and number of beds has been analyzed in case studies I and II due to the scale of the process – hydrogen production is a typical large-scale process where a large number of beds and complex configurations are typically employed. On the other hand, air separation (case study III) is a small to medium scale process and a standard two-bed configuration is used.

2.7.3. Formulation of the optimization problem

The objective of this thesis is to apply the optimization framework on a wide range of PSA processes. Thus, a typical medium/large scale process has been investigated: hydrogen recovery from SMROG. A typical objective is maximization of the total profit (Smith and Westerberg, 1991, Cruz et al, 2003 and 2005). However, a rigorous objective function which takes into account all of the above factors has to deal with too many uncertainties (such as pricing, fluctuations in the market, and many other economic parameters), generally requires a lot of information of different nature (difficult to compare and systematically analyze), and produce misleading results. Thus, the mathematical

formulation of the optimization problem being solved in this work ought to focus on the optimization of the most important process variables.

2.7.3.1. Case study I: Hydrogen recovery from SMROG (single layer)

The main objective in this case study is to investigate the effect of multi-bed PSA configurations, number of pressure equalizations, and additional operating steps that may significantly improve the overall performance. The most commonly used performance indicator - product recovery for the given minimal requirements in product purity will be employed. In addition, in order to get a fair comparison between various multi-bed PSA configurations, it is necessary to define a set of conditions that have to be met. Thus, the total cycle time, the amount of feed and the amount of adsorbent will be kept constant (that is the productivity of the adsorbent will be kept constant). Also, the feed is available at high pressures; therefore no matter how high feed pressure is - no compression is needed. Based on the parametric studies, and the sensitivity analysis, the most significant process parameters in this case study are the feed pressure and flowrate, column geometry (length/diameter ratio), and purge/feed ratio. The relative sensitivity values of the recovery (objective function) and purity (constraint) with respect to the most important process variables have been calculated using gPROMS and given in Table 2.43. Relative sensitivity represents the average ratio between the sensitivity of the purity/recovery on the particular variable and the corresponding highest sensitivity. This way, it is possible to compare and asses the relative importance of the decision variables on the objective function or constraints and, if necessary, eliminate those with the lowest influence.

Table 2.43. Typical sensitivity ratios (Case studies I and II)

Optimized variable	Purity*	Recovery (obj. fn.)
Pfeed	0.5	1
P/F	1.0	0.4
L/D	0.1	0.01
AC/Z	0.001	0.01

* Given as a minimum requirement

Sensitivity of variable x with respect to the model parameter p is defined as $S = \frac{\partial x(t)}{\partial p}$. In gPROMS sensitivities are calculated automatically on the following way. If we consider a problem of N unknowns and one parameter p where the model equations are $f(x, p) = 0,\ x \in \{x_1, x_2, ..., x_N\}$, the solution of the problem at point (x^*, p^*) is: $f(x^*, p^*) = 0$. If we now consider the effect of a small change in parameter δp, the solution of the system becomes $f(x^* + \delta x, p + \delta p) = 0$. If we perform a Taylor expansion around point (x^*, p^*) and take the limit $\delta p \to 0$, after some simple mathematical operations we

get: $\frac{\partial x}{\partial p} = -\left[\frac{\partial f}{\partial x}\left(x^*, p^*\right)\right]^{-1} \frac{\partial f}{\partial p}\left(x^*, p^*\right)$ where the left hand side term represents the local sensitivity of solution with respect to parameter p at the point $\left(x^*, p^*\right)$, and the first right hand side term is the Jacobian matrix of the system. If several parameters are being considered the formula derived may be applied to each one separately. Local sensitivity can be used now to calculate relative change in the objective function or the key variables from variation in each parameter: $\left[\textit{Relative change in } x_j\right] = \frac{1}{x_j}\left(\frac{\partial x_j}{\partial p}\right) \cdot \Delta p$, where the term $\frac{\partial x_j}{\partial p}$ is the local sensitivity coefficient and Δp is the variation in parameter p.

In this case, the feed pressure and the purge/feed ratio were found to be the most important variables, while the cycle and step times have the lowest sensitivities (more than three orders of magnitude lower than the other does) and thus their values will be fixed in all configurations. Also, the cycle time is assumed constant and will not be considered. Hence, the optimization problem can be formulated as the maximization of hydrogen recovery for a given productivity and minimum requirements in product purity, while optimizing the number of beds and cycle configuration, feed pressure, purge/feed ratio, and column length to diameter ratio (cycle and step times, the amount of adsorbent and gas valve constants are kept constant):

$$
\begin{aligned}
&\textit{Max} \quad \textit{Recovery}_{H_2} \\
&\textit{s.t.} \quad \textit{Model Equations} \\
&\qquad \textit{Purity}_{H_2} \geq \textit{min. Purity}_{H_2} \\
&\qquad \textit{Productivity} = \textit{const} \\
&\qquad N_{beds} \in \{1,2,4,5,8\} \\
&\qquad \textit{Configurations} \in \{C1, C2, C4, C5a, C5b, C8\} \\
&\qquad LB \leq P_{feed} \leq UB \\
&\qquad LB \leq \textit{Purge}/\textit{Feed} \leq UB \\
&\qquad LB \leq \frac{L}{D} \leq UB
\end{aligned}
\tag{2.93}
$$

where LB and UB denote the lower and upper bounds of optimization variables, respectively.

2.7.3.2. Case study II: Hydrogen recovery from SMROG (double layer)

The fact that different adsorbents exhibit different selectivity can be exploited to improve separation quality by combining two or more adsorbent layers in a single column. Many studies (Yang and Lee, 1998; Lee et al, 1999; Park et al, 1998, 2000) showed the existence of an optimal carbon to zeolite ratio. In this thesis, we systematically exploit the combined effects of multi-bed PSA configurations and activated carbon/zeolite ratio on the process performance. Thus, similarly to case study I, the optimization problem can be formulated as a maximization of hydrogen recovery for a given productivity and minimum

requirements in product purity, while optimizing the number of beds and cycle configuration, feed pressure, purge/feed ratio, and carbon/zeolite ratio for constant cycle and step time durations, column volume (that is amount of adsorbent), column length to diameter ratio, and gas valve constants:

$$\begin{aligned} &Max \quad Recovery_{H_2} \\ &s.t. \quad Model\ Equations \\ &\quad Purity_{H_2} \geq min.\ Purity_{H_2} \\ &\quad Productivity = const \\ &\quad N_{beds} \in \{1,2,4,5,8\} \\ &\quad Configurations \in \{C1, C2, C4, C5a, C5b, C8\} \\ &\quad LB \leq P_{feed} \leq UB \\ &\quad LB \leq Purge/Feed \leq UB \\ &\quad LB \leq Carbon/Zeolite \leq UB \end{aligned} \tag{2.94}$$

2.7.3.3. Case study III: Oxygen production from air

The objective in this case study is to investigate effects of various design and operating parameters on process performance. Air separation is the most frequently small (to medium) scale process since the cryogenic distillation is still economically better choice for large-scale production. Thus, usually a small number of beds is employed (in this study a two bed configuration is used). Feed is freely available at 1 bar and a compression is necessary. Desorption is performed at 1 bar, hence no vacuum pumps are needed. Based on parametric studies and a sensitivity analysis given in Table 2.44, the most significant process parameters were found to be particle size, feed pressure and flowrate, column geometry (length/diameter ratio), feed/purge ratio, cycle and step times. Due to the free availability of air, the process performance in this study cannot be expressed as a function of product recovery since the process of oxygen production is not considered as a recovery of the valuable product from the mixture (like the separation of hydrogen from SMROG). Therefore, the recovery in this study is of secondary importance (compared to the importance of the operating costs). The optimization problem being solved is formulated as the minimization of power consumption to produce oxygen at minimum required purity and of a specified flowrate, while optimizing the feed pressure and flowrate, purge/feed ratio, particle size, column length/diameter ratio (for the constant bed diameter), and step time durations:

$$
\begin{aligned}
&Min \quad Power\ for\ air\ compression \\
&s.t. \quad Model\ Equations \\
&\quad Purity_{O_2} \geq min.\ Purity_{O_2} \\
&\quad \dot{N}_{O_2} = required\ \dot{N}_{O_2} \\
&\quad N_{beds} \in \{2\} \\
&\quad Configurations \in \{C2\} \\
&\quad LB \leq Q_{feed} \leq UB \\
&\quad LB \leq P_{feed} \leq UB \\
&\quad LB \leq Purge/Feed \leq UB \\
&\quad LB \leq \frac{L}{D} \leq UB \\
&\quad LB \leq R_p \leq UB \\
&\quad LB \leq \tau_{adsorption} \leq UB \\
&\quad LB \leq \tau_{blowdown} \leq UB
\end{aligned}
\tag{2.95}
$$

Table 2.44. Typical sensitivity ratios (Case study III)

Control variable	Purity (constraint)	Power (obj. fn.)
Pfeed	0.3	1
P/F	1	0.2
L/D	0.01	0.4
Rp	0.001	0.01
τ_{ADS}	0.01	0.03
τ_{BLOW}	0.001	0.003
Qfeed	0.003	0.03

2.7.4. Optimization results

All optimization problems have been solved using the gPROMS/gOPT tool. The latter employs the rSQP non-linear programming code, implementing a reduced sequential quadratic programming algorithm. Transport properties and adsorption isotherm parameters and other relevant data have been adopted from the work of Park et al (1998, 2000) (case studies I and II), and Jee et al, 2003 (case study III) and summarized in Table 2.45 to Table 2.49. Runtime parameters are given in Table 2.50 and Table 2.51. Axial domain is discretized by using orthogonal collocation of finite elements method of third order and 30 elements. The CPU time strongly depends on the complexity of the particular optimization problem. Optimization times (on the AMD Athlon machine running at 2.2GHz) for both case studies are given in Table 2.52.

Table 2.45. Various design, operating and transport characteristics (Case studies I and II)

Parameter	Value	Units
Temperature of the feed	297	K
Temperature of the purge gas	297	K
Purge gas pressure	1e5	Pa
Molar fraction of H_2 in feed	0.755	-
Molar fraction of CO in feed	0.040	-
Molar fraction of CH_4 in feed	0.035	-
Molar fraction of CO_2 in feed	0.170	-
Heat axial dispersion coefficient	1e-4	m^2/s
Mass axial dispersion coefficient	1e-4	m^2/s
Activated carbon		
Particle density	850	kg/m^3
Particle radius	0.003	m
Bed void fraction	0.36	-
LDF coefficient of H_2	1.0	1/s
LDF coefficient of CO	0.3	1/s
LDF coefficient of CH_4	0.4	1/s
LDF coefficient of CO_2	0.1	1/s
Heat capacity of the particles	878.64	J/(kg·K)
Zeolite 5A		
Particle density	1080	kg/m^3
Particle radius	0.0016	m
Bed void fraction	0.36	-
LDF coefficient of H_2	1.0	1/s
LDF coefficient of CO	0.15	1/s
LDF coefficient of CH_4	0.2	1/s
LDF coefficient of CO_2	0.05	1/s
Heat capacity of the particles	962.32	J/(kg·K)

Table 2.46. Various design, operating and transport characteristics (Case study III)

Parameter	Value	Units
Temperature of the feed	297	K
Temperature of the purge gas	297	K
Purge gas pressure	1e5	Pa
Bed void fraction	0.314	-
Bed inner diameter	0.1	m
Molar fraction of O_2 in feed	0.21	-
Molar fraction of N_2 in feed	0.79	-
Particle density	1160	kg/m^3
Heat capacity of the particles	920	J/(kg·K)
LDF coefficient of O_2	0.15	1/s
LDF coefficient of N_2	0.05	1/s
Heat axial dispersion coefficient	1e-4	m^2/s
Mass axial dispersion coefficient	1e-4	m^2/s

Table 2.47. Langmuir parameters and heat of adsorption for activated carbon

Comp.	$a_1 x10^3$ (mol/g)	a_2 (K)	$b_1 x10^9$ (Pa^{-1})	b_2 (K)	$-\Delta H_{ads}$ (J/mol)
H_2	4.32	0.00	5.040	850.5	7861.73
CO	0.92	0.52	5.896	1730.9	16677.42
CH_4	-1.70	1.98	19.952	1446.7	18752.69
CO_2	-14.20	6.63	24.775	1496.6	25572.61

Table 2.48. Langmuir parameters and heat of adsorption for zeolite 5A

Comp.	$a_1 x10^3$ (mol/g)	a_2 (K)	$b_1 x10^9$ (Pa^{-1})	b_2 (K)	$-\Delta H_{ads}$ (J/mol)
H_2	4.32	0.00	5.040	850.5	7861.73
CO	0.92	0.52	5.896	1730.9	16677.42
CH_4	-1.70	1.98	19.952	1446.7	18752.69
CO_2	-14.20	6.63	24.775	1496.6	25572.61

Table 2.49. LRC parameters and heat of adsorption for zeolite 5A

Comp.	$a_1 x10^3$ (mol/g)	$a_2 x10^6$ (mol/g·K)	$b_1 x10^6$ (atm^{-1})	b_2 (K)	n_1 (-)	n_2 (K)	$-\Delta H_{ads}$ (J/mol)
O_2	7.151	-18.20	5419	662.6	-1.101	656.4	5508
N_2	6.210	-12.70	198.6	1970	2.266	-396.5	16378

Table 2.50. Runtime parameters (Case studies I and II)

Parameter	Configuration					
	C1	C2	C4	C5a	C5b	C8
$\tau_{Press,\ s}$	120	60	60	48	48	60
$\tau_{Ads,\ s}$	120	120	120	96	96	90
$\tau_{PEQ1,\ s}$	-	60	60	48	48	30
$\tau_{PEQ2,\ s}$	-	-	-	48	48	30
$\tau_{PEQ3,\ s}$	-	-	-	-	-	30
$\tau_{CoCD,\ s}$	-	-	60	-	48	-
$\tau_{Purge,\ s}$	120	60	60	48	48	60
$\tau_{Blow,\ s}$	120	120	60	96	48	90
$\tau_{cycle,\ s}$	480	480	480	480	480	480

Table 2.51. Runtime parameters (Case study III)

Parameter	Configuration C2
$\tau_{Press,\ s}$	50
$\tau_{Ads,\ s}$	100
$\tau_{PEQ1,\ s}$	50
$\tau_{Blow,\ s}$	50
$\tau_{Purge,\ s}$	100
$\tau_{cycle,\ s}$	400

Table 2.52. Optimization durations

Case study	Duration, h					
	C1	C2	C4	C5a	C5b	C8
I	7	11	20	17	25	26
II	9	29	43	37	51	48
III		60				

2.7.4.1. Case study I: Hydrogen recovery from SMROG (single layer)

The objective here is to maximize product recovery for a given minimum requirement in product purity while optimizing purge/feed ratio (0.5–2.5), feed pressure (5–30bar), and L/D ratio (5–15), where the values in the parenthesis indicate upper and lower bounds of the optimization variables. Two optimization runs have been conducted for two different constraints on product purity: 99.9 and 99.99%. All studies have been carried out keeping the cycle time, amount of adsorbent and adsorbent productivity constant. This way it is possible to analyze the separation quality for a given minimum purity and different process designs ensuring that the same amount of feed is processed during the same period of time. A comparison of the optimization results (for purity 99.90 and 99.99%) and the base case design (L/D ratio=5, purge/feed ratio=1, feed pressure=25bar) is shown in figures 2.53 to 2.58.

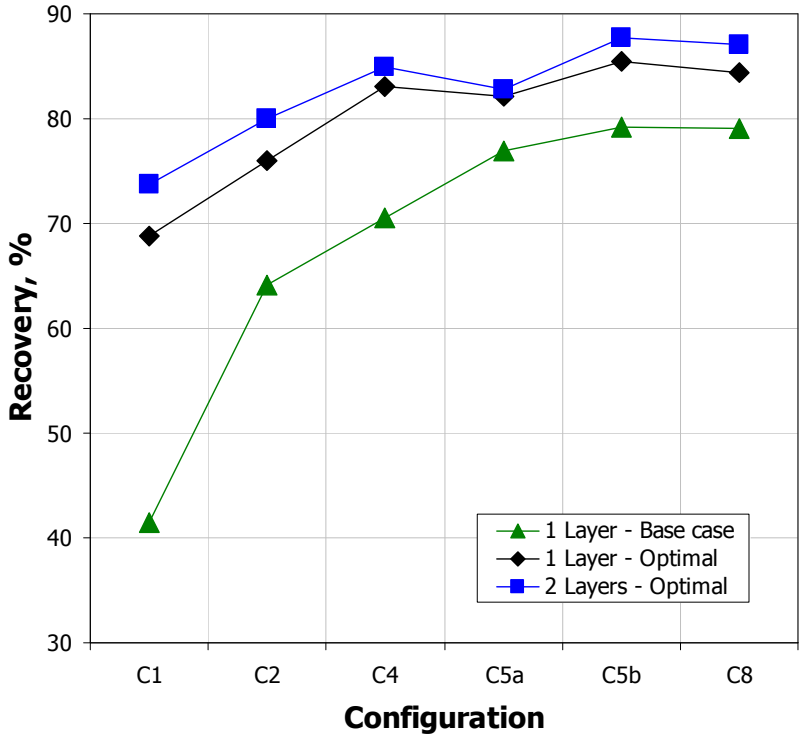

Figure 2.53. Case study I, II: optimal recovery (purity 99.9^{+} %)

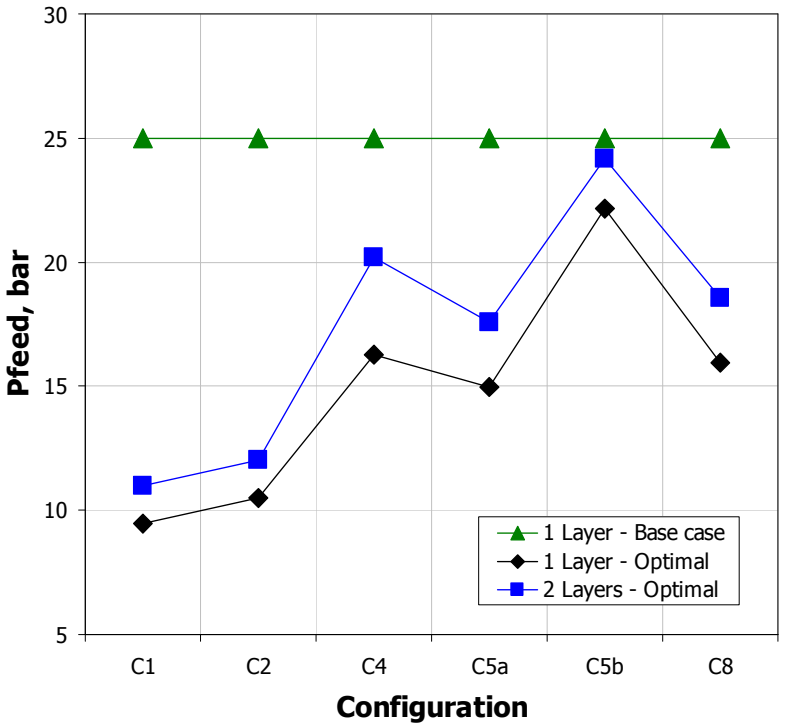

Figure 2.54. Case study I, II: optimal feed pressure (purity 99.9$^+$ %)

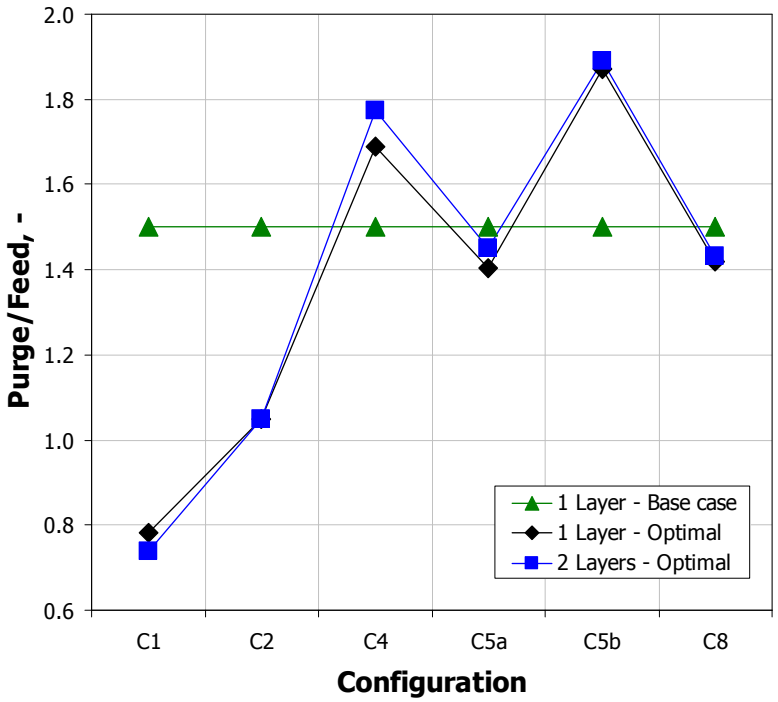

Figure 2.55. Case study I, II: optimal purge/feed ratio (purity 99.9$^+$ %)

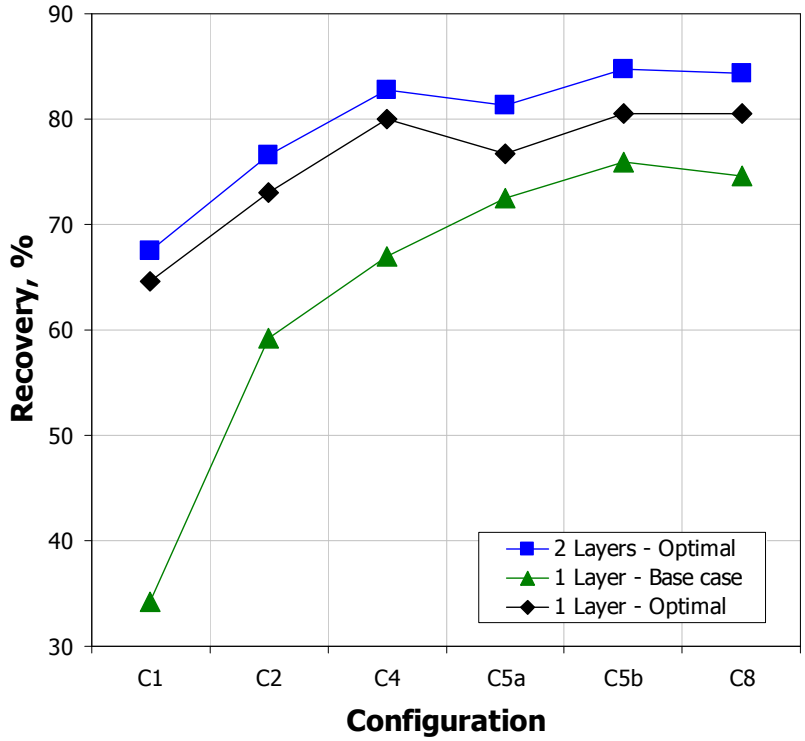

Figure 2.56. Case study I, II: optimal recovery (purity 99.99^{+} %)

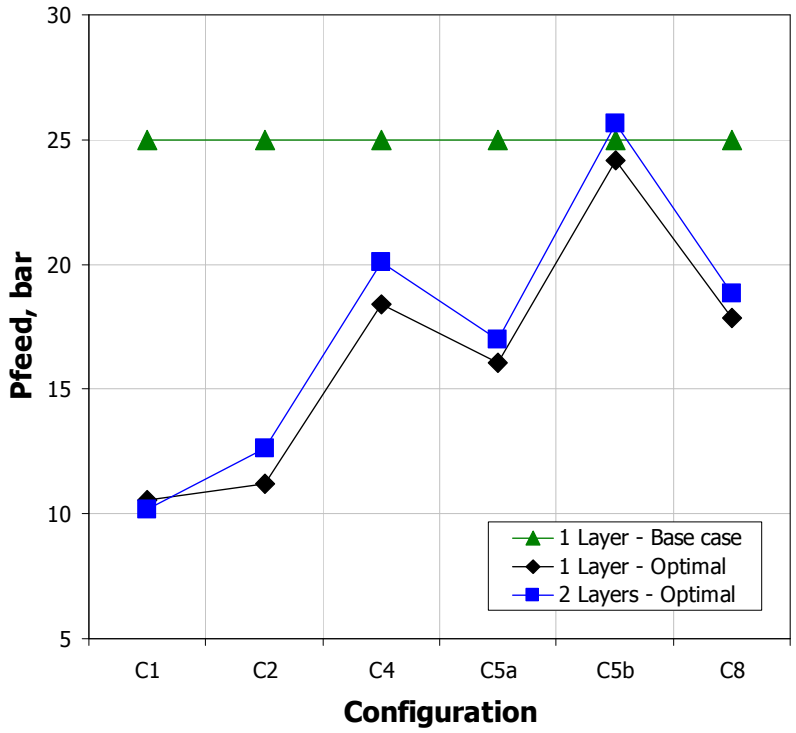

Figure 2.57. Case study I, II: optimal feed pressure (purity 99.99^{+} %)

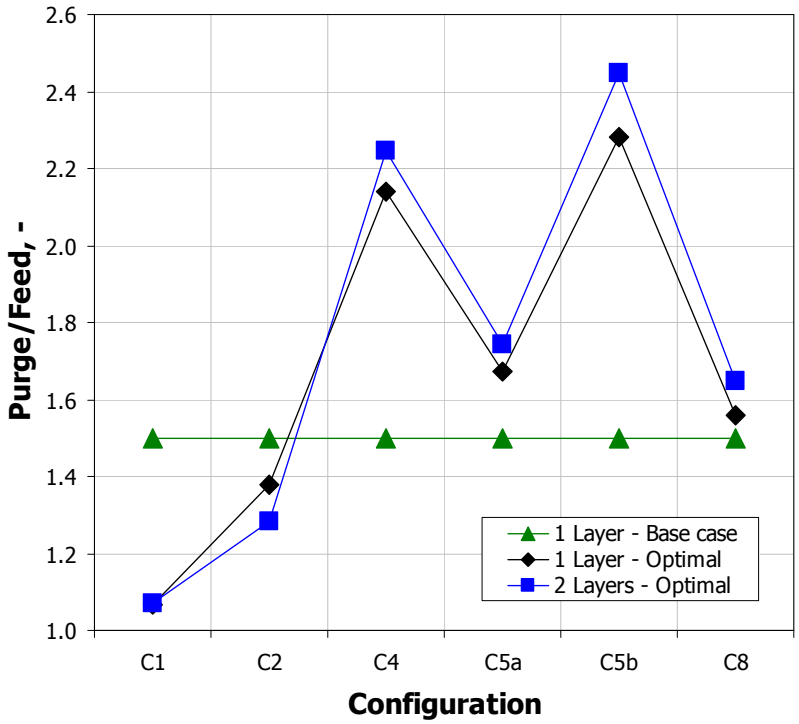

Figure 2.58. Case study I, II: optimal purge/feed ratio (purity 99.99^{+} %)

2.7.4.2. Case study II: Hydrogen recovery from SMROG (double layer)

The objective is the same as in case study I representing maximization of product recovery for given minimum requirements in product purity while optimizing purge/feed ratio (0.5–2.5), feed pressure (5–30bar), and carbon/zeolite ratio (0–1) for fixed L/D ratio (5). Again two optimization runs have been carried out changing the minimum requirements in product purity (99.9 and 99.99%). Optimization results are summarized in Figure 2.53 to Figure 2.58, and. Again, the same trends hold for 99.90% and 99.99% purity. Figure 2.59 and Figure 2.60 illustrates a comparison of the optimal carbon/zeolite ratios obtained for 99.90 and 99.99% minimum purity requirements.

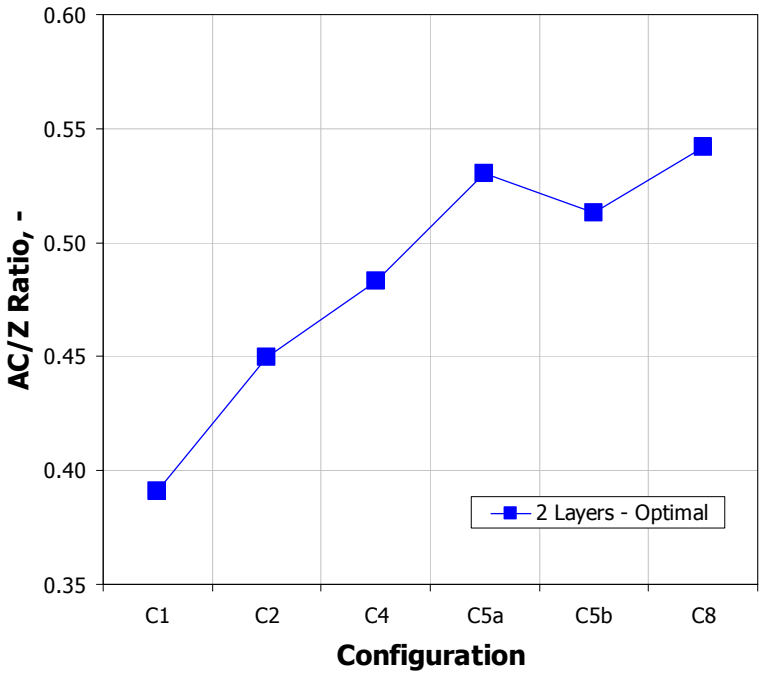

Figure 2.59. Case study II: optimal carbon/zeolite ratio (purity 99.9^{+} %)

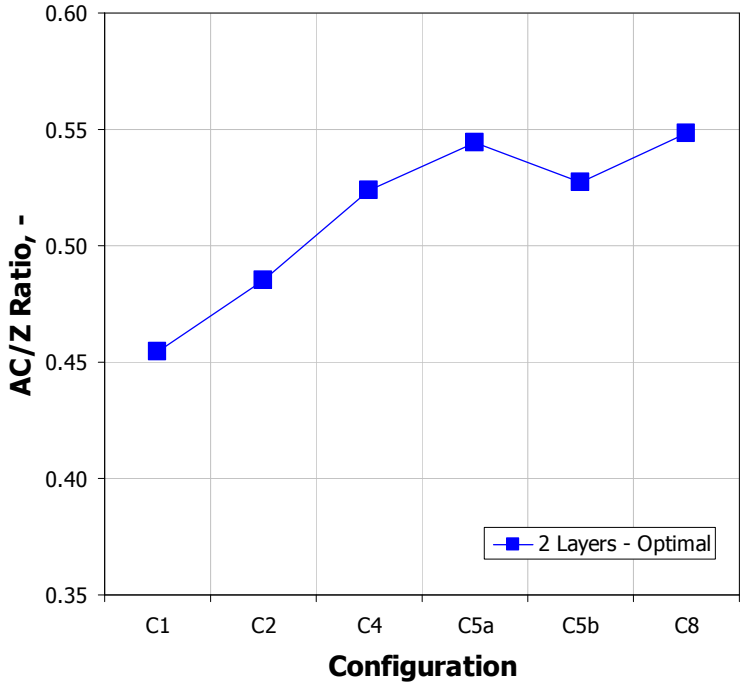

Figure 2.60. Case study II: optimal carbon/zeolite ratio (purity 99.99^{+}%)

2.7.4.3. Case study III: Oxygen production from air

The objective here is to minimize power consumption for given minimum requirements in product purity and product flowrate while optimizing the feed pressure (3-12bar), the feed flowrate (20-40 L_{STP}/min), purge/feed ratio (0.5-2.0), step times for constant cycle time: blowdown ($0.1\tau_c$-$0.15\tau_c$), adsorption ($0.2\tau_c$-$0.3\tau_c$), particle radius (0.3-2.5mm), column L/D ratio (3-10). Minimum oxygen purity requirements are fixed to 99.5^{+}%. Since there is no practical difference between oxygen and argon characteristics the actual oxygen purity is at the level of 95% while the remaining consists of argon. Configuration C2 has been used and pressurization is done co-currently by using the feed stream. Optimization results are summarized in Figure 2.61 to Figure 2.66.

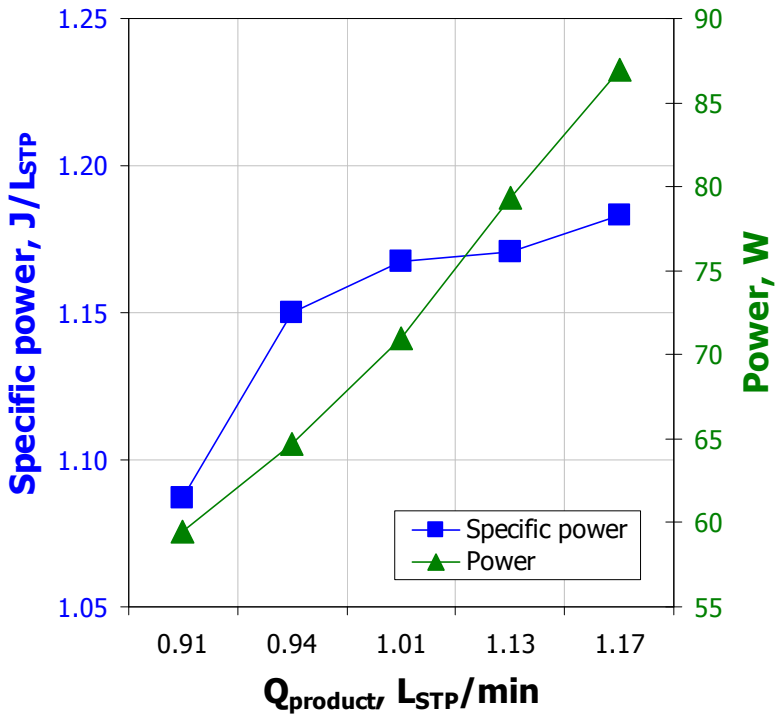

Figure 2.61. Case study III: optimal power and specific power (purity 99.5^{+} %)

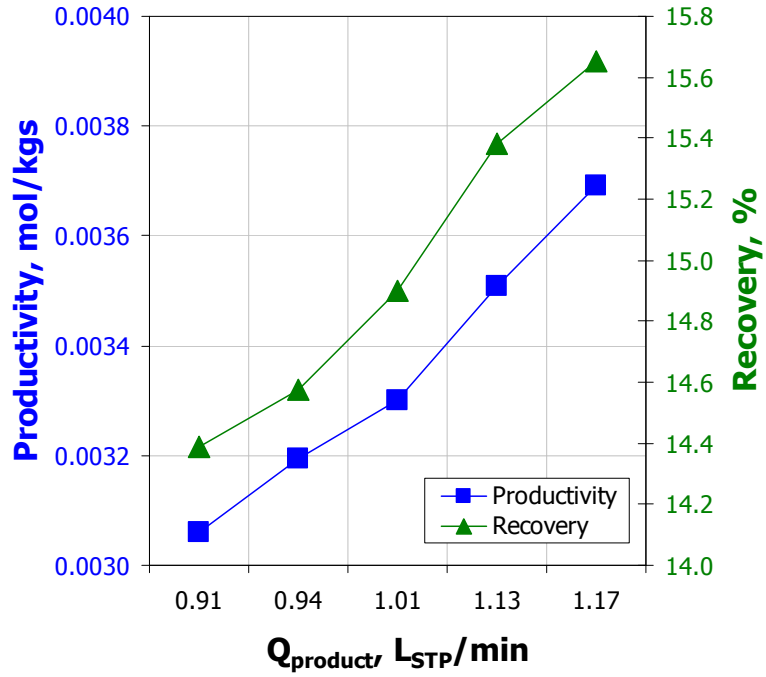

Figure 2.62. Case study III: optimal productivity and recovery (purity 99.5^{+} %)

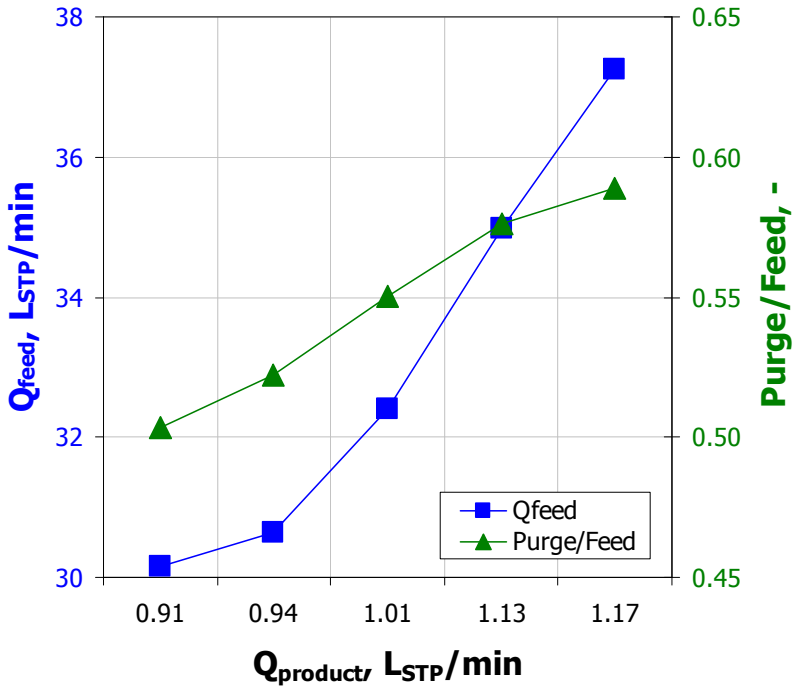

Figure 2.63. Case study III: optimal feed flowrate and purge/feed ratio (purity 99.5^{+} %)

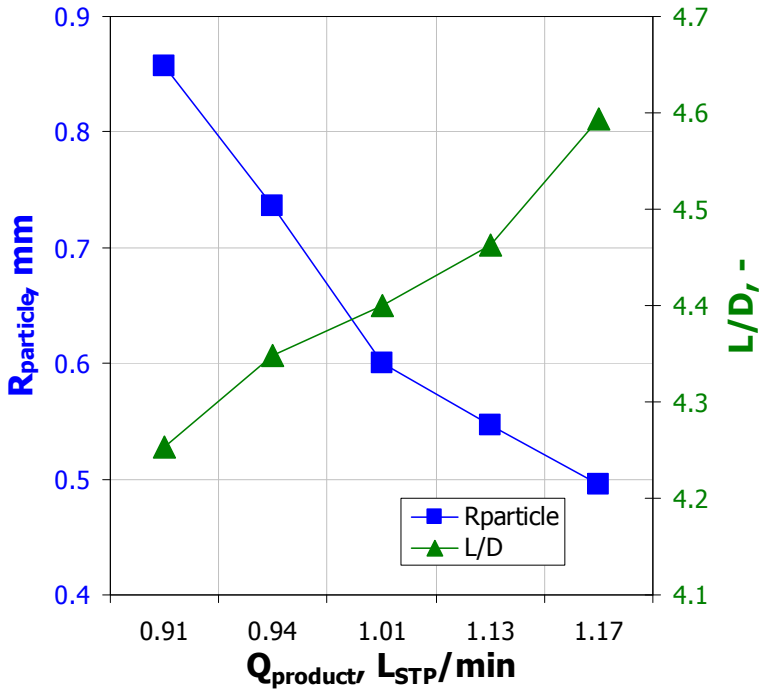

Figure 2.64. Case study III: optimal particle radius and L/D ratio (purity 99.5^{+} %)

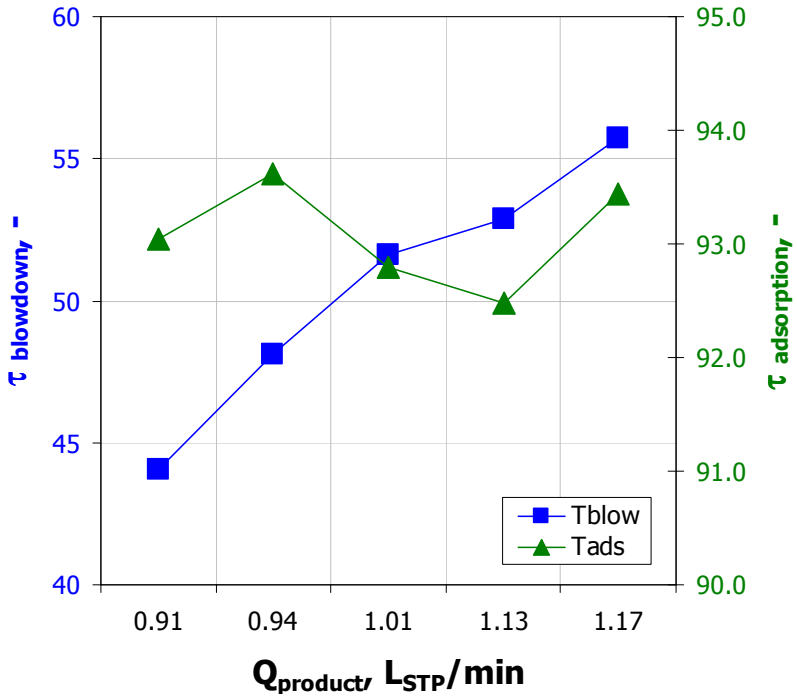

Figure 2.65. Case study III: optimal step times (purity 99.5^{+} %)

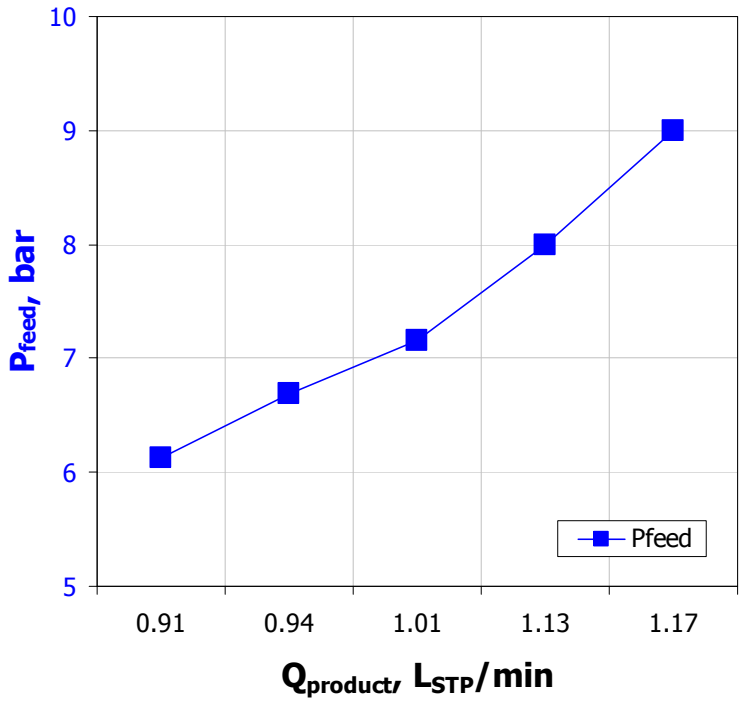

Figure 2.66. Case study III: optimal feed pressure (purity 99.5^{+} %)

2.7.5. Discussion

2.7.5.1. Case studies I and II

Comparison of the base case scenario with the optimized case indicates that the product recovery can be improved by 6-33%. It is clear that the recovery increases as the number of beds increase due to several subsequent co-current depressurization steps which conserve void gas. The recovery of configurations involving only pressure equalizations steps (C1, C2, C5a and C8) increases and reaches a maximum value (Figure 2.53). An interesting result is the improved process performance of configuration C4 compared to C5a, and configuration C5b compared to C8. Although they include one pressure equalization step less, they employ an additional co-current depressurization step to purge other columns, thus resulting in an improved recovery. Tables 2.53 to 2.55 reveal that as the number of equalizations increase, the final pressure decreases and the waste gas contains less hydrogen. This is due to the large amount of pure product spent during pressure equalizations, which affects the composition of waste gas. On the other hand, if we compare the final equalization pressures for configurations C4 and C5a, and C5b and C8 we observe a different trend: the final pressure in C4 is lower compared to C5a while it is higher in C5b compared to C8. On the other hand, the feed pressure is significantly higher in C4 and C5b compared to C5a and C8. Furthermore, the amount of void gas needed for two pressure equalizations (C4), one pressure equalization and one co-current depressurization providing purge (C5b) is higher compared to the corresponding amount spent in configurations C5a and C8. This leads to a better utilization of the void gases.

However, these effects strongly depend on the operating variables (such as feed pressure) and the system under consideration and it might not always be possible to exploit them.

Table 2.53. The feed and the final pressure after the last pressure equalization (Case studies I and II)

Configuration	Pressure, bar	
	Feed	Final eq.
C1	10.16	10.16
C2	12.61	5.90
C4	20.09	5.64
C5a	16.96	5.93
C5b	25.66	4.18
C8	18.82	3.46

Table 2.54. Average waste gas composition after blowdown step (Case studies I and II)

Configuration	Composition, %			
	H_2	CO	CH_4	CO_2
C1	73	5	4	18
C2	59	7	6	28
C4	50	8	7	35
C5a	50	8	7	35
C5b	48	8	7	37
C8	48	8	7	37

Table 2.55. Average waste gas composition after purge step (Case studies I and II)

Configuration	Composition, %			
	H_2	CO	CH_4	CO_2
C1	38	7	6	49
C2	34	8	7	51
C4	33	9	8	50
C5a	31	9	8	52
C5b	32	9	8	51
C8	31	9	8	53

The purge/feed ratio increases as the number of beds increases since the concentration front moves toward the end of the column due to many co-current depressurization steps,

thus requiring more purge gas to rinse the column. In addition, configurations C4 and C5b require much higher purge/feed ratios compared to the configurations C5 and C8 despite the same number of co-current depressurization steps. This is due to the existence of an additional co-current depressurization step used to provide purge, where void gas is used to rinse the columns (not pure hydrogen). Therefore, an increase in purge/feed ratio does not decrease the product recovery.

The feed pressure increases as the number of beds increases because higher pressures are needed to ensure feasible subsequent pressure equalization steps. The optimal feed pressure in C4 and C5b is higher compared to C5a and C8, respectively, due to the higher amount of gas needed for purge compared to the amount of gas spent in the last pressure equalization. This fact may be the limiting factor if the feed is not available at high enough pressure.

The results show that higher L/D ratios are always preferable in both cases. This can be attributed to the fact that longer columns had better support for re-adsorption of impurities as the concentration fronts move toward the end of the column during pressure equalization steps.

The different selectivity of activated carbon and zeolite adsorbents can be exploited as long as carbon dioxide does not break through the activated carbon layer. This is due to the specific shape of CO_2 isotherm on zeolite 5A which makes the regeneration step infeasible at atmospheric pressure. The concentration profiles (configuration C8) in the column after adsorption step (given in Figure 2.67a-d) show that the position where the CO_2 fraction drops to very low value corresponds to the optimal carbon/zeolite ratio (~0.55). In other words, without any additional optimization constraints, CO_2 is prevented to break through the carbon layer. Similar results stand for all other configurations. Furthermore, the carbon/zeolite ratio slightly increases as the number of beds increases because the CO_2 concentration front penetrates more deeply the bed during pressure equalization steps, thus leading to a higher amount of activated carbon needed. Configurations C4 and C5b require slightly lower carbon/zeolite ratios compared to C5a and C8, due to the higher feed pressure and consequently the higher adsorption capacity thus leading to a shorter activated carbon layer.

Similar configurations have been investigated by Park et al (2000) and Golden and Sircar (2000). Park et al (2000) used four columns (one column less) to perform the same schedule as in this work. The only difference in the schedule is that the co-current depressurization step takes place after the first pressure equalization while in this work it occurs after the second one. In addition, a number of other parameters were different (column geometry, feed flowrate, feed pressure, cycle time, step times, feed composition etc) except the mass transfer and isotherm data. Golden and Sircar (2000) presented an industrial process (Polybed) consisting of ten beds and the identical sequence of operating steps. These configurations are directly comparable with our results since the only difference is in number of beds which is twice higher, therefore allowing higher capacity of the plant. The input parameters are also different. Comparison of available input data and results obtained for 99.99^{+}% purity is provided in Table 2.56. The results indicate a slightly lower recovery in the 4-bed study and a more than one percent higher in the 10-bed industrial Polybed process. Comparing the total content of impurities, we can observe that this is highest in the 4-bed study (27.64%), 24.5% in our study and 22.86% in the 10-bed one. In addition, it should be noted than the four-bed study has not been optimized and thus an even higher recovery may be obtained using a formal optimization procedure. The

optimal active carbon fractions are 0.6-0.5, 0.768 and 0.528 in the 4-bed, 10-bed and our work, respectively. This is an expected trend since the CO_2 content is highest in the 10-bed study and lower in our work. Thus, a longer activated carbon layer is necessary to adsorb all CO_2 and prevent it from entering a zeolite layer.

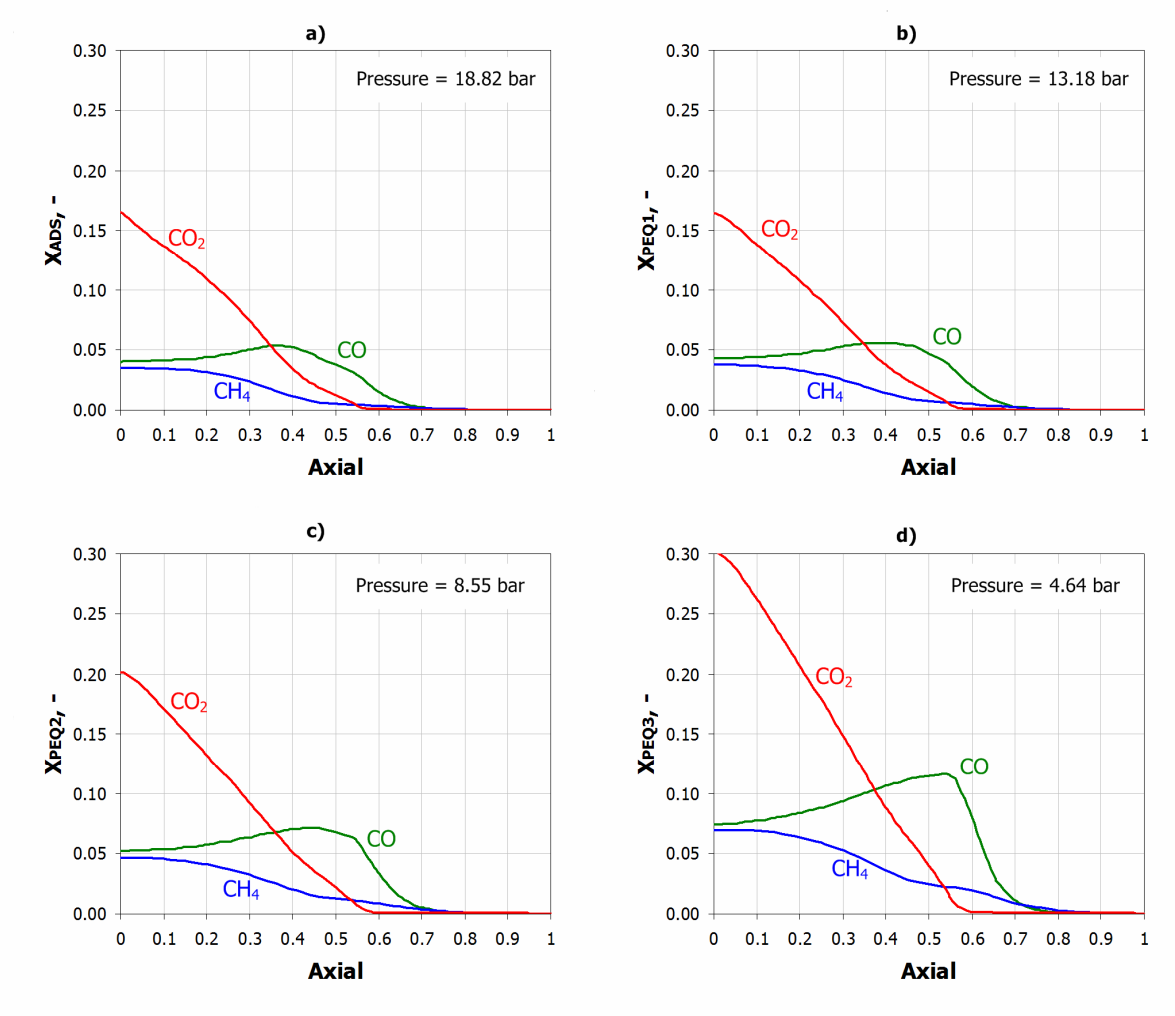

Figure 2.67. Concentration profiles (configuration C8, two layers): a) after adsorption step, b) after 1st pressure equalization, c) after 2nd pressure equalization, d) after 3rd pressure equalization

Table 2.56. Comparison of the results

	Park, 2000	Sircar, 2000	This work
N_{beds}	4	10	5
N_{PEQs}	2	2	2
N_{CoCD}	1	1	1
Capacity	Lab scale	High	Medium
Purity, %	99.99	99.999	99.99
Recovery, %	84	86	84.77
P_{feed}, bar	23.6	20.7	25.6
Act. carbon fraction, -	0.6-0.5	0.768	0.528
Feed composition, %			
H_2	72.36	77.10	75.50
CO_2	21.18	22.50	17.00
CO	2.49	0.35	4.00
CH_4	3.97	0.013	3.50
$\Sigma_{impurities}$, %	27.64	22.86	24.50
τ_{cycle}, min	6	13.33	8

As it was previously shown, it is difficult to compare different configurations without accurate economical data. However, the following general conclusions can be drawn from the results: a) the best configuration is C5b (five beds, two pressure equalizations, one co-current depressurization); b) by employing multi-bed configurations it is possible to achieve up to 18% higher recovery for the same purity; c) in the case that multicomponent mixtures are being separated it is a good idea to employ more than one adsorbent layer as up to 5% higher recovery can be obtained; c) as the number of beds and co-current depressurization steps increase, the product recovery asymptotically approaches the maximum value; this increase is higher at a lower number of beds/co-current depressurizations thus, at least two co-current depressurizations are necessary to get a good balance between increased capital costs of the columns and higher recovery; d) much higher feed pressures are needed to make several subsequent co-current depressurization steps feasible, something that can be a limiting factor; e) it appears that almost nothing can be gained by introducing a fourth co-current depressurization step.

2.7.5.2. Case study III

In order to compare the optimization results in this work to the results of existing oxygen generators some performance factor should be defined. A convenient performance indicator is the work needed to produce one liter of oxygen at a standard temperature and pressure (L_{STP}) and at a given oxygen flowrate. For instance, the work per liter of a PSA plant producing $5L_{STP}$/min demanding 300W is 1 J/L_{STP}. In typical industrial units this ratio is in the range of less than 1 (for high capacity plants) to more than 2 J/L_{STP} (for low capacity plants). Keeping in mind the low capacity of the unit, the optimization results (presented in Figure 2.61) show the potential advantages offered by the proposed optimization approach. It should be noted that the power requirements in this work are theoretical and in a real study, all non-idealities have to be taken into account. The oxygen recovery, as it is mentioned before, is not one of the primary performance indicators due to

the free availability of air. However, it is reported in the literature (Chiang et al, 1994) that high purity oxygen+argon (99.7^{+}%) can be produced with 10% recovery at a pressure ratio of 6.4. In addition, 98.2% purity can be achieved for 15% recovery and at a pressure ratio of 4.3. In this thesis, the optimized purity is 99.5% for a recovery in the range of 14-15% and pressure ratios 6-9 (given in Figure 2.62 and Figure 2.66).

All other decision variables show the expected trends (according to the parametric analysis). As the product flowrate increases the feed flowrate and purge/feed ratio increase (given in Figure 2.63), the particle radius decrease and the length/diameter ratio increase (illustrated in Figure 2.64), and the feed pressure increases (shown in Figure 2.66). According to Figure 2.65, the duration of blowdown step increase (to increase the amount of impurities removed during the blowdown).

Chapter 3

Membranes

3.1. Introduction

Gas separation by membrane systems is a promising technology offering potentially low energy consumption, possibility for continuous operation, dramatically lower investment costs, ease of operation and overall cost effectiveness. Membranes were known to have the potential to separate important gas mixtures long before 1980, but the technology to fabricate high-performance membranes and modules economically was lacking. The development of high-flux anisotropic membranes and large-surface-area membrane modules for reverse osmosis applications occurred in the late 1960s and early 1970s. Permea (now a division of Air Products) then adapted this technology to membrane gas separation. Its poly-sulfone hollow-fiber membrane was an immediate success, particularly for the separation and recovery of hydrogen from the purge gas streams of ammonia plants. This success encouraged other companies to advance their own technologies and during the past 20 years the use of membrane gas separation processes has grown rapidly. More than 90% of the developed membranes involves the separation of non-condensable gases: nitrogen from air, carbon dioxide from methane, hydrogen or methane from various mixtures, natural gas separations etc. Also, a large potential for membrane gas separation lies in separating mixtures containing condensable gases such as the $C3^+$ hydrocarbons from methane or hydrogen, propylene from propane, and n-butane from isobutene. Currently, only eight or nine polymer materials have been used to make at least 90% of the total installed gas separation membrane base and several hundred new polymer materials have been reported in the past few years.

Typical industrial processes where membranes are employed are:

- Separation of hydrogen from gases like nitrogen and methane

- Recovery of hydrogen from product streams of ammonia plants
- Recovery of hydrogen in oil refinery processes
- Separation of methane from biogas
- Enrichment of air by oxygen for medical or metallurgical purposes
- Removal of water vapour from natural gas
- Removal of CO_2 from natural gas
- Removal of H_2S from natural gas
- Removal of volatile organic liquids from air of exhaust streams
- Desiccation

Usually nonporous polymeric membranes are used in gas separations. There, vapours and gases are separated due to their different solubility and diffusivity in polymers. Polymers in glassy state, generally more effective for separation, predominantly differentiate in diffusivity. Small molecules of penetrants move among polymer chains according to the formation of local gaps by thermal motion of polymer segments. Free volume of the polymer, its distribution and local changes of distribution are of the utmost importance. Then diffusivity of a penetrant depends mainly on the size of its molecule.

Porous membranes are also utilized for the gas separation. The pores diameter must be smaller than the mean free path of gas molecules. Under normal condition (100 kPa, 300 K) this figure is about 50 nm. Then the gas flux through the pore is proportional to molecules velocity i.e. inversely proportional to square root of the molecule mass. It is known as Knudsen diffusion. Gas flux through a porous membrane is much higher than through a nonporous one – 3 to 5 orders of magnitude.

Over 430 patents have been issued since 2000 for hydrogen selective membranes (Ritter and Ebner, 2007) where four classes of membranes dominate: O_2 permeable membranes, H_2 permeable inorganic membranes, H_2 permeable polymeric membranes, and CO_2 permeable membranes.

Oxygen Permselective Membranes

The development of improved oxygen permselective membranes is essential for the commercial implementation of syngas production via partial oxidation (POX). POX is an exothermic process, which produces a lower H_2/CO ratio (1⁄42) than steam reforming and provides advantages in syngas production, Fischer-Tropsch chemistry and other gas to liquid processes. POX processes can operate at lower temperatures and pressures providing energy savings.

Hydrogen Permselective Inorganic Membranes

The use of hydrogen selective membranes to enhance hydrocarbon conversions for hydrogen and syngas production has been receiving considerable attention. Selective separation of hydrogen at high temperatures is appealing for hydrogen and ammonia production plants, as it lowers the CO content, which subsequently reduces operational and capital costs for PSA units and methanators. These cost reductions are further maximized if hydrogen selective membranes are incorporated into hybrid SMR, POX or WGS reactors.

Hydrogen Permselective Polymeric Membranes

Hydrogen permselective polymeric membranes are widely used for hydrogen recovery from refinery streams at low temperatures. As mentioned above, polymeric membranes that are selective towards hydrogen over heavier gases, like carbon dioxide, can be used for hydrogen recovery in tail streams of PSA units.

Carbon Dioxide Permselective Membranes

Carbon dioxide is a highly permeable gas; generally, only hydrogen and helium are more permeable. In fact, at low temperatures, the solubility selectivity of carbon dioxide/hydrogen dominates the diffusivity advantages of H_2 and membranes have been developed with selectivity towards carbon dioxide. Rubbery type membranes are preferred for carbon dioxide/hydrogen separation.

3.2. Principles of operation

The main principle of the membrane technology is to allow one component of a mixture to permeate the membrane freely, while hindering permeation of other components (Figure 3.1). Thus, the separation process depends upon the different transport rates of different components through membrane and it is driven by a difference in the gas partial pressure across the membrane. The most common processes are pressure-driven processes, such as reverse osmosis, ultra- and micro-filtration and gas separation, concentration-driven such as dialysis, partial-pressure-driven, such as pervaporation, and electrical-potential-driven processes, such as electrolysis and electrodialysis. In gas separations, typically a high pressure gas mixture is applied on one side of membrane (called retentate) while the product is removed from the other side (called permeate). The ranges of membrane based separations are presented in Figure 3.2.

The key properties determining membrane performance are high selectivity and fluxes; good mechanical, chemical, and thermal stability under operating conditions; low fouling tendency and good compatibility with the operation environment; and cost-effective and defective free production. Membranes are produced as flat sheets, hollow fibers, capillaries or tubes. For practical operations, membranes are installed in a suitable device, which is referred to as membrane module. There are many different types of membrane modules. Their key properties are high packing density, good control of concentration polarization and membrane fouling, low operating and maintenance costs and cost-efficient production.

Permeability and selectivity are only two of the criteria that must be met to produce a useful membrane; others include the ability to form stable, thin, low-cost membranes that can be packaged into high-surface-area modules. To obtain high permeation rates, the selective layer of gas separation membranes must be extremely thin. Typical membranes have effective thicknesses of less than 0.5 μm and often less than 0.1 μm. These membranes have a thin, dense, nonporous skin layer that performs the separation, supported on a finely micro-porous substrate made from the same material that provides mechanical strength.

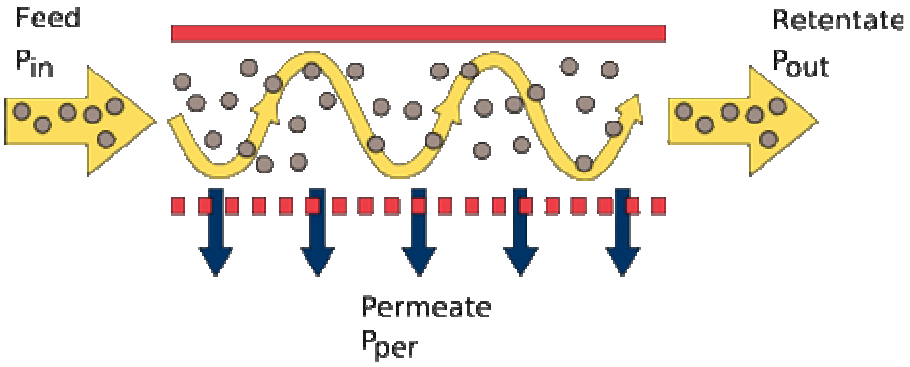

Figure 3.1 Principle of a membrane operation

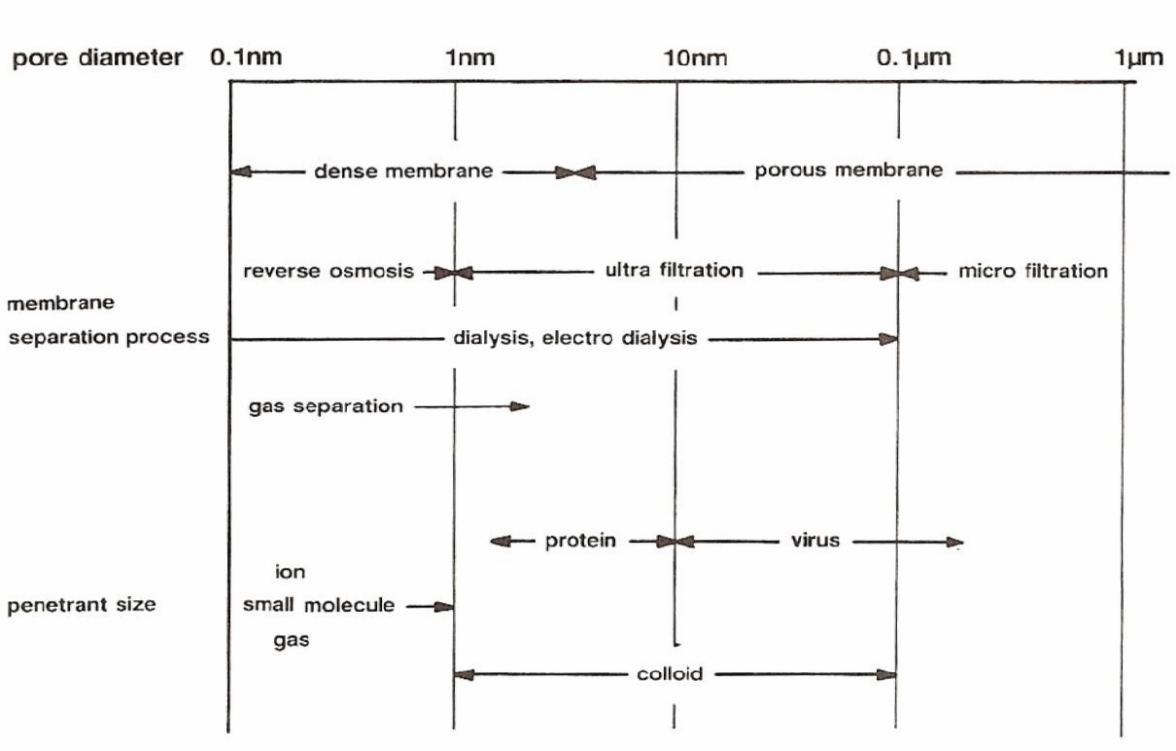

Figure 3.2 Ranges of membrane based separations

3.3. Literature review

Theoretical approaches for modelling diffusion in microporous structures generally fall into two different categories: a kinetic approach and an approach based on irreversible thermodynamics. The kinetic approach is based on random walk models and/or transition state theory appropriately modified to account for several additional phenomena such as multilayer adsorption, surface heterogenity and energy barriers (Yang et al, 1973; Chena and Yang, 1992; Sikavitsas and Yang, 1995). The irreversible thermodynamics approach considers the chemical potential gradient as the driving force for diffusion (Kärger and Büllow, 1975; Kärger and Ruthven, 1992). Multicomponent interactions occur through competitive equilibrium and/or diffusional sorbate-sorbate interactions. In this case, the driving force exerted on any particular species is balanced by the friction this species experiences with all other species present in the mixture and can be accurately described by the Generalized Maxwell-Stefan (GMS) model for diffusion (Van de Graaf et al, 1999; Krishna, 2001; Kapteijn at al, 2000). Arguably, the Maxwell-Stefan formulation provides the most general, and the most convenient approach for describing mass transport which takes proper account of thermodynamic non-idealities and influence of external force fields. Furthermore, the Maxwell-Stefan approach can be extended to handle diffusion in macro- and microporous catalysts, adsorbents and membranes. Krishna and Wesselingh (1997) presented a comprehensive review on the application of the Maxwell-Stefan approach, as well as several examples illustrating the inadequacy of the Ficks's approach to modelling multi-component diffusion in micro-porous media. The applicability and advantages of the Maxwell-Stefan approach have been extensively analyzed in several contributions in the literature by Krishna et al (1993, 1997, 2000, 2003, 2004, 2005, 2006 and 2007), Van de Graaf et al (1998, 1999, 2000), and Baker (1987, 1994, 1996, 1998, 2001).

3.4. Mathematical modelling

Transport phenomena in porous solids have been the subject of many studies. Quantitative solutions are obtained only in few cases for relatively simple cases such as the permeation of a single gas. Separation of gas mixtures is much more complicated due to complex membrane architecture, large pressure gradients and extensive component interactions. In this work, a generic membrane unit model has been developed. It comprises three low-level models:

- Permeate and retentate compartments (essentially the same transport phenomena)
- Porous membrane
- Macroporous support layer

All lower level models are treated as black boxes. For example, any type of membranes can be modelled as long as the membrane model can calculate the mass flux through the membrane for given pressure, temperature and composition at the interfaces. The mass flux calculated in the membrane model serve as a glue between the models: flux continuity equations must be satisfied at the interface between the retentate compartment and the membrane, between the membrane and the porous support, and between the porous support and the permeate compartment. The membrane unit topology is illustrated in Figure 3.3.

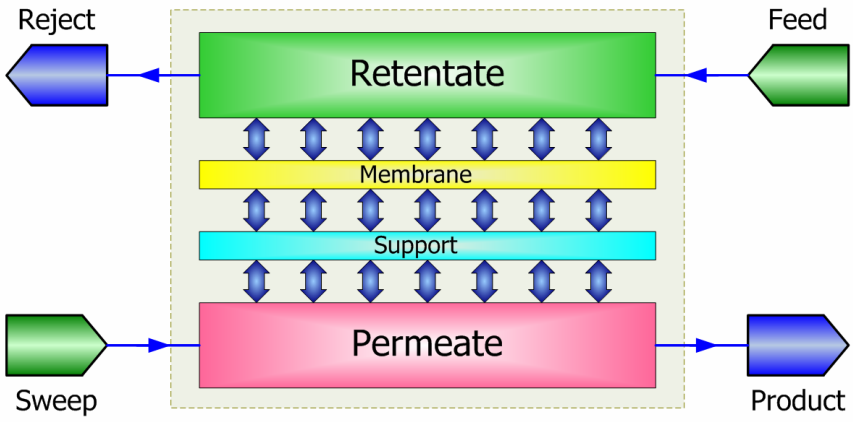

Figure 3.3 The topology of the membrane unit

3.4.1. Permeate/Retentate compartments

The Permeate/Retentate compartments topology is shown in Figure 3.4. The compartments are connected to the support layer and the membrane, respectively, while the proper boundary conditions are selected at each of two interfaces to ensure flux continuity between them.

The main assumptions made in the model are:

- Ideal gas law holds
- Isothermal operation
- Negligible pressure drop
- The flow pattern is described by the axially dispersed plug flow
- The flux through the interface of the compartment with the membrane (N_i) is calculated in the membrane model and given as a boundary condition

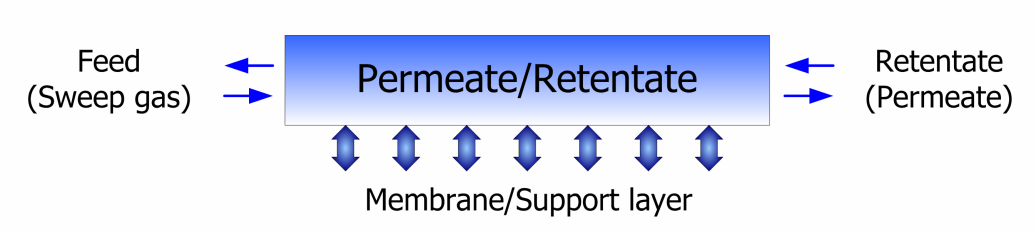

Figure 3.4 Topology of the Permeate/Retentate compartment model

Mass balance for the axially dispersed plug flow is given by the following equation:

$$\frac{\partial(uC_i)}{\partial z} - D_{z,i}\frac{\partial^2 C_i}{\partial z^2} + a_V N_i = 0,\ i = 1, N_{comp},\ z \in (0, L) \tag{3.1}$$

The generation term in the equation 3.1 contains the molar flux N_i at each position along the compartment. The molar flux is calculated in the membrane model and coupled at the interfaces between the compartments and the membrane/support by the boundary conditions equations.

The total pressure is constant and given by:

$$P = RT\sum_i C_i,\ \forall z \in (0,\ L) \tag{3.2}$$

The boundary conditions at the inlet/outlet of the compartment depend on the operating mode of the module. Two operating modes have been developed:

- Co-current mode

$$u\left(C_i\big|_{z=0} - C_i^{in}\right) = D_{z,i}\frac{\partial C_i\big|_{z=0}}{\partial z},\ i = 1,\ N_{comp} \tag{3.3}$$

$$\left.\frac{\partial C_i}{\partial z}\right|_{z=L} = 0,\ i = 1,\ N_{comp} \tag{3.4}$$

$$u\big|_{z=0} = u_{in} \tag{3.5}$$

$$\left.\frac{\partial u}{\partial z}\right|_{z=L} = 0 \tag{3.6}$$

- Counter-current mode

$$u\left(C_i\big|_{z=L} - C_i^{in}\right) = D_{z,i}\,\frac{\partial\, C_i\big|_{z=L}}{\partial z},\ i = 1,\ N_{comp} \tag{3.7}$$

$$\left.\frac{\partial C_i}{\partial z}\right|_{z=0} = 0,\ i = 1,\ N_{comp} \tag{3.8}$$

$$u\big|_{z=L} = u_{in} \tag{3.9}$$

$$\left.\frac{\partial u}{\partial z}\right|_{z=0} = 0 \tag{3.10}$$

3.4.2. Porous membrane

The generalized Maxwell-Stefan (GMS) equations provide an adequate basis for the description of multicomponent mass transfer in porous media (Krishna, 1993). The Maxwell-Stefan approach is a convenient way to describe diffusion in porous media and yields coefficients that are directly amenable to physical interpretations. The GMS equations are based on the assumption that movement of species is caused by a driving force, which is balanced by the friction that the moving species experience from each other and their surroundings. Taking the gradient of the thermodynamic potential as the driving force and treating vacancies as participating species (representing zeolite) Krishna (1993) derived equations for the diffusion of adsorbed species.

Following the approach proposed by Krishna and Baur (2004) it is possible to independently combine the methods for computing the phase equlibria, the thermodynamic correction factor and the square matrix of inverse Maxwell-Stefan coefficients. A list of the implemented options is given below.

a) Methods for calculating the phase equilibrium:

- Multicomponent Langmuir isotherm (single or dual site)
- Ideal Adsorbed Solution (IAS) theory
- Real Adsorbed Solution (RAS) theory

b) Methods for the thermodynamic correction factor Γ:

- Unity matrix (no correction)
- Based on multicomponent Langmuir isotherm (single or dual site)
- Based on IAS theory
- Based on RAS theory

c) Methods for the square matrix of inverse Maxwell-Stefan coefficients $Đ_{ij}$:

- No binary diffusional interactions
- Binary interaction estimated from Vignes equation

The porous membrane topology is presented in Figure 3.5. The membrane is connected at one side to a retentate compartment and to a support layer at the other, and the boundary conditions at each of two interfaces ensure the mass flux continuity between them.

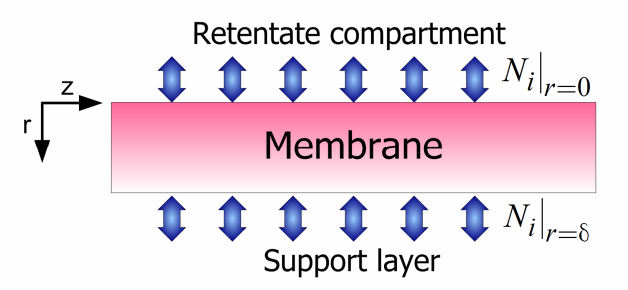

Figure 3.5 Topology of the membrane model

The main assumptions made in the model are:

- Ideal gas behaviour
- Isothermal and the steady state operation
- All adsorption happens at the membrane interfaces ($r = 0$ and $r = \delta$)
- At the steady state, gas is in equilibrium with the membrane surface
- Inside the membrane gas is transported by surface diffusion
- The flux is constant along the membrane (r axis direction):

$$\frac{\partial N_i}{\partial r} = 0,\ \forall z \in [0,\ L],\ i = 1,\ N_{comp} \tag{3.11}$$

Three options are available to describe multi-component diffusion in micro-porous media (adsorbate phase):

a) Assuming that the Fick law applies (useful during the initialization of the DAE system):

$$N_i = -\frac{\rho q_i^{sat} Đ_i}{RT}\frac{\partial \theta_i}{\partial r},\ i = 1, N_{comp},\ z \in [0, L],\ r \in [0, \delta_m) \tag{3.12}$$

b) Assuming friction between molecules less important than friction with the wall; in that case $Đ_{ij}$ is much larger than $Đ_i$ and this case is referred to as the "single-file" diffusion mode and given by the following equation:

$$N_i = -\frac{\rho q_i^{sat} Đ_i}{RT}\sum_{j=1}^{N_{comp}} \Gamma_{ij}\frac{\partial \theta_i}{\partial r},\ i, j = 1, N_{comp},\ z \in [0, L],\ r \in [0, \delta_m) \tag{3.13}$$

c) If molecule-molecule interactions cannot be neglected, the general Maxwell-Stefan equations are used:

$$\frac{\theta_i}{RT}\frac{\partial \mu_i}{\partial r} = \sum_{\substack{j=1 \\ j \neq i}}^{N_{comp}} \frac{q_j N_i - q_i N_j}{q_i^{sat} q_j^{sat} Đ_{ij}} + \frac{N_i}{q_i^{sat} Đ_i},\ i, j = 1, N_{comp},\ z \in [0, L],\ r \in [0, \delta_m) \tag{3.14}$$

For calculation of the cross-term diffusivities $Đ_{ij}$ Krishna (1993) proposed to use the empirical relation of Vignes to determine $Đ_{ij}$ from the single-component diffusivities:

$$Đ_{ij} = Đ_i^{\frac{\theta_i}{\theta_i + \theta_j}} Đ_j^{\frac{\theta_j}{\theta_i + \theta_j}},\ i, j = 1, N_{comp},\ z \in [0, L],\ r \in [0, \delta_m) \tag{3.15}$$

The gradient of the surface chemical potential $\frac{\partial \mu_i}{\partial r}$ in equation 3.14 may be expressed in terms of the gradients of the surface occupancies by introduction of the thermodynamic factor Γ:

$$\frac{\theta_i}{RT}\frac{\partial \mu_i}{\partial r} = \sum_{j=1}^{N_{comp}} \Gamma_{ij}\frac{\partial \theta_i}{\partial r},\ i,j = 1, N_{comp},\ z \in [0, L],\ r \in [0, \delta_m] \tag{3.16}$$

where the thermodynamic factor Γ is given by:

$$\Gamma_{ij} = \theta_i \frac{\partial \ln p_i}{\partial \theta_j} = \frac{q_j^{sat}}{q_i^{sat}}\frac{q_i}{p_i}\frac{\partial p_i}{\partial q_j} = \frac{\theta_i}{p_i}\frac{\partial p_i}{\partial \theta_j},\ i,j = 1, N_{comp},\ z \in [0, L],\ r \in [0, \delta_m] \tag{3.17}$$

In general, the partial derivative $\frac{\partial p_i}{\partial \theta_j}$ depends on the adsorption isotherm employed as follows:

$$\frac{\partial p_i}{\partial \theta_j} = \frac{\partial p_i\left(T, P, \theta, adsorption\ isotherm\right)}{\partial \theta_j} \tag{3.18}$$

- In the case that the Extended Langmuir adsorption isotherm is used, the partial derivative $\frac{\partial p_i}{\partial \theta_j}$ can be derived from the isotherm equation and given in an explicit form as follows:

$$\Gamma_{ij} = \frac{\theta_i}{p_i}\frac{\partial p_i}{\partial \theta_j} = \begin{cases} 1 + \dfrac{\theta_i}{1 - \sum_k \theta_k}, i = j \\ \dfrac{\theta_i}{1 - \sum_k \theta_k}, i \neq j \end{cases},\ \forall z \in [0,\ L],\ i,j,k = 1,\ N_{comp} \tag{3.19}$$

- If the IAS or RAS is used, the partial derivative $\frac{\partial p_i}{\partial \theta_j}$ cannot be given in an explicit form and has to be calculated numerically. Here a first order perturbation method is used. The procedure is the following:

  I) Calculate the equilibrium for the given T and p_i by using the following set of equations 3.20 to 3.28 (O'Brien and Myers, 1988):

$$x_i^* p_i^0 \gamma_i = p_i, \forall z \in [0,\ L],\ i = 1, \ldots, N_{comp} \tag{3.20}$$

  where:

$$\gamma_i = 1 \ \text{– for IAS} \tag{3.21}$$

$$\gamma_i = f\left(T, P, x\right) \ \text{– for RAS (Wilson correlation for instance)} \tag{3.22}$$

$$\pi_i^* = \int_0^{p_i^0} \frac{q_{pure,i}^*\left(T, P, x, adsorption\ isotherm\right)}{p} dp \tag{3.23}$$

$$\xrightarrow[isotherm]{Langmuir} \pi_i^* = q_i^{sat} \log\left(1 + b_i p_i^0\right), \forall z \in [0,\ L],\ i = 1, \ldots, N_{comp}$$

$$\pi_i^* = \pi_{i+1}^*, \forall z \in [0,\ L],\ i = 1, \ldots, N_{comp} - 1 \tag{3.24}$$

$$q^*_{pure,i} = q^{sat}_i \frac{b_i p^0_i}{1+b_i p^0_i},\ \forall z \in [0,\ L],\ i = 1,\ldots,N_{comp} \tag{3.25}$$

$$\sum x^*_i = 1, \forall z \in [0,\ L],\ i = 1,\ldots,N_{comp} \tag{3.26}$$

$$\frac{1}{q_{total}} = \sum_i \frac{x^*_i}{q^*_{pure,i}}, \forall z \in [0,\ L],\ i = 1,\ldots,N_{comp} \tag{3.27}$$

$$q^*_i = x^*_i q_{total}, \forall z \in [0,\ L],\ i = 1,\ldots,N_{comp} \tag{3.28}$$

II) Now we need to calculate $\left(N_{comp}\right)^2$ values of the partial derivative $\frac{\partial p_i}{\partial \theta_j}$, one for each (i, j) pair. We can apply the centre finite difference scheme:

$$\frac{\partial p_i}{\partial \theta_j} = \frac{p^{II}_{i,j} - p^{I}_{i,j}}{2\Delta\theta}, \forall z \in [0,\ L], \forall r \in [0,\ \delta_m],\ i, j = 1,\ldots,N_{comp} \tag{3.29}$$

To do so we have to repeat the previous calculation (system of equations 3.20 to 3.28) twice for each (i, j) pair to obtain two values of p_i : $p^I_{i,j}$ by using $\theta^I_{i,j}$ and $p^{II}_{i,j}$ by using $\theta^{II}_{i,j}$. The values of $\theta^I_{i,j}$ and $\theta^{II}_{i,j}$ are calculated by perturbing θ_i calculated in the step I per each component:

$$\theta^I_{i,j} = \begin{cases} \theta_i - \Delta\theta,\ i = j \\ \theta_i,\ i \neq j \end{cases}, \forall z \in [0,\ L], \forall r \in [0,\ \delta_m],\ i, j = 1,\ldots,N_{comp} \tag{3.30}$$

$$\theta^{II}_{i,j} = \begin{cases} \theta_i + \Delta\theta,\ i = j \\ \theta_i,\ i \neq j \end{cases}, \forall z \in [0,\ L], \forall r \in [0,\ \delta_m],\ i, j = 1,\ldots,N_{comp} \tag{3.31}$$

Putting the above procedure into a single set of equations, we get the system of $2\times\left(N_{comp}\right)^2$ equations, which represent the change of partial pressure of all components for differential change in the loading of each component. For example, for binary component system, we end up with the following equations:

$$\theta^I_{1,1} = \theta_1 - \Delta\theta, \forall z \in [0,\ L], \forall r \in [0,\ \delta_m],\ i, j = 1,\ldots,N_{comp}$$

$$\theta^I_{1,2} = \theta_2, \forall z \in [0,\ L], \forall r \in [0,\ \delta_m],\ i, j = 1,\ldots,N_{comp}$$

$$\theta^I_{2,1} = \theta_1, \forall z \in [0,\ L], \forall r \in [0,\ \delta_m],\ i, j = 1,\ldots,N_{comp}$$

$$\theta^I_{2,2} = \theta_2 - \Delta\theta, \forall z \in [0,\ L], \forall r \in [0,\ \delta_m],\ i, j = 1,\ldots,N_{comp}$$

$$p^I_{1,1} = f\left(T, \theta_1 - \Delta\theta, \theta_2\right)$$

$$p^I_{1,2} = f\left(T, \theta_1, \theta_2 - \Delta\theta\right)$$

$$p^I_{2,1} = f\left(T, \theta_1 - \Delta\theta, \theta_2\right)$$

$$p^I_{2,2} = f\left(T, \theta_1, \theta_2 - \Delta\theta\right)$$

and

$$\theta_{1,1}^{II} = \theta_1 + \Delta\theta, \forall z \in [0,\ L], \forall r \in [0,\ \delta_m],\ i, j = 1, \ldots, N_{comp}$$

$$\theta_{1,2}^{II} = \theta_2, \forall z \in [0,\ L], \forall r \in [0,\ \delta_m],\ i, j = 1, \ldots, N_{comp}$$

$$\theta_{2,1}^{II} = \theta_1, \forall z \in [0,\ L], \forall r \in [0,\ \delta_m],\ i, j = 1, \ldots, N_{comp}$$

$$\theta_{2,2}^{II} = \theta_2 + \Delta\theta, \forall z \in [0,\ L], \forall r \in [0,\ \delta_m],\ i, j = 1, \ldots, N_{comp}$$

$$p_{1,1}^{II} = f\left(T, \theta_1 + \Delta\theta, \theta_2\right)$$

$$p_{1,2}^{II} = f\left(T, \theta_1, \theta_2 + \Delta\theta\right)$$

$$p_{2,1}^{II} = f\left(T, \theta_1 - \Delta\theta, \theta_2\right)$$

$$p_{2,2}^{II} = f\left(T, \theta_1, \theta_2 - \Delta\theta\right)$$

At the steady state, gas is in equilibrium with the membrane surface, given by:

$$\theta_i\big|_{r=0} = \frac{q_i^*\left(T, P, x\right)\big|_{r=0}}{q_i^{sat}} = f\left(P, T, x, ads.\ isotherm\right),\ \forall z \in [0,\ L],\ i = 1,\ N_{comp} \tag{3.32}$$

$$\theta_i\big|_{r=\delta m} = \frac{q_i^*\left(T, P, x\right)\big|_{r=\delta m}}{q_i^{sat}} = f\left(P, T, x, ads.\ isotherm\right),\ \forall z \in [0,\ L],\ i = 1,\ N_{comp} \tag{3.33}$$

3.4.3. Support layer

In general, the resistance of the support layer cannot be neglected. Although diffusion in the support is relatively fast, compared to diffusion in the zeolite layer, the support causes significant partial-pressure gradient due to its thickness and low porosity and that affects the boundary condition at the membrane-support interface (van de Graaf, Kapteijn and Moulijn, 1999).

The general Maxwell-Stefan equations can be used to calculate the partial-pressure gradient in the support layer, now applied to gas-phase diffusion (Krishna, 1993). According to Krishna, 1993, three fundamentally different diffusion mechanisms exist inside the pores of the porous media:

- Bulk (free molecular) diffusion where molecule-molecule collisions dominate over molecule-wall collisions; it becomes significant for large pore sizes and high system pressures
- Knudsen diffusion where molecule-wall collisions dominate; it is predominant when the mean free path of the molecular species is much higher than the pore diameter
- Surface diffusion of adsorbed molecular species along the pore surface; it is predominant for micro-pores and for strongly adsorbed species

In the case when the media is a porous support, the free molecular diffusion is predominant and the contribution of the other two mechanisms is very low because the pores are large and the support is inert.

The porous membrane topology is presented in Figure 3.6. The support layer is connected at two sides to the membrane and the permeate compartment, and the boundary conditions at each of two interfaces ensure mass flux continuity between them.

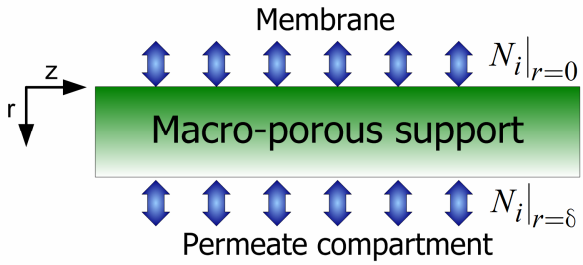

Figure 3.6 Topology of the support layer

The main assumptions made in the model are:

- Ideal gas behaviour
- Isothermal and the steady state operation
- The support layer is inert and macroporous
- Gas is transported by molecular diffusion (pores large enough so that Knudsen diffusion is negligible)
- The flux is constant along support layer and equal to the flux through the membrane:

$$\frac{\partial N_i}{\partial r} = const,\ \forall z \in [0,\ L],\ i = 1,\ N_{comp} \tag{3.34}$$

To describe multi-component diffusion in the gas phase of the macro-porous media two options are available in this thesis:

a) Assuming that the Fick law applies (useful during the initialization of the DAE system):

$$N_i = -\frac{\varepsilon Đ_{ij}}{RT}\frac{\partial p_i}{\partial r},\ i = 1, N_{comp},\ z \in [0, L],\ r \in (0, \delta_s] \tag{3.35}$$

b) If molecule-molecule interactions cannot be neglected, the GMS equations (with no Knudsen diffusivity term) are used (Krishna 1993):

$$-\frac{1}{RT}\frac{\partial p_i}{\partial r} = \sum_{j=1}^{N_{comp}} \frac{x_j N_i - x_i N_j}{\varepsilon Đ_{ij}},\ i, j = 1, N_{comp},\ z \in [0, L],\ r \in (0, \delta_s] \tag{3.36}$$

If sweep gas is used, equation 3.36 is given in the following form:

$$-\frac{1}{RT}\frac{\partial p_i}{\partial r} = \sum_{j=1}^{N_{comp}} \frac{x_j N_i - x_i N_j}{\varepsilon Đ_{ij}} + \frac{x_{inert} N_i - x_i N_{inert}}{\varepsilon Đ_{i,inert}},\ i, j = 1, N_{comp}, z \in [0, L],\ r \in (0, \delta_s]$$

where:

$$N_{inert} = 0$$

$$x_{inert} = 1 - \sum_{NoComp} x_j$$

$$Đ_{i,inert} = Đ_i$$

Finally, the GMS equations in the case when sweep gas is used become:

$$-\frac{1}{RT}\frac{\partial p_i}{\partial r} = \sum_{j=1}^{N_{comp}} \frac{x_j N_i - x_i N_j}{\varepsilon Đ_{ij}} + \frac{\left(1 - \sum_{NoComp} x_j\right) N_i}{\varepsilon Đ_i},\ i, j = 1, N_{comp},\ z \in [0, L],\ r \in (0, \delta_s] \tag{3.37}$$

3.5. Simulation case studies

3.5.1. Separation of hydrocarbons: GMS – EL

To validate the developed generic membrane model, described by the Generalized Maxwell-Stefan (GMS) equations and the extended Langmuir (EL) isotherm, a comparison of the work of van der Graaf et al (1999) and Vareltzis et al (2003) is made. The composite membrane used in this study consisted of a top layer of silicalite-1, supported on a stainless-steel support. The geometrical characteristics of the membrane are adopted from the work of van der Graaf et al (1999) and they are given in Table 3.1 to Table 3.3. The sweep gas (helium) with a flowrate of 1.0×10^{-4} $(m^3/min)_{STP}$ has been used at the permeate side to remove the permeating components.

Table 3.1 Membrane parameters

Parameter	Value
Membrane surface area, m^2	2×10^{-4}
Effective thickness of the zeolite layer, m	10×10^{-6}
Density of the zeolite layer, g/m^3	1.8×10^{6}
Thickness of the support, m	3.0×10^{-3}
Porosity of the support	0.2

Table 3.2 Diffusion parameters

Temperature, K	Zeolite layer*		Support layer**	
	$Đ_i^s$, $10^{-10} m^2/s$	$Đ_{He}$, $10^{-5} m^2/s$	$Đ_{C_1,C_2}$, $10^{-5} m^2/s$	$Đ_{C_1,C_3}$, $10^{-5} m^2/s$
Methane (C_1)				
273	8.64	5.6	1.4	
303	10.4	6.7	1.7	1.4
338	15.2	8.1	2.0	
373	20.7	9.6	2.4	
Ethane (C_2)				
273	0.95	4.0		
303	1.50	4.8		
338	3.14	5.8		
373	5.83	6.9		
Propane (C_3)				
	0.34	3.9		

* Calculated from single-component permeation data
** Calculated from the empirical relation of Fuller

Table 3.3 Adsorption parameters

Temperature, K	K_i, 10^{-6} Pa^{-1} *		q_{sat}, mmol/g *
	Methane	Ethane	
273	7.0*	203*	1.92*
303	3.1	57	1.85
338	1.4	17	1.78
373	0.7	6.0	1.71
	Methane	Propane	
303	4.0	650	1.58

* Extrapolated from data at 303, 338, and 373K

Mixture permeation experiments were performed as:

- a function of composition, keeping the total hydrocarbon pressure at the feed side atmospheric
- as a function of pressure, keeping the ratio between components the same and increasing the total pressure at the feed side, and
- as a function of temperature.

The total feed flow was 100×10^{-6} $(m^3/min)_{STP}$. The results of these experiments are given in Figure 3.8 to Figure 3.12, together with the predicted fluxes and selectivities using the GMS (for "single-file" diffusion mode, $D_{ij}=\infty$) model and the GMS model. The original results of van der Graaf et al. (1999) are given in the bottom part of the figures. Solid lines represent results for GMS while dashed lines represent GMS (for "single-file" diffusion mode, $D_{ij}=\infty$). The comparison shows a very good agreement between results in the original and this work.

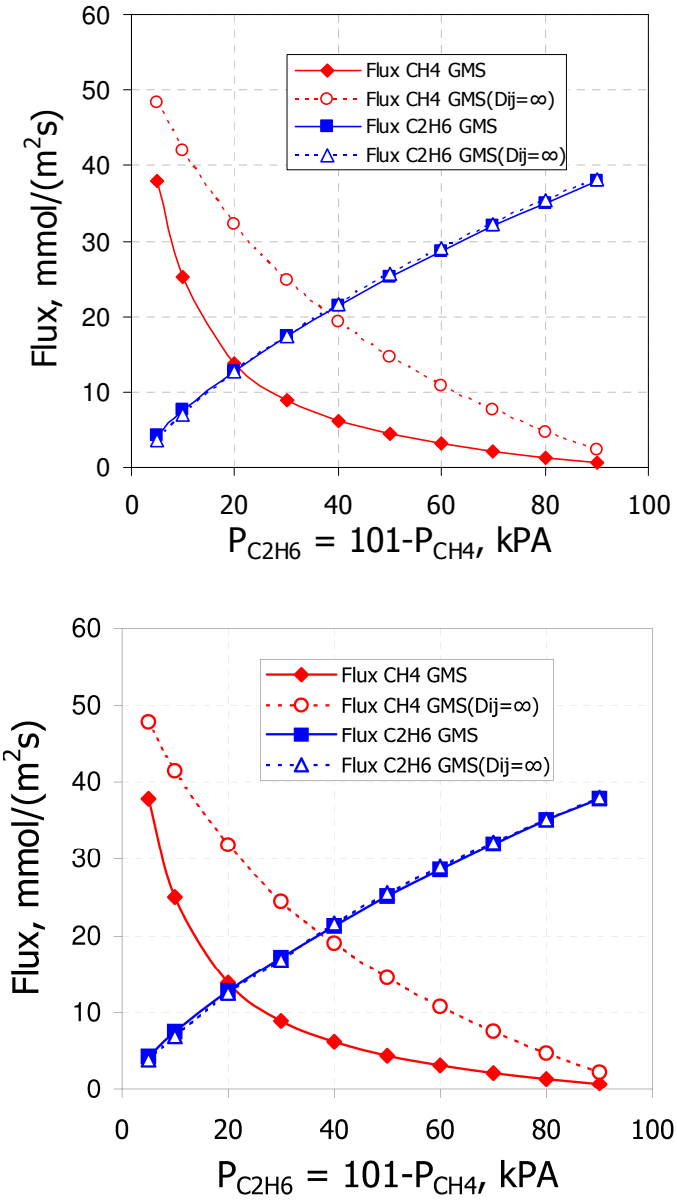

Figure 3.7 Methane/Ethane permeation fluxes as a function of ethane composition at 303K; (above: this thesis; below: van der Graaf et al, 1999)

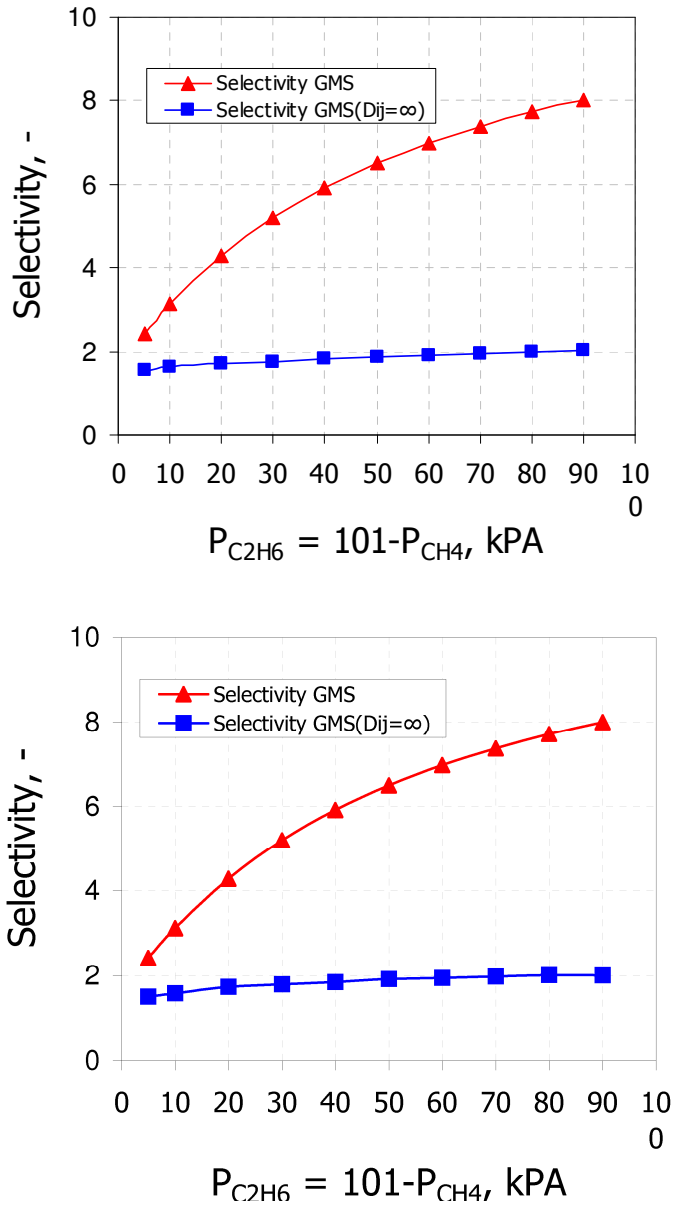

Figure 3.8 Selectivity toward ethane as a function of ethane composition at 303K; (above: this thesis; below: van der Graaf et al, 1999)

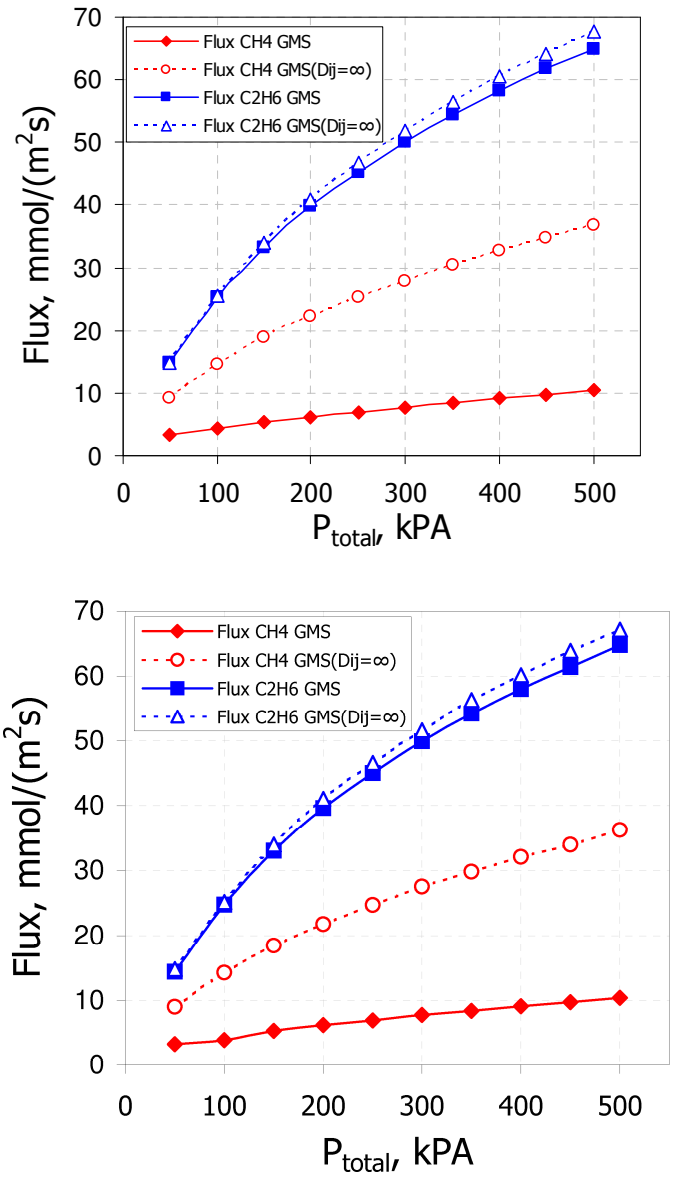

Figure 3.9 Methane/Ethane permeation fluxes as a function of total pressure at 303K (1:1 mixture); (above: this thesis; below: van der Graaf et al, 1999)

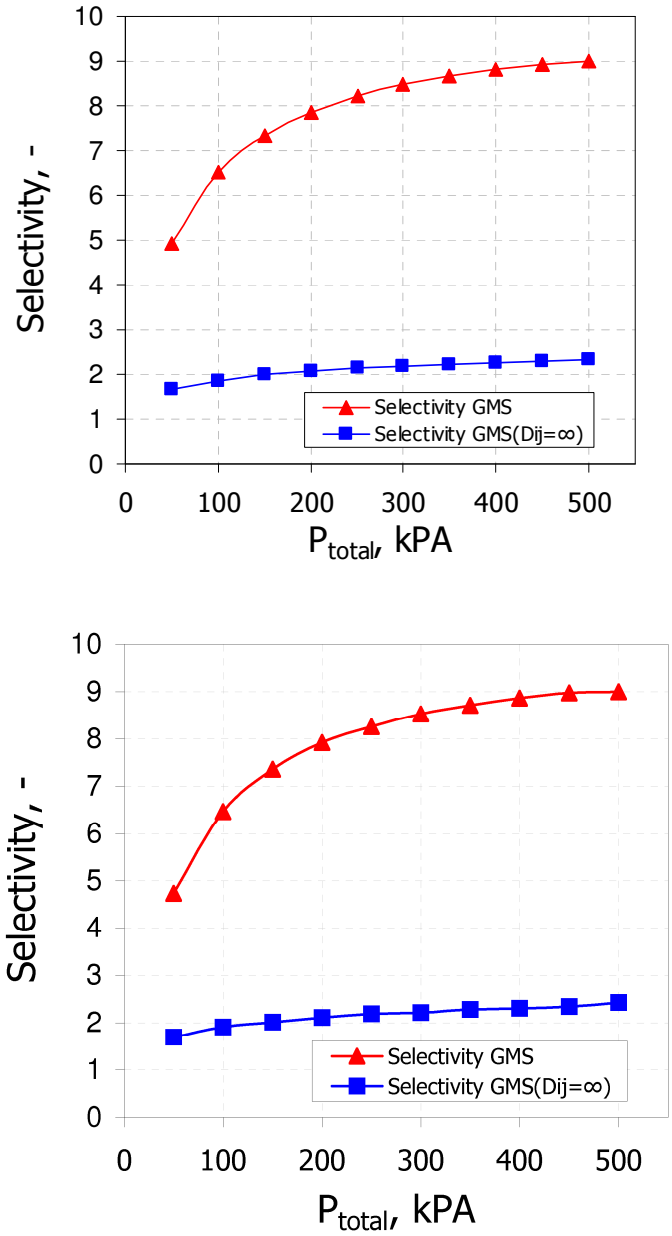

Figure 3.10 Selectivity toward ethane as a function of total pressure at 303K (1:1 mixture); (above: this thesis; below: van der Graaf et al, 1999)

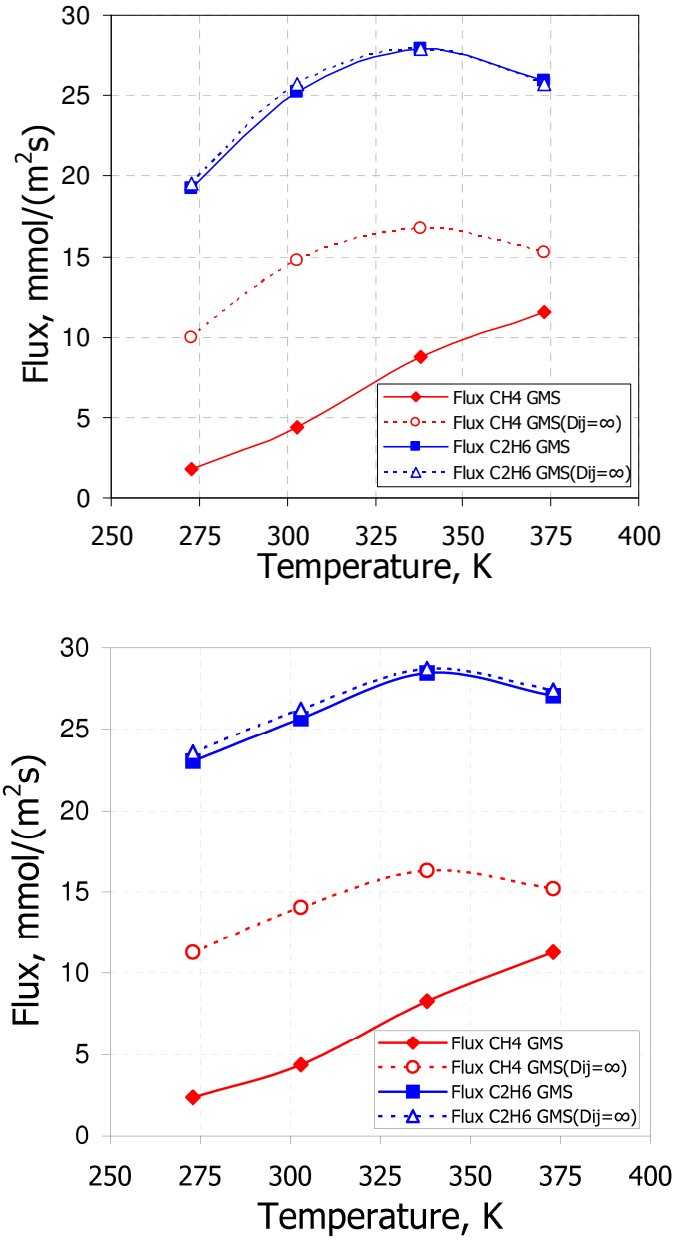

Figure 3.11 Methane/Ethane permeation fluxes as a function of temperature (1:1 mixture, P_{tot}=1bar); (above: this thesis; below: van der Graaf et al, 1999)

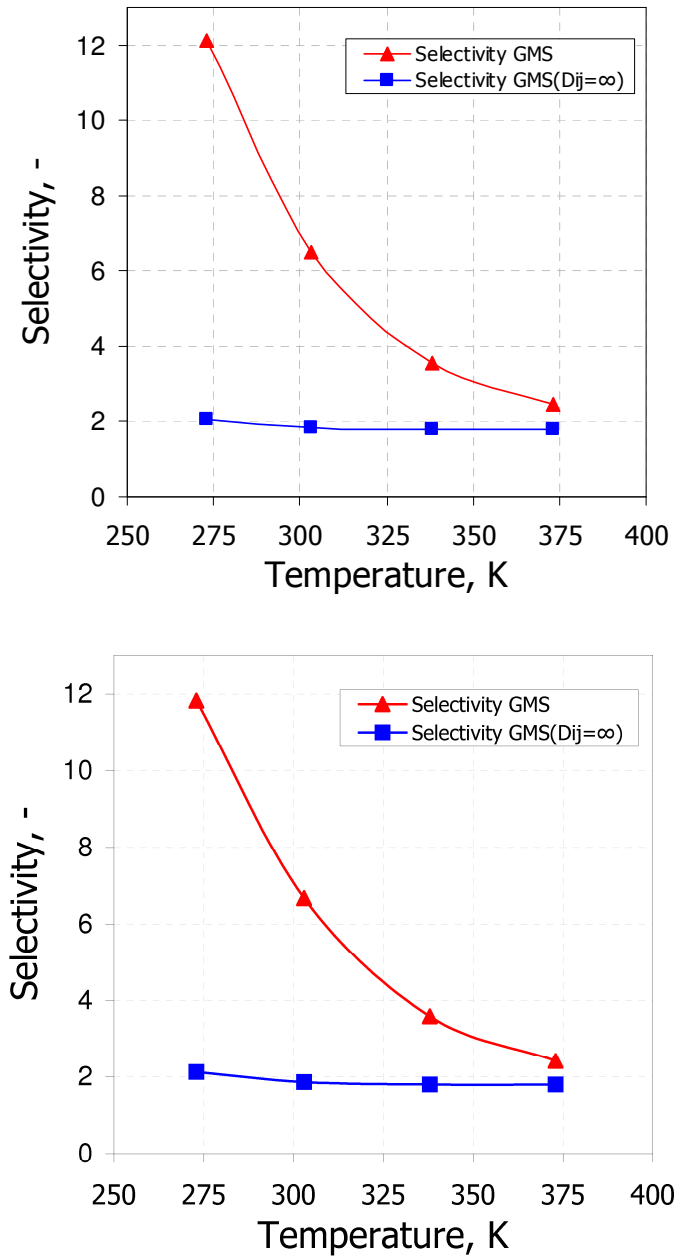

Figure 3.12 Selectivity toward ethane as a function of temperature (1:1 mixture, P_{tot}=1bar); (above: this thesis; below: van der Graaf et al, 1999)

3.5.2. Separation of hydrocarbons: GMS – IAS vs. GMS – EL

To validate the membrane model, in the separation of hydrocarbons a comparison is made with the work of of Kaptaijn et al, 2000. To remain thermodynamically consistent and to apply the extended single-site Langmuir isotherm in the mixture permeation simulations, Van de Graaf et al, 1999 re-estimated the methane adsorption parameters from the single-component methane adsorption data by fixing the methane saturation loading to that of the other component in their calculation. Geometrical and diffusion parameters are the same as in the work of van der Graaf et al, 1999 given in the previous section.

The simulation results based on the IAS approach for ethane/methane are given in Figure 3.13 while results for propane/methane are given in Figure 3.14. Furthermore, the original experimental data and the extended Langmuir isotherm simulations with equal saturation loadings for each component are included. The total hydrocarbon permeate pressure was kept fixed at 20 and 10 kPa, respectively, to approach the experimental conditions. These two examples were selected since the single-site Langmuir approach gave the largest deviation for the selectivity. In both cases, the experimental data exhibit a declining tendency for the selectivity, while the Langmuir model evolves to a limiting value. It is noted here that the IAS predicton with the equal saturation loadings is the same as the extended Langmuir model. The IAS approach with the different saturation loadings is clearly able to predict the decreasing trends of the experimental data in both figures. For the 1:1 ethane/methane mixture the increasing total pressure is relatively more favourable for the methane adsorption (as shown in Figure 3.13), while the ethane selectivity decreases. In the propane/methane mixture a similar reason holds for the variation in composition. So, these subtle details in the permeation selectivities become apparent only if the different values of the saturation loadings are taken into consideration in the mixture adsorption, and, consequently, in the diffusion equations. The model without the D_{ij} interaction terms is not capable of predicting the results for propane/methane.

Again, predictions of the proposed modelling framework are in a very good agreement with the previous literature contribution (Kapteijn et al, 2000).

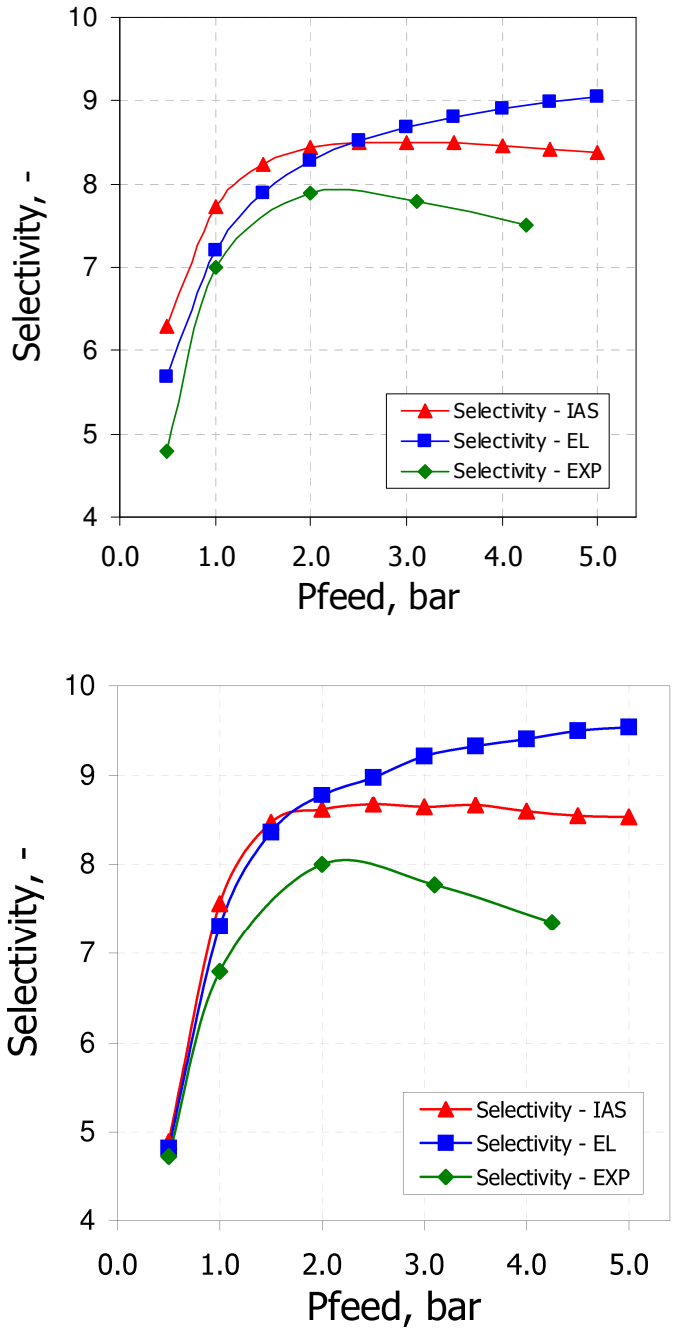

Figure 3.13 Comparison of selectivities for binary mixture permeation through a silicalite-1 membrane for ethane/methane equimolar feed mixture at 303 K as a function of the total feed pressure, permeate pressure 20 kPa; (above: this thesis; below: Kapteijn et al, 2000)

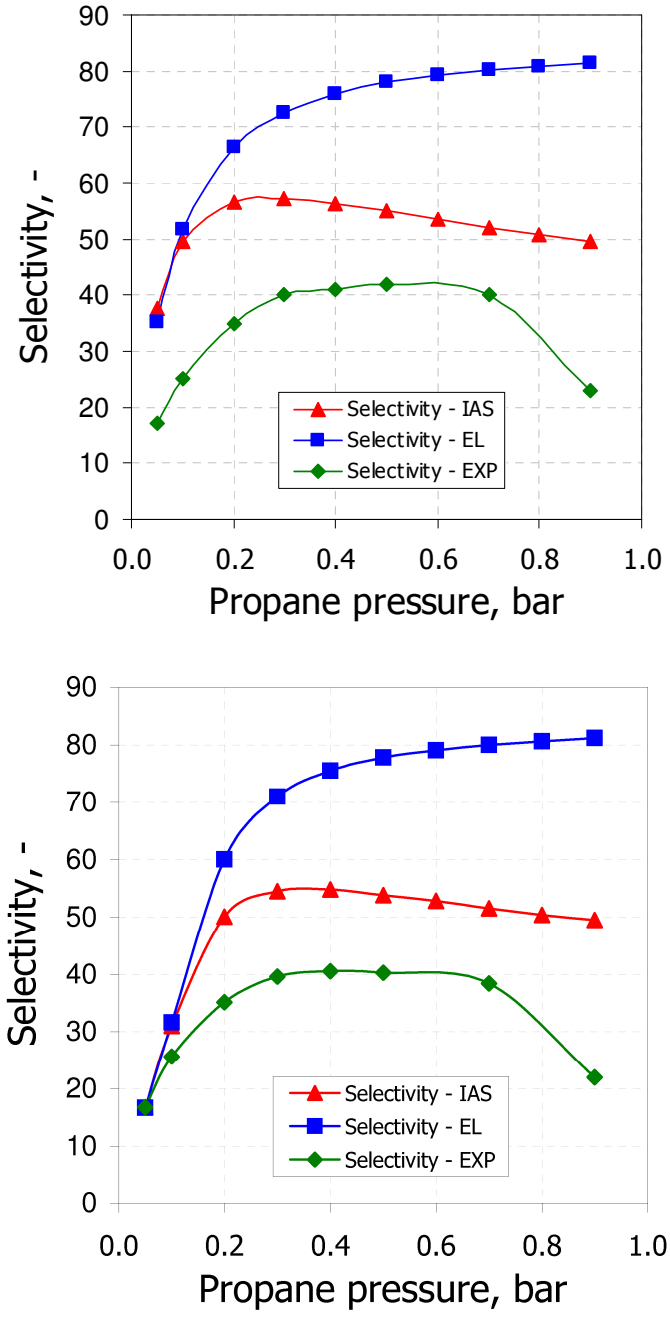

Figure 3.14 Comparison of selectivities for binary mixture permeation through a silicalite-1 membrane for propane/methane mixture at 303 K and 100 kPa total feed pressure as a function of the propane pressure, permeate pressure 10 kPa; (above: this thesis; below: Kapteijn et al, 2000)

3.5.3. Separation of hydrocarbons: GMS – IAS vs. GMS – RAS vs. GMS – CBMC

The work of Krishna and Paschek (2000) has been used to verify the Real Adsorption Solution Theory model to predict mixture loadings, and to compare the results obtained by using IAS/RAS to the results from Configurational-bias Monte-Carlo (CBMC) simulations.

In order to illustrate various features of hydrocarbon mixture isotherm characteristics, the CBMC simulations were performed for the following systems:

- methane/ethane (can be considered as an ideal mixture)
- methane/propane (can be considered as an ideal mixture)
- ethane/propane (can be considered as an ideal mixture)
- n-butane/iso-butane (cannot be considered as an ideal mixture)

For the pure component linear and branched alkanes studied here, the dual-site Langmuir (DSL) model was found to be applicable in all the cases. The adsorption parameter values used for the calculations are given in Table 3.4.

The activity coefficients γ in the equation 3.20 have been calculated by using the Wilson model:

$$\ln \gamma_1 = 1 - \ln\left(x_1 + x_2\Lambda_{12}\right) - \frac{x_1}{x_1 + x_2\Lambda_{12}} - \frac{x_2\Lambda_{21}}{x_2 + x_1\Lambda_{21}} \tag{3.38}$$

$$\ln \gamma_2 = 1 - \ln\left(x_2 + x_1\Lambda_{21}\right) - \frac{x_2}{x_2 + x_1\Lambda_{21}} - \frac{x_1\Lambda_{12}}{x_1 + x_2\Lambda_{12}} \tag{3.39}$$

Parameters of the Wilson model are given in the Table 3.5. Once more, predictions of the proposed modelling framework are in a very good agreement with the previous literature contribution (Krishna and Paschek, 2000).

Table 3.4 Pure component parameters for dual-site Langmuir model

Temperature, K	Site A		Site B	
	b_i, Pa^{-1}	θ_i, molecules per unit cell	b_i, Pa^{-1}	θ_i, molecules per unit cell
Methane				
300	$4.86 \cdot 10^{-6}$	11	$2.38 \cdot 10^{-7}$	8
303	$4.6 \cdot 10^{-6}$	11	$2.0 \cdot 10^{-7}$	8
Ethane				
300	$9.73 \cdot 10^{-5}$	12	$4.38 \cdot 10^{-7}$	3
303	$8.28 \cdot 10^{-5}$	12	$3.73 \cdot 10^{-7}$	3
Propane				
300	$9.64 \cdot 10^{-4}$	11	$5.06 \cdot 10^{-6}$	1
303	$7.95 \cdot 10^{-4}$	11	$1.59 \cdot 10^{-6}$	1
n-Butane				
300	$1.6 \cdot 10^{-2}$	9	$1.1 \cdot 10^{-5}$	1
iso-Butane				
300	$2.84 \cdot 10^{-2}$	4	$4.3. \cdot 10^{-6}$	6

Table 3.5 Wilson non-ideality parameters for mixture isotherms

Temperature, K	Wilson parameters	
	Λ_{12}	Λ_{21}
Methane-ethane		
303	1	1
Methane-propane		
303	1	1
Ethane-propane		
300	1	1
n-Butane-iso-butane		
300	6.95	1.005

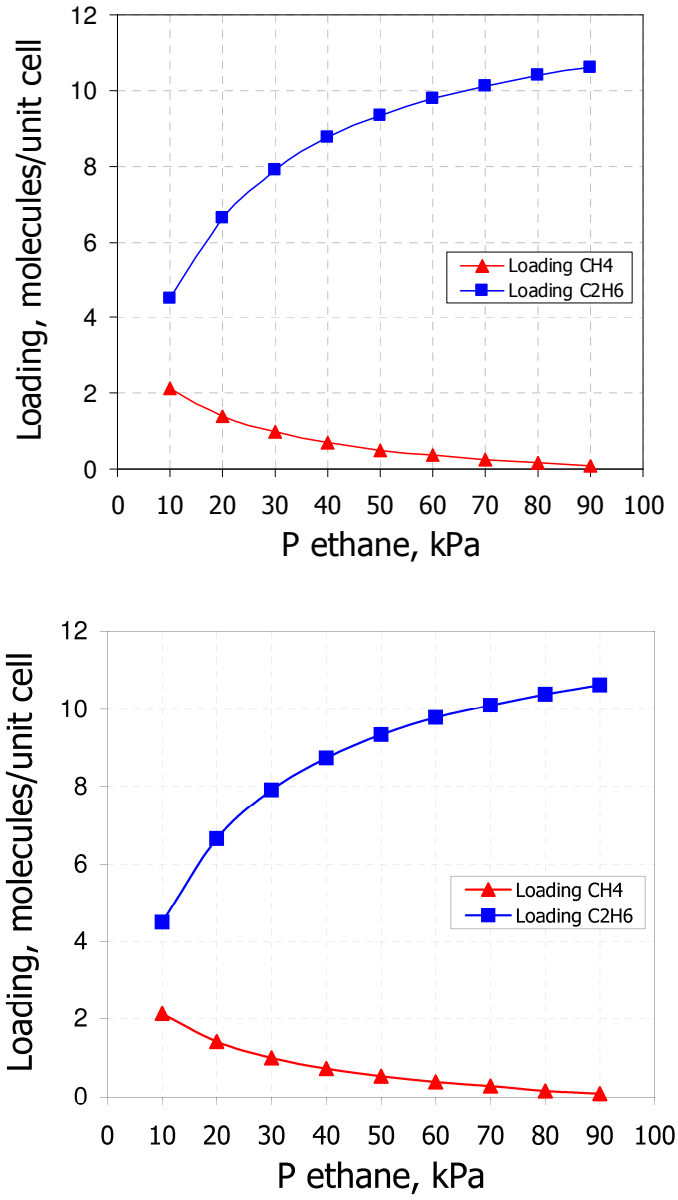

Figure 3.15 Comparison of IAS and CBMC mixture loadings for Methane-Ethane mixture at T=303K in silicalite and P_{total}=100kPa; (above: this thesis; below: Krishna and Paschek, 2000)

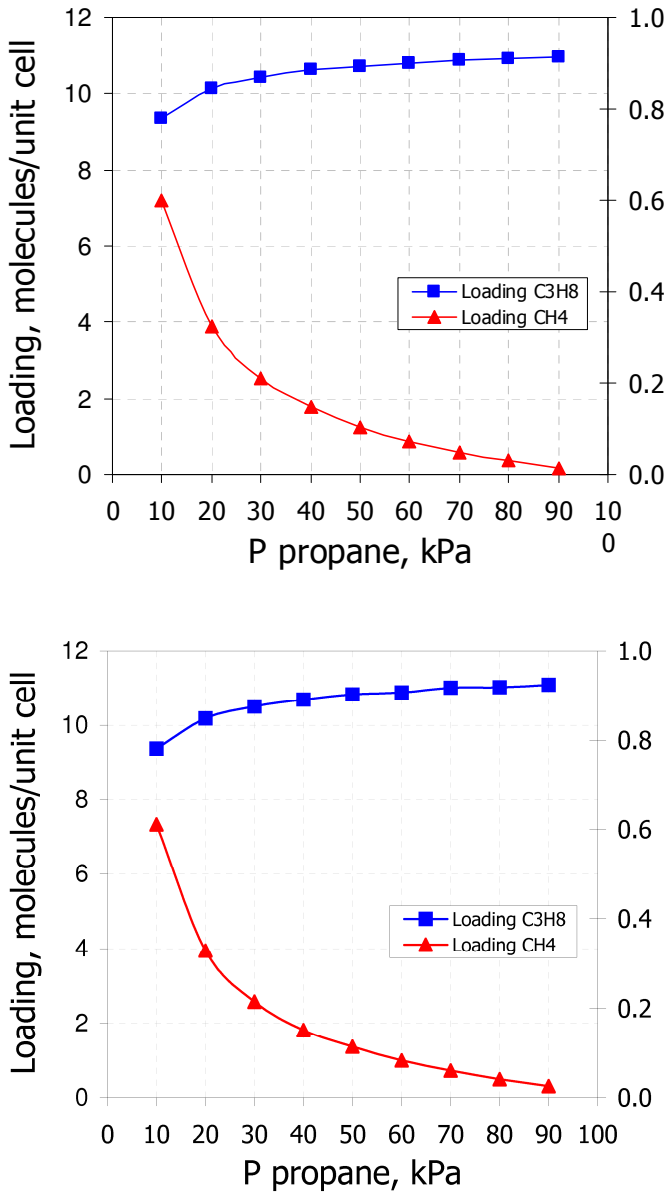

Figure 3.16 Comparison of IAS and CBMC mixture loadings for Methane-Propane mixture at T=303K in silicalite and P_{total}=100kPa; (above: this thesis; below: Krishna and Paschek, 2000)

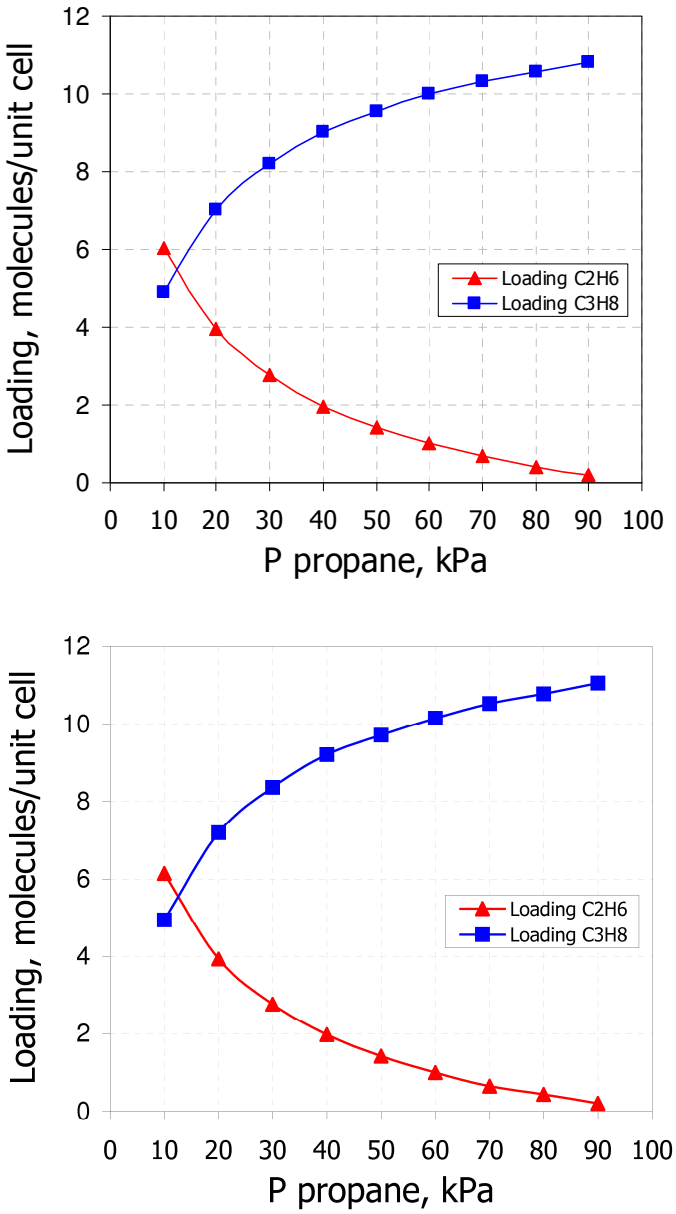

Figure 3.17 Comparison of IAS and CBMC mixture loadings for Ethane-Propane mixture at T=303K in silicalite and P_{total}=100kPa; (above: this thesis; below: Krishna and Paschek, 2000)

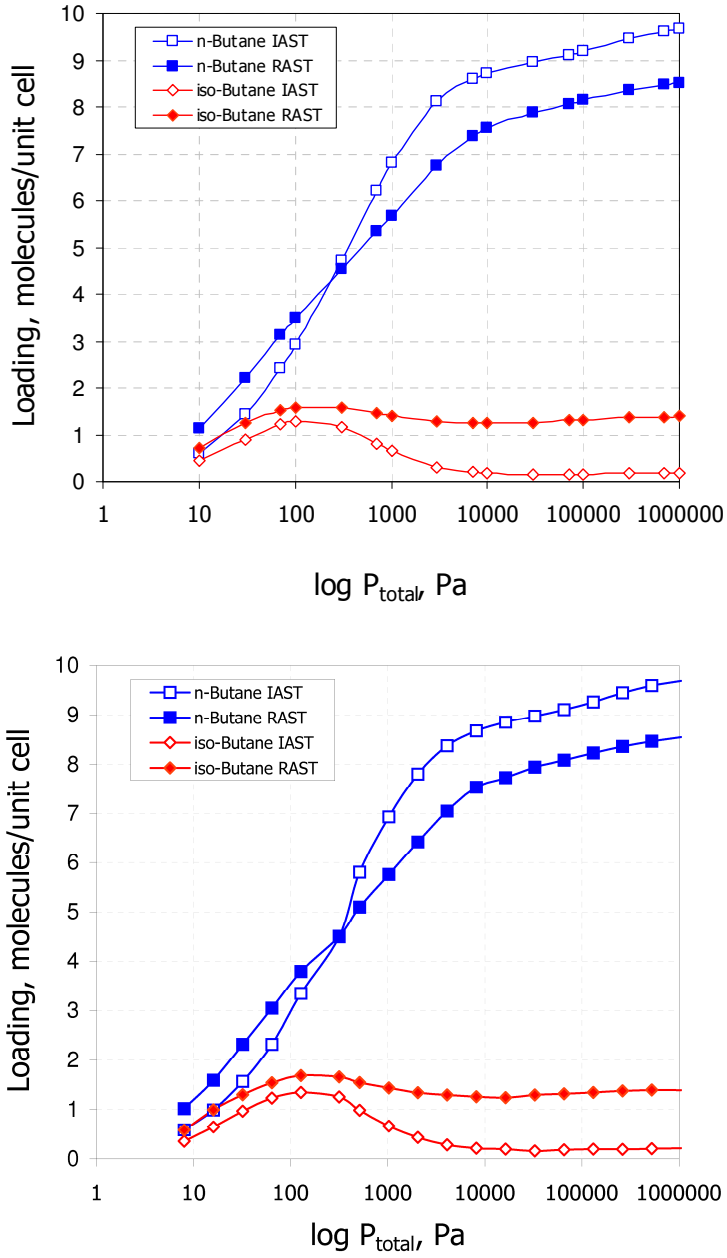

Figure 3.18 Comparison of IAS, RAS and CBMC mixture loadings for n-Butane/iso-Butane at 303K in silicalite; (above: this thesis; below: Krishna and Paschek, 2000)

Chapter 4

Hybrid PSA/Membrane

4.1. Introduction

Hybrid units are commonly used as a “multifunctional" equipment that couples and uncouples elementary processes (transfer-reaction-separation) to increase productivity and/or selectivity with respect to the desired product and to facilitate the separation of undesired by-products. Numerous separation processes involving unit operation hybridization exist. For instance, the concept of reactive or catalytic distillation has been commercialized successfully in petroleum processing and manufactoring of chemicals were reactive distillation is often employed. These hybrid units have been used to help to achieve higher conversions and yields in chemical reactors compared to conventional reactor configurations. However, the modelling and simulation of hybrid PSA/membrane systems has received rather limited attention in the open literature compared to modelling of PSA and membranes. Although there is some published work on the development of hybrid PSA/membrane systems there are no many practical applications yet. The majority is linked to hydrogen production/purification from various chemical and petrochemical sources (Ritter and Ebner, 2007). Other example of using hybrid PSA/membrane schemes focus on the production of oxygen and nitrogen from air for aircraft on-board application where bulk separation by membrane is followed by adsorption process for further purification (Zolandz and Fleming, 1992). In addition, several patents have been issued for various applications, including helium recovery hydrogen purification, acid gas removal and nitrogen production (Feng et al, 1997).

4.2. Principles of operation

A successful hybrid scheme of PSA/membrane process has to exploit the most important features of two technologies. Membrane technology is not mature yet to provide high selectivity, thus the product purity is at a lower level compared to PSA. However, membranes offer high fluxes, low energy consumption, possibility for continuous operation, lower investment costs and ease of operation. On the other hand PSA is able to produce extra pure gases at high recovery, but at the cost of higher capital investments (typical industrial PSA units utilize layered beds containing up to four adsorbents and, depending on the production volume, anywhere between four and sixteen columns) and complex operation due to a large number of a time-dependent variables and very complex column interconnections. By combining these two technologies, it may be possible to retain extra high product purity but at higher recovery and at significantly lower operating costs. In the case of hydrogen production, waste gases of a high calorific value and with lower carbon monoxide and carbon dioxide content would be a separation target. A typical hybrid configuration is presented in Figure 4.1.

4.3. Literature review

Membrane permeation and pressure swing adsorption are two widely used processes for gas separation. As it was shown in the previous chapters, these processes are very often considered to be alternatives or complements to the more conventional cryogenic separation process. Membrane separation is based on the difference in the rate of permeation through a membrane, while adsorption separation depends on the difference in either the rate or the equilibrium on an adsorbent. Membrane gas separation is pressure driven and normally operates continuously, whereas PSA is a cyclic process in which adsorbers undergo adsorption at a high pressure and desorption at a reduced pressure cyclically, thereby making it suitable for processing a gas mixture in a continuous fashion. A concise comparison between current PSA and membrane processes is given by Ruthven (1994).

Generally speaking, gas permeation with the present generation of membranes is less selective than adsorption. Hence, membrane process is very efficient for bulk separation while PSA is suitable for producing higher purities. In several commercial applications, hybrid process schemes that combine membrane and PSA have been employed. Zolandz and Fleming (1992) presented a process for the production of O_2 and N_2 from air for aircrafts where bulk separation by membrane is followed by PSA for further purification. Mercea and Hwang (1994) studied oxygen production from air by PSA on zeolite followed by oxygen purification by a membrane. In addition, several hybrid configurations have been proposed in international patents for various applications. Those hybrid schemes can be simply classified into two categories: membrane followed by PSA, and PSA followed by membrane. In the first case, the membrane is mainly used for bulk separation and the concentrated product stream from membrane is fed to PSA for purification. If a high purity is not demanded, the less concentrated stream from membrane can be fed to PSA to increase recovery. In the second case, the waste gas from PSA is fed to membrane to increase recovery, and the waste gas from membrane can be used to purge adsorption columns.

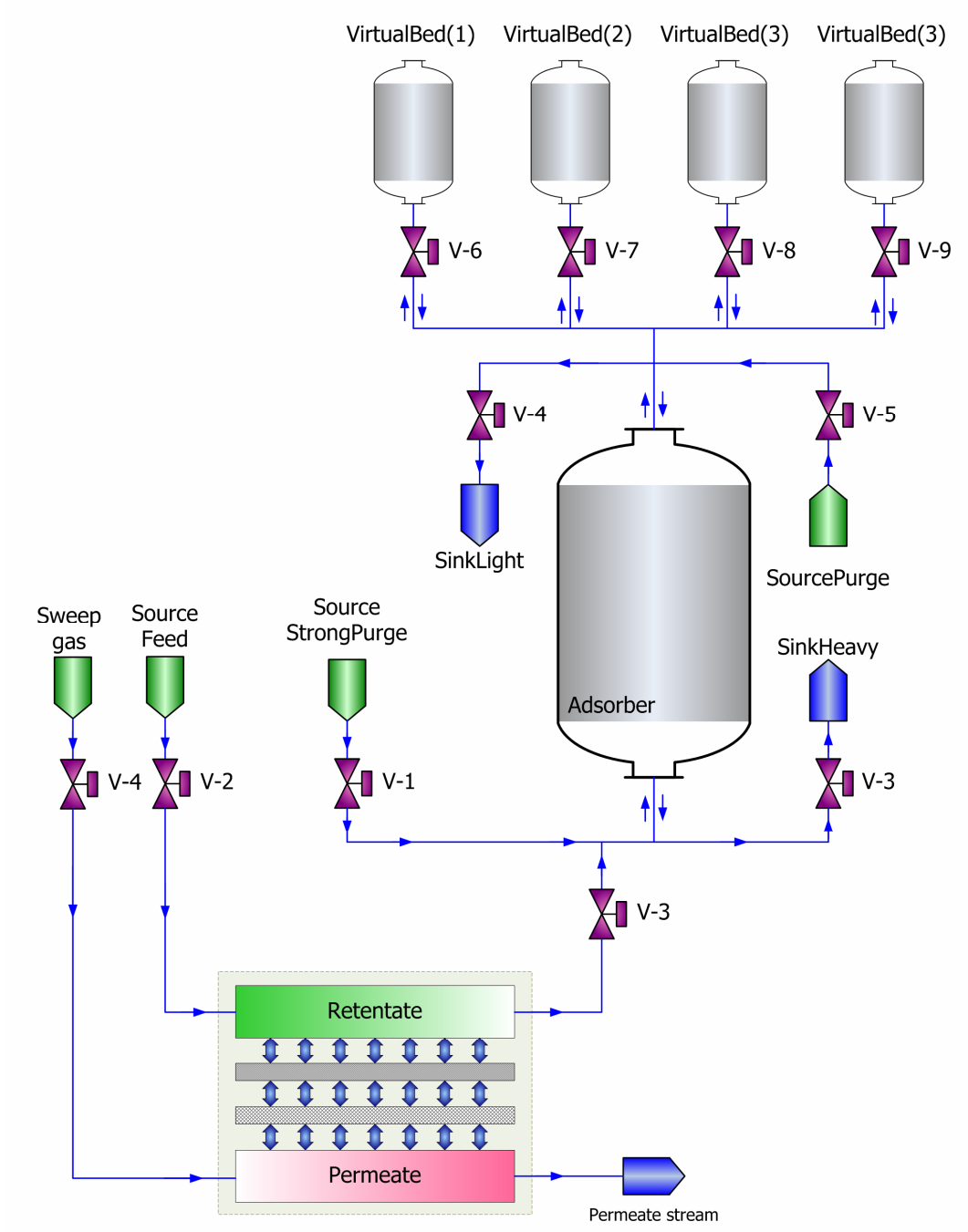

Figure 4.1 Sample hybrid PSA-Membrane configuration

Feng et al (1998) proposed a novel process that incorporates membrane permeation into cyclic process of PSA. This integration is not a simple combination of two process components. Unlike in the traditional membrane processes where pressures are kept constant, the pressure in the integrated permeation/adsorption system is changing as the permeation proceeds with time. Permeation processes with varying pressure were analyzed parametrically to study the feasibility of integrating permeation with cyclic PSA processes. Two configurations were investigated: membrane-assisted feed gas pressurization, and membrane-assisted co-current depressurization. A bench scale unit was assembled and tested for hydrogen purification. It was shown that compared to the simple adsorption process, both product purity and recovery could be improved by using the integrated process, and the improvement was especially remarkable for the cases where the feed gas mixture contained impurities that were difficult to remove by adsorption.

Esteves and Mota (2002) developed a hybrid gas separation process, designed and optimized for cyclic steady-state operation in terms of product purity and recovery. The feasibility of the integrated process presented here is assessed through the effect of the various operating parameters on separation performance.

The same authors in 2007 developed novel membrane/PSA schemes for gas separation, which cover both cooperative and opposing regions of the selectivity for the two stand-alone units. Hybrid scheme A, is applicable when the more permeable component is the least adsorbed one, whereas hybrid process B is suitable when the more permeable component is also the more adsorbed one. The former scheme was thoroughly evaluated for H_2/CH_4 separation on activated carbon and a polysulfone membrane with a typical selectivity H_2/CH_4 of 35. The membrane works as a prebulk separation unit and is coupled to the intrinsically dynamic periodic operation of the PSA in a way that the operating pressure of the PSA unit is used as the driving force for permeation. In contrast to a conventional PSA process, adsorption beds for the integrated system are fed with a varying-composition gas stream, initially rich in the more permeable but less adsorbed component, which is progressively enriched in the other component having opposite behaviour. The hybrid process behaviour was analyzed and compared with the conventional PSA unit. The effect of various operating parameters, such as permeation throughput, total feed amount per cycle, purge-to-feed ratio, and adsorption and blowdown pressures, is assessed through detailed process simulation. The simulation results show that the inclusion of a membrane module into the cyclic adsorption process improves the separation performance when compared to the stand-alone PSA. Depending on the values of the operating parameters, the integrated cycle gives H_2 and CH_4 products with purities within the ranges of 83-97% and 81-99%, respectively. The product recoveries obtained are in the ranges of 77-99% for H_2 and 81-98% for CH_4. The results presented suggested that a pre-established PSA process, already in operation, could be advantageously coupled with a suitable membrane module, according to one of the proposed schemes, to enhance product purity and recovery. Whether the obtained improvements are large enough to overcome capital and extra operating costs for a given separation, must be assessed on a case per case basis.

An important conclusion drawn from these works is that the membrane permeation can be an effective aid in the pressurization and high-pressure adsorption steps of a typical PSA process. The results also indicate the feasibility of incorporating membrane permeation into the blowdown step of the PSA cycle, so that the operating pressure range available from the PSA can be used as the driving force for permeation. Therefore, a complete understanding of these hybrid processes for gas separation is crucial, mainly

because benefits, such as product quality, plant minimization, environmental impact, and energetic cost reductions, are arising.

4.4. Mathematical modelling

As it was presented in previous chapters, all models have been developed according to the gPROMS PML standard library, and PSA and membrane models can be easily interconnected. Thus, hybrid schemes can be simply developed by dragging and dropping those models into the flowsheet and no additional modelling is necessary.

4.5. Analysis

The hybrid PSA/membrane modelling and optimization framework have been specifically applied on the process of hydrogen recovery from SMROG. The general objective of using hybrid PSA/Membrane units is to achieve one or more of the following goals:

- To increase product purity and/or recovery
- To increase the productivity of the adsorbent (that is to process more feed by the same amount of adsorbents, or the same amount of feed by the lower amount of adsorbents)
- To decrease capital costs (by decreasing the columns size)
- To fractionate some unwanted components (for instance CO and CO_2)
- To separate some valuable components from the mixture which are usually wasted

Although PSA technology is already capable to produce hydrogen of very high purity (99.999^{+} %), further improvements are neither possible (nor necessary). Thus, by employing different hybrid schemes it is possible to achieve other abovementioned goals (to increase recovery and adsorbent productivity, to remove CO_2 and produce fuel gas of higher calorific value and lower CO_2 contents, to decrease the size of columns/amount of the adsorbent).

In order to systematically investigate the coupling of PSA and membrane units two base schemes have been recognized:

I) PSA serves as the main bulk separation unit

II) Membrane serves as the main bulk separation unit

Base scheme I assumes that membrane is an aid to PSA module providing the following functionality:

- Membrane(s) attached to feed stream (pressurization and adsorption step):
  - to remove impurities from feed stream
  - to fractionate the waste gasses from attached membrane by producing the secondary product(s) or to remove impurities(such as CO or CO_2)

- Membrane(s) attached to waste gases streams (blowdown and purge steps):
  - to recover product from membrane waste gasses
  - to remove impurities from waste gasses mixture (such as CO or CO_2)
  - to fractionate the waste gasses mixture by producing the secondary product(s)
- Membranes(s) attached to both feed and waste gases streams:
  - all of the abovementioned
- Membrane(s) attached to product stream (adsorption step):
  - to purify crude product from PSA unit

Base scheme II assumes that PSA is an aid to membrane module providing the following functionality:

- PSA attached to permeate stream:
  - to recover product from membrane waste gasses
  - to remove impurities from membrane waste gasses
- PSA attached to retentate stream:
  - to purify crude product mixture from membrane

In the work of Esteves and Mota (2007) the hybrid concept exploited the base scheme II and was formulated to address both cooperative and opposing regions of the selectivity for the two stand-alone units, and two main schemes were developed:

- Scheme A, in which the more permeable component is the least adsorbed one
- Scheme B, in which the more permeable component is the more adsorbed one

In this work, the focus was put on the base scheme I which can be exploited in many different ways. In a general case, we have several streams entering or leaving a column:

- At the top of the column: product, depressurization, purge and pressurization (by pure light product) streams
- At the bottom of the column: feed, pressurization (by using feed), blowdown and purge streams

All streams are presented in Figure 4.2. Obviously, there is no purpose to attach a membrane on a product stream as purity is already high enough. A depressurization stream is used to pressurize or purge other columns, and it is pure enough as well. The same stands for all streams at the top of the column. However, all streams at the bottom of the column can be pre- or post-processed by using a membrane unit (or several of them). Feed and pressurization streams can be processed in order to decrease the level of impurities allowed to enter the column during pressurization and adsorption steps. On the other hand, the waste gases that leave the column during blowdown and purge steps can be processed in order to either increase the recovery of the light product, recover some valuable component that is commonly wasted, or to decrease the level of pollutants (CO and CO_2) which severely affect the environment.

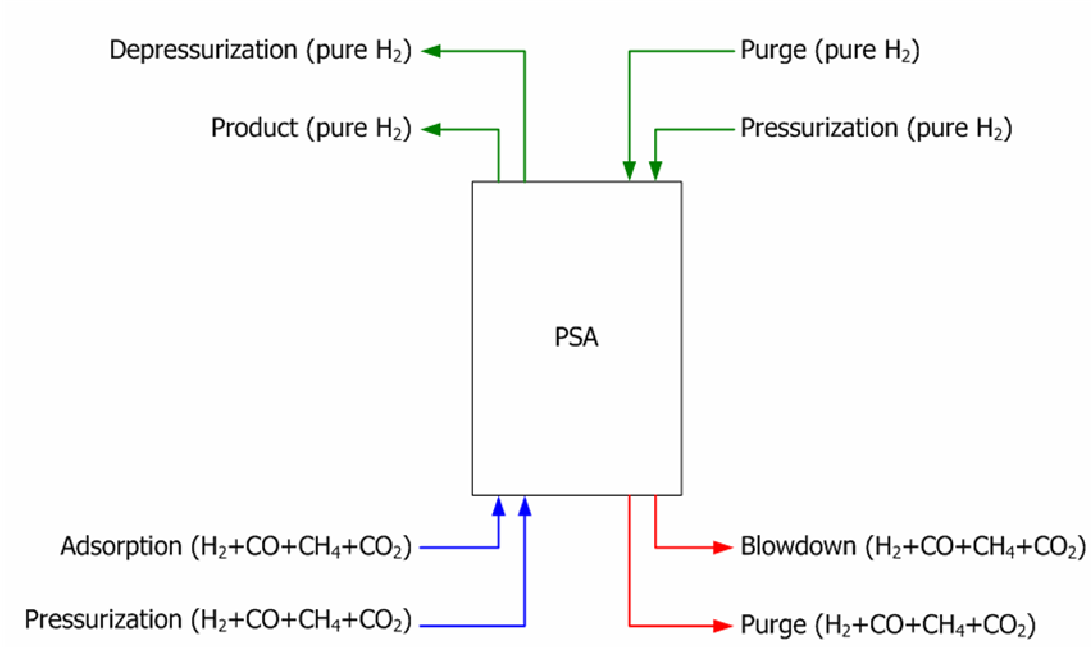

Figure 4.2 PSA inlet /outlet streams

Thus, bearing in mind the abovementioned analysis, three different configurations have been recognized as feasible:

- Membrane attached to feed stream (adsorption): *Mem-PSA*
- Membrane attached to waste gas streams (blowdown, purge): *PSA-Mem*
- Membranes attached to both feed and waste gas streams: *Mem-PSA-Mem*

The next question that arises is what type of membrane should be employed? Since the objective in this work is to use a PSA as the main separation unit, the logical answer is to use a carbon-dioxide selective membrane to decrease the level of carbon monoxide and carbon dioxide that enter the column. Using for instance a hydrogen selective membrane, PSA is transformed into the auxiliary unit.

Following a similar logic, and keeping in mind the fact that waste gases are the most often used as a fuel for the previous steps in steam methane reforming process, the carbon-dioxide selective membrane should be employed again. The objective is twofold: to produce a fuel gas of a higher calorific value (by increasing the content of H_2 and CH_4) and to decrease the level of CO and CO_2 in the waste gases.

The detailed analysis (advantages and disadvantages) of all configurations is presented in the following section.

4.5.1. Membrane attached to feed stream (Mem-PSA)

This hybrid scheme consists of a membrane unit that serves as a feed source for a PSA unit. PSA is connected to a retentate stream of the membrane (as shown in Figure 4.3). The objective in this case study is to maximize the overall hydrogen recovery, while at the same time trying to decrease carbon dioxide content in a retentate stream which is connected to the PSA unit. Therefore, two objectives should be considered simultaneously:

- Maximization of the overall hydrogen recovery, and
- Minimization of carbon-dioxide content in the retentate stream

In order to consider the above objectives simultaneously we can construct a Pareto curve by solving an optimization problem for maximizing the overall hydrogen recovery while imposing a bound on the carbon dioxide concentration. By solving this optimization problem for different bounds on the carbon dioxide concentration, we can get the optimal overall recovery as a function of the allowed carbon dioxide concentration in the retentate stream. This way we can investigate the trade off between hydrogen recovery and carbon dioxide content in the feed.

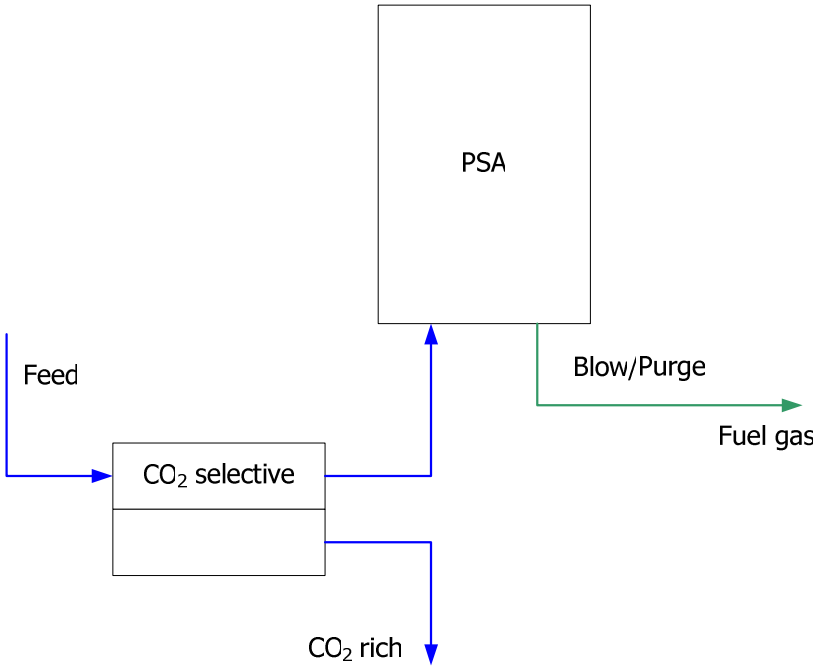

Figure 4.3 Hybrid Case 1: Mem-PSA

4.5.2. Membrane attached to waste gases stream (PSA-Mem)

This hybrid scheme consists of a PSA unit that serves as a feed source for a membrane unit. The membrane feed inlet is connected to a blowdown/purge streams of the PSA (as shown in Figure 4.4). The objective in this hybrid scheme is to investigate possibilities of producing a fuel gas of a higher calorific value. Thus, here we have two objectives: a) to maximize hydrogen recovery; b) to decrease CO_2 content in a waste gas stream. While these two problems are not linked to each other, since the primary objective is to maximize hydrogen recovery, the optimization problem can be split into two smaller problems. First, the PSA unit is optimized. Then, starting with the waste gases from the PSA unit (combined blowdown and purge off gases) using an average composition, flowrate and temperature the second problem is solved. Obviously, the first problem is identical to the PSA-Only case. Therefore, the results from PSA-Only case will be used here as a starting point.

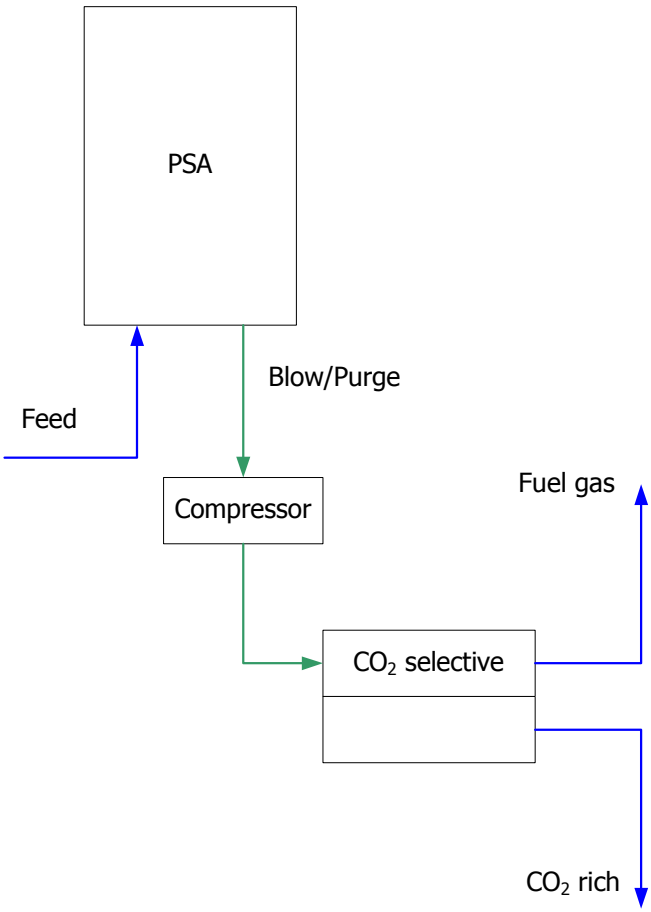

Figure 4.4 Hybrid Case 2: PSA-Mem

4.5.3. Membranes attached to both feed and waste gases streams (Mem-PSA-Mem)

This hybrid scheme consists of the Mem-PSA scheme (membrane + PSA) with an additional membrane unit. Membrane feed inlet is connected to a blowdown/purge streams of the PSA (Figure 4.5). All the conclusions made for the PSA-Mem case hold here as well: the main objective of this hybrid scheme is to investigate possibilities of producing a fuel gas of a higher calorific value. Thus, we have two objectives and we can split the optimization problem into two smaller problems. In this case, the PSA and the first membrane unit will be optimized together; then, starting with the waste gases from the PSA unit (combined blowdown and purge off gases) of the average composition, flowrate and temperature the second problem is solved. The first problem is identical to the Mem-PSA case and the results from that case will be used here as a starting point.

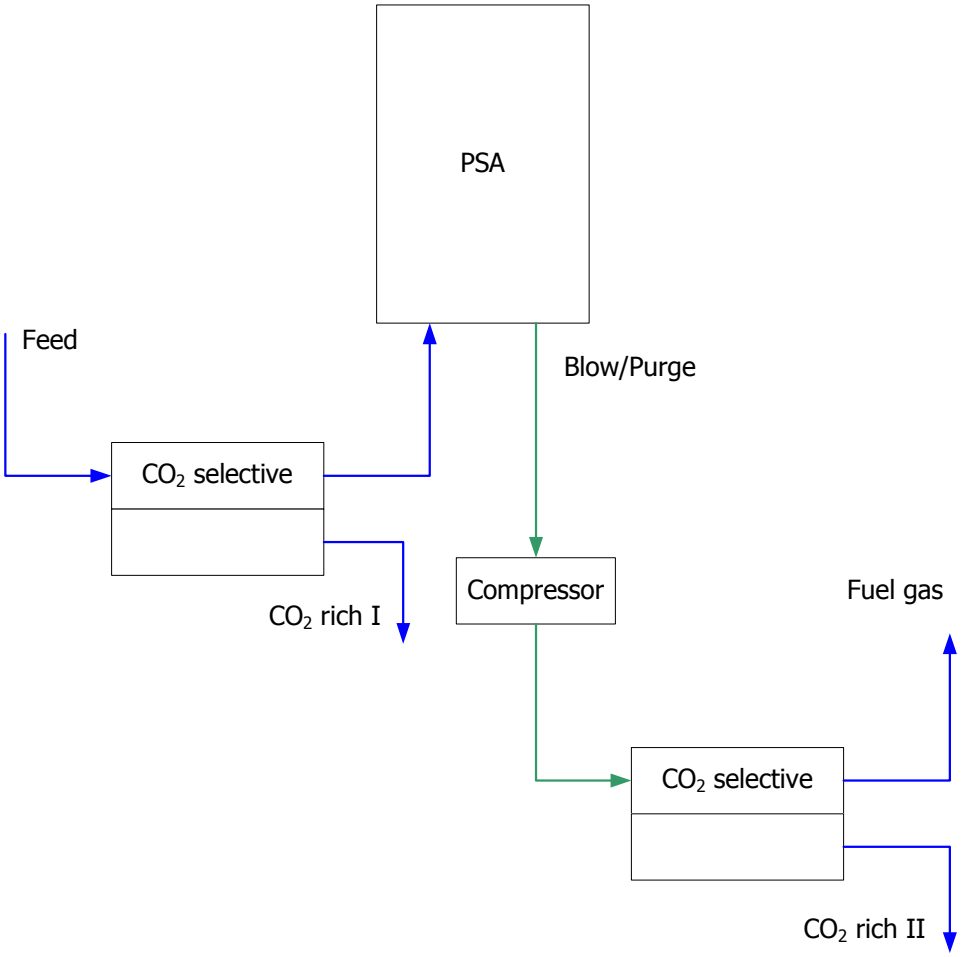

Figure 4.5 Hybrid Case 3: Mem-PSA-Mem

4.6. Optimization case studies

To analyze the benefits of hybrid PSA/membrane schemes, three hybrid schemes have been compared to the base, PSA-Only case. The input to all four configurations is the steam methane reformer off gas of the same characteristics, given in Table 4.1. For all four cases, configurations C1, C2, C4, C5a, C5b and C8 have been employed and two adsorbent layers have been used (activated carbon and zeolite 5A). Silicalite-1 membrane (CO_2 selective, with a stainless steel support layer) has been selected. All transport and equilibrium properties for PSA are equivalent to those in Chapter 2. Adsorption isotherm data and surface diffusion coefficients for Silicalite-1 membrane are adopted from the work of Baker et al (1997) and given in Table 4.2 and Table 4.3. Base case parameters for membrane are given in Table 4.4 while PSA runtime parameters are given in Table 4.5. Molecular diffusivities through the metal support are calculated by using Chapman-Enskog equation.

Table 4.1 Feed characteristics

Parameter	**Value**			
Composition, %	H_2	CO	CH_4	CO_2
	75.5	4.0	3.5	17.0
Flowrate, lit_{STP}/s	2.5			
Temperature, K	303			

Table 4.2 Diffusion coefficients and activation energies for diffusion

Comp.	**$D_{S,0}$ (10^{-8} m^2/s)**	**$E_{D,S}$ (kJ/mol)**
H_2	1.5	2.1
CO	0.9	7.1
CH_4	3.9	8.8
CO_2	0.7	9.6

Table 4.3 Langmuir parameters for Silicalite-1

Comp.	**Q^{sat} (mol/kg)**	**ΔS (J/molK)**	**ΔH_{ads} (kJ/mol)**
H_2	5.4	-43	5.9
CO	5.1	-55	17.9
CH_4	4.5	-70	22.6
CO_2	5.0	-58	24.1

Table 4.4 Base case parameters (membrane)

Property	Value
Membrane surface, m^2	0.5
Membrane thickness, m	1×10^{-5}
Support thickness, m	3×10^{-3}
Feed pressure, bar	10
Permeate pressure, Pa	1×10^{5}
Feed temperature, K	303

Table 4.5 PSA runtime parameters (all case studies)

Parameter	Configuration					
	C1	C2	C4	C5a	C5b	C8
$\tau_{Press,\ s}$	120	60	60	48	48	60
$\tau_{Ads,\ s}$	120	120	120	96	96	90
$\tau_{PEQ1,\ s}$	-	60	60	48	48	30
$\tau_{PEQ2,\ s}$	-	-	-	48	48	30
$\tau_{PEQ3,\ s}$	-	-	-	-	-	30
$\tau_{CoCD,\ s}$	-	-	60	-	48	-
$\tau_{Purge,\ s}$	120	60	60	48	48	60
$\tau_{Blow,\ s}$	120	120	60	96	48	90
$\tau_{cycle,\ s}$	480	480	480	480	480	480

4.6.1. Formulation of the optimization problem

The main objective is to analyze a range of medium scale hybrid PSA/Membrane processes and compare their separation performance to the base PSA-Only case. Several design and operating parameters have been systematically optimized. The effects of multi-bed PSA configurations, number of pressure equalizations, multiple adsorbent layers as well as various membrane characteristics (such as area, thickness, and support thickness) have been investigated.

In order to get a fair comparison between the various configurations involving PSA, it is necessary to define certain assumptions. Here, the total cycle time, the amount of feed and the bed diameter will be kept constant (to make comparison of columns easier). Based on the conclusions from previous case studies (Chapter 2), the most significant process parameters in this case study are the feed pressure, column geometry (length/diameter ratio), carbon/zeolite and purge/feed ratios.

4.6.1.1. Case 1: PSA-Only

The optimization problem can be formulated as the maximization of hydrogen recovery for given minimum requirements in product purity, while optimizing the number of beds and cycle configuration, feed pressure, purge/feed ratio, carbon to zeolite ratio, and column length to diameter ratio (cycle and step times, the amount of feed and column diameter are kept constant):

$$\begin{aligned} &Max \quad Recovery_{H_2} \\ &s.t. \quad Model\ Equations \\ &\quad Purity_{H_2} \geq 99.99\% \\ &\quad N_{beds} \in \{1,2,4,5,8\} \\ &\quad Configurations \in \{C1, C2, C4, C5a, C5b, C8\} \\ &\quad LB \leq P_{feed} \leq UB \\ &\quad LB \leq \frac{Purge}{Feed} ratio \leq UB \\ &\quad LB \leq \frac{L}{D} \leq UB \\ &\quad LB \leq \frac{Carbon}{Zeolite} ratio \leq UB \end{aligned} \tag{4.1}$$

where LB and UB denote the lower and upper bounds of optimization variables, respectively.

4.6.1.2. Case 2: Mem-PSA

The objective in this case study is to maximize hydrogen recovery while trying to minimize carbon dioxide content in the retentate stream that enters PSA unit. Therefore, several changes have to be introduced compared to the PSA-Only case.

First, the objective function in this case must be the maximization of the overall hydrogen recovery (a combined recovery of the membrane and the PSA unit).

Second, three new design optimization variables have to be added to the optimization problem: membrane area, thickness and support thickness. Permeate side pressure and temperature will be kept constant.

Finally, two problems came forth during preliminary optimization runs:

- If a feed pressure is considered common for PSA and membrane, much lower hydrogen recovery can be obtained compared to PSA-Only case. Thus, it is desirable to allow PSA and membrane feed pressures to be different, by introducing an additional constraint that PSA feed pressure must be lower or equal to membrane feed pressure. This approach produced satisfactorily results.
- By setting the objective function as the maximization of the overall recovery several numerical errors/problems have been encountered. Hence, a new constraint had to

be introduced representing the maximum concentration of CO_2 in the retentate stream.

Keeping all of above facts in mind, the optimization problem can be formulated now as the maximization of overall hydrogen recovery for given minimum requirements in product purity and maximum allowed carbon dioxide concentration in retentate stream, while optimizing the number of beds and cycle configuration, feed pressure, purge to feed ratio, carbon to zeolite ratio, column length to diameter ratio, membrane area, membrane and support thickness (cycle and step times, the amount of feed, column diameter, permeate side pressure and temperature are kept constant) with an additional constraint regarding pressures of feed streams of the membrane and the PSA unit:

$$
\begin{aligned}
&Max \quad OverallRecovery_{H_2} \\
&s.t. \quad Model\ Equations \\
&\quad Purity_{H_2} \geq 99.99\% \\
&\quad N_{beds} \in \{1,2,4,5,8\} \\
&\quad Configurations \in \{C1, C2, C4, C5a, C5b, C8\} \\
&\quad LB \leq P_{feed}^{PSA} \leq UB \\
&\quad LB \leq \frac{Purge}{Feed} ratio \leq UB \\
&\quad LB \leq \frac{L}{D} \leq UB \\
&\quad LB \leq \frac{Carbon}{Zeolite} ratio \leq UB \\
&\quad LB \leq A_{membrane} \leq UB \\
&\quad LB \leq \delta_{membrane} \leq UB \\
&\quad LB \leq \delta_{support} \leq UB \\
&\quad LB \leq P_{feed}^{Membrane} \leq UB \\
&\quad P_{feed}^{PSA} \leq P_{feed}^{Membrane} \\
&\quad X_{CO_2} = \{3,4,5\ and\ 6\%\}
\end{aligned}
\tag{4.2}
$$

where LB and UB denote the lower and upper bounds of optimization variables, respectively.

In our case four different cases have been investigated where CO_2 concentration was fixed to 3, 4, 5 and 6% (keeping in mind that the CO_2 concentration in feed is 17.5%). This way a Pareto curve can be constructed with the overall recovery given as a function of CO_2 concentration after membrane unit and to investigate the trade off between hydrogen recovery and carbon dioxide content.

4.6.1.3. Case 3: PSA-Mem

In this case, PSA and membrane can be optimized separately, as it is previously explained in the analysis section. Here CO_2 selective membrane has been attached to a waste gas stream (during blowdown and purge steps) in order to decrease CO/CO_2 content, thus produce a fuel-gas of a higher calorific value. The flowrate, composition and temperature of waste gases after blowdown and purge steps are firstly averaged and then sent to the membrane.

Keeping all of the above facts in mind, the optimization problem can be split into two smaller problems, corresponding to the optimization of the PSA unit and then optimization of the membrane unit. Since the problems are considered separately as two sub-problems, they should not affect each other. Consequently, the optimization results of the first problem should be equal to the results from the PSA-Only case (which is actually the case, as it will be shown in the section with the results). The mathematical formulation of the PSA optimization problem is given previously by the problem 4.1. The membrane optimization problem can be formulated as the maximization of H_2 and CH_4 content in the retentate stream, while optimizing the membrane area and thickness, and support thickness (permeate side pressure is kept constant, while the temperature is equal to the average temperature of waste gases):

$$\begin{aligned} &Max \ \left(x_{H_2} + x_{CH_4}\right) in\ retentate \\ &s.t. \quad Model\ Equations \\ &\qquad LB \le P_{feed} \le UB \\ &\qquad LB \le A_{membrane} \le UB \\ &\qquad LB \le \delta_{membrane} \le UB \\ &\qquad LB \le \delta_{support} \le UB \end{aligned} \tag{4.3}$$

4.6.1.4. Case 4: Mem-PSA-Mem

Following the same approach as in PSA-Mem case, the membrane unit is attached to a feed stream and Mem-PSA part of the unit can be optimized separately from the membrane attached to waste gas streams. Again, the optimization problem can be split into two smaller sequential problems. Similar to the previous case, the mathematical formulation for the Mem-PSA optimization problem is given by the problem 4.2, while the mathematical formulation for the membrane attached to waste gas streams is given by the problem 4.3.

4.6.2. Optimization results and discussion

All optimization problems have been solved using the gPROMS/gOPT tool. The axial domains for each layer have been discretized using orthogonal collocation of finite elements method (OCFEM) of third order and 20 elements (total of 40 elements per column). Axial domains in the retentate and permeate compartments have been discretized using OCFEM of third order and 20 elements. Radial domain in the membrane model has been discretized using OCFEM of third order and four elements. The CPU time depends on the complexity of the particular optimization problem. CPU times (on AMD Phenom II X4 810 running on 2.6 GHz) are given in Table 4.6.

Table 4.6. Computational statistics

Case study	CPU, hours					
	C1	**C2**	**C4**	**C5a**	**C5b**	**C8**
PSA-Only	5	10	18	15	30	20
Mem-PSA	14	41	56	49	60	54
PSA-Mem*	0.1	0.1	0.1	0.1	0.1	0.1
Mem-PSA-Mem*	0.1	0.1	0.1	0.1	0.1	0.1

* optimization of membrane only

4.6.2.1. Case 1 and 2: PSA-Only and Mem-PSA

The objective here is to compare the separation performance of the hybrid scheme to the PSA-Only case. Upper and lower bounds of the optimization variables were as follows:

- Purge/feed ratio (0.5–2.5)
- Feed pressure (5–30 bar)
- Carbon/zeolite ratio (0.25 – 0.75)
- Length/diameter ratio (5–15)
- Membrane area (0.1–5 m^2)
- Membrane thickness ($0.1 \cdot 10^{-5}$–$5 \cdot 10^{-5}$ m)
- Support thickness (1–10 mm)

The optimization results are presented in Figures 4.6 to 4.44 and Tables 4.7 to 4.12. The overall conclusion is that, by using a hybrid scheme, it is possible to increase the hydrogen recovery (around 2%), significantly decrease column size (up to 46%), significantly reduce carbon dioxide content (up to 74%) and increase hydrogen content (up to 106%) in waste gases stream compared to PSA-Only case. It should be noted that the carbon dioxide stream produced by the membrane is of a moderate purity (not suitable for immediate sequestration but can be further processed).

In this case, an increase in adsorbent productivity is achieved by decreasing the column size (that is by decreasing an amount of adsorbent). This way the same amount of feed can be processed by the lower amount of the adsorbent. However, an increase in adsorbent productivity is available by leaving the column size intact so that more feed can be processed by the same amount of adsorbent due to a lower impurity content. The later may be a preferred option in the case of the existing PSA plant.

A detailed analysis of the results is presented below.

Recovery

A comparison of the PSA-Only and Mem-PSA recovery is given in Figures 4.6 to 4.9. We can observe a trade-off between hydrogen recovery and CO_2 content allowed to enter PSA columns. As the CO_2 content increases recovery increases as well. Hence, some other indicators are needed to choose an optimal value (economical analysis and capital costs data, for instance).

Comparison of the overall recovery in Mem-PSA case for different content of CO_2 is given in Figure 4.10. Again, it can be noted that as the CO_2 content increases the recovery also increases (for all configurations). Only two points are exceptions (C2-3% and C5b-3%), which can be attributed to potential numerical issues.

Comparison of the recovery of membrane only, PSA only and the overall recovery for Mem-PSA case (for PSA configurations C1 to C8) is given in Figures 4.11 to 4.14. It can be seen that the difference between overall recovery and the recovery of the PSA unit decreases as the CO_2 content increases. This result is expected and shows that the overall recovery will reach PSA recovery when the CO_2 content becomes equal to PSA-Only case.

Comparison of the recovery of membrane unit only, PSA unit only and the overall recovery for Mem-PSA case (for different CO_2 content and configurations C4, C5b and C8) is given in Figures 4.15 to 4.17. The conclusion is that the membrane recovery increases as the CO_2 content increases (for less hydrogen is lost through the membrane; this is also given in Figure 4.39), while the PSA recovery slightly decreases as the CO_2 content increases. However, the overall recovery increases as the CO_2 content increases because the absolute value of the membrane recovery increase is higher than the recovery decrease of the PSA.

Length/diameter ratio

Comparison of PSA-Only and Mem-PSA length/diameter ratio is given in Figures 4.18 to 4.21. Since the bed diameter has been kept constant these results directly represent the difference in columns size (or in the other words a difference in the amount of the adsorbent). It can be observed that length/diameter ratio follows identical trend, but it is always lower compared to PSA-Only case, which can be attributed to a much higher CO_2 content in feed in PSA-Only case; consequently, longer columns are needed to achieve the same purity.

Figure 4.22 illustrates that as the CO_2 content increases the length/diameter ratio increases as well (for all configurations). Only one point is the exception (C1-4%), which can be attributed to the numerical issues. This is an expected result since the amount of impurities increases thus longer columns are necessary to achieve the same purity.

Difference (given as percentage) in length/diameter ratio between PSA-Only and Mem-PSA case is shown in Figure 4.23. It can be concluded that it is possible to achieve a reduction in column size (that is in amount of an adsorbent) up to 46% (in 3% CO_2 case). In other words, the capital costs and the adsorbent productivity can be significantly improved by using this hybrid scheme.

Carbon/zeolite ratio

Comparison of the PSA-Only and Mem-PSA carbon/zeolite ratio is shown in Figures 4.24 to 4.27. It can be seen that the carbon/zeolite ratio is always lower compared to PSA-Only case. This trend is expected since the CO_2 content is lower thus the activated carbon layer can be shorter. Only one point is the exception (configuration C5a), which can be attributed to the numerical issues.

Comparison of the Mem-PSA carbon/zeolite ratio for different content of CO_2 is given in Figure 4.28. It can be noted that as the CO_2 content increases the carbon/zeolite ratio increases as well (for all configurations) because of a higher amount of CO_2 in the feed stream. Thus, the activated carbon layer must be longer to produce hydrogen of the same purity.

Feed pressure

Comparison of the PSA-Only and Mem-PSA feed pressure is given in Figures 4.28 to 4.32. No single conclusion can be made based on the trend of the results. However, from Figure 4.33 it can be concluded that as the CO_2 content increases the feed pressure also increases (for all configurations except C4 and C5b). This can be attributed to the fact that a higher amount of impurities demands a higher feed pressure to shift phase equilibrium and produce the same purity. In addition, it is shown that optimal feed pressures for configurations C4 and C5b always hit the lower bound of 16 and 18 bars, respectively. This can be attributed to the fact that in those configurations quite high lower bound had to be introduced to avoid numerical problems. Problems arise during optimization, when a high purge/feed ratio and a low feed pressure is selected by the optimization solver. In these cases, the amount of gas needed for purge is so high that there is no enough gas in a column, thus the pressure at the end of purge step will be below 1 bar (which is not feasible, but mathematically correct). Therefore, in order to prevent such scenarios “a barrier” (that is a high lower bound for feed pressure) had to be introduced.

Purge/Feed ratio

Comparison of the PSA-Only and Mem-PSA purge/feed ratio is given in Figures 4.34 to 4.37. It can be seen that the purge/feed ratio follows the same trend and that it is always higher compared to PSA-Only case. From Figure 4.38 it can be noted that as the CO_2 content increases the purge/feed ratio increases as well (for all configurations). This can be explained by the fact that more gas is needed to purge columns when the amount of impurities is higher. Only two points are exceptions (C1-3% and C2-3%), which can be attributed to the numerical issues.

Membrane results

Comparison of the optimal membrane area, membrane thickness and support thickness for Mem-PSA case is given in Figures 4.40 to 4.42, while the retentate and permeate flowrates are given in Figure 4.43 and Figure 4.44, respectively. All trends are as it was expected:

- when a higher CO_2 content is allowed to leave the membrane unit - the membrane area is lower

- membrane thickness increases as the allowed CO_2 content increases
- support thickness decreases as the allowed CO_2 content increases
- retentate flowrate increases as the allowed CO_2 content increases
- permeate flowrate decreases as the allowed CO_2 content increases

Quite low values of the membrane stage-cut (fraction of feed permeated, θ_m) have been observed: 0.15 to 0.22. This is in agreement with the objective to maximize the hydrogen recovery (effectively demanding the minimal losses through a membrane). Therefore, the low membrane stage-cut values are expected and sought after.

Waste gases

Comparison of averaged PSA waste gas compositions for PSA-Only and Mem-PSA cases is given in Table 4.7 and Table 4.9, while retentate/permeate compositions are shown in Table 4.8. Differences in hydrogen and carbon dioxide content (given as a percentage) are shown in Table 4.10. It is observed that by using this hybrid scheme, it is possible to achieve up to 106% higher hydrogen content and up to 74% lower carbon dioxide content in waste gases compared to PSA-Only case. More specifically, carbon dioxide content decreases from 38.3 – 50.9% in PSA-Only to 9.9 – 16.2% in Mem-PSA case, while hydrogen content increases from 27.2 – 44.6% in PSA-Only to 56.3 – 73.7% in Mem-PSA case.

Differences in waste gas flowrates (given as percentage) are shown in Table 4.11. Obviously, waste gas flowrate is ~50% lower compared to PSA-Only case due to the amount of impurities removed in the membrane unit.

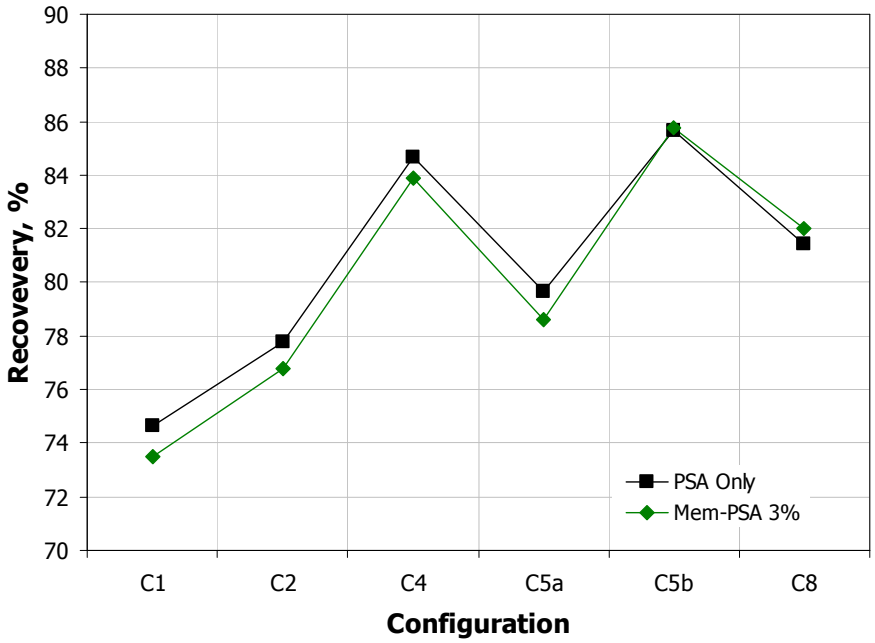

Figure 4.6 Comparison of the recovery: PSA-Only vs. Mem-PSA (X_{CO2}=3%)

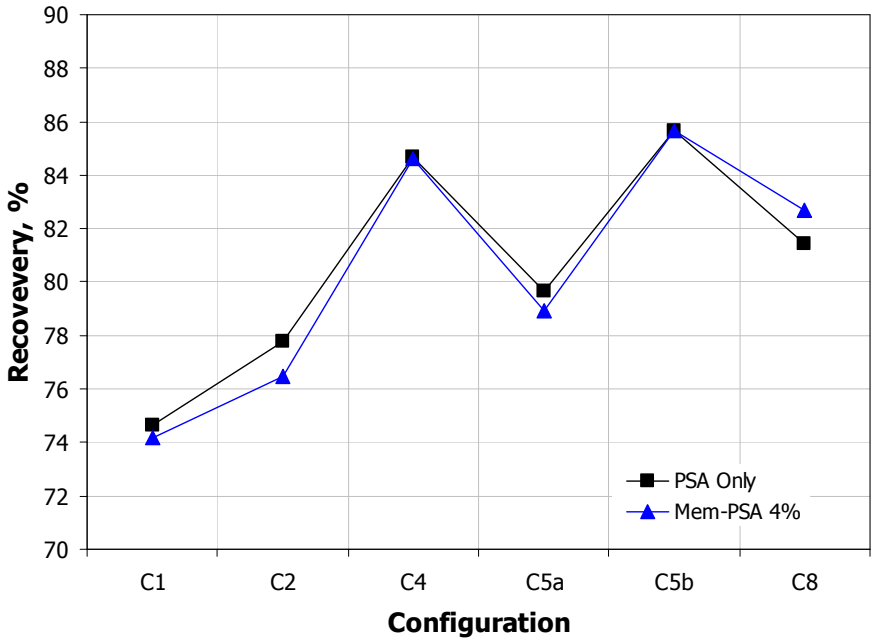

Figure 4.7 Comparison of the recovery: PSA-Only vs. Mem-PSA (X_{CO2}=4%)

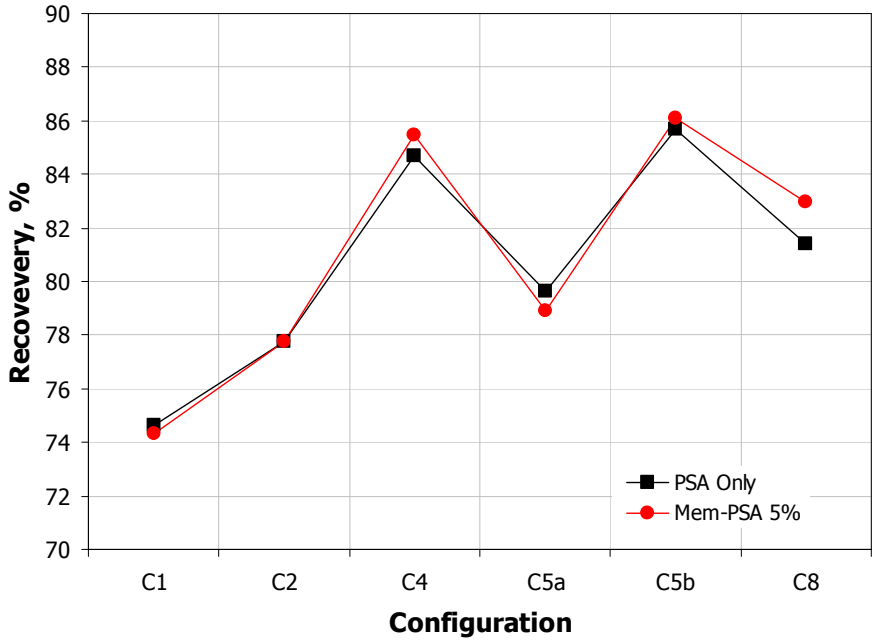

Figure 4.8 Comparison of the recovery: PSA-Only vs. Mem-PSA (X_{CO2}=5%)

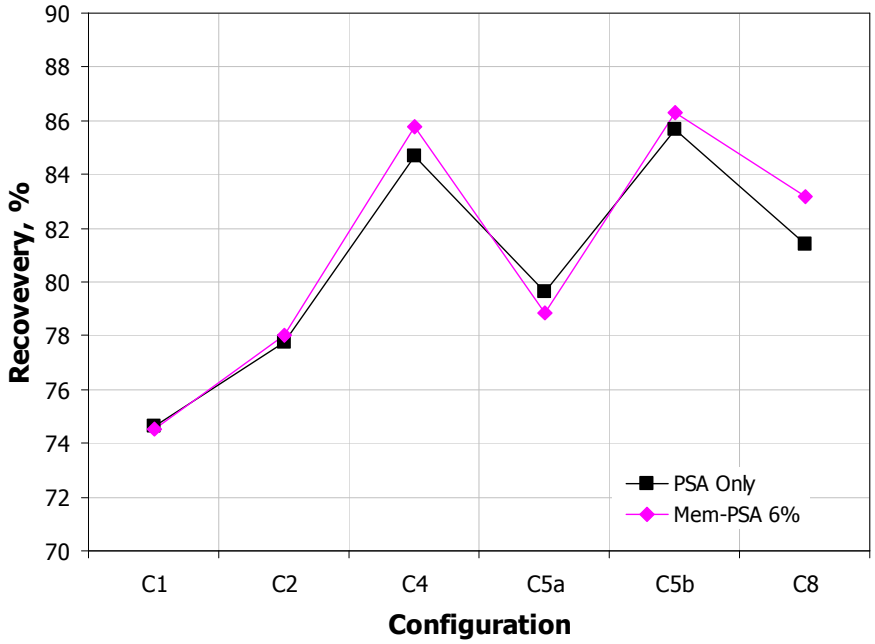

Figure 4.9 Comparison of the recovery: PSA-Only vs. Mem-PSA (X_{CO2}=6%)

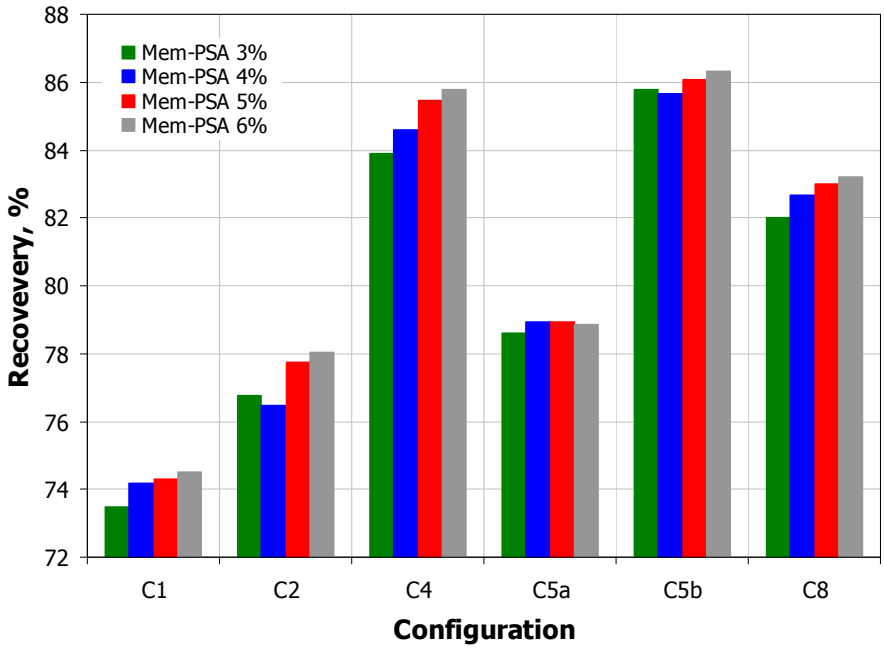

Figure 4.10 Comparison of the overall recovery (Mem-PSA case)

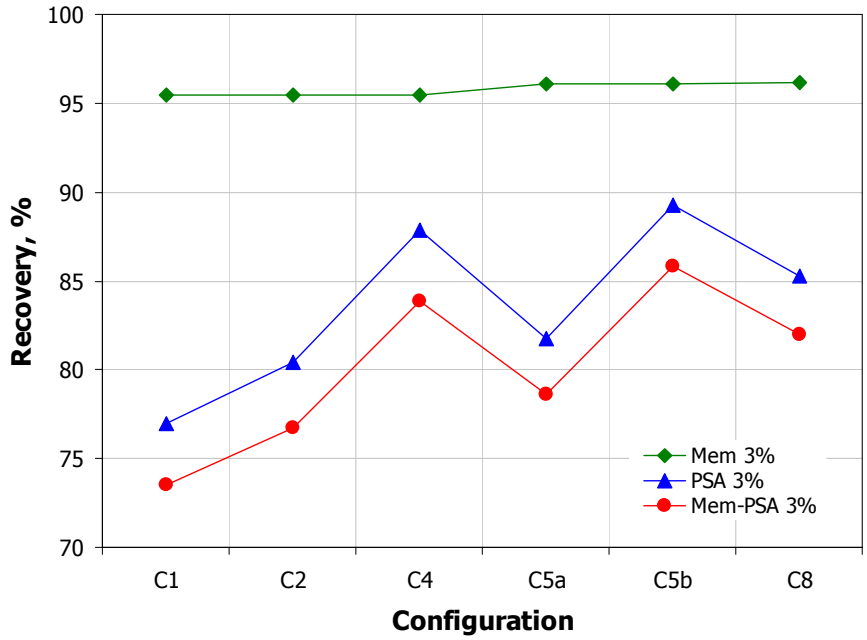

Figure 4.11 Comparison of the recovery: Membrane vs. PSA vs. Overall (Mem-PSA case, X_{CO2}=3%)

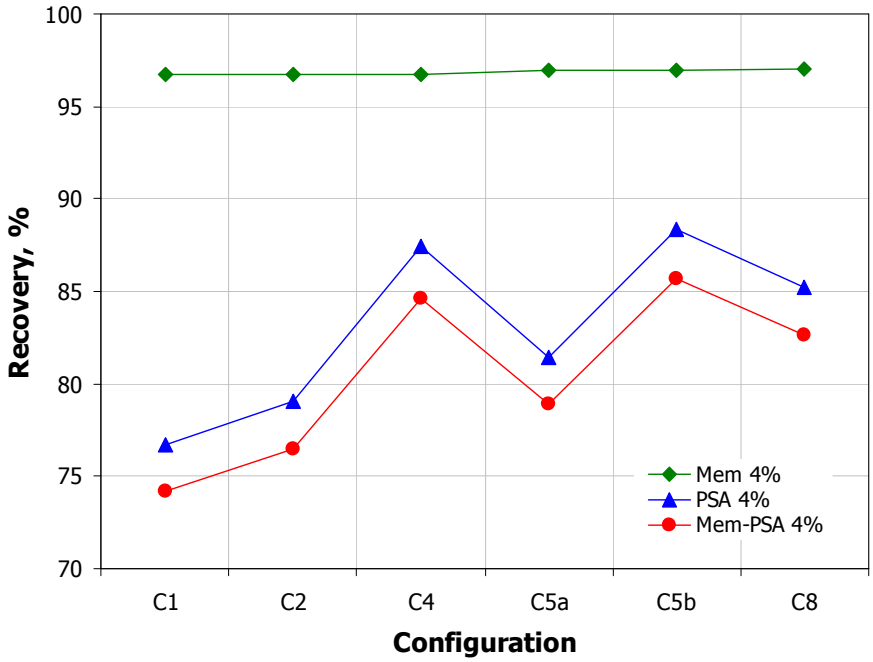

Figure 4.12 Comparison of the recovery: Membrane vs. PSA vs. Overall (Mem-PSA case, X_{CO2}=4%)

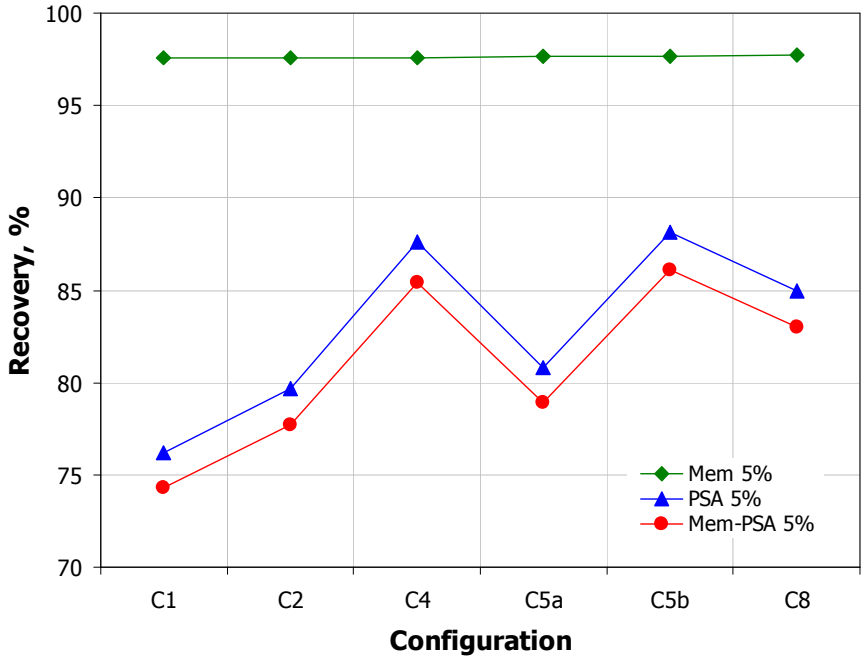

Figure 4.13 Comparison of the recovery: Membrane vs. PSA vs. Overall (Mem-PSA case, X_{CO2}=5%)

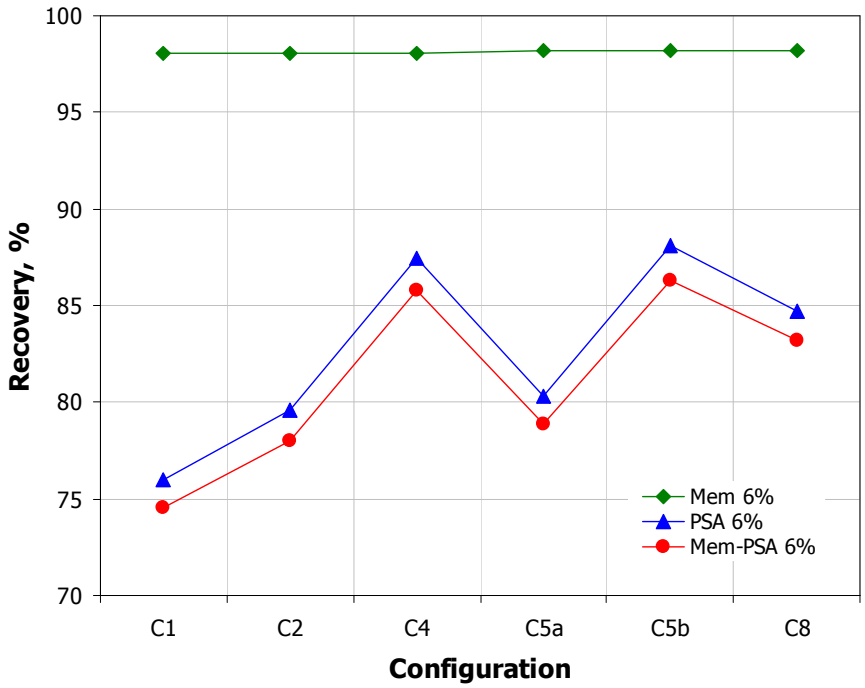

Figure 4.14 Comparison of the recovery: Membrane vs. PSA vs. Overall (Mem-PSA case, X_{CO2}=6%)

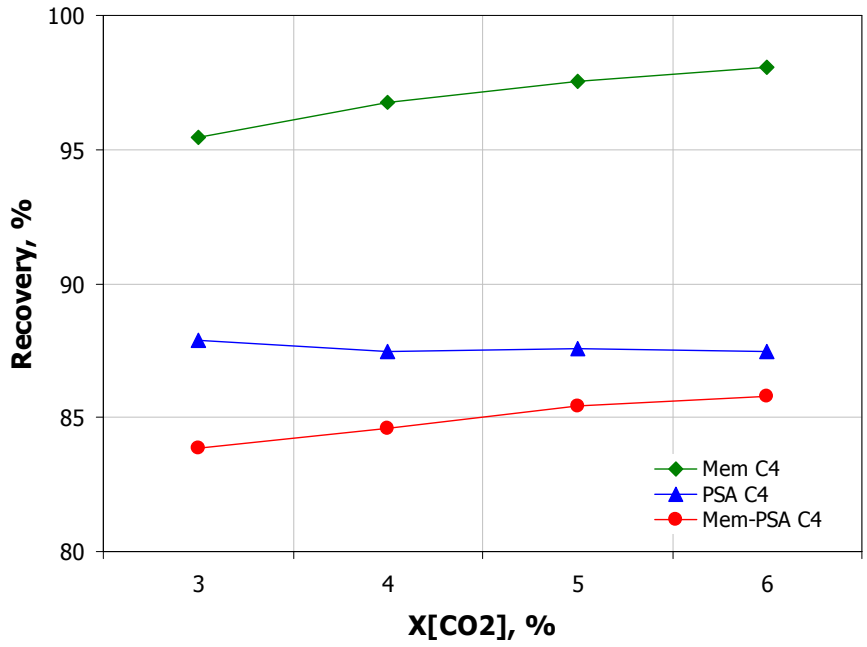

Figure 4.15 Comparison of the recovery: Membrane vs. PSA vs. Overall (Mem-PSA case, configuration C4)

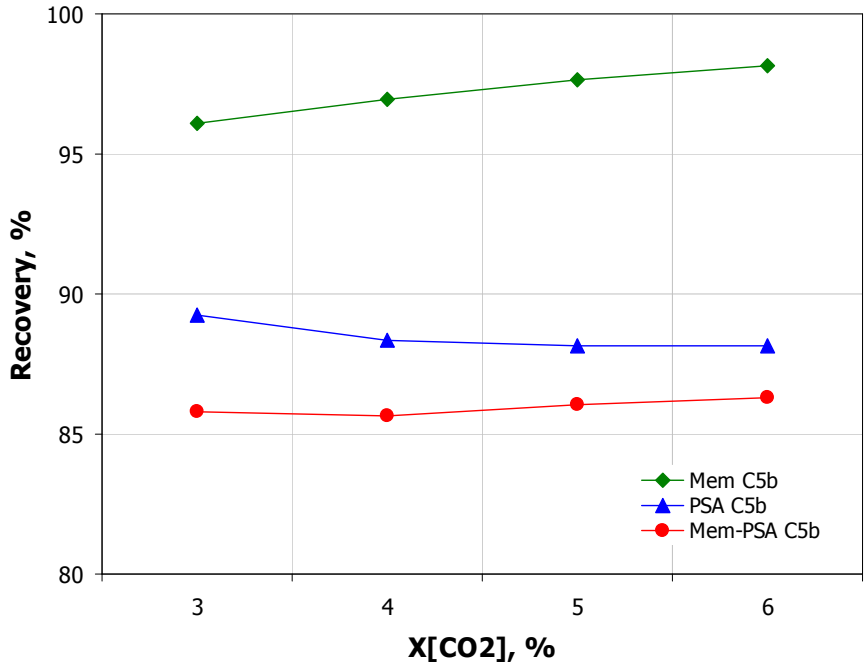

Figure 4.16 Comparison of the recovery: Membrane vs. PSA vs. Overall (Mem-PSA case, configuration C5b)

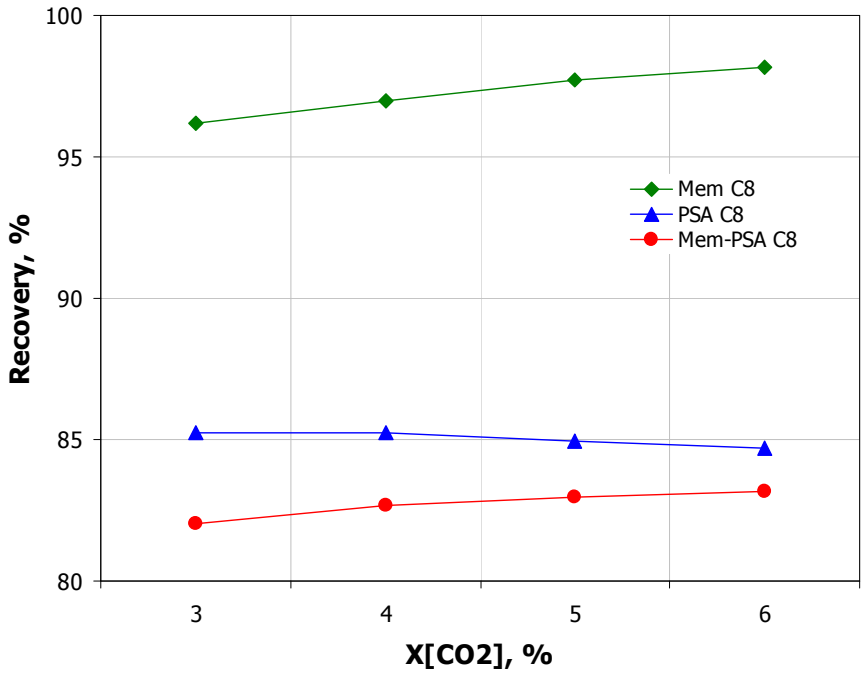

Figure 4.17 Comparison of the recovery: Membrane vs. PSA vs. Overall (Mem-PSA case, configuration C8)

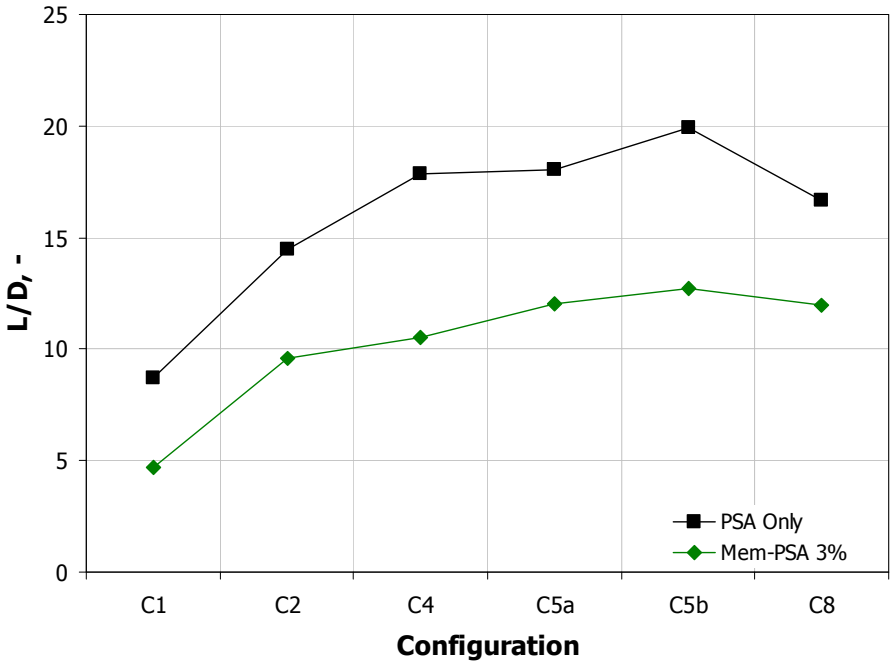

Figure 4.18 Comparison of L/D ratio: Mem-PSA vs. PSA-Only (X_{CO2}=3%)

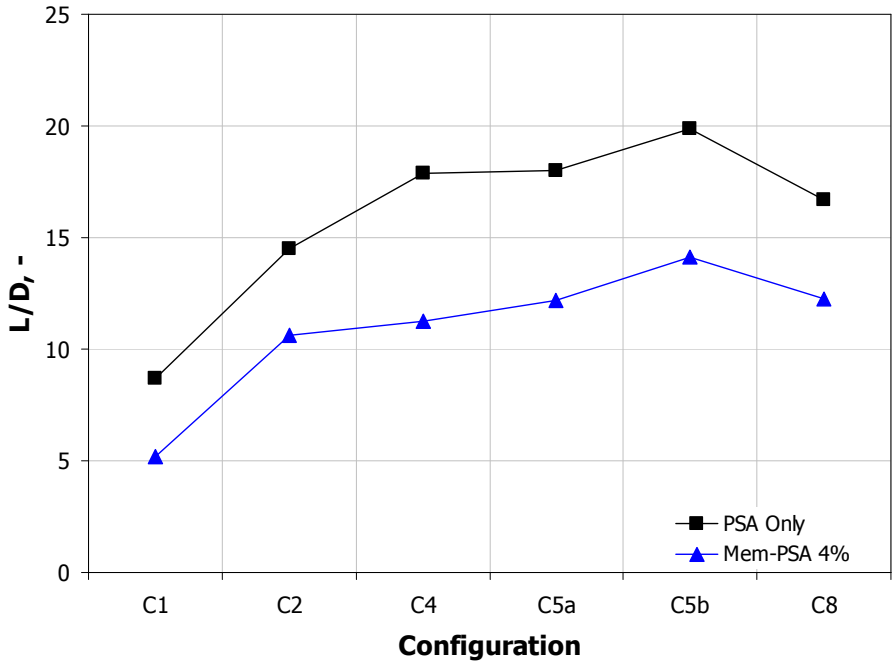

Figure 4.19 Comparison of L/D ratio: Mem-PSA vs. PSA-Only (X_{CO2}=4%)

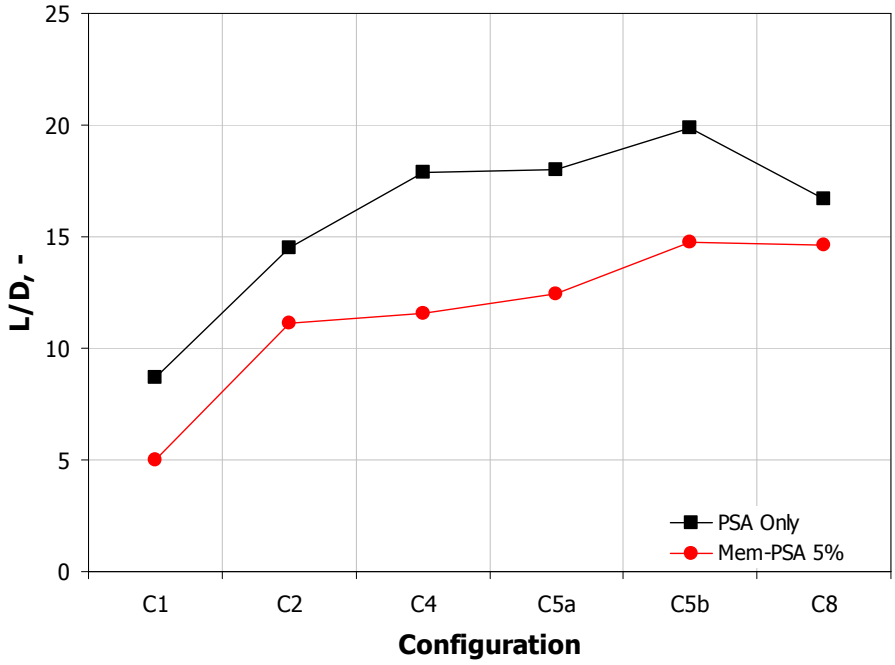

Figure 4.20 Comparison of L/D ratio: Mem-PSA vs. PSA-Only (X_{CO2}=5%)

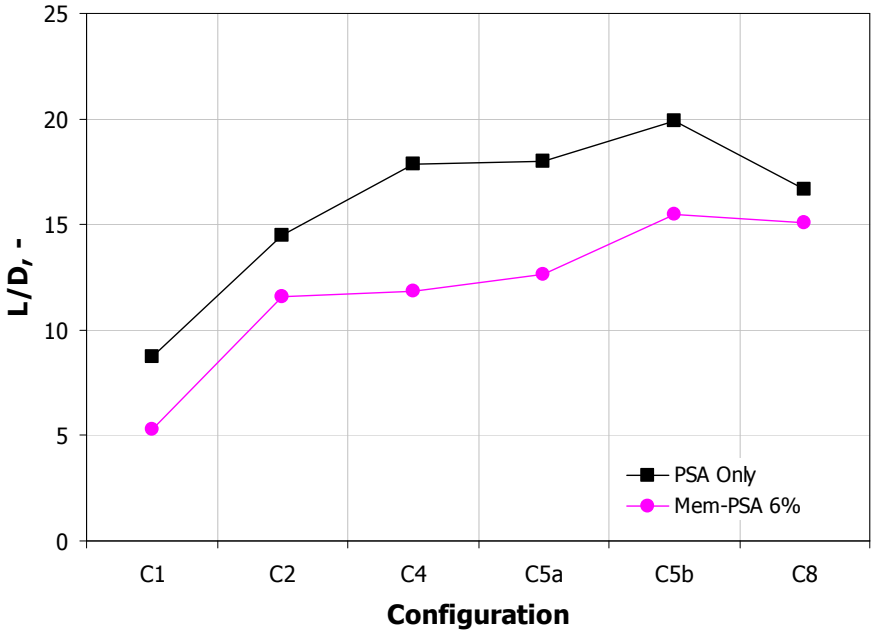

Figure 4.21 Comparison of L/D ratio: Mem-PSA vs. PSA-Only (X_{CO2}=6%)

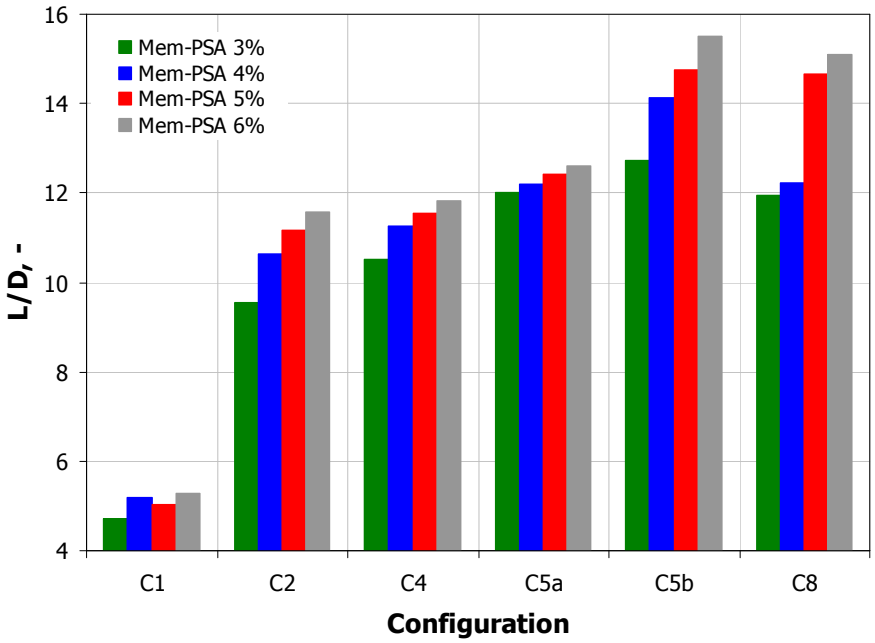

Figure 4.22 Comparison of L/D ratio (Mem-PSA case)

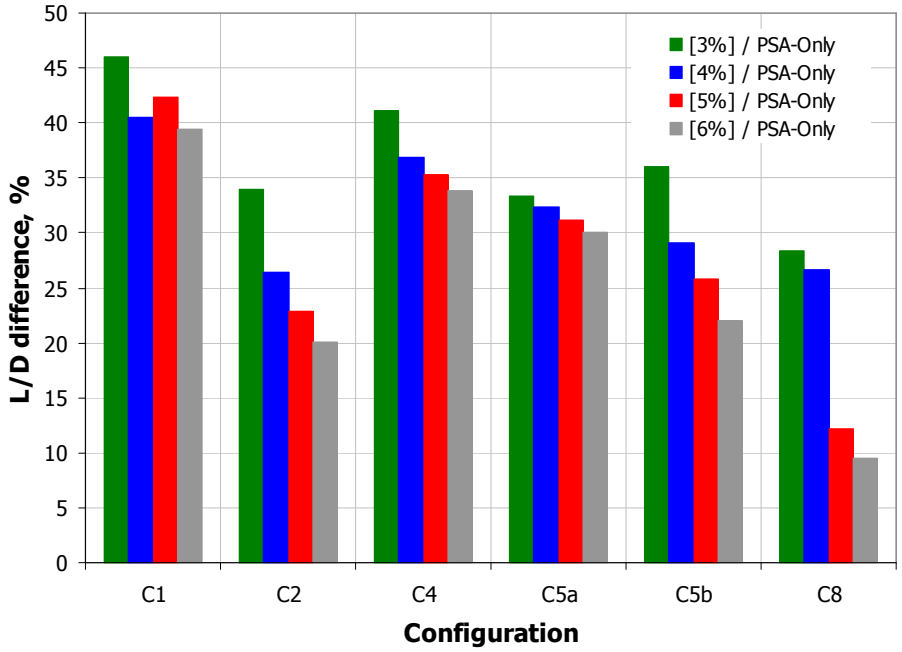

Figure 4.23 Difference between L/D of PSA-Only and Mem-PSA case (given in %)

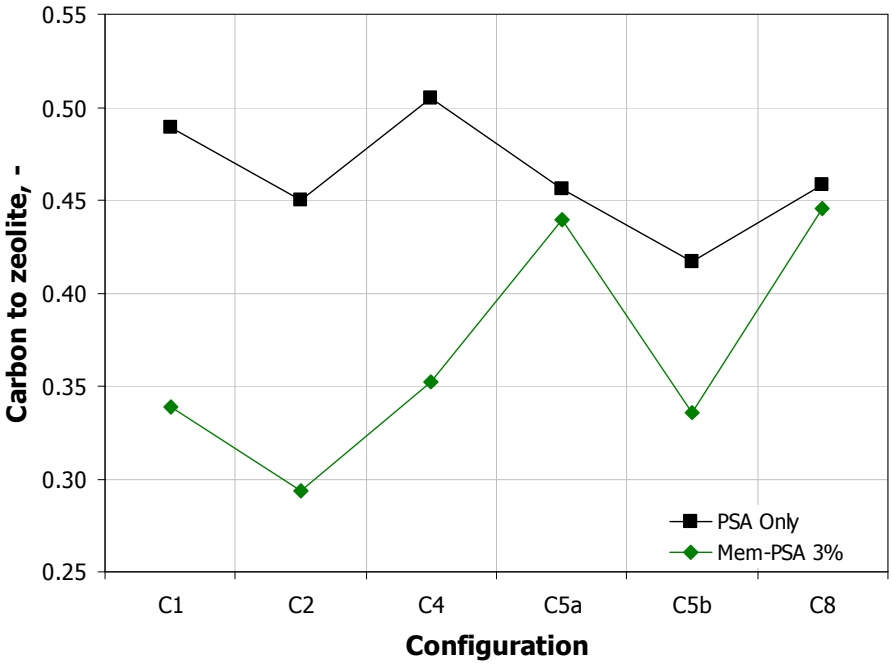

Figure 4.24 Comparison of AC/Z ratio: Mem-PSA vs. PSA-Only (X_{CO2}=3%)

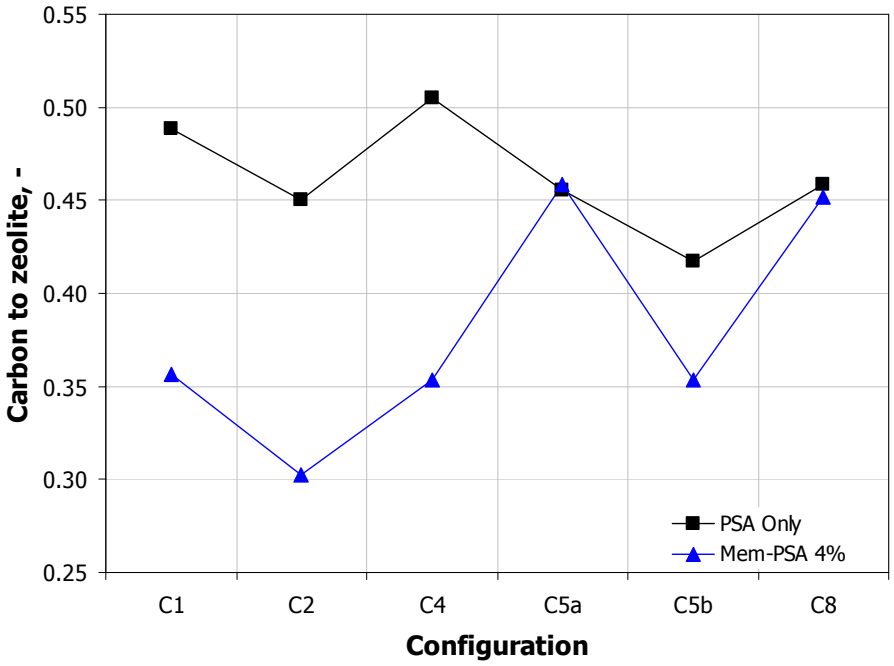

Figure 4.25 Comparison of AC/Z ratio: Mem-PSA vs. PSA-Only (X_{CO2}=4%)

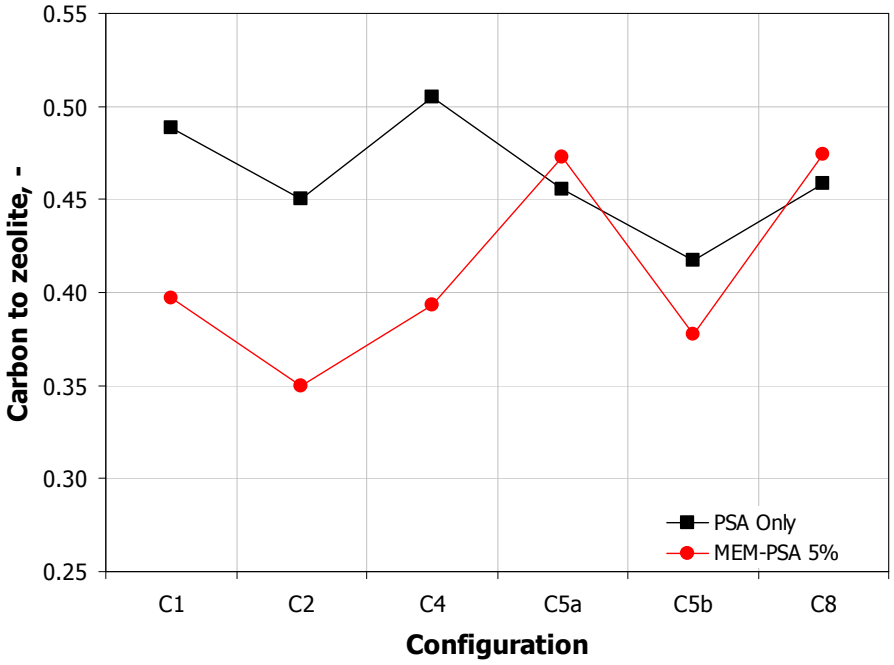

Figure 4.26 Comparison of AC/Z ratio: Mem-PSA vs. PSA-Only (X_{CO2}=5%)

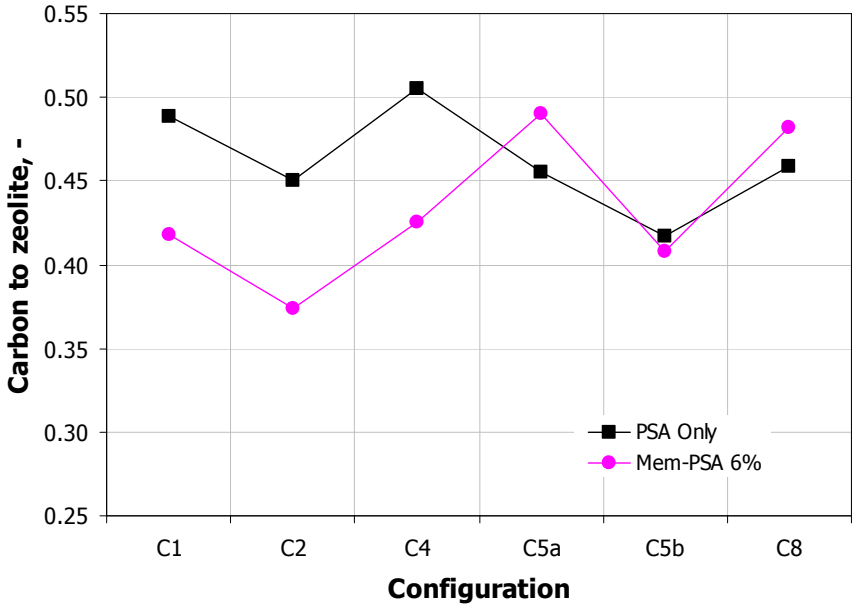

Figure 4.27 Comparison of AC/Z ratio: Mem-PSA vs. PSA-Only (X_{CO2}=6%)

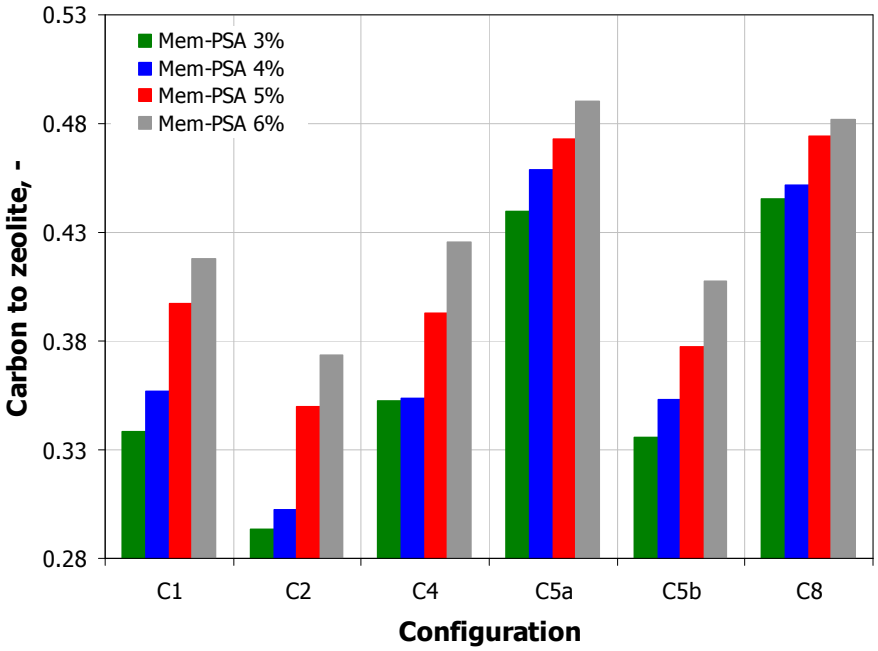

Figure 4.28 Comparison of AC/Z ratio (Mem-PSA case)

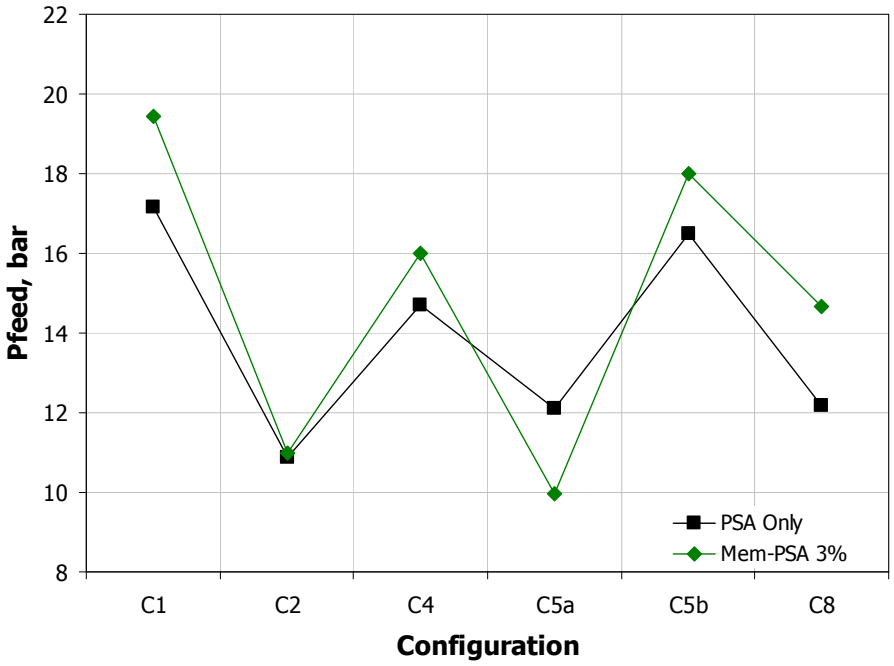

Figure 4.29 Comparison of P_{feed}: Mem-PSA vs. PSA-Only (X_{CO2}=3%)

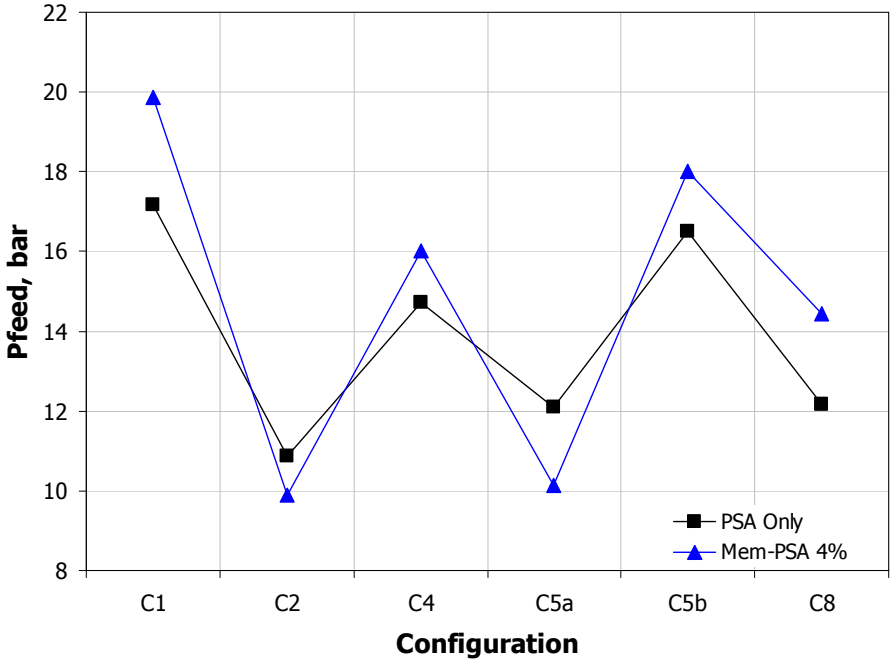

Figure 4.30 Comparison of P_{feed}: Mem-PSA vs. PSA-Only (X_{CO2}=4%)

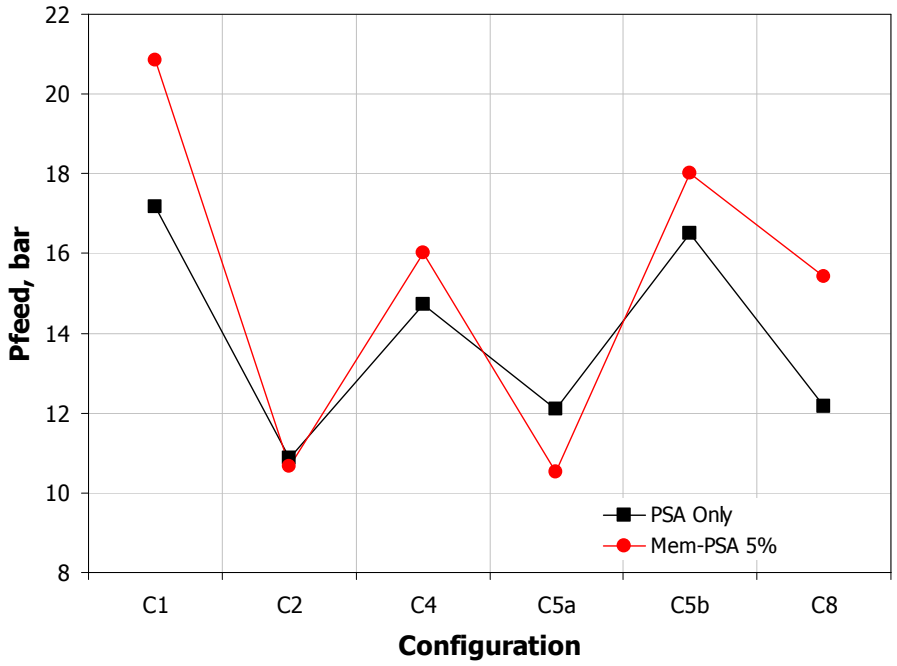

Figure 4.31 Comparison of P_{feed}: Mem-PSA vs. PSA-Only (X_{CO2}=5%)

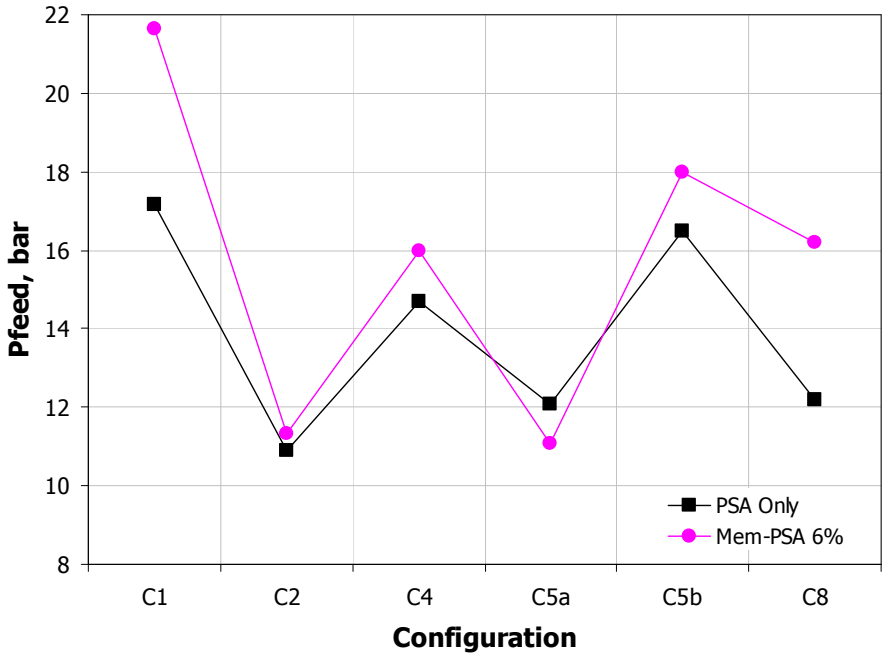

Figure 4.32 Comparison of P_{feed}: Mem-PSA vs. PSA-Only (X_{CO2}=6%)

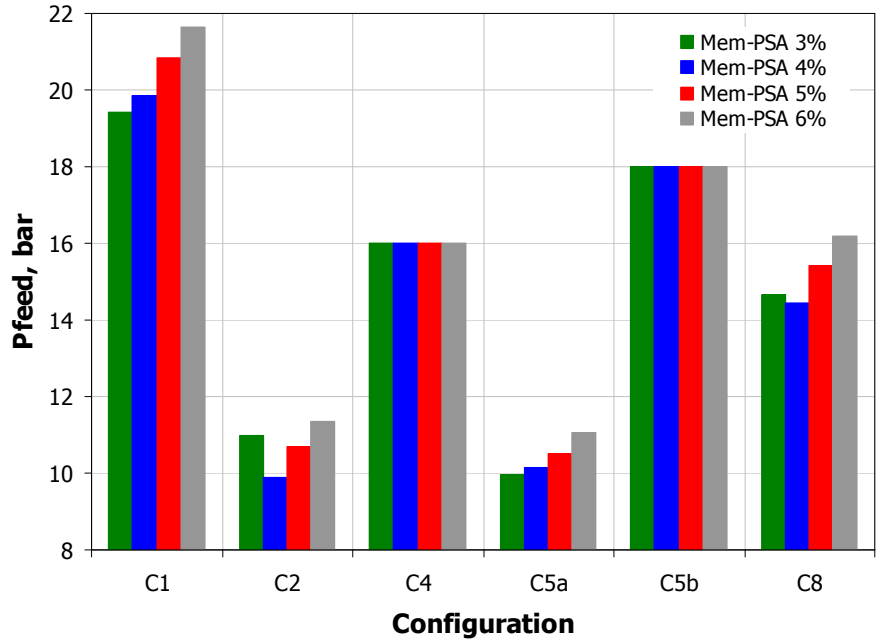

Figure 4.33 Comparison of P_{feed} (Mem-PSA case)

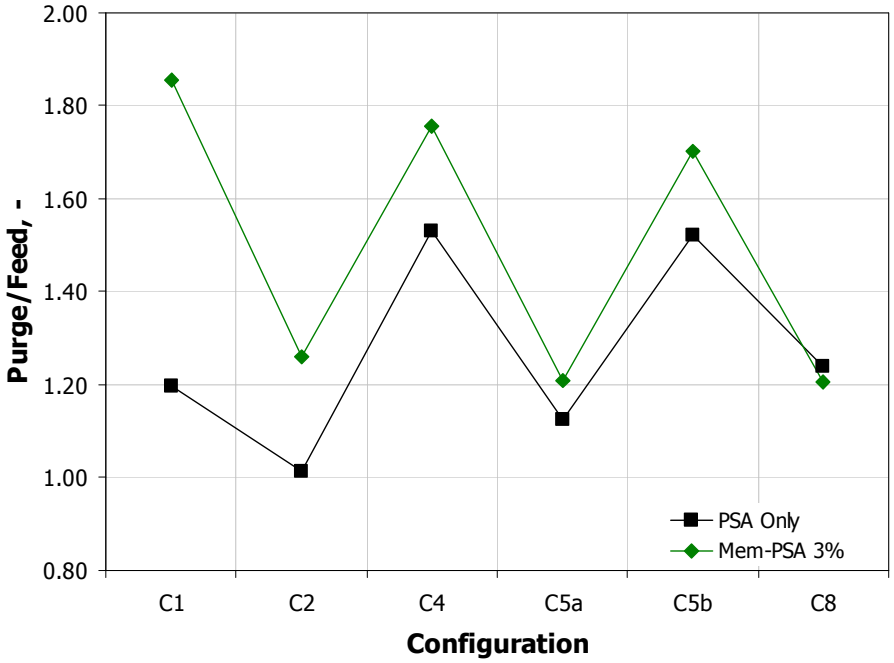

Figure 4.34 Comparison of Purge/feed ratio: Mem-PSA vs. PSA-Only (X_{CO2}=3%)

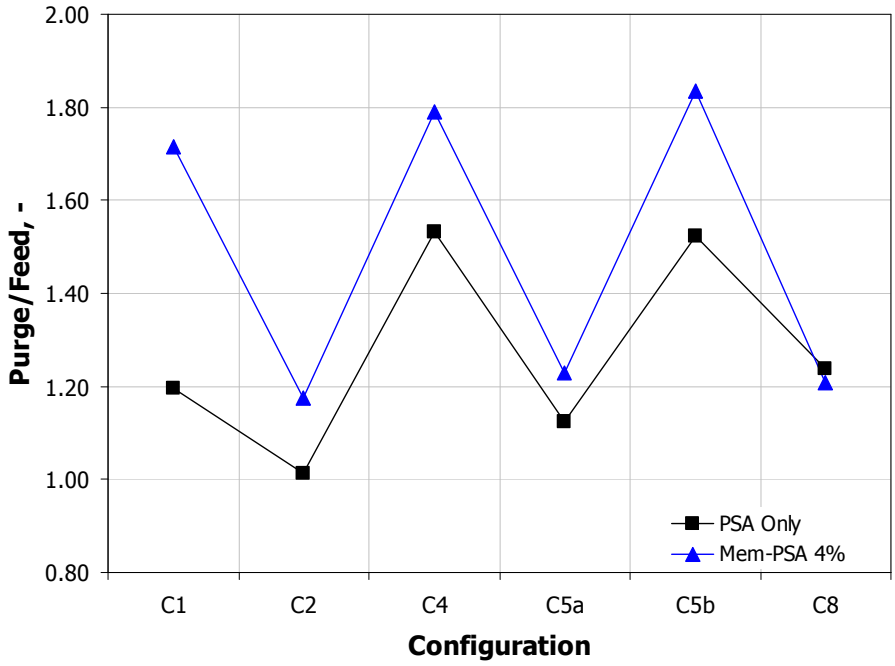

Figure 4.35 Comparison of Purge/feed ratio: Mem-PSA vs. PSA-Only (X_{CO2}=4%)

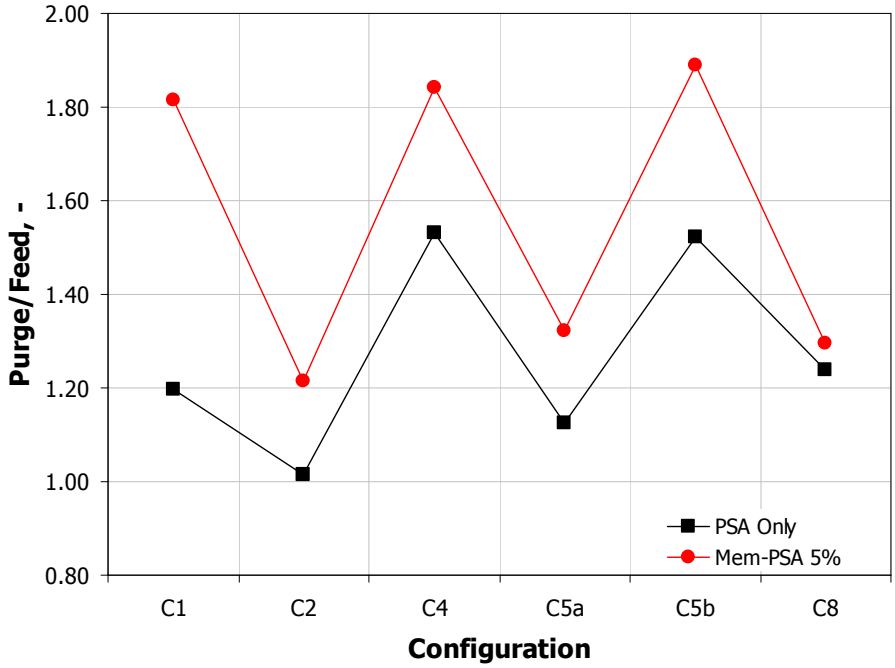

Figure 4.36 Comparison of Purge/feed ratio: Mem-PSA vs. PSA-Only (X_{CO2}=5%)

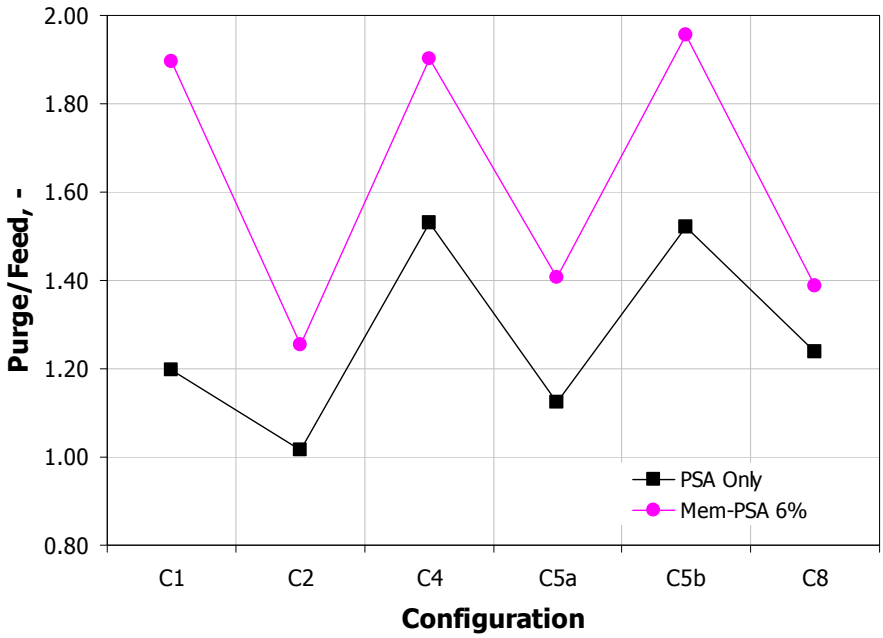

Figure 4.37 Comparison of Purge/feed ratio: Mem-PSA vs. PSA-Only (X_{CO2}=6%)

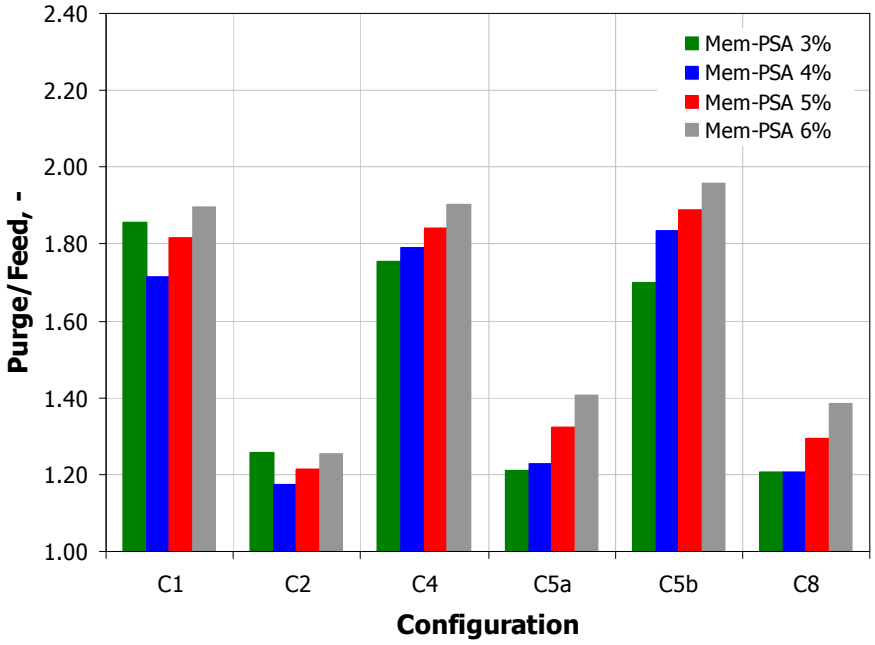

Figure 4.38 Comparison of Purge/feed ratio (Mem-PSA case)

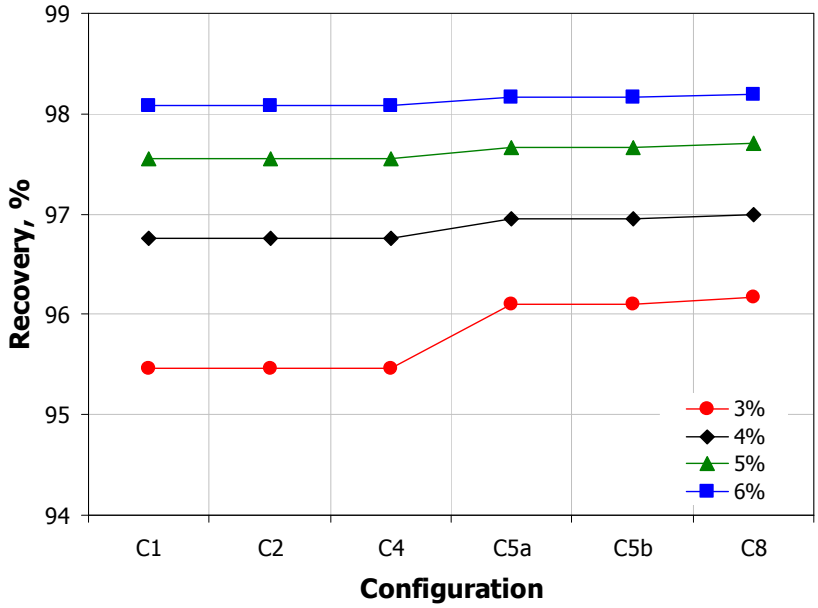

Figure 4.39 Comparison of the membrane recovery (Mem-PSA case)

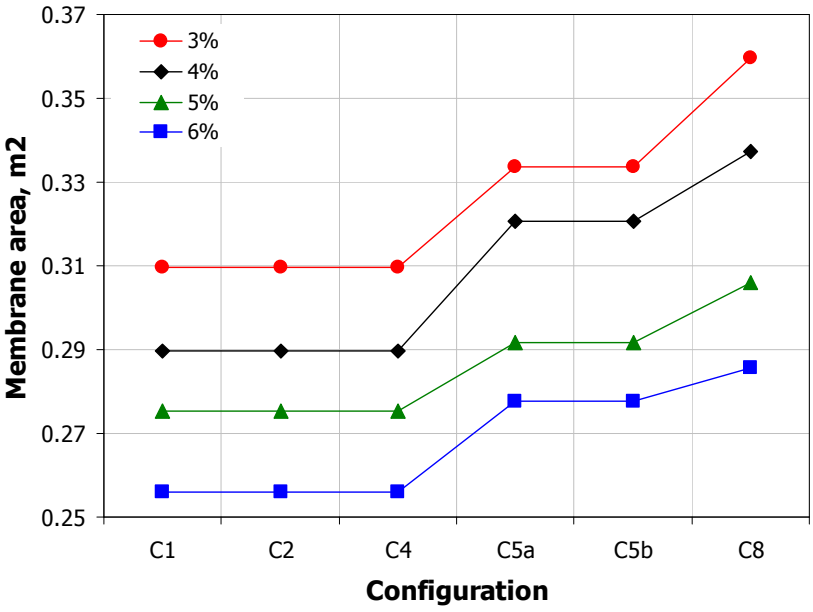

Figure 4.40 Comparison of the membrane area (Mem-PSA case)

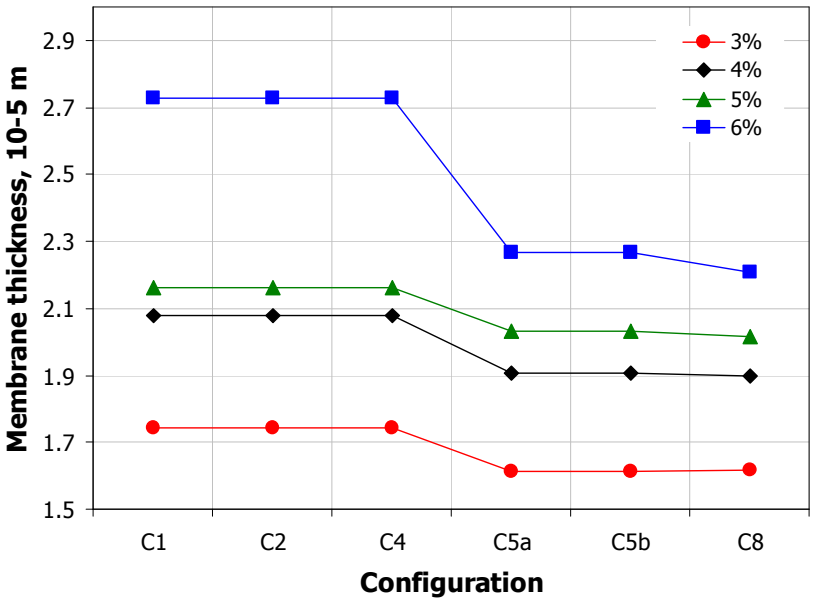

Figure 4.41 Comparison of the membrane thickness (Mem-PSA case)

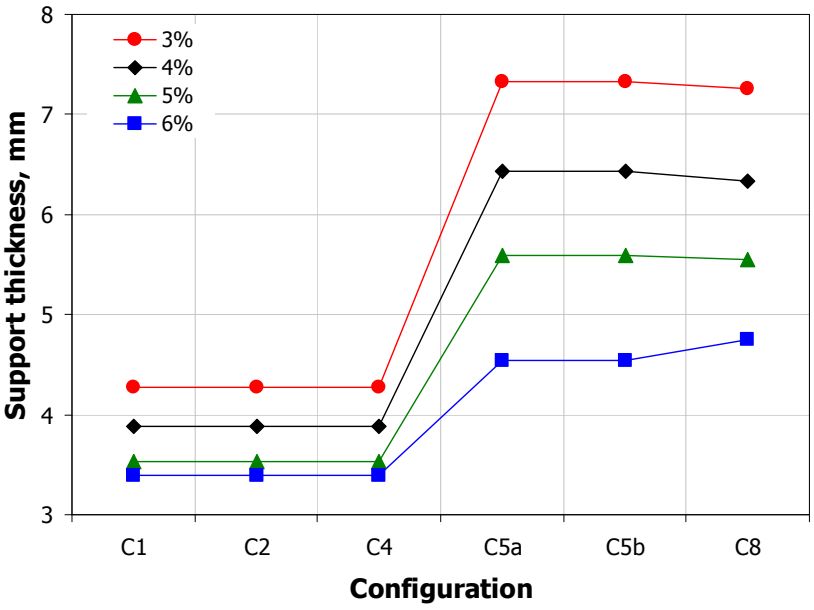

Figure 4.42 Comparison of the membrane support thickness (Mem-PSA case)

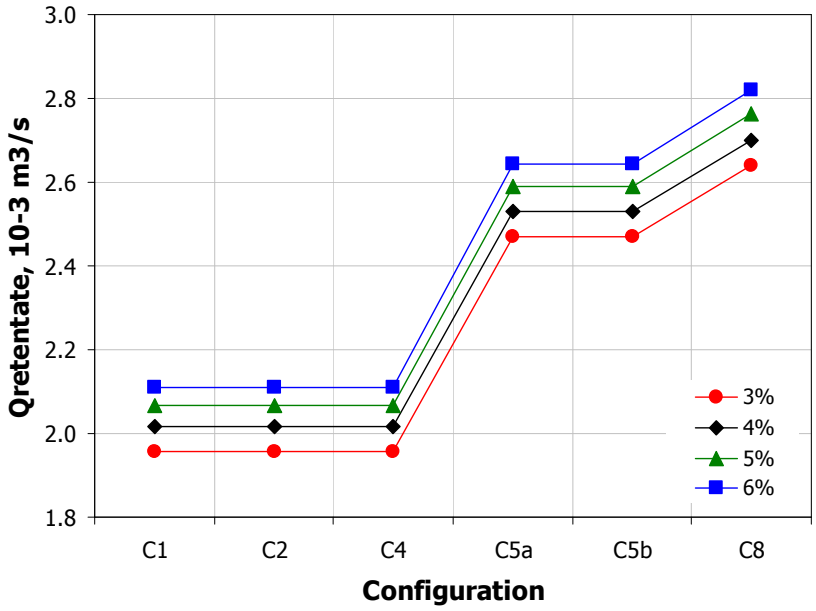

Figure 4.43 Comparison of the membrane retentate flowrates (Mem-PSA case)

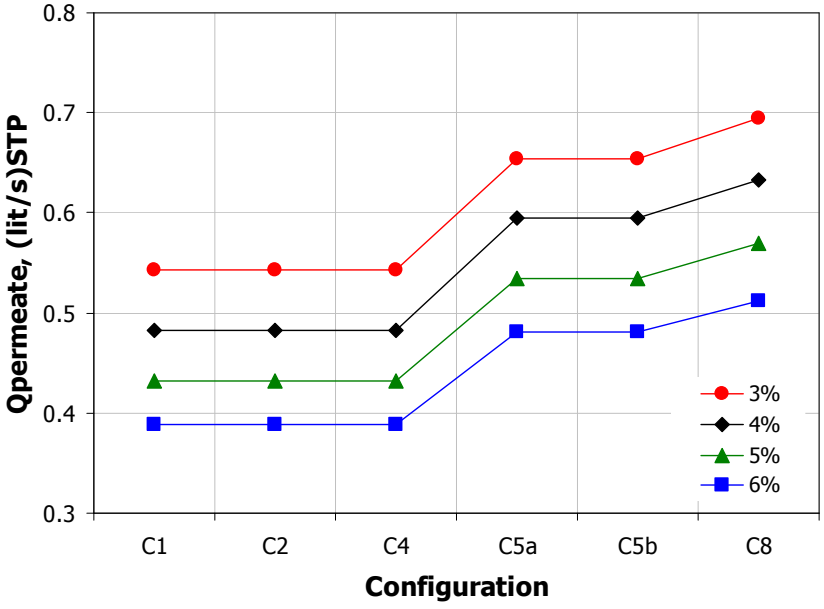

Figure 4.44 Comparison of the membrane permeate flowrates (Mem-PSA case)

Table 4.7 PSA averaged waste gas compositions (PSA-Only case)

Config.	H_2	CO	CH_4	CO_2
C1	0.446328	0.091633	0.079067	0.382972
C2	0.391365	0.101102	0.086686	0.420847
C4	0.324356	0.115205	0.088491	0.471948
C5a	0.393019	0.101880	0.086310	0.418792
C5b	0.272536	0.112716	0.105122	0.509626
C8	0.306308	0.100415	0.100376	0.492901

Table 4.8 Membrane retentate/permeate compositions (Mem-PSA case, 3%)

	Retentate molar fractions				Permeate molar fractions			
Config.	H_2	CO	CH_4	CO_2	H_2	CO	CH_4	CO_2
C1	0.92108	0.02682	0.02210	0.03000	0.18894	0.09048	0.08405	0.63654
C2	0.92108	0.02682	0.02210	0.03000	0.18894	0.09048	0.08405	0.63654
C4	0.92108	0.02682	0.02210	0.03000	0.18894	0.09048	0.08405	0.63654
C5a	0.91743	0.02881	0.02377	0.03000	0.16522	0.08622	0.08095	0.66761
C5b	0.91743	0.02881	0.02377	0.03000	0.16522	0.08622	0.08095	0.66761
C8	0.91715	0.02895	0.02390	0.03000	0.16072	0.08582	0.08057	0.67288

Table 4.9 PSA averaged waste gas compositions (Mem-PSA case, 3%)

Config.	H_2	CO	CH_4	CO_2
C1	0.73699	0.09005	0.07400	0.09897
C2	0.70340	0.10036	0.08285	0.11340
C4	0.60199	0.13576	0.11055	0.15170
C5a	0.68489	0.10962	0.08663	0.11885
C5b	0.56268	0.15125	0.12426	0.16181
C8	0.63256	0.12672	0.10505	0.13567

Table 4.10 Difference in waste gas H_2 and CO_2 compositions: PSA-Only vs Mem-PSA (3%)

Config.	ΔH_2, %	ΔCO_2, %
C1	65.12	74.16
C2	79.73	73.05
C4	85.59	67.86
C5a	74.26	71.62
C5b	106.46	68.25
C8	106.51	72.48

Table 4.11 Waste gas flowrates: PSA-Only vs Mem-PSA (3%)

Config.	Q_{waste}, lit_{STP}/s		ΔQ_{waste}, %
	PSA-Only	Mem-PSA 3%	
C1	0.5595	0.2953	- 47.23
C2	0.6853	0.3526	- 48.55
C4	0.9458	0.4005	- 57.65
C5a	0.8581	0.4471	- 47.89
C5b	1.0652	0.4897	- 54.03
C8	0.7024	0.3668	- 47.77

Table 4.12 Membrane cut (Mem-PSA case)

Config.	3%	4%	5%	6%
C1	0.2174	0.1928	0.1728	0.1554
C2	0.2174	0.1928	0.1728	0.1554
C4	0.2174	0.1928	0.1728	0.1554
C5a	0.2091	0.1904	0.1712	0.1542
C5b	0.2091	0.1904	0.1712	0.1542
C8	0.2083	0.1897	0.1708	0.1538

4.6.2.2. Case 3: PSA-Mem

The main objective of this case study is to investigate the potential of producing a fuel gas of a higher calorific value. Since the maximization of the overall hydrogen recovery is not linked to the production of a better quality fuel gas - those two optimization problems have been split into two separate ones. Thus, the optimization results of the first problem in this case study are equal to optimization results of the PSA-Only case. The optimization results of the second problem (optimization of the membrane) are given in Table 4.13 and Table 4.14. It can be seen that a very high quality fuel gas can be obtained (95 to 97% of hydrogen and methane combined). However, the retentate flowrate is rather low, compared to the feed flowrate, and it is only a small fraction of it (8-23%) as it can be seen from the values of the fraction of feed permeated (θ_m) shown in Table 4.13. Moreover, hydrogen content in the permeate stream is still rather high (17-38%), the carbon dioxide stream produced by the membrane is of a moderate purity (not suitable for immediate sequestration but can be further processed) and the operating costs (power requirements) are higher because of the use of a compressor.

Table 4.13 Membrane optimization results (PSA-Mem case)

Config.	A_{memb}	d_{memb}	P_{feed}, bar	d_{supp}	X_{H2+CH4},%	$Q_{retentate}$, lit_{STP}/s	$Q_{permeate}$, lit_{STP}/s	θ_m, -
C1	0.2219	0.6842	12.3153	3.6075	96.7748	0.062971	0.496499	0.8875
C2	0.2120	0.6760	12.4800	4.2400	96.3464	0.095783	0.589497	0.8602
C4	0.3449	0.8515	12.3112	4.8801	96.1100	0.090422	0.855418	0.9044
C5a	0.2081	0.6838	12.3241	4.1621	95.4681	0.200758	0.657985	0.7668
C5b	0.3194	0.9263	12.4916	4.6424	95.0343	0.140054	0.925146	0.8685
C8	0.2127	0.6747	12.5066	4.2533	96.0255	0.058830	0.643530	0.9162

Table 4.14 Membrane retentate/permeate compositions (PSA-Mem case)

	Retentate molar fractions				Permeate molar fractions			
Config.	**H_2**	**CO**	**CH_4**	**CO_2**	**H_2**	**CO**	**CH_4**	**CO_2**
C1	0.95549	0.01620	0.01226	0.01606	0.37992	0.10090	0.08731	0.43187
C2	0.94700	0.02144	0.01583	0.01509	0.29993	0.11351	0.09777	0.48880
C4	0.94510	0.02442	0.01600	0.01448	0.25831	0.12406	0.09562	0.52201
C5a	0.93339	0.02856	0.02076	0.01676	0.22838	0.12352	0.10571	0.54240
C5b	0.92464	0.03310	0.02575	0.01656	0.17448	0.12398	0.11644	0.58510
C8	0.94075	0.02301	0.01950	0.01674	0.24805	0.10692	0.10723	0.53779

4.6.2.3. Case 4: Mem-PSA-Mem

Similarly to the previous study, the main objective of this case is to investigate the potential of producing a fuel gas of a higher calorific value. Again, the optimization problem has been split into two smaller problems. The optimization results of the first problem in this case study are equal to optimization results in Mem-PSA case. The optimization results of the second problem are given in Figures 4.45 to 4.48, Table 4.15 and 4.16. It can be seen that a very high quality fuel gas can be obtained (95.5 to 97% of H_2 and CH_4 combined). However, the retentate flowrate is again rather low, compared to the feed flowrate, and it is only a small fraction of it (9-22%) as it can be seen from the values of the fraction of feed permeated (θ_m) shown in Table 4.15. Moreover, hydrogen content in the permeate stream is rather high (46-69%), the carbon dioxide stream produced by the membrane is of a moderate purity (not suitable for immediate sequestration) and the operating costs (power requirements) are higher because of the use of a compressor.

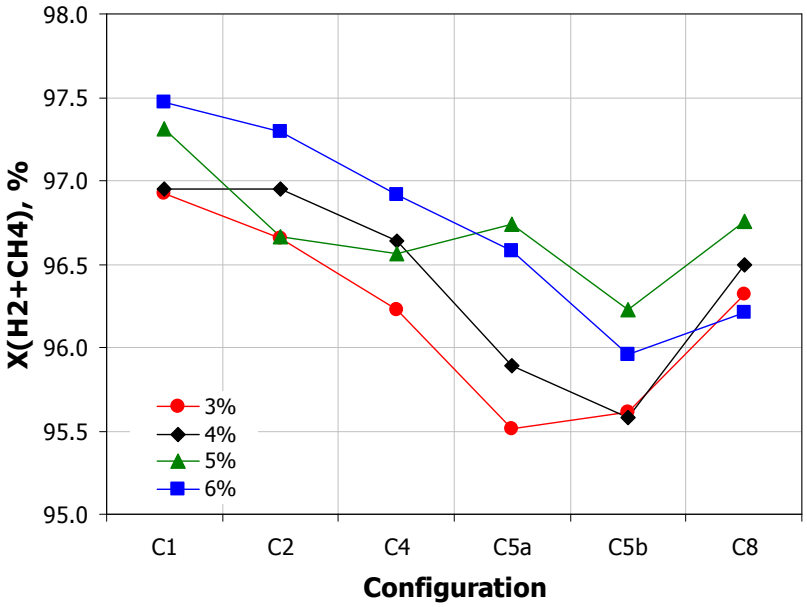

Figure 4.45 Comparison of the membrane H_2 and CH_4 purity (Mem-PSA-Mem case)

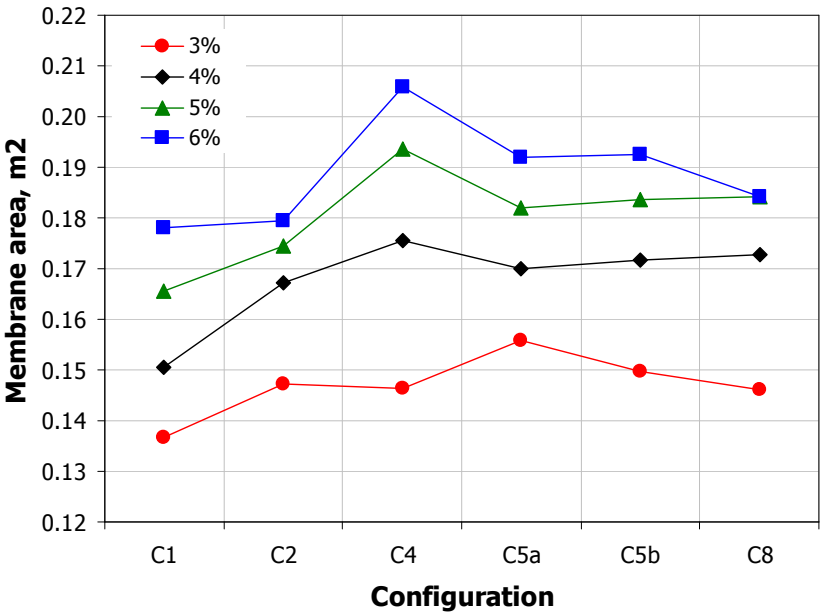

Figure 4.46 Comparison of the membrane area (Mem-PSA-Mem case)

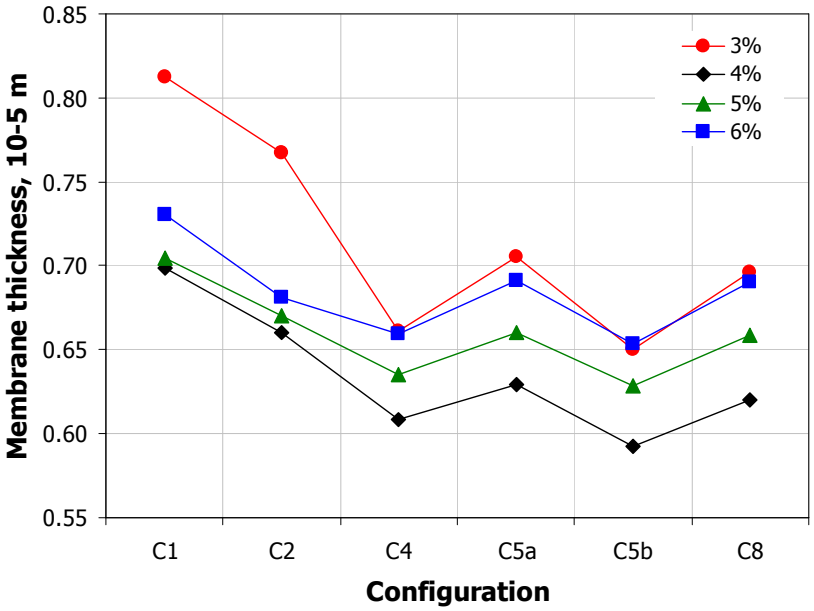

Figure 4.47 Comparison of the membrane thickness (Mem-PSA-Mem case)

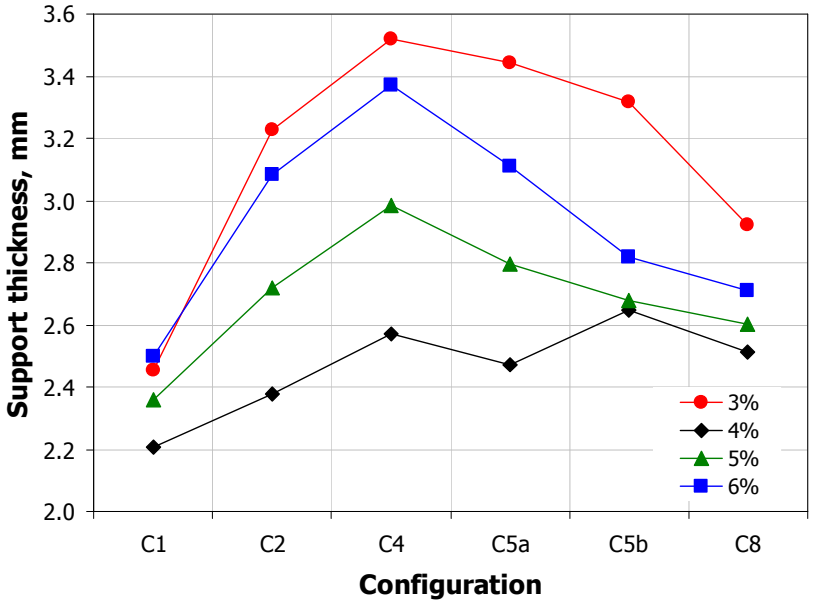

Figure 4.48 Support thickness (Mem-PSA-Mem case)

Table 4.15 Optimization results (Mem-PSA-Mem case, 3%)

Config.	A_{memb}	d_{memb}	P_{feed}, bar	d_{supp}	X_{H2+CH4},%	$Q_{retentate}$, lit_{STP}/s	$Q_{permeate}$, lit_{STP}/s	θ_m, -
C1	6.4362	0.1367	0.8122	2.4560	96.9210	0.053063	0.242191	0.8203
C2	6.8611	0.1472	0.7671	3.2252	96.6542	0.076715	0.275840	0.7824
C4	7.4080	0.1464	0.6613	3.5186	96.2252	0.053746	0.336804	0.8409
C5a	7.1418	0.1559	0.7054	3.4428	95.5145	0.038815	0.408299	0.9132
C5b	7.5875	0.1498	0.6499	3.3159	95.6123	0.105803	0.383857	0.7839
C8	7.1447	0.1462	0.6963	2.9203	96.3220	0.039315	0.327525	0.8928

Table 4.16 Membrane compositions (Mem-PSA-Mem case, 3%)

	Retentate molar fractions				Permeate molar fractions			
Config.	**H_2**	**CO**	**CH_4**	**CO_2**	**H_2**	**CO**	**CH_4**	**CO_2**
C1	0.95431	0.01990	0.01491	0.01088	0.68801	0.10568	0.08721	0.11910
C2	0.95134	0.02170	0.01610	0.01086	0.63271	0.12253	0.10171	0.14305
C4	0.94335	0.02665	0.01908	0.01092	0.53537	0.15661	0.12811	0.17991
C5a	0.96098	0.01933	0.01311	0.00658	0.65399	0.11812	0.09446	0.13242
C5b	0.93405	0.03230	0.02290	0.01075	0.45852	0.18402	0.15230	0.20516
C8	0.94896	0.02375	0.01736	0.00993	0.59237	0.13941	0.11594	0.15228

Chapter 5

Conclusions and future work

In this chapter, we summarise the main contributions of this thesis and consider some possible directions for future work.

The focus of our work has been on three main aspects:

- The detailed and generic modelling and optimization of PSA and membrane processes
- The modelling of hybrid PSA/membrane schemes
- The application of the above processes in a wide range of gas separation problems of significant industrial interest

We consider each of these separately below.

In this thesis, a novel mathematical framework for simulation and optimization of PSA and porous membranes as well as hybrid PSA/membrane units has been established. The framework comprises three major parts.

In the first part, a detailed modelling of typical modern multi-bed industrial PSA units consisting of several multi-layered adsorption columns operating in tandem has been presented. The coupled set of mixed algebraic and partial differential equations for mass, heat and momentum balance at bulk gas and particle levels, gas-solid phase equilibrium equations and complex boundary conditions represent the core of the modelling framework. The modelling framework is sufficiently general to support arbitrary number of beds, all feasible bed configurations, all operating steps and all feasible inter-bed connectivities. Four different mass transfer mechanisms (local equilibrium, linear driving force, surface diffusion and particle diffusion), three thermal operating modes (isothermal, adiabatic and non-isothermal) and several approaches to model gas-solid phase equilibrium (Henry's law or extended Langmuir adsorption isotherms and Ideal/Real Adsorbed

Solution theory) have been implemented. Two approaches to modelling of bed interactions in a multi-bed PSA process have been developed: a) bed network super-structure approach (the most complete one, where all columns are simulated), b) *VirtualBeds* approach (a modified *Unibed* approach employed to reduce the size of the DAE system and speed up process simulation). Two approaches to control the execution of a PSA process have been proposed: a) by using a set of operating procedures to govern the bed network super-structure (generated by an auxiliary program for automatic generation of operating procedures, which generates operating procedures for the whole network of beds according to the given number of beds and sequence of operating steps in one bed); b) a novel, more robust approach by using a state transition network (STN) to govern the state of adsorbent columns and gas valves (implemented as a deterministic Finite State Machine where the next possible state is uniquely determined for a given current state and input values).

The modelling framework has been applied on two most common separation processes (oxygen and nitrogen production from air) and simulation results have been compared to the results available in the literature.

Then, a medium scale hydrogen recovery from steam methane reforming off gas process has been used to investigate the effects of number of beds on the separation quality and analyse the trade-offs between capital and operating costs and separation quality.

Finally, two large-scale multi-component separation processes (oxygen production from air and hydrogen recovery from steam methane reforming off gas) have been used to illustrate the applicability and potential of the proposed approach in terms of power consumption minimization and improvement of product purity and recovery. The number of beds, PSA cycle configuration and various operating and design parameters have been systematically optimized using recent advances on process optimization. It has been shown that by employing multi-bed configurations it is possible to achieve up to 18% higher recovery for the same purity. In addition, by using more than one adsorbent layer up to 5% higher recovery can be obtained compared to single adsorbent cases.

In the second part, a detailed modelling framework of porous membranes for gas separations has been presented. The state-of-the-art general Stefan-Maxwell equations have been coupled with Ideal/Real Adsorbed Solution theory to model mass transfer phenomena within a porous solid and porous support. The modelling framework has been applied on several hydrocarbons separation processes and results compared with experimental or molecular simulations data.

In the last part, a hybrid PSA/membrane concept has been analysed and applied on hydrogen production from SMROG. Several hybrid schemes have been analyzed and possibilities for process improvement were critically discussed. Three distinct hybrid configurations have been studied: membrane attached to feed stream (Mem-PSA), membrane attached to waste gas streams (PSA-Mem) and membranes attached to both feed and waste gases streams (Mem-PSA-Mem).

The overall hydrogen recovery for given minimum requirements in product purity has been systematically maximized using recent advances on process optimization while optimizing the number of beds, PSA cycle configuration and various PSA and membrane operating and design parameters. The optimization results have been compared to the optimization results of the PSA only case. Benefits of hybrid systems have been assessed in terms of reduction of adsorption columns size, improvements in the overall hydrogen recovery, reduction of the carbon dioxide content in the feed and waste gas streams and

improvements in a calorific value of the waste gas streams (used as a fuel in the steam methane reforming process). Major improvements include: significant reduction in column size (up to 46%), increase in overall hydrogen recovery (~2%), reduction of carbon dioxide content (up to 74%) and increase of hydrogen content (up to 106%) in PSA waste gases, and fuel gas (from PSA waste gases) of a higher calorific value (~96% of hydrogen and methane combined).

In summary, the contributions of this thesis have been:

- An integrated modelling, simulation and optimization framework for complex gas separation processes has been developed including: Pressure Swing Adsorption, Membrane and hybrid PSA/Membrane processes
- Two approaches to modelling of bed interactions in a multi-bed PSA process have been developed: a) bed network super-structure approach; b) VirtualBeds approach
- Two approaches to control the execution of a PSA process have been proposed: a) by using a set of operating procedures to govern the bed network super-structure; b) by using a state transition network approach to govern the state of adsorbent columns and gas valves
- Developed modelling and optimization framework has been applied on several typical industrial separation processes and the number of beds, PSA cycle configuration and various operating and design parameters have been systematically optimized using recent advances on process optimization
- Several hybrid PSA/Membrane schemes have been analyzed and possibilities for process improvement were critically discussed in terms of reduction of adsorption columns size, improvements in the overall hydrogen recovery, reduction of the carbon dioxide content in the feed and waste gas streams and improvements in a calorific value of the waste gas streams

5.1. Recommendations for Future Directions

A range of issues requiring further investigation has been revealed in the course of this thesis. In particular:

- The synthesis of hybrid PSA/membranes processes using process systems engineering approach. Here, it would be interesting to consider the application of advanced mixed-integer dynamic optimisation techniques for the integrated synthesis problems in which the number and types of membrane and PSA units along with their optimal connections and design and operating conditions would be optimally defined. This approach would not require a priory postulation of the hybrid scheme and it will automatically define the optimal flowsheet
- The integrated design and control of hybrid PSA/membrane process. The integrated scheme very likely suffers from optimal and robust control. Here the application of integrated design and control approaches would offer significant opportunities to explore the synergistic benefits between process design and control in view of

designing both operable and economically attractive processes under uncertainty, disturbances and tight operating constraints

- The detailed modelling and optimization of more effective hydrogen and carbon dioxide selective membranes
- The multi-objective optimization of hybrid PSA/membrane schemes. The analysis in the previous chapters revealed that several objectives exist when optimizing hybrid process. The e-constraint approach would offer a Pareto curve of inferior solutions by providing an optimal set of points/solutions each corresponding to an optimal value of the first objectives (e.g. purity) under a certain upper or lower bound on the second objectives

Referenced Papers from this Thesis

Journal publications:

- Nikolic, D.; Giovanoglou, A.; Georgiadis, M.C.; Kikkinides, E.S. *Generic modeling framework for gas separations using multibed pressure swing adsorption processes*. Ind. Eng. Chem. Res. **2008**, 47, 3156.
- Nikolic, D.; Kikkinides, E.S.; Georgiadis, M.C. *Optimization of Multibed PSA Processes*. Ind. Eng. Chem. Res. **2009**, 48, 5388.
- *Book chapter: Modeling of Pressure Swing Adsorption Processes* in J. Banga, M. Georgiadis, E. Pistikopoulos;. Volume 7: Dynamic Process Modelling, Process Systems Engineering (7 Volume Set), **2010**, Wiley-VCH, edited by E. Pistikopoulos, M. Georgiadis and V. Dua
- In preparation:
    - Nikolic, D.; Georgiadis, M.C.; Kikkinides, E.S. *A generic modelling and optimization framework for membrane-based gas separations processes*. To be submitted to publication in Computers & Chemical Engineering.
    - Nikolic, D.; Georgiadis, M.C.; Kikkinides, E.S. *Modelling and optimization of hybrid PSA/Membrane processes*. To be submitted to publication in Industrial & Engineering Chemistry Research

Conference publications:

- Nikolic, D.; Georgiadis, M.C.; Kikkinides, E.S. *Modelling and optimization of multibed pressure swing adsorption flowsheets*, Process Integration, Modelling and Optimisation for Energy Saving and Pollution Reduction (PRES) **2006**, Prague
- Nikolic, D.; Georgiadis, M.C.; Kikkinides, E.S. *Modelling and optimization of multibed Pressure swing adsorption flowsheets*, European Symposium on Computer-Aided Process Engineering (ESCAPE) 17, **2007**, Bucharest, Romania
- Nikolic, D.; Georgiadis, M.C.; Kikkinides, E.S. *Modeling and optimization of single and multi-layer pressure swing adsorption systems*, European Congress of Chemical Engineering (ECCE) 6, **2007**, Copenhagen, Denmark
- Nikolic, D.; Giovanoglou, A.; Georgiadis, M.C.; Kikkinides, E.S. *Simultaneous production of hydrogen and carbon dioxide from steam methane off gas using multibed pressure swing adsorption systems*, Process Integration, Modelling and Optimisation for Energy Saving and Pollution Reduction (**2007**), Ischia, Italy
- Nikolic, D.; Georgiadis, M.C.; Kikkinides, E.S. *An optimization framework of multibed pressure swing adsorption systems*, European Symposium on Computer-Aided Process Engineering (ESCAPE) 18, **2008**, Lyon, France.

Chapter 6

Nomenclature

a_V = specific area, m^2/ m^3

a_1 = Langmuir isotherm parameter, mol/kg

a_2 = Langmuir isotherm parameter, K

b_1 = Langmuir isotherm parameter, 1/Pa

b_2 = Langmuir isotherm parameter, K

b = Langmuir isotherm parameter, m^3/mol

C = molar concentrations of gas phase in bulk gas, mol/m^3

C^p = molar concentrations of gas phase in particles, mol/m^3

c_p = heat capacity of bulk gas, J/(kg·K)

$c_{p,pg}$ = heat capacity of gas within pellets, J/(kg·K)

c_p^p = heat capacity of the particles, J/(kg·K)

C_v = valve constant

D = bed diameter, m

D_e = effective diffusivity coefficient, m^2/s

$Đ$ = Stefan Maxwell diffisivity

D_m = molecular diffusion coefficient, m^2/s

D_s = surface diffusion coefficient, m^2/s

D_z = axial dispersion coefficient, m^2/s

F = molar flowrate, mol/s

F_{feed} = feed molar flowrate, mol/s

$F_{product}$ = product molar flowrate, mol/s

ΔH_{ads} = heat of adsorption, J/mol

H = Henry's parameter, m^3/kg

k_f = mass transfer coefficient, m^2/s

k_h = heat transfer coefficient, $J/(m^2 \cdot K \cdot s)$

$k_{h,wall}$ = heat transfer coefficient for the column wall, $J/(m^2 \cdot K \cdot s)$

L = bed length, m

N_{comp} = number of components, -

N_i = molar flux, mol/m^2s

Q = adsorbed amount, mol/kg

Q^* = adsorbed amount in equilibrium state with gas phase (in the mixture), mol/kg

Q^*_{pure} = adsorbed amount in equilibrium state with gas phase (pure component), mol/kg

Q_{total} = total adsorbed amount, mol/kg

Q_m = Langmuir isotherm parameter, mol/kg

P = total pressure, Pa

P^0 = pressure that gives the same spreading pressure in a multicomponent mixture, Pa

p_i = partial pressure, Pa

q_i^{sat} = monolayer saturation capacity of zeolite, mol/kg

q_{total} = the total amount adsorbed, mol/kg

R_p = particle diamater, m

R_{bed} = bed radius, m

R_p = pellet radius, m

sp = stem position of a gas valve

$sp_{PressCoC}$ = stem position of a gas valve during co-current pressurization, -

$sp_{PressCC}$ = stem position of a gas valve during counter-current pressurization, -

sp_{AdsIn} = stem position of a gas valve during adsorption (inlet valve), -

sp_{AdsOut} = stem position of a gas valve during adsorption (outlet valve), -

sp_{Blow} = stem position of a gas valve during blowdown, -

$sp_{PurgeIn}$ = stem position of a gas valve during purge (inlet valve), -

$sp_{PurgeOut}$ = stem position of a gas valve during purge (outlet valve), -

sp_{PEQ1} = stem position of a gas valve during pressure equalization, -

sp_{PEQ2} = stem position of a gas valve during pressure equalization, -

sp_{PEQ3} = stem position of a gas valve during pressure equalization, -

T = temperature of bulk gas, K

T^p = temperature of particles, K

u = interstitial velocity, m/s

x = molar fraction in gas phase, -

x^* = molar fraction in adsorbed phase, -

Z = compressibility factor, -

CC = counter-current pressurization

Ads = adsorption

Ads^{CC} = adsorption while at the same time repressurizing the other column

EQD1, *EQD2*, *EQD3* = co-current depressurizations (pressure equalization)

EQR1, *EQR2*, *EQR3* = counter-current repressurization (pressure equalization)

CoCD = co-current depressurization providing purge

Blow = counter-current blowdown

Purge = counter-current purge

Greek letters:

δ_m = membrane thickness, m

δ_s = thickness of the support, m

ε_{bed} = bed porosity, -

ε_p = pellet porosity, -

γ = activity, -

Γ = thermodynamic factor, -

θ = fractional coverage, -

θ_m = membrane cut (fraction of feed permeated), -

ρ = density of bulk gas, kg/m^3

μ = viscosity of bulk gas, Pas

μ = chemical potential, J

λ = thermal conductivity of bulk gas, J/(m·K)

λ^p = thermal conductivity of the particles, J/(m·K)

π^* = reduced spreading pressure, -

ρ_{pg} = density of gas within pellets, kg/m^3

ρ^p = density of the particles, kg/m^3

τ = tortuosity, -

Chapter 7

List of references

[1] Yang, R.T.; Fenn, J.B.; Haller, G.L. Modification to the Higashi model for surface diffusion. AIChE Journal, **1973**, 19, 1052.

[2] Kawazoe, K.; Takeuchi, Y. Mass transfer in adsorption on bidisperse porous materials: Macro and micropore series diffusion model. J. Chem. Eng. Jpn. **1974**, 7.

[3] Kärger, J.; Bülow, M. Theoretical prediction of uptake behaviour in adsorption kinetics of binary gas mixtures using irreversible thermodynamics. Chem. Eng. Sci. **1975**, 30, 893.

[4] Wakao, N.; Funazkri, T. Effect of fluid dispersion coefficients on particle-to-fluid mass transfer coefficients in packed beds: Correlation of Sherwood numbers. Chem. Eng. Sci. **1978**, 33, 1375.

[5] Wakao, N,: Kaguei, S.; Funazkri, T. Effect of fluid dispersion coefficients on particle-to-fluid heat transfer coefficients in packed beds: Correlation of Nusselt numbers. Chem. Eng. Sci. **1979**, 34, 325.

[6] Ruthven, D. M. Principles of adsorption and adsorption processes; Wiley: New York, **1984**.

[7] Raghavan, N.; Ruthven D.; Pressure swing adsorption. Part III: numerical simulation of a kinetically controlled bulk gas separation. AIChE J., **1985**, 31, 2017.

[8] Raghavan, N.; Hassan M.; Ruthven, D.M. Numerical simulation of a PSA system using a pore diffusion model. Chem. Eng. Sci. **1986**, 41, 2787.

[9] Doong, S.J.; Yang, R.T. Bulk separation of multicomponent gas mixtures by pressure swing adsorption: Pore/surface diffusion and equilibrium models. AIChE J. **1986**, 32, 397.

[10] Yang, R.T.; Doong, S.J. Parametric study of the pressure swing adsorption process for gas separation: A criterion for pore diffusion limitation. Chem. Eng. Commun. **1986**, 41, 163.

[11] Doong, S.J.; Yang, R.T. Bidisperse pore diffusion model for zeolite pressure swing adsorption. AIChE J. **1987**, 33, 1045.

[12] Yang, R. T. Gas separation by adsorption processes; Butterworths: Boston, **1987**.

[13] Hassan, M.M.; Raghavan, N.S.; Ruthven, D.M. Numerical simulation of a pressure swing air separation system a comparative study of finite difference and collocation methods. Can. J. Chem. Eng. **1987**, 65, 512.

[14] Wankat, P.C. Intensification of sorption processes, *Ind. Eng. Chem. Res*. **1987**, 26, 1579.

[15] Raghavan, N.S.; Hassan, M.M.; Ruthven, D.M. Pressure swing air separation on a carbon molecular sieve- II. Investigation of a modified cycle with pressure equalization and no purge. Chem. Eng. Sci. **1987**, 42, 2037.

[16] Shin, H.S.; Knaebel, K.S. Pressure swing adsorption: A theoretical study of diffusion-induced separation. AIChE J. **1987**, 33, 654.

[17] Shin, H.S.; Knaebel, K.S. Pressure swing adsorption: An experimental study of diffusion-induced separation. AIChE J. **1988**, 34, 1409.

[18] O'Brien, J.A.; Myers, A.L. A comprehensive technique for equilibrium calculations in adsorbed mixtures: The generalized FastIAS method. Ind. Eng. Chem. Res. **1988**, 27, 2085.

[19] Farooq, S.; Ruthven, D.M. Numerical simulation of a pressure swing adsorption oxygen unit. Chem. Eng. Sci. **1989**, 44, 2809.

[20] Kapoor, A.; Yang, R.T. Kinetic separation of methane-carbon mixture by adsorption on molecular sieve carbon. Chem. Eng. Sci. **1989**, 44, 1723.

[21] Suh, S.S.; Wankat, P.C. A new pressure adsorption process for high enrichment and recovery. Chem. Eng. Sci. **1989**, 44, 567.

[22] Ruthven, D.M.; Farooq S. Air separation by pressure swing adsorption. Gas Sep. Purif. **1990**, 4, 141.

[23] Ackley, M.W.; Yang, R.T. Kinetic separation by pressure swing adsorption: Method of characteristics model. AIChE J. **1990**, 36, 1229.

[24] Smith, O.J.; Westerberg, A.W. Mixed-integer programming for pressure swing adsorption cycle scheduling. Chem. Eng. Sci. **1990**, 45, 2833.

[25] Smith, O.J.; Westerberg, A.W. The optimal design of pressure swing adsorption systems. Chem. Eng. Sci. **1991**, 46, 2967.

[26] Zolandz, R. R.; Fleming, G. K. Design of gas permeation systems, in Membrane Handbook. Editors W.S. Ho and K.K. Sirkar. **1992**.

[27] Ruthven, D.M. Diffusion of Oxygen and Nitrogen in Carbon Molecular Sieve. Chem. Eng. Sci. **1992**, 47, 4305.

[28] Alpay, E.; Scot, D.M. The linear driving force model for the fast-cycle adsorption and desorption in a spherical particle. Chem. Eng. Sci. **1992**, 47, 499.

[29] Chena, Y.D.; Yang, R.T. Predicting binary Fickian diffusivities from pure-component Fickian diffusivities for surface diffusion. Chem. Eng. Sci. **1992**, 47, 3895.

[30] Zolandz, R.R.; Fleming, G.K. Gas Permeation. In: Membrane Handbook, eds. Ho, W.S.W, Sirkar, K.K. Van Nostrand Reinhold, New York, USA, **1992.**

[31] Kärger, J.; Ruthven, D.M. Diffusion in Zeolites and Other Microporous Solids, **1992**, John Wiley, New York.

[32] Krishna, R. A unified approach to the modeling of intraparticle diffusion in adsorption processes. Gas Sep. Purif. **1993**, 7, 92.

[33] Kikkinides, E.S.; Yang, R.T. Effects of bed pressure drop on isothermal and adiabatic adsorber dynamics. Chem. Eng. Sci. **1993**, 48, 1545.

[34] Kikkinides, E.S.; Yang, R.T. Concentration and recovery of CO_2 from flue gas by pressure swing adsorption. Ind. Eng. Chem. Res. **1993**, 32, 2714.

[35] Lu, Z.P.; Loureiro, J.M.; Le Van, M.D; Rodrigues, A.E. Pressure swing adsorption processes - Intraparticle diffusion/convection models. Ind. Eng. Chem. Res. **1993**, 32, 2740.

[36] Chou, C.T.; Huang, W.C. Incorporation of a valve equation into the simulation of a pressure swing adsorption process. Chem. Eng. Sci. **1994a**, 49, 75.

[37] Chou, C.T.; Huang, W.C. Simulation of a four-bed pressure swing adsorption process for oxygen enrichment. Ind. Eng. Chem. Res. **1994b**, 33, 1250.

[38] Lu, Z.P.; Rodrigues, A.E. Pressure swing adsorption reactors: simulation of three-step one-bed process. AIChE J. **1994**, 40, 1118.

[39] Mercea, P.; Hwang, S.T. Oxygen Separation from Air by a Combined Pressure Swing Adsorption and Continuous Membrane Column Process, J. Memb. Sci., **1994**, 88, 132.

[40] Ruthven, D.M.; Farooq, S.; Knaebel, K.S. Pressure swing adsorption; VCH Publishers: New York. **1994**.

[41] Ruthven, D.M. PSA vs membrane processes for gas separation. Membrane Quarterly, **1994**, 9, 3, 7.

[42] Sikavitsas, V.I.; Yang, R.T. Predicting multicomponent diffusivities for diffusion on surfaces and in molecular sieves with energy heterogeneity. Chem. Eng. Sci. **1995**, 50, 3057.

[43] Le Van, M.D. Pressure swing adsorption: Equilibrium theory for purification and enrichment. Ind. Eng. Chem. Res. **1995**, 34, 2655.

[44] Yang, J.; Han, S.; Cho, C.; Lee, C.H., Lee, H. Bulk separation of hydrogen mixtures by a one-column PSA process, Separations Technology. **1995**, 5, 239.

[45] Warmuzinski, K.; Tanczyk, M. Multicomponent pressure swing adsorption. Part I. Modelling of large-scale PSA installations. Chem. Eng. Process. **1997**, 36, 89.

[46] Krishna, R.; Wesselingh, J. A. The Maxwell-Stefan approach to mass transfer. Chem. Eng. Sci. **1997**, 52, 861.

[47] Van de Graaf, J.M.; Van der Bijl, E.; Stol, A.; Kapteijn, F.; Moulijn, J.A. Effect of operating conditions and membrane quality on the separation performance of composite silicalite-1 membranes, Ind. Eng. Chem. Res., **1998**, 37, 4071.

[48] Feng, X.; Pan, C. Y.; Ivory, J.; Ghosh, D. Integrated Membrane/Adsorption Process for Gas Separation. Chem. Eng. Sci. **1998**, 53, 1689.

[49] Baker, R. W. Steam Cracker Gas Separation Process. U.S. Patent 5,785,739, **1998**.

[50] Warmuzinski, K.; Tanczyk, M. Multicomponent pressure swing adsorption. Part II. Experimental verification of the model. Chem. Eng. Process. **1998**, 37, 301.

[51] Nilchan, S.; Pantelides, C.C. On the optimisation of periodic adsorption processes. Adsorption. **1998**, 4, 113.

[52] Park, J.H.; Kim, J.N.; Cho, S.H.; Kim, J.D.; Yang, R.T., Adsorber dynamics and optimal design of layered beds for multicomponent gas adsorption, Chem. Eng. Sci. **1998**, 53, 3951.

[53] Serbezov, A.; Sotirchos, S.V. Mathematical modelling of multicomponent nonisothermal adsorption in sorbent particles under pressure swing conditions. Adsorption. **1998**, 4, 93.

[54] Botte, G.G.; Zhang, R.Y.; Ritter, J.A. On the use of different parabolic concentration profiles for nonlinear adsorption and diffusion in a single particle. Chem Eng. Sci. **1998**, 24, 4135.

[55] Yang, J.; Lee, C.H. Adsorption dynamics of a layered bed PSA for H_2 recovery from coke oven gas. *AIChE J.* **1998**, 44, 1325.

[56] Lee, C.H.; Yang, J.; Ahn, H. Effects of carbon-to-zeolite ratio on layered bed H_2 PSA for coke oven gas, AIChE J. **1999**, 45, 535.

[57] S. Sircar, W.E. Waldron, M.B. Rao, M. Anand. Hydrogen production by hybrid SMR–PSA–SSF membrane system. Separation and Purification Technology, **1999**, 17, 11.

[58] Van de Graaf, J. M.; Kapteijn, F.; Moulijn, J. A. Modeling permeation of binary mixtures through zeolite membranes. AIChE J. **1999**, 45, 497.

[59] Baker, R. W.; Lokhandwala, K. A. Membrane-Based Conditioning for Adsorption System Feed Gases. U.S. Patent 6,011,192, **2000**.

[60] van de Graaf, J.M.; Kapteijn, F.; Moulijn, J.A. Diffusivities of light alkanes in a silicalite-1 membrane layer, Microporous Mesoporous Mater. **2000**, 35, 267.

[61] Kapteijn, F.; Moulijn, J. A.; Krishna, R. The generalized Maxwell-Stefan model for diffusion in zeolites: Sorbate molecules with different saturation loadings. Chem. Eng. Sci. **2000**, 55, 2923.

[62] Pantelides, C.C. The mathematical modelling of the dynamic behaviour of process systems. Imperial College of Science, Technology and Medicine, London, **2000**.

[63] Chou, C.T.; Chen, C.Y. Carbon dioxide recovery by vacuum swing adsorption. Sep. Purif. Technol. **2000**, 39, 51.

[64] Chahbani, M.H.; Tondeur, D. Mass transfer kinetics in pressure swing adsorption. Sep. Purif. Technol. **2000**, 20, 185.

[65] Park, J.H.; Kim, J.N.; Cho, S.H., Performance analysis of four-bed H_2 PSA process using layered beds, AIChE J. **2000**, 46, 790.

[66] Barg, C.; Fereira, J.M.P.; Trierweiler, J.O.; Secchi, A.R. Simulation and optimization of an industrial PSA unit. Braz. J. Chem. Eng. **2000**, 17.

[67] Sircar, S.; Golden, T.C. Purification of hydrogen by pressure swing adsorption, Sep. Sci. Technol. **2000**, 35, 667.

[68] Waldron, W.E.; Sircar, S. Parametric Study of a Pressure Swing Adsorption Process. Adsorption. **2000**, 6, 179.

[69] Rajasree, R.; Moharir, A.S. Simulation based synthesis, design and optimization of pressure swing adsorption (PSA) processes. Comput. Chem. Eng. **2000**, 24, 2493.

[70] Mendes, A.M.M.; Costa, C.A.V.; Rodrigues A.E. PSA simulation using particle complex models, Sep. Purif. Technol. **2001**, 24, 1.

[71] Drioli, E.; Romano, M. Progress and New Perspectives on Integrated Membrane Operations for Sustainable Industrial Growth. Ind. Eng. Chem. Res. **2001**, 40, 1277.

[72] Baker, R. W.; Lokhandwala, K. A.; He, Z.; Pinnau, I. Process including PSA and Membrane Separation, for Separating Hydrogen from Hydrocarbons. U.S. Patent 6,183,628, **2001**.

[73] Esteves, I.A.A.C.; Mota, J.P.B. Simulation of a New Hybrid Membrane/Pressure Swing Adsorption Process for Gas Separation. Desalination, **2002**, 148, 275.

[74] Baker, R.W. Future Directions of Membrane Gas Separation Technology, Ind. Eng. Chem. Res. **2002**, 41, 1393.

[75] Gardner, T.Q.; Falconer, J.L.; Noble, R.D. Adsorption, Diffusion properties of zeolite membranes by transient permeation, Desalination, 149, **2002**, 435.

[76] Jee, J.G.; Park, M.K.; Yoo, H.K.; Lee, K; Lee, C.H. Adsorption and desorption characteristics of air on zeolite 5A, 10X, and 13X fixed beds, *Sep. Sci. Technol*, **2002**, 37, 3465.

[77] Esteves, I.A.A.C.; Mota, J.P.B. Simulation of a new hybrid membrane/pressure swing adsorption process for gas separation. Desalination, **2002**, 148, 275.

[78] Vareltzis, P.; Kikkinides E.S., Georgiadis M.C., On the optimization of gas separation processes using zeolite membranes. Trans IChemE, **2003**, 81, 525.

[79] De Bruijn, F.T.; Sun, L.; Z. Olujic, P.J. Jansens, F. Kapteijn, Influence of the support layer on the flux limitation in pervaporation, J. Membr. Sci. 223, **2003**, 141.

[80] Krishna, R.; Baur, R. Modelling issues in zeolite based separation processes. Sep. Purif. Technol. **2003**, 33, 213.

[81] Cruz, P.; Alves, M.B.; Magalhaes, F.D.; Mendes, A. Solution of hyperbolic PDEs using a stable adaptive multiresolution method. Chem. Eng. Sci. **2003**, 58, 1777.

[82] Cruz, P.; Alves, M.B.; Magalhaes, F.D.; Mendes, A. Cyclic adsorption separation processes: analysis strategy and optimization procedure. Chem. Eng. Sci. **2003**, 58, 3143.

[83] Ko, D.; Siriwardane, R.; Biegler, L. T. Optimization of a pressure-swing adsorption process using zeolite 13X for CO_2 sequestration. Ind. Eng. Chem. Res. **2003**, 42, 339.

[84] Jain, S.; Moharir, A.S.; Li, P.; Wozny, G., Heuristic design of pressure swing adsorption: a preliminary study, Sep. Purif. Technol. **2003**, 33, 25.

[85] Jiang, L.; Biegler, L. T.; Fox, V. G. Simulation and optimization of pressure-swing adsorption systems for air separation. AIChE J. **2003**, 49, 1140.

[86] Jiang, L.; Biegler, L.T.; Fox, V.G. Simulation and optimal design of multiple-bed pressure swing adsorption systems. AIChE J. **2004**, 50, 2904.

[87] Kim, M.B.; Jee, J.G.; Bae, Y.S.; Lee C.H. Parametric study of pressure swing adsorption process to purify oxygen using carbon molecular sieve. AIChE J. **2004**.

[88] Chang, D.; Min, J.; Moon, K.; Park, Y. K.; Jeon, J.K.; Ihm, S.K. Robust numerical simulation of pressure swing adsorption process with strong adsorbate CO_2. Chem. Eng. Sci. **2004**, 59, 2715.

[89] Krishna, R.; Paschek, D.; Baur, R. Modelling the occupancy dependence of diffusivities in zeolites. Microporous Mesoporous Mater. **2004**, 76, 233.

[90] Krishna, R.; Baur, R. Diffusion, Adsorption and Reaction in Zeolites: Modelling and Numerical Issues; University of Amsterdam, The Netherlands, **2004**; http://www.science.uva.nl/research/cr/zeolite.

[91] Cruz, P.; Magalhaes, F.D.; Mendes, A. On the optimization of cyclic adsorption separation processes. AIChE J. **2005**, 51, 1377.

[92] Ko, D.; Siriwardane, R.; Biegler, L.T. Optimization of pressure swing adsorption and fractionated vacuum pressure swing adsorption processes for CO_2 capture. Ind. Eng. Chem. Res. **2005**, 44, 8084.

[93] Jee, J.; Kim, M.; Lee, C. Pressure Swing Adsorption Processes to Purify Oxygen Using a Carbon Molecular Sieve. Chem. Eng. Sci. **2005**, 60, 869.

[94] Knaebel, S.P.; Ko, D.; Biegler, L.T. Simulation and optimization of a pressure swing adsorption system: Recovering hydrogen from methane. Adsorption. **2005**, 11, 615.

[95] Kim, M.B.; Jee, J.G.; Bae, Y.S.; Lee, C.H. Parametric study of pressure swing adsorption process to purify oxygen using carbon molecular sieve, Ind. Eng. Chem. Res. **2005**, 44, 7208.

[96] Ahn, H; Brandani, S. A new numerical method for accurate simulation of fast cyclic adsorption processes. Adsorption. **2005**, 11, 113.

[97] Grande, C.A.; Rodrigues A.E., Propane/propylene separation by pressure swing adsorption using zeolite 4A. Ind. Eng. Chem. Res. **2005**, 44, 8815.

[98] Jiang, L.; Biegler, L.T.; Fox, V.G. Design and optimization of pressure swing adsorption systems with parallel implementation. Comput. Chem. Eng. **2005**, 29, 393.

[99] Skoulidas, A.I.; Sholl, D.S. Multiscale models of sweep gas and porous support effects on zeolite membranes, AIChE J. 51, **2005**, 867.

[100] Krishna, R.; van Baten, J. M. Diffusion of alkane mixtures in zeolites. Validating the Maxwell-Stefan formulation using MD simulations. J. Phys. Chem. **2005**, 109, 6386.

[101] Krishna, R.; van Baten, J. M. Influence of isotherm inflection on the diffusivities of C5-C8 linear alkanes in MFI zeolite. Chem. Phys. Lett. **2005**, 407, 159.

[102] Krishna, R.; van Baten, J. M. Kinetic Monte Carlo simulations of the loading dependence of diffusion in zeolites. Chem. Eng. Technol. **2005**, 28, 160.

[103] Process Systems Enterprise Ltd. http://www.psenterprise.com. **2006**.

[104] Reynolds, S.P.; Ebner, A.D.; Ritter, J.A., Stripping PSA cycles for CO_2 recovery from flue gas at high temperature using a hydrotalcite-like adsorbent. Ind. Eng. Chem. Res. **2006**, 45, 4278.

[105] Reynolds, S.P.; Ebner, A.D.; Ritter J.A. Enriching PSA cycle for the production of nitrogen from air. Ind. Eng. Chem. Res. **2006**, 45, 3256.

[106] Zhu, W.; Hrabanek, P.; Gora, L.; Kapteijn, F.; Moulijn, J. A. Role of Adsorption in the Permeation of CH_4 and CO_2 through a Silicalite-1 Membrane. Ind. Eng. Chem. Res. **2006**, 45, 767.

[107] Krishna, R.; van Baten, J. M. Linking the loading dependence of the Maxwell-Stefan diffusivity of linear alkanes in zeolites with the thermodynamic correction factor. Chem. Phys. Lett. **2006**, 420, 545.

[108] Krishna, R.; van Baten, J. M.; Garcıa-Perez, E.; Calero, S. Incorporating the loading dependence of the Maxwell-Stefan diffusivity in the modeling of CH_4 and CO_2 permeation across zeolite membranes. Ind. Eng. Chem. Res. **2007**, 46.

[109] Ritter, J.A.; Ebner, A.D. State-of-the-Art Adsorption and Membrane Separation Processes for Hydrogen Production in the Chemical and Petrochemical Industries, Separation Science and Technology, **2007**, 42, 1123.

[110] Sankararao, B.; Gupta, S.K. Multi-objective optimization of pressure swing adsorbers for air separation, *Ind. Eng. Chem. Res.*, **2007**, 46, 3751.

[111] Esteves, I.A.A.C.; Mota, J.P.B. Gas Separation by a Novel Hybrid Membrane / Pressure Swing Adsorption Process. AIChE Journal, **2007**, 46, 5723.

[112] Nikolic, D.; Giovanoglou, A.; Georgiadis, M.C.; Kikkinides, E.S. Generic modeling framework for gas separations using multibed pressure swing adsorption processes. *Ind. Eng. Chem. Res.* **2008**, 47, 3156.

[113] Nikolic, D.; Kikkinides, E.S.; Georgiadis, M.C. Optimization of Multibed PSA Processes. *Ind. Eng. Chem. Res.* **2009**, 48, 5388.